Investigating the Effects of the Microglial Inflammatory Response on Iron Metabolism in Dopaminergic Neurons

Dr Tamara Alireza

Imperial College London
Faculty of Medicine
Department of Medicine
Division of Brain Sciences
Centre for Neuroinflammation and Neurodegeneration

A thesis submitted in fulfilment of the requirements set for the degree of Doctor of Philosophy in the Faculty of Medicine, Imperial College London

October 2017

Declaration of Originality

I hereby declare that this thesis is entirely of my own composition for the fulfilment of the doctorate degree from Imperial College London, and has not been previously submitted in any other form or at any other time for another degree or diploma at any university or other institution of tertiary education. Information derived from the published or unpublished work of others has an accompanying acknowledgement in the text and a full reference list provided at the end.

Tamara Alireza
28th October 2017

Acknowledgements

I would like to thank my supervisor Professor David Dexter for providing me with the opportunity to undertake this project in the first place, and helping to see it to completion.

A great deal of the work needed to complete this thesis could not have been possible without the help and support of other students and collaborators who were willing to take the time to teach me various techniques. I am extremely grateful to you all. From the Dexter group, thank you to Ian Harrison for welcoming me to the lab and teaching me everything you knew about PCRs, even when you had to figure it all out for yourself first, and to Mike Hurley for helping when the PCRs didn't work out quite as planned. Muchisimas gracias Dan for introducing me to the world of cell culture. Thanks Claire for being my desk buddy, you were sorely missed when you left. To Darya, thank you so much for providing me with my primary cells and for teaching me how to culture them. You were so supportive and kind to me, and I am truly thankful. To Felwah for maintaining a semblance of unity within our group, you are so lovely and helpful in many things. I wish you the best in the completion of your own project.

Then to members of other groups, I am truly indebted to those of you who took the precious time out of your own projects to explain things I could not have learnt without you. To Maria Weinert, thank you for educating me on the confocal microscope and for setting me on the right path to use another microscope instead. To Ilaria Palmisano, thank you so much for the induction to use the white wash microscope and for your support with analysis. Thank you Maria Teresa for all your help with flow cytometry, and your patience while I tried to figure out the settings. Last but certainly not least, thank you Miriam Ries for single-handedly enriching my PhD experience outside of the lab, by bringing all the groups together with the weekly cake clubs, for organising get-togethers, and for bringing me into the Pint of Science team. You made it a much more enjoyable time that was not all about the work.

Thank you to Amar, Sander, Luca, Bahaa, Stefan, and Claudia for being so lovely, keeping me entertained during all this writing, and always keeping me supplied with matcha tea. To my family for your unending support and love, I could not have done it without you. Thank you for your patience in letting me moan, and for your encouragement to not let me quit. Hayat thanks for always checking in on me and helping me get through this writing. Dania, you were the best editor. Chachi, thanks for being there for me, and helping with the sources. Mama and Baba you guys are the best, from unending moral support and editing, to saving me from disaster when the computer crashed. I cannot express how much I love and appreciate everything you have done for me. I owe it all to you.

Abstract

Parkinson's disease (PD) is a chronic progressive neurodegenerative disorder characterised by selective loss of dopaminergic neurons in the substantia nigra. Drugs are the principal method of symptom treatment, yet remain unable to reverse underlying neurodegeneration. As PD prevalence increases with aging populations, greater emphasis falls on understanding pathogenesis to establish an effective neuroprotective strategy. Current research identifies iron accretion as a potential pathogenic factor.

Iron is crucial for healthy cellular physiology, however, dysregulation can be highly neurotoxic. Since iron cannot be excreted, levels must be tightly controlled via specific iron regulatory proteins (IRP), including hepcidin, transferrin receptors, divalent metal transporter 1, ferritin, ferroportin, aconitase 1, and iron response element-binding protein 2. Iron accumulation has been established in neurodegenerative diseases, including Alzheimer's, Multiple Sclerosis, and PD. While the instigating causes remain unknown, inflammation is a common factor. Activated microglia mediate the inflammatory response, and can release cytotoxic substances leading to iron-induced toxicity. Since dopaminergic neurons in PD are vulnerable to iron overload and inflammation, it is vital to determine what promotes changes to IRP expression leading to iron accumulation.

It is hypothesised that chronic microglial activation and ensuing pro-inflammatory factors can dysregulate neuronal iron. Such changes may result from alterations in key IRP gene expression, with downstream cascades leading to neuronal degeneration. Results herein provide evidence of microglial inflammatory factor involvement on neuronal iron metabolism in an *in vitro* model of dopaminergic neurons. Specifically, IL6, TNF and new evidence of hydrogen peroxide instigate significant alterations in expression of HAMP, TfR and DMT1, causing iron elevations. Co-culture experiments established astrocytic iron buffering mechanisms able to provide sufficient neuroprotection to abolish observed gene expression changes. Lastly, experiments conclude that neuronal death occurs mainly via apoptotic pathways. Collectively, results support the instigative role of inflammation on altering neuronal iron handling. Such discoveries could lead to potential improvements in therapeutic strategies for PD.

Investigating the Role of the Microglial Inflammatory Response on Iron Metabolism in Dopaminergic Neurons

List of Tables

Chapter One

Chapter Two

Chapter Three

List of Figures

Chapter One

Chapter Two

Chapter Three

Chapter Four

Chapter Five

Chapter Six

Chapter Seven

Chapter Eight

Chapter Nine

Abbreviations

6-OHDA	6-Hydroxydopamine
AAAD	Aromatic L-amino Acid Decarboxylase
Abb	Annexin-Binding Buffer
Aco1	Aconitase 1
ANOVA	Analysis of Variance
APS	Ammonium Persulfate
ßME	ß-mercaptoethanol
BSA	Bovine Serum Albumin
CD200R	CD200 Receptor
cDNA	Complementary DNA
CI	Complex I
CO_2	Carbon Dioxide
C_T	Threshold Cycle
c/w	Cells per well
DAT	Dopamine Transporter
DCytb	Duodenal Cytochrome b
dH_2O	Deionised water
DMEM	Dulbecco's Modified Eagle Medium (microglial growth medium)
DMSO	Dimethyl Sulfoxide
DMT1	Divalent Metal Transporter 1
DNA	Deoxyribonucleic Acid
E	Embryonic
ECL	Electrochemiluminescent
ELISA	Enzyme Linked Immunosorbent Assay
ETC	Electron Transport Chain
FAC	Ferric Ammonium Citrate
FAM	6-carboxyfluorescein
FBS	Foetal Bovine Serum
Fe	Iron
$FeCl_3$	Ferric Chloride
FtH1	Ferritin Heavy Chain
FPN	Ferroportin
Fxn	Frataxin
gDNA	Genomic DNA
GFAP	Glial Fibrillary Acidic Protein
GPx	Glutathione Peroxidase
GSH	Glutathione
H_2O_2	Hydrogen Peroxide
HAMP	Hepcidin
HBSS	Hank's Balanced Salt Solutions
HCl	Hydrochloric Acid
HCP-1	Haem Carrier Protein 1
HEX	Hexachlorofluorescein
HO-1	Haem Oxygenase 1
HRP	Horse Radish Peroxidase
Iba1	Ionised Calcium-Binding Adapter Molecule 1
IL	Interleukin
iNOS	inducible Nitric Oxide Synthase
IRE	Iron Responsive Element
IREB2	Iron Response Element-Binding Protein 2
IRP	Iron Regulatory Protein
ISC	Iron Sulphur Cluster
$KMnO_4$	Potassium Permanganate

Levodopa	Levo-dihydroxy-phenylalanine
LPS	Lipopolysaccharide
LRRK2	Leucine-Rich Repeat Kinase 2
M199	Medium 199 (astrocytic growth medium)
MAO	Monoamine Oxidase
MAOBI	Monoamine Oxidase Type B Inhibitor
MCM	Microglial Conditioned Medium
MHC	Major Histocompatibility Complex
MMP	Matrix Metalloproteinase
Mn-SOD	Manganese Superoxide Dismutase
MPTP	1-methyl-4-1,2,3,6-tetrahydropyridine
MSD	Mesoscale Discovery
mt	Mitochondrial
MT	MitoTracker
MTP	Mitochondrial Transmembrane Potential
MTS	(3-(4,5-dimethylthiazol-2-yl)-5-(3-carboxymethoxyphenyl)-2-(4-sulfophenyl)-2H-tetrazolium, inner salt)
N9	Microglial mouse cell line
N27	Dopaminergic neuronal rat cell line
NADH	Nicotinamide Adenine Dinuleotide (Reduced Form)
NADPH	Nicotinamide Adenine Dinucleotide Phosphate
NaOH	Sodium Hydroxide
NeuN	Neuronal Nuclei
NGS	Normal Goat Serum
NO	Nitric Oxide
Nox	NADPH Oxidase
NR	Neutral Red
NSAID	Nonsteroidal anti-inflammatory drug
$ONOO^-$	Peroxynitrite
OS	Oxidative Stress
PAGE	Polyacrylamide Gel Electrophoresis
PARK7	DJ-1
PBS	Phosphate Buffered Saline
PD	Parkinson's Disease
PES	Phenazine Ethosulfate
PFA	Paraformaldehyde
PI	Protease Inhibitors
PI	Propidium Iodide
PINK1	PTEN-Induced Putative Kinase 1
PRKN	Parkin
PS	Phosphatidylserine
PTP	Permeability Transition Pore
PVDF	Polyvinylidene Difluoride
qRT-PCR	Quantitative Real-Time Polymerase Chain Reaction
RIPA	Radio-Immunoprecipitation Assay
RNS	Reactive Nitrogen Species
ROS	Reactive Oxygen Species
RPMI	Roswell Park Memorial Institute (neuronal growth medium)
RT	Reverse Transcription
RTP	Room Temperature
RT-PCR	Reverse Transcription- Polymerase Chain Reaction
S	Sulphur
SDS	Sodium Dodecylsulphate
SEM	Standard Error Mean
SN	Substantia Nigra

SNCA	Alpa-Synuclein Gene
SNpc	Substantia Nigra pars compacta
SOD	Superoxide Dismutase
SOD1	Superoxide Dismutase 1
SPECT	Single Photon Emission Computed Tomography
TBS-T	Tris Buffered Saline- Tween20
TEMED	Tetramethylethylenediamine
Tf	Transferrin
TfR	Transferrin Receptor
TH	Tyrosine Hydroxylase
TNF	Tumour Necrosis Factor
Tf	Transferrin
TfR	Transferrin Receptor
UPS	Ubiquitin Protease System
UTR	Untranslated Region
wp	Well plate

CHAPTER 1:

Introduction

1. Introduction

1.1 Overview

Parkinson's disease (PD) is a chronic progressive disorder, and the second most prevalent neurodegenerative disease after Alzheimer's. With an increasing incidence over the age of 60, an aging population leaves greater risk of occurrence, which stresses the necessity for remedial discoveries. Current treatment is less curative and often includes detrimental long term side effects, with a limited focus on dopamine replacement therapy, rather than systemic hindrance of neurodegenerative progression. Recent evidence has placed emphasis on the role of oxidative stress and excess iron on neuronal demise. Iron accumulation has been established at sites of neuronal damage in several neurodegenerative disorders, and is believed to exacerbate already stressed conditions due its redox cycling abilities. Iron regulation occurs by homeostasis from several iron regulatory proteins, which are believed to be imbalanced during inflammatory situations. This introduction synopsises prevailing treatments, as well as symptomatological and pathophysiological evidence on PD. It will also evaluate current knowledge concerning inflammation and iron accumulation in the PD brain.

1.2 Parkinson's Disease

1.2.1 Background

Medical literature specifies ancient incidence of parkinsonian cases throughout history, including writings from Galen (~175 AD), Leonardo da Vinci (~1500), and Dutch scientist Franciscus Sylvius de la Boë (~1660) who helped distinguish between tremors during movement from those produced at rest (Calne, 1989; Raudino, 2012). In 1817, London surgeon James Parkinson famously published a patient case study entitled "An Essay on the Shaking Palsy", which provided a formal description of specific disease progression, and distinguished shaking palsy from old age and other confounding diseases (Parkinson, 2002). The term Parkinson's disease was coined several years later by French neurologist Jean Martin Charcot, who recognised James Parkinson's work and named the disease after him (Lees, 2007). Elaboration of parkinsonian clinical characteristics and neuropathology developed significantly in the following years, with increasing worldwide prevalence.

1.2.2 Epidemiology

Incidence of age-related neurodegenerative disease rises concomitantly with life expectancy. Recent advancements in medicine have led to aging global populations, and prevalence studies have determined significant projected increases in the number of PD patients. Current PD occurrence in the world's ten most highly populated countries lies around 4.2 million, which is expected to more than double to 8.67 million cases in the next 13 years (Dorsey, 2007; Elbaz, 2016). Analysis of worldwide PD prevalence data reveals lower disease presentation under the age of 50, but a significantly increasing frequency with age thereafter. Occurrence increases from 0.11% between ages 50-59 years up to 2% in patients over the age of 80 (von Campenhausen, 2005; de Lau, 2006; Pringsheim, 2014), with the mean age of disease onset currently at 65 years (Connolly, 2014). Medical advancements and technology have synchronously provided an increasing trend in age. As the older demographic increases, so would the incidence of neurodegenerative disease and its socio-economic encumbrance.

There are several non-genetic and environmental risk factors, however, many results are inconclusive. Geographic location is believed to have an effect, with a decreased prevalence observed in Asia compared to Europe, North America, and Australia (Pringsheim, 2014). Differences from race and ethnicity are confirmed, with highest incidence in Hispanics, followed in descending order by Caucasians, Asians, and Blacks (Van Den Eeden, 2003). It is postulated that gender may benefit females, as males between 50-59 years demonstrate increased prevalence of disease (male:134/100,000; females: 41/100,000) (Van Den Eeden,

2003; Pringsheim, 2014). Oestrogen has been shown to provide neuroprotective effects capable of delaying disease onset, and thus is speculated to account for the variation in gender (Gajjar, 2003). Iron is also implicated, as excess iron can have destructive consequences, and women are at greater risk of deficiencies (Haaxma, 2007). However, results remain inconclusive due to conflicting evidence (de Rijk, 1997). A possible correlation between increased dietary iron and greater PD risk has also been determined (Johnson, 1999), although contradictory evidence of no correlation was also found (Anderson, 1999). Environmental risks include farming, pesticide, welding and heavy metal exposure (Noyce, 2012). Dietary effects involve a greater PD risk from high dairy and saturated fat consumption (Johnson, 1999; Thacker, 2008). Controversy also lies in PD correlation to excessive head injuries, with studies showing conflicting results of either affirmed positive risk or no significant change in risk (Seidler, 1996; Fang, 2012). Conversely, smoking and coffee are consistently proven to diminish PD risk, with a potential neuroprotective role for nicotine and caffeine (de Lau, 2006; Noyce, 2012).

1.2.3 Familial Forms

Familial history of PD is a significant risk factor, accounting for an estimated 15% of PD cases, with relative risk higher for early disease onset (Thacker, 2008). The remaining majority of cases are idiopathic, with a generally later disease onset. Autosomal dominant or recessive mutations may occur in several different genes, respectively including Leucine-rich repeat kinase 2 (LRRK2) and α-synuclein (SNCA), as well as recessive DJ-1 (PARK7), parkin (PRKN), and PTEN-induced putative kinase 1 (PINK1), amongst others (Table 1.1).

Cellular function of LRRK2 and SNCA remain largely unknown, although the former's mutations account for more than 50% of cases, varying by ethnicity (Nuytemans, 2010). PARK7 serves as a hydrogen peroxide (H_2O_2)-triggered oxidative stress (OS) sensor and antioxidant against dopamine toxicity (Mitsumoto, 2001; Lev, 2009). Loss of function can lead to unregulated H_2O_2 accumulation. PRKN is an ubiquitin ligase with a role in the ubiquitin proteasome system (UPS) of protein degradation, functioning by triggering impaired mitochondria for mitophagy (Zheng, 2013). Loss of function can result in accumulation of dysfunctional proteins and cellular debris that would affect physiological functioning. PINK1 is a mitochondrial kinase that is imported into healthy mitochondria for degradation (Zheng, 2013). Damaged mitochondria allow only partial PINK1 entrance, leaving an external domain to activate and recruit PRKN for mitophagy. Compromised mitochondrial function, and persistence of damaged mitochondria would cause reductions in energy production and

significantly augmented levels of damaging free radicals. Cumulative analysis of known PD mutations points to an essential role of OS and loss of mitochondrial function.

Table 1.1 Gene Mutations Instigating Familial Parkinson's Disease
Some of the common gene mutations found to cause familial PD, their mode of inheritance, and age of onset. Gene mutations associated with mitochondrial dysfunction can lead to energy depletion, deficient Complex I activity, and increased formation of reactive oxygen species, which in turn feeds further mitochondrial dysfunction. (Adapted from Dexter, 2013). *Abbreviations: OS=oxidative stress, ROS=reactive oxidative species.*

Gene	Locus	Mode of Inheritance	Age of onset (years)	Mode of Mutational Action to Trigger PD
LRRK2	PARK8	Autosomal Dominant	32-79	Induces Apoptosis
SNCA	PARK1/4	Autosomal Dominant	20-85	α-synuclein Misfolding
DJ1	PARK7	Autosomal Recessive	20-40	Loss of H_2O_2/ROS Scavenger Activity Loss of Protection from OS
PRKN	PARK2	Autosomal Recessive	16-72	Ubiquitin & Mitochondrial Dysfunction
PINK1	PARK6	Autosomal Recessive	20-40	Mitochondrial Dysfunction

1.3 Clinical Symptoms

1.3.1 Motor

Chronic debilitating symptoms of PD can negatively affect patient quality of life. The major PD clinical motor symptoms cause a loss of fine motor skills and include postural instability, tremor at rest, rigidity and bradykinesia. The first feature may be defined as impaired balance, which occurs at later stages causing patients to have a greater fall risk. It is difficult to treat, and thus may be particularly disabling (Grimbergen, 2009). Resting tremors consist of uncontrolled movements resulting in shaking of limbs whilst relaxed, but which subside during voluntary movement or sleep (Pallis, 1971). Rigidity includes stiffness, jerking and heavy limbs, which may cause patient suffering when co-presenting with bradykinesia. Bradykinesia is demarcated by slow movement, and impairments in initiating both voluntary and involuntary movement. Early disease stages typically demonstrate unilateral symptom occurrence, which can spread to bilateral limbs with time. Slower reaction speeds may progress to involuntary manifestations, such as dysphagia, which can have significant choking complications in the elderly when combined with disintegrated mastication and lingual movement (Leopold, 1996; Wang, 2002).

1.3.2 Non-motor

Non-motor symptoms may develop prior to motor symptoms, or occur concurrently with disease progression. A major symptom is development of cognitive decline, with relative risk falling between 1.7-5.9% (Elbaz, 2016). There are various other PD symptoms, including psychosis, depression, cognitive dysfunction, dysregulation of sleep cycles, constipation, and anosmia (Table 1.2) (Chaudhuri, 2006). Disease advancement can escalate presentation of these symptoms, causing considerable patient impairment and decreased quality of life.

Table 1.2 Non-Motor Symptoms in Parkinson's Disease
List of non-motor symptoms exhibited in PD patients at various stages of disease, separated into four categories of neuropsychiatric disorders, sleep dysfunction, autonomic problems and gastrointestinal difficulties (Chaudhuri, 2006). *Abbreviations: REM= Rapid Eye Movement.*

Neuropsychiatric	Sleep Dysfunction	Autonomic	Gastrointestinal
Depression & Anxiety	Restless Legs	Incontinence	Ageusia
Attention Deficits	REM sleep disorder	Bladder Problems	Dyshpagia
Hallucinations & Delusions	Non-REM sleep disorders	Orthostatic Hypotension	Choking
Dementia	Insomnia	Profuse Sweating	Reflux
Obsessive & Compulsive Behaviours	Daytime Somnolence	Sexual Dysfunctions	Nausea
Panic Attacks	Intense Dreams	Erectile Impotence	Constipation
Confusion	Inspiration & Expiration Difficulties While Sleeping	Xerostomia	Faecal Incontinence

1.3.3 Pathology

Parkinson's pathology commences prior to observable symptoms, with degeneration already at significant levels by onset of motor deficits due to physiological compensatory regulations (Thacker, 2008). The basal ganglia consist of a collection of related subcortical nuclei involved in motor control and movement selection (Kravitz, 2010). Dopamine or 2-(3,4-dihydroxyphenyl)ethylamine (DA) is member of the catecholamine family of neurotransmitters, mostly concentrated within the striatum, and produced by nigrostriatal dopaminergic neurons (Herlinger, 1995). Dopaminergic neuron somas within the substantia nigra pars compacta (SNpc) form the nigrostriatal pathway with their axons projecting up to the corpus striatum for dopamine release (Tieu, 2003). The dopaminergic system appears to maintain a principal role in modulating voluntary movement (Hermida-Ameijeiras, 2004). Post-mortem studies have determined that PD is a progressive neurodegenerative disorder pathologically typified by a chronic, selective degeneration of nigrostriatal dopaminergic neurons, with a subsequent diminution in dopamine concentrations and neurotransmission (Wills, 2010). Neuropathological studies indicate an upward moving disease progression from the dorsal IX/X motor nucleus or intermediate reticular zone towards the cerebral cortex (Braak, 2003) (Figure 1.1). Nigrostriatal projections control initiation of movement, hence PD degeneration translates to the clinical loss of control. Fading nigrostriatal dopamine levels eventually manifest as disruptions in motor control and observed non-motor symptoms. Melanin-containing dopaminergic neurons within the mesencephalic SNpc are affected most, with neuronal degeneration and reduction of melanin resulting in pathological depigmentation.

Presynaptic α-synuclein protein aggregation into spherical perikaryal Lewy body formations or spindle-like Lewy neurites within diseased and dying neurons is a pathological hallmark of disease (Baba, 1998). It has been postulated that Lewy bodies demarcate dying neurons, however do not directly affect cell degeneration (Schulz-Schaeffer, 2010). The precise reason for protein aggregation remains to be determined, however, overexpression of α-synuclein in PD and mutations in the SNCA gene point to significant connotations with disease. Excessive α-synuclein aggregates can disrupt membrane permeability and cause mitochondrial dysfunction, which ultimately leads to neurotoxic production of reactive oxygen species (ROS) (Schulz-Schaeffer, 2010). Protein accumulation at the presynaptic membrane may also interfere with dopamine release, causing further functional disruption. Other pathophysiological signs include inflammation, increased OS, and diminished mitochondrial function. When combined, these features can lead to irreversible dopaminergic neuron degeneration.

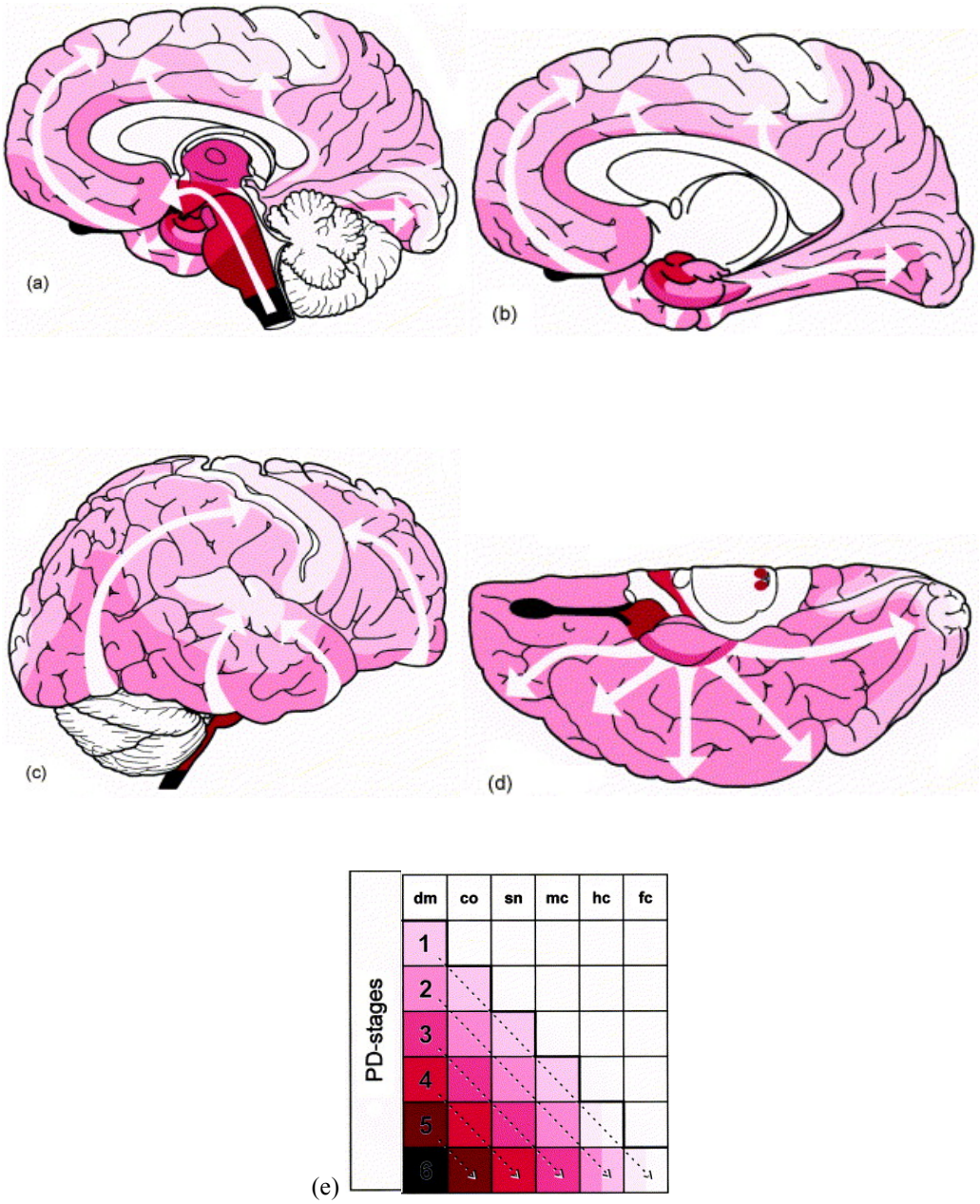

Figure 1.1 Braak Stages Showing Intraneuronal Progression of PD Pathology

These images represent the subcortical and cortical progression of PD brain pathology and α-synuclein expansion seen from different views (a-d) as developed by Braak (2003). The simplified diagram (e) represents a topographical development of PD lesion progression, traveling from left to right and progressing from top to bottom. The increasing shading intensity represents increasing disease severity, with lighter colours characterising less pathology, while darker colours portray more severe pathology. White arrows represent course of disease pathology. *(Image adapted from Braak, 2003). Abbreviations: co=coeruleus-subcoeruleus complex, dm=dorsal motor nucleus of the glossopharyngeal and vagal nerves, fc=first order sensory association areas, premotor areas and primary sensory and motor fields, hc=high order sensory association areas and prefrontal fields, sn=substantia nigra, mc=temporal mesocortex.*

1.3.4 Diagnosis

Definitive PD diagnoses remain elusive due to varying rates of individual disease progression and lack of conclusive evidence until pathological determination of nigral Lewy body inclusions at autopsy. Instead, current assessment relies on patient history, environmental and genetic risk factors, non-motor symptoms, as well as clinical presentation of at least two of the major motor symptoms, providing a diagnostic accuracy between 76-98% (Hughes, 1992). Several clinical diagnostic criteria exist, such as that recently posited as the Movement Disorder Society Clinical Diagnostic Criteria for Parkinson's Disease. These criteria for clinically established PD require the necessary criterion of presentation with parkinsonism, followed by two or more supportive criteria, and simultaneous lack of any exclusion criteria or red flags (Table 1.3) (Postuma, 2015). While PD remains the principal source of parkinsonism symptoms, they may still be attributed to diseases other than Parkinson's. Thus, exclusion of these factors via application of diagnostic criteria is necessary to establish a definitive PD diagnoses.

Research into superior diagnostic tools at earlier stages of disease has recently provided new methods. Improved technology has added functional imaging as another method of preclinical assessment providing support to any potential PD diagnosis. While there are several methods, the most specificity for confirmed PD diagnoses is determination of presynaptic dopamine transporters (DAT) via single photon emission computed tomography (SPECT) (Antonini, 2004). This method is able to identify abnormalities in striatal dopamine at earlier stages of disease progression, which is useful for clinical confirmation of disease (Brooks, 2010). Olfactory screening is one of the more recent forms of preclinical assessment in neurodegenerative diseases, where patients exhibit anosmia from a loss of olfactory processing (Haehner, 2007; Iannilli, 2017).

Table 1.3 Movement Disorder Society Clinical Diagnostic Criteria for Established Parkinson's Disease
Clinical diagnostic criteria to determine established PD (Postuma, 2015). Clinically established PD requires establishment of parkinsonism, along with two or more supportive criteria, plus absence of any exclusion criteria or red flags.

- 1st necessary criterion: Parkinsonism diagnosis, including bradykinesia + at least one of rest tremor or rigidity

Supportive Criteria

- Positive reaction to dopaminergic supplementation therapy
- Development of Levodopa-stimulated dyskinesia
- Rest tremor of one or more limbs
- Manifestation of anosmia or cardiac sympathetic denervation

Exclusion Criteria

- Cerebellar abnormalities
- Downward vertical supranuclear gaze palsy
- Either frontotemporal dementia or aphasia
- Selectively lower limb parkinsonism
- Drug-induced parkinsonism
- Deficiency in response to levodopa treatment
- Cortical sensory loss
- Normal presynaptic dopaminergic imaging
- Concomitant condition able to instigate parkinsonism

Red Flags

- Quick advancement of postural impairments
- Lack of motor symptom progression
- Presentation of severe dysphonia, dysarthria, or dysphagia
- Breathing dysfunction
- Autonomic failure, including orthostatic hypotension or urinary difficulties
- Repeated falls
- Intense extremity contractures
- Lack of common PD non-motor factors
- Pyramidal tract difficulties
- Bilateral parkinsonism

1.4 Treatment

1.4.1 Pharmacotherapy

Absence of effective neuroprotective strategies to slow or reverse disease progression means PD remains an incurable disease. However, certain therapeutic treatments are available to manage symptoms and improve patient quality of life. Since the principal neuropathological outcome of PD involves degeneration of nigrostriatal dopaminergic neurons and a concomitant neurochemical reduction in the dopamine neurotransmitter, the leading form of pharmacotherapy involves replacement of dopamine. Medication is administered from onset of functional impairment, and differs according to the individual symptoms. Medical administration of dopamine would be ineffective due to its inability to cross the blood brain barrier (BBB), so instead the dopamine precursor levo-dihydroxy-phenylalanine (Levodopa) is prescribed.

Levodopa is able to cross into the central nervous system where it can be metabolised into dopamine in the presence of aromatic L-amino acid decarboxylase (AAAD) enzymes. This replacement therapy is effective at alleviating symptoms, including motor deficits, sleeping difficulties, fatigue and hallucinations, and thus remains the standard form of treatment (Martinez-Ramirez, 2016). However, levodopa administration results in only an estimated 1% crossing into the brain from AAAD metabolism occurring in the periphery, so co-administration with an inhibitor is common (Martinez-Ramirez, 2016). Eventual inception of drug-induced debilitating dyskinesias occurs in 30-50% of patients after about 3-5 years (Fahn, 2004). Levodopa is regularly co-administered with AAAD inhibitors, such as Benserazide or Carbidopa, to avoid peripheral levodopa conversion to dopamine and to increase bioavailability in the brain (Nutt, 1985). Individualised therapy modifies dosages to improve relief from symptoms with simultaneous minimisation of drug-induced dyskinesias. Correlations have been drawn between greater levodopa dosage and worsened motor symptoms, so prescriptions may be reduced with adjuvant therapies or alternative monotherapies at earlier stages of disease (Cereda, 2017). These may include monoamine oxidase type B (MAOB) inhibitors (MAOBI), such as selegiline, dopamine agonists, such as pramipexole, or surgical techniques. MAOB enzymes catalyse the breakdown of dopamine into its metabolites, so MAOBIs inhibit MAOB activity, thereby augmenting synaptic dopamine bioavailability (Cereda, 2017). Dopamine agonists act upon postsynaptic dopaminergic receptors to mimic the actions of striatal dopamine, and have shown efficacy as a monotherapy relief in early PD or as a later stage supplement to levodopa (Bennett, 1999; Pinter, 1999). Deep brain stimulation is the most common surgical therapy, whereby stimulation of the subthalamic nuclei situated adjacent to

the SNpc, leads to significant reductions in motor dysfunction and improved quality of life (Obeso, 2001; Weaver, 2009).

Treatment of non-motor symptoms is also an essential aspect of PD therapy, as occurrence may begin at earlier stages of disease, and they significantly affect patient quality of life. While dementia and cognitive impairments currently remain incurable, pharmacotherapy may ease symptoms (Martinez-Ramirez, 2016). Antidepressants, antipsychotics and antianxiety medications may also be administered, while there are also treatments available for gastrointestinal difficulties, sleeping abnormalities, orthostatic hypotension, and sexual dysfunction. As PD prevalence increases with an aging population, greater emphasis falls on understanding disease pathogenesis in order to establish more effective neuroprotective strategies and more curative treatments.

1.5 Pathogenesis

1.5.1 Proteopathy: α-synuclein and Lewy Bodies

PD is typically characterised as a movement disorder due to diminishing dopamine neurotransmitter levels from loss of dopaminergic neurons in the SNpc, which results in a fading pigmentation of neuromelanin within the SNpc. Yet another distinguishing feature of sporadic PD involves Lewy body (LB) intraneuronal inclusions, consisting of abnormal α-synuclein protein aggregates which disrupt normal cellular functioning, and are found in other forms of neurodegeneration such as dementia with Lewy bodies or familial Alzheimer's disease (Revesz, 1997; Lippa, 1998; Kotzbauer, 2001). Under physiological conditions, the soluble presynaptic α-synuclein protein has a role in neurotransmission regulation, however, mutations result in its conformation to insoluble fibrils that can accumulate to form LBs (Goedert, 2001). Aggregation of such LB inclusions can begin to hinder other cellular function, binding mitochondrial membranes and disrupting cellular respiration, and since α-synuclein-containing LBs are present in both idiopathic and familial PD, it insinuates a pathogenic role in PD (Nakamura, 2011; Mullin, 2013). This eventually results in a loss of neuronal viability (Lippa, 1998), with α-synuclein directly proportional to increased toxicity in cultured neurons (Nakamura, 2011), and thus contributes to progression of Parkinson's neurodegeneration.

1.5.2 Oxidative Stress and Mitochondrial Dysfunction

OS is the consequence of a pro-oxidant environment, rich in reactive oxygen species (ROS), accompanied by insufficient antioxidant levels and impaired damage repair, resulting in an imbalanced oxidant build-up from deficient cellular ROS clearance. Persistent OS can eventually lead to loss of cell viability, as reactive species are able to inflict damage to lipid membranes, proteins, and DNA modifications (Zhou, 2008). Several different PD models are implemented to elicit an inflammatory response leading to neurodegenerative demise of dopaminergic neurons, including 1-methyl-4-phenyl-1,2,3,6-tetrahydropyridine (MPTP), rotenone, and 6-hydroxydomaine (6-OHDA). While each neurotoxin provokes degenerative cascades via independent means, the triggering mechanism of cell death is via OS (Niranjan, 2014). This insinuates a significant role of OS in induction of parkinsonian degeneration.

Neurons have proportionately high metabolic needs to maintain neurotransmission supplies, requiring copious oxygen consumption and ATP production to satisfy their great demand (Kann, 2006). While the brain makes up an average of only 2% body weight, it takes up 20% of the body's total oxygen levels, thus having a greater rate of oxidative metabolism than any other organ, and a concomitant amplified ROS production (Dringen, 2000). These

high energy requirements are met by mitochondrial oxidative metabolism. Yet, mitochondria remain the principal generators of free radicals and oxidative species, which are by-products of cellular respiration from oxygen handling in the electron transport chain during respiration (Niranjan, 2014). The first electron transfer to oxygen results in formation of the superoxide radical, while a second electron acceptance forms H_2O_2, a third results in the highly damaging hydroxyl radical, and a fourth creates a water molecule (Jesberger, 1991). Free radicals are atoms containing one or more free unpaired electrons in its outer orbit, making it highly reactive (Jesberger, 1991). Oxygen free radicals form during aerobic metabolism, and comprise of any chemical enclosed by an outer orbital shell with an oxygen atom and free electron (Ikeda, 1990). The greatest sources of oxygen free radical production include cellular oxidation by the mitochondrial electron transport chain, and catecholamine auto-oxidation. As neurons require copious amounts of energy, and dopamine is a catecholamine, this places dopaminergic neurons at greater risk of free radical-mediated OS. Under physiological conditions, the mitochondrial antioxidant arsenal is able to detoxify excess ROS levels, and prevent toxic oxidant concentrations (Zhou, 2008). However, mitochondrial defects and disruption to the electron transport chain would rapidly augment free radical production, and in turn, escalate OS, and overwhelm the protective antioxidant system. Such dependency on efficient mitochondrial functioning means that any mitochondrial dysfunction is met with substantial deleterious consequences, leaving neuronal populations vulnerable to high oxidant exposure. Nigral dopaminergic neurons have proven to be particularly susceptible to degenerative effects of OS, due to their greater exposure to reactive oxygen species compared with other neuronal populations. Auto-oxidation and enzymatic deamination of dopamine specifically exposes them to additional reactive species in the form of hydrogen peroxide (H_2O_2). During PD pathogenesis, as dopaminergic neurons begin to die, a compensatory increase in dopamine turnover exposes these neurons to an overabundance of H_2O_2. While excess H_2O_2 can be converted into water with the help of glutathione reduction, these antioxidant concentrations are naturally low within the SN, but further reduced in PD (Sian, 1994; Sofic, 1992). Additionally, a high oxidant environment can interact with RNS and labile intracellular iron, producing highly reactive and damaging oxidant species capable of oxidising lipid membranes and contributing to cell death (Alvarez, 1995). This serves to ensure that dopaminergic neuronal populations remain highly susceptible to OS.

Free radicals are produced exponentially, so that very high antioxidant levels would be required in order to successfully neutralise a state of OS (Demopoulos, 1982). Antioxidants serve as a biological defence against radical-mediated cellular damage, functioning by

deactivating free radicals to prevent their accumulation from reaching noxious levels (Valko, 2004). If chronic OS were to arise and override the levels of available antioxidants, the pathophysiology of oxidant toxicity occurs via several mechanisms. Unpaired electrons are extremely volatile, able to react with different substances such as proteins, lipids and nucleic acids, thereby disrupting cellular processes (Jesberger, 1991). Phospholipid cell membranes are comprised of polyunsaturated fatty acids, which are highly vulnerable to destruction by ROS as radicals react with them to remove electrons (Zhou, 2008). Oxidative degradation of these lipid membranes, otherwise known as lipid peroxidation, damages cellular membranes, and eventually affects cell viability (Mishra, 1990). Products of lipid peroxidation, such as reactive aldehydes, are free radicals themselves that can add to cell damage. They have been shown to have an autocatalytic cascading effect reacting with neighbouring lipids to mediate further damage to neuronal membranes, resulting in distorted membrane utility and eventual neurodegeneration (Mark, 1997). Additionally, neuronal lysosomal membranes may also break down as a result of exposure to ROS such as the hydroxyl radical (OH^*), which would cause release of harmful lysosomal hydrolytic enzymes (Fong, 1973). Release of iron from ferritin storage may also occur via lysosomal proteolysis, which adds another source of iron during already toxic conditions of OS (Kidane, 2006). ROS can also induce structural alterations to amino acids and proteins, with phenylalanine, tyrosine and cysteine being particularly sensitive to oxidant damage (Jesberger, 1991). In terms of Parkinson's pathology, phenylalanine is the precursor for tyrosine, while tyrosine is a crucial element in dopamine synthesis. Cysteine is a source of sulphur for scaffolding of iron-sulphur clusters, as is present in the IRP1 homologous protein cytosolic aconitase (Bandyopadhyay, 2008; Liu, 2010). If free radicals such as OH^* reach nuclear DNA, they are able to elicit strand breaks (Valko, 2004). Continuous free radical exposure and limited neuronal defences result in their significant contribution to neuronal degeneration in various conditions and neurodegenerative diseases. Any disruptions to mitochondrial functioning could increase free radical production, while simultaneously causing metabolic inhibition, both which would have devastating consequences on neuronal viability.

Mitochondrial defects were first implicated in PD with the discovery that exposure to the prodrug MPTP resulted in parkinsonism (Langston, 1983). The MPTP metabolite MPP^+ inhibits mitochondrial activity of Complex I (CI), which would augment free radical production and disrupt mitochondrial function via compromised electron transport (Nakamura, 2011). It is postulated that dopaminergic neurons are particularly sensitive to loss of CI function, as evidenced by rotenone treatment. Rotenone selectively impedes CNS CI activity,

however, toxicity is reserved solely for the dopaminergic neurons (Sherer, 2003). Similarly, genetic mutations in familial PD cases, such as in PINK1 or SNCA, directly involve mitochondria (Lin, 2006). Thus, mitochondrial dysfunction in PD, with a concurrent rise in OS within overly-sensitive dopaminergic neurons, may play a significant injurious role in the neurodegenerative cascade. In the presence of labile intracellular iron, this can have disastrous consequences on physiological cellular functioning.

1.5.3 Iron

1.5.3.1 Cellular Iron

Iron is an essential element, with numerous functions crucial for physiological cellular functioning. Roles include acting as haem cofactor for oxygen transport via haemoglobin, acting as cofactor for various enzymes including tyrosine hydroxylase (Zecca, 2004), synthesis of DNA and iron proteins, ATP generation in mitochondrial electron transport (Zucca, 2017), formation of iron-sulphur clusters, participation in redox cycling (Winterbourn, 1995; Moos, 2000), myelin synthesis, and involvement in dopamine, serotonin and catecholamine neurotransmitter synthesis (Beard, 1993). Iron incidence is additionally involved in transcriptional and translational control of certain protein expression, such as transferrin receptors, hepcidin or ferritin (Dayani, 2004). Uptake of iron into the brain first occurs during development as non-transferrin bound iron may enter prior to full formation of the blood brain barrier (Hare, 2013). Thereafter, iron uptake decelerates, with a slower, more controlled accumulation occurring instead by transferrin receptor-mediated endocytosis across the blood brain barrier via TfR1 on capillary endothelial cell luminal membranes (Jefferies, 1984; Rouault, 2006). This physical barrier carefully regulates nutrient entry of molecules such as iron, ensuring that any peripheral changes are not necessarily reflected in the brain (Ward, 2014). Upon entering endothelial cells, transferrin is recycled back to the blood, and iron is able to be transported throughout the central nervous system (Moos, 2000). Brain iron levels reach high concentrations at birth, followed by descending concentrations for the following two postnatal weeks, then increasing concentrations thereafter until death (Höck, 1975). SNpc iron measures about 20ng/mg for the first year, escalating to 200ng/mg by old age (Zecca, 2001). Studies support these correlations, consistently proving that healthy brains demonstrate age-induced amplifications to iron levels within specific regions (Bartzokis, 1997; Xu, 2008; Adisetiyo, 2012).

The body maintains a total iron concentration between 3-4g, most of which is used in bone marrow for red blood cell production (Kohgo, 2008). It is predominantly found in haemoglobin, as well as in myoglobin, enzymes, iron-sulphur clusters, and in iron transport

and storage proteins (Zucca, 2017). Iron does not have a mechanism for excretion from the body, instead upon phagocytosis of expired cells, iron is released by macrophages for recycling (Rhodes, 2008). The only loss of iron occurs from sloughing of skin cells or intestinal epithelial cells, or via bleeding, which is why women tend to have lower iron levels than men (Soldin, 2004). Iron levels are replenished by absorption of dietary intake at intestinal duodenal enterocytes (Belaidi, 2016). There are two types of iron: haem and non-haem. Haem iron is derived from meats, with absorption carried out by the haem carrier protein (HCP1). Once in the cytosol, haem is broken down by haem oxygenase 1 (HO-1) to release ferrous iron (Kohgo, 2008; Belaidi, 2016). Non-haem iron mostly consists of ferric iron originating from plants, with absorption occurring by duodenal cytochrome b (DCytb) reduction to ferrous iron, followed by passage across the apical membrane by divalent metal transporter (DMT1) (Belaidi, 2016). Once in the cytosol, this ferrous iron comprises the labile iron pool (LIP), which contains chelatable redox-active iron (Zucca, 2017). Ferrous iron may remain in the LIP for immediate use in various cellular functions, or may either be exported to other cells for use, or oxidised for storage in an unreactive form. The brain requires essential provision of iron like all organs, so iron transport across the blood brain barrier is critical to maintaining healthy function. For example, iron deficiency in human infants between 3-16 months can lead to incomplete development, deficits in both cognition and behaviour, hypomyelination, and deficits to neurotransmitter synthesis and auditory function (Roncagliolo, 1998; Shankar, 2000; Bear, 2003). Function failed to regularise even after iron supplementation, suggesting a critical iron requirement in the CNS during brain development (Roncagliolo, 1998). This irreversible deficiency was also established in animal studies within the timeframe of 7-25 days in severely iron-deficient postnatal rats, which also exhibited incomplete restoration of iron in certain brain regions, even with supplementary iron repletion (Dallman, 1975; Piñero, 2000). Animal models with dietary iron insufficiency also presented with reduced nigrostriatal dopaminergic neuron transmission, leading to irreversible cognitive deficits such as defective learning capabilities (Youdim, 1989). These results point to the importance of adequate iron provision during brain development. While sufficient iron concentrations are vital, excess iron can prove highly neurotoxic, so it must be carefully controlled by iron regulatory proteins to maintain a constant state of iron homeostasis.

1.5.3.2 Iron Regulatory Proteins

Since iron is one of the only elements unable to be passively excreted from the body, homeostatic levels are very carefully regulated via a highly coordinated system of iron regulatory proteins (IRP) to ensure balanced iron transport for provision of biochemical processes, whilst maintaining low concentrations of reactive free iron (Gerlach, 1994). Hepatic iron regulation is well defined, with a similar system believed to occur in the brain (Figure 1.2). Ferric iron attaches to the bilobal blood plasma glycoprotein transferrin (Tf), containing two homologous high-affinity ferric iron binding domains, each containing one Fe^{3+}-binding site (Berg, 2001). Following binding of 2 ferric atoms, the empty apotransferrin is transformed to holotransferrin. Affinity to iron is pH dependent, with high affinity in plasma pH (~7.4), and very low affinity at a more acidic pH ($\leq$ 4.5). Iron saturation of plasma transferrin is about 33%, leaving a significant percentage available for rapid iron uptake during conditions of iron overload in avoidance of iron-mediated toxicity (Ponka, 1999). Transferrin functions to chelate iron and prevent free plasma iron-mediated toxicity, as well as to facilitate iron transport to sites for absorption, utilisation, and storage (Ponka, 1999). Upon formation, the Fe^{3+}-transferrin complex is able to bind transmembrane glycoprotein transferrin receptors (TfR) that allow for cellular iron acquisition.

Transferrin receptors maintain a role in cellular iron regulation, as expression directly affects the amount of iron imported into cells. The affinity of transferrin for the receptors increases with iron saturation, with apotransferrin having lowest affinity, and diferric transferrin having the greatest, so that the majority of iron delivered to cells is from diferric transferrin (Young, 1984). This diferricTf-TfR complex is then internalised by receptor-mediated endocytosis via clathrin-coated pits (Mousavi, 2004). The endocytic vesicles have a lower pH, whereby acidification lowers the affinity of ferric iron for Tf, releasing it into the endosome. Situated on the apical membrane is a proton-coupled ferrous iron transporter, known as divalent metal ion transporter (DMT1), and an endosomal ferrireductase DCytb (Rouault, 2006). As DMT1 can only transport ferrous iron, released ferric ions are crucially reduced by DCytb to allow movement of iron into the cellular cytosol. Upon completion, the apotransferrin-TfR complex is recycled back to the cell membrane. The ferrous iron can then join the labile iron pool for cellular utilisation, or the majority travels to the mitochondria for direct use in processes such as haem synthesis or iron sulphur cluster (ISC) biogenesis and assembly (Pandey, 2015). Mitochondrial ISC assembly occurs by sulphur mobilisation from cysteine, and transference to a scaffolding protein with iron to complete the ISC structure (Pandey, 2015). Mitochondria play a role in iron regulation, whereby their production of iron sulphur clusters is monitored.

Any defects to ISC biosynthesis and failed assembly, as may occur from cysteine sensitivity to OS-mediated damage, can trigger the cytosolic iron-responsive transcription factor Aft1 to induce transcriptional regulation for increased cellular iron acquisition (Banerjee, 2007; Lill, 2012). Alternatively, ferric iron can be transferred in a non-reactive bioavailable form for long-term storage in ferritin molecules.

Ferritin, an intracellular iron storage molecule, oxidises iron via ferroxidase activity to store it in a nonreactive ferric form as hydrous ferric oxide (Miyazaki, 2002). This prevents iron-mediated toxicity and allows for controlled release whenever iron is required for mitochondrial haem synthesis or export. Ferritin is mostly cytosolic, but low levels are found in serum. The protein is comprised of 24 subunits forming a hollow core nanocage. Ferritin is able to bind up to 4500 ferric iron atoms, however, leaves a significant buffer for situations of toxic iron overload by generally only using up about 20% (Samokyszyn, 1988). There are two main subunits: heavy (H)-chain and light (L)-chain. H-ferritin, more prevalent in neurons, is used for fast access to iron and less long-term storage, with an iron oxidation site to help oxidise iron for storage, while L-ferritin is for long-term storage and more prevalent in glia (Miyazaki, 2002). The brain expresses the greatest ferritin levels of any organ after the liver (Dayani, 2004), substantiating the importance of a sufficient iron reserve for efficient brain functioning. Iron mobilisation from ferritin storage may occur via reduction to ferrous iron (Dognin, 1975; Funk, 1985) by reductants including superoxide (Samokyszyn, 1988), otherwise permanent mobilisation depends on cytosolic iron concentrations. This process entails either cytosolic proteasomal degradation, where iron has been released from ferritin and the nanocage becomes tagged for ubiquitin-mediated proteasomal degradation, or total lysosomal degradation occurs during high stress conditions (Kidane, 2006). Alternatively, haemosiderin is another cellular iron storage protein, storing unreactive ferric iron in a form that is not easily accessible (Quintana, 2006). Haemosiderin has a similar composition to ferritin, formed as a product of ferritin degradation, and is upregulated during haemorrhage and iron overload conditions (Ward, 2000). If iron is not stored, it may also be exported out of the cell.

Ferroportin (FPN) serves as the primary iron exporter of ferrous iron. FPN expression leads to reduced cellular iron, including release of ferritin iron via proteasomal activity (Nemeth, 2004). Once ferrous iron is released by FPN, the membrane-bound or plasma copper-dependent glycoprotein ceruloplasmin with ferroxidase activity is able to oxidise it into ferric iron to allow for subsequent binding with plasma apotransferrin (Patel, 1997; Xu, 2004). Ceruloplasmin is homologous to intestinal hephaestin. During high iron conditions, the regulatory peptide hormone hepcidin is upregulated. Hepcidin binds FPN on the apical plasma membrane,

resulting in FPN internalisation and degradation. This cellular iron sequestration additionally diminishes serum iron (Rouault, 2006). Thus, by affecting iron egress, hepcidin is able to control both cellular and plasma iron levels. Transferrin saturation functions as an indicator of systemic iron, with diferric Tf able to affect hepcidin expression (Muckenthaler, 2008). Inflammation (Ganz, 2003) IL6, and iron overload (Ilyin, 2003) are able to induce hepcidin expression, causing ferroportin internalisation, and leading to hypoferremia of inflammation, while hypoxia, iron deficiency and anaemia decrease expression (Nemeth, 2004). While hepcidin is able to shift iron from overloaded plasma by sequestration into cells, if not carefully monitored, the enhanced iron retention can initiate the damaging cascade of iron-catalysed OS.

A homologous pair of iron-sensing iron regulatory proteins (IRP1 and IRP2) exist within the cytoplasm. They maintain a post-transcriptional control of gene expression for proteins related to iron regulation, such as TfR, ferritin and DMT1. IRP1 is able to detect iron concentrations via its reversible conversion from IRP1 to cytosolic aconitase (Aco1) with addition of an iron-sulphur [4Fe-4S] cluster (ISC). Disassembly of this ISC is triggered by low iron levels (Brand, 2004). IRP2 (also IREb2) loses function and is targeted for proteasomal degradation in iron-replete cells. These IRP proteins function as part of a regulatory system of post-transcriptional iron regulatory control that involves iron responsive elements.

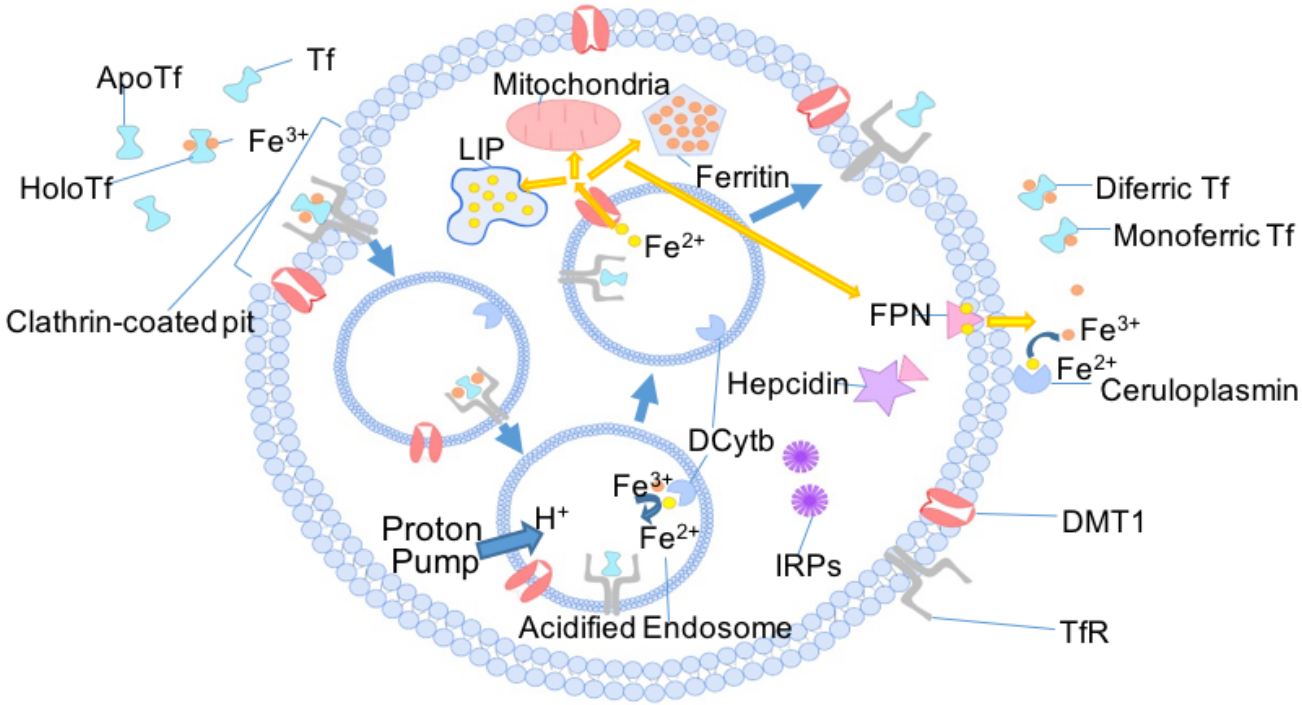

Figure 1.2 Proteins Involved in Iron Regulation
This schematic representation of iron regulatory proteins exemplifies a model of non-haem iron regulation in the periphery. It is thought to also characterise that in the central nervous system. Free ferric iron attaches to the blood plasma glycoprotein transferrin (Tf). Two ferric ions (Fe^{3+}) bind Tf, which gains high affinity for transferrin receptors (TfR). Upon TfR binding, the diferric holotransferrin enters the cell by receptor-mediated endocytosis in clathrin-coated pits. Proton pumps lower endosomal pH, removing ferric affinity for transferrin. The released ferric ions are reduced to ferrous iron (Fe^{2+}) by an endosomal ferrireductase duodenal cytochrome b (DCytb), whereby the divalent metal transporter (DMT1) is then able to transport the ferrous iron through the endosomal membrane into the cytosol. From there, ferrous iron either enters the transit labile iron pool (LIP) for contribution to cellular processes, or enters mitochondria for use in processes such as ISC biosynthesis. Alternatively, it may be stored in a non-reactive bioavailable form within ferritin storage proteins, or exported out of the cell via ferroportin (FPN), whereupon the plasma or membrane-bound ceruloplasmin ferroxidase oxidises exported iron to allow for its subsequent chelation by plasma transferrin. The apotransferrin (apoTf) is recycled back to the plasma membrane, where reduced acidity releases it back into plasma. Hepcidin is an important iron regulator, whose expression is induced by inflammation, transferrin saturation and low iron levels. It is able to bind FPN, causing its internalisation and degradation, and thereby sequestering iron into cells by preventing export. As a result, hepcidin is able to alter both plasma and cellular iron levels. IRP1 and IRP2 are cytosolic iron sensors that are able to elicit post-transcriptional control over several iron regulatory proteins, including TfR, DMT1, FPN and ferritin.

1.5.3.3 IRP/IRE System

The availability of iron is determined by its degree of uptake, export or storage, so regulation of any of these mechanisms can alter total concentrations. Intracellular iron levels are maintained by regulation from two structurally homologous cytosolic iron-sensing iron regulatory protein (IRP) isoforms (IRP1 and IRP2). These IRPs are able to sense cytoplasmic iron levels, and maintain homeostasis by exerting post-transcriptional control of gene expression for key iron regulatory proteins based on the propensity of IRP1 and IRP2 to bind nucleotide sequences in noncoding untranslated regions (UTR) of iron responsive elements (IRE) (Muckenthaler, 2008). The nucleotide sequences form hairpin loops, to which either IRP isoform may bind. There are two separate UTRs of specific mRNAs encoding for iron regulation, 5'UTR and 3'UTR. IRPs have high affinity to bind IREs during iron depletion (Ponka, 1999). IRP binding in the 5'UTR prevents ribosomal docking, thus inhibiting mRNA translation, leading to decreased protein expression. IRP binding in the 3'UTR prevents nuclease-mediated degradation of transcripts, stabilising the mRNA and increasing protein expression. Increases in the labile iron pool leads to a loss of IRP binding activity. An iron sulphur [4Fe-4S] cluster binds IRP1, in formation of cytosolic aconitase, which inactivates IRP1 and blocks IRE binding sites. IRP2 is then targeted for proteasome degradation (Ponka, 1999). As a result, no binding activity occurs in the 5'UTRs, allowing for ribosomal docking and increased protein expression. In the 3'UTR, the mRNA is no longer stabilised, allowing nuclease-mediated degradation to occur, thereby decreasing protein expression. In this way, the IRP/IRE system is able to modify expression of mRNAs encoding for proteins such as TfR, DMT1, FtH1, and FPN, depending on whether the specific mRNA presents IREs in the 3' (TfR, DMT1) or 5' (FtH1, FPN) UTRs (Figure 1.3).

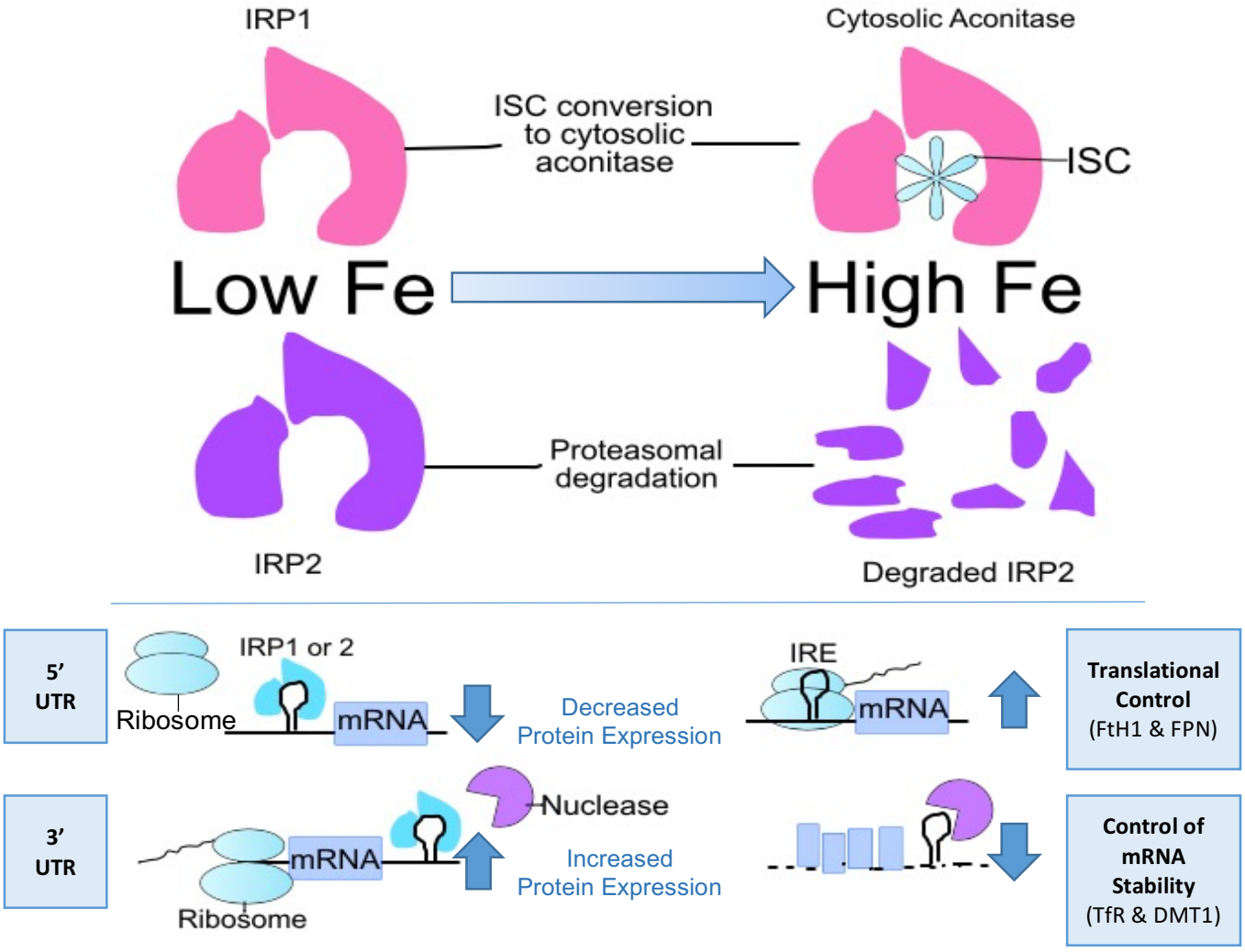

Figure 1.3 IRP/IRE System

The IRP/IRE system helps to regulate iron metabolism, and responds very quickly to any fluctuations in iron. Iron regulatory proteins (IRP1 and IRP2) are cytosolic iron sensors which bind to iron response elements (IRE) with high affinity during conditions of iron depletion. IREs are nucleotide sequences within either 3' or 5' noncoding untranslated regions (UTR) of mRNAs coding proteins involved in iron metabolism. These nucleotide sequences form hairpin stem-loops to which both IRP isoforms may bind. In low iron, IRPs bind to IREs. In the 5' UTR, bound IRPs prevent ribosomal docking, thus lowering protein expression. This occurs in ferritin and ferroportin, so less iron would be stored or exported, in an attempt to increase cellular iron concentrations. In the 3' UTR, bound IRPs prevent nuclease-mediated degradation, thus stabilising the mRNA to increase protein expression. This occurs in TfR and DMT1, so more iron would be imported into the cell, in attempt to increase cellular iron. When cellular iron levels are at high levels, IRPs lose affinity to bind IREs. An iron sulphur cluster binds to IRP1, blocking IRE binding sites and converting its function to a cytosolic aconitase. IRP2 becomes targeted for proteasomal degradation. As a result, in the 5' UTR, ribosomes may now dock, and translation proceeds to increase protein expression. This would occur in ferritin and ferroportin, so more iron is stored and exported to lower intracellular free iron. In the 3' UTR, the IRE is no longer protected, and thus mRNA is destabilised and exposed for nuclease-mediated degradation. This would decrease protein expression, which would occur in TfR and DMT1, resulting in less iron import into the cell. In this way, the IRP/IRE system is able to respond quickly to any changes in intracellular iron, in order to maintain equilibrium with sufficient iron levels for cellular functioning whilst avoiding reaching toxic iron concentrations. *Abbreviations: Fe= Iron, IRE=Iron Responsive Element, IRP= Iron Regulatory Protein, ISC= Iron Sulphur Cluster, mRNA=messenger Ribonucleic Acid, UTR=Untranslated Region.*

1.5.3.4 Toxicity

While sufficient iron provision is critical to maintain physiological cellular functioning, iron properties can also cause substantial damage during conditions of iron overload. As excess iron is not excreted from the body, it is easily possible for a diseased state or certain genetic iron disorders to quickly escalate towards toxic iron accumulation. Iron reversibly alternates between two oxidation states within aqueous solutions: Fe^{2+} ferrous and Fe^{3+} ferric iron. This property allows it to participate in crucial cyclic oxidation-reduction reactions, however, also allows for production of cytotoxic free radicals and oxidising species in the presence of ROS (Winterbourn, 1995). One of the greatest means of iron-mediated toxicity is participation of labile ferrous iron in the Fenton and Haber-Weiss reactions (Equations 1-3) (Figure 1.4) to produce hydroxyl radicals (OH^*). Sources of iron may include non-transferrin bound iron, labile plasma iron, labile iron pool, or iron released from components such as iron-sulphur clusters or ferritin after exposure to radicals. This free iron is toxic due to its ability to catalyse OH* production from H_2O_2 (Equation 2). The hydroxyl radical is then able to react with the majority of biological molecules, causing damage to proteins, nucleic acids, lipids and carbohydrates. This includes DNA strand breakage and mutations, lipid peroxidation, inactivation of mitochondrial oxidative metabolism enzymes, and even cellular death via apoptosis (Lin, 1997). Additionally, ROS can trigger neuronal apoptosis, by activating cellular death pathways (Das, 2014). It is posited that overburdened cells are hypersensitive to ROS, and exposure may then trigger their apoptotic death, while also signalling initiation of antioxidant defence mechanisms to surrounding cells (Levine, 1994). Iron has also been found to directly accelerate formation of α-synuclein aggregates into fibrils (Uversky, 2001). To avoid such detrimental consequences, ideally, iron would be stabilised by chelation to Tf or ferritin, in a form inert to reducing agents to prevent Fenton chemistry from occurring. However, high OS conditions and the resultant exposure to free radicals may cause homeostatic dysregulation. Neurodegenerative effects of OS are significantly exacerbated by dysregulated levels of iron. This is corroborated by the protective properties of iron chelation.

1. $O_2^{*-} + Fe^{3+} \rightarrow Fe^{2+} + O_2$
(superoxide radical + ferric iron → ferrous iron + oxygen)

2. $H_2O_2 + Fe^{2+} \rightarrow Fe^{3+} + OH^* + OH^-$ FENTON REACTION
(ferrous iron + hydrogen peroxide→ ferric iron + hydroxyl radical + hydroxide ion)

3. $O_2^{*-} + H_2O_2 \rightarrow OH^* + OH^- + O_2$ HABER-WEISS REACTION

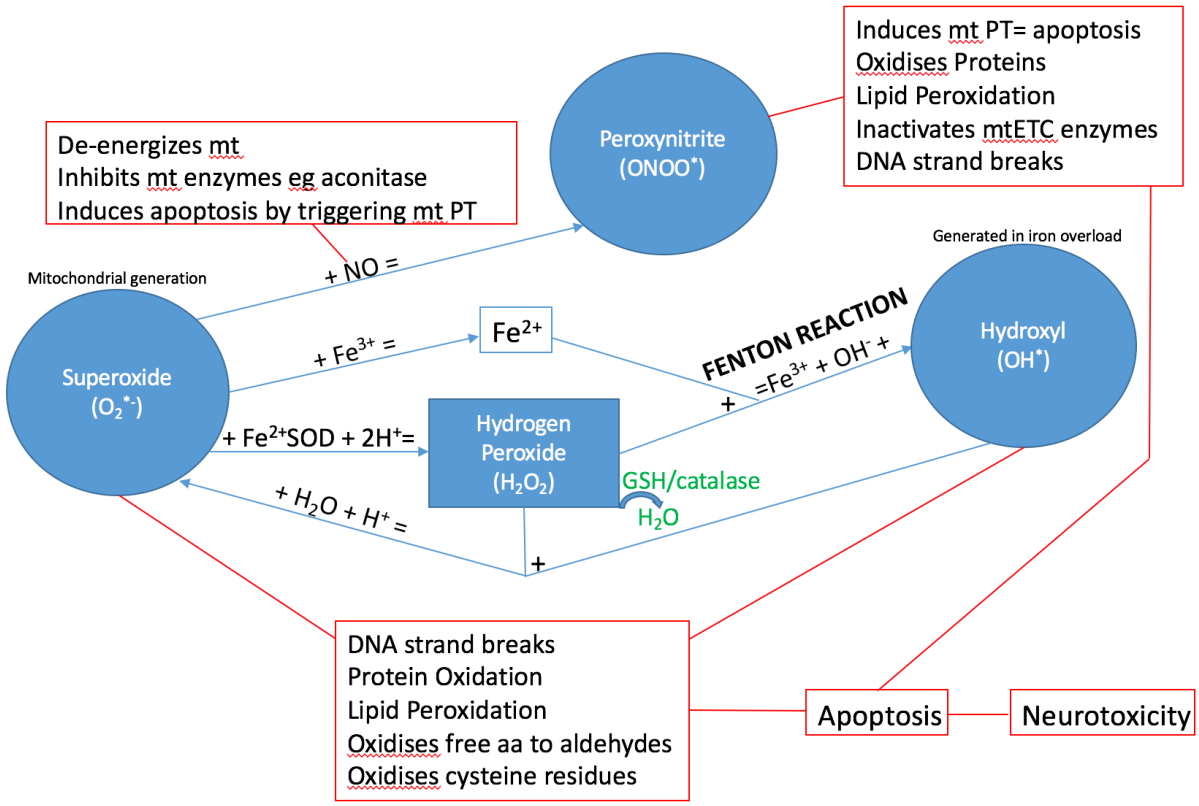

Figure 1.4 Iron in Free Radical-Mediated Toxicity
This schematic represents reactions and relationships between iron, reactive oxidant species and free radicals. Mitochondrial generation of superoxide radicals can react with nitric oxide to form the toxic peroxynitrite radical. Alternatively, superoxide can reduce ferric iron to ferrous iron, which feeds the Fenton reaction. Superoxide dismutation to H_2O_2 also feeds the Fenton reaction, which ultimately results in hydroxyl radical formation. High oxidant conditions during iron overload will produce greater quantities of hydroxyl, which can lead to OS and eventually to neurotoxicity. The metalloenzyme superoxide dismutase can decompose superoxide into H_2O_2. Antioxidants such as catalase or glutathione are then able to dismutate H_2O_2 into nontoxic components. *Blue circles represent free radicals. Blue arrows represent chemical reactions. Red lines represent toxic effects. Abbreviations: aa=amino acids, ETC=electron transport chain, GSH=glutathione, H_2O=water, H_2O_2=hydrogen peroxide, mt=mitochondria, NO=nitric oxide, OH^*=hydroxyl radical, OH^-=hydroxide, ONOO=peroxynitrite, PT=permeability transition, SOD=superoxide dismutase.*

Positive effects from studies using iron chelating agent treatments point to the toxic properties of excess iron, and signify the importance for controlling or reducing superfluous iron levels. Iron chelator deferoxamine has been shown to reduce both brain edema (Ikeda, 1991) and cancer proliferation (Dayani, 2004), while clioquinol and transgenic ferritin over-expression protect against MPTP toxicity (Kaur, 2003). The iron chelator VK-28 is able to cross the blood brain barrier, allowing it to chelate labile brain iron. VK-28 treatment in rats was able to attenuate iron-mediated lipid peroxidation to the mitochondrial membrane (Ben-Shachar, 2004). Similarly, injections of the desferal chelator prevents iron-mediated cytotoxicity in dopaminergic neurons (Ben-Shachar, 2004), while scavenging antioxidant green tea catechin EGCG protects against MPTP-mediated neurodegeneration (Levites, 2002). A human case of neurodegenerative brain iron accumulation presented with assuaged

dyskinesias following treatment with deferiprone chelators (Forni, 2008). Deferiprone treatment also reported improvements to early-stage Parkinson's patients in a pilot clinical trial (Devos, 2014). These results emphasise the prominent role of chronic iron accumulation on perpetuation of OS and eventual neurodegeneration, accentuating a potential target for neuroprotection in degenerative diseases such as PD. The role of iron-mediated toxicity and OS is further supported by beneficial antioxidant treatments. Treatment with antioxidant scavengers providing glutathione peroxidase type actions, was able to mitigate MPTP and 6-OHDA toxicity (Cadet, 1998; Moussaoui, 2000). While radical scavenging green tea extracts provided protection from iron-inflicted lipid peroxidation in mitochondrial membranes following 6-OHDA treatment (Levites, 2002). Studies investigating neuroprotective effects of both iron chelators and antioxidants in conjunction as multi-functional treatments proved very successful (Zheng, 2005). For these reasons, efficient functioning of iron homeostatic mechanisms is necessary to limit cellular exposure to labile iron. Unfortunately, inflammation in neurodegenerative disease has demonstrated the capacity for dysregulating expression of iron proteins.

Diseased conditions can lead to a pro-oxidant environment, with substantial effects on the iron regulatory system. Ferritin acts as an additional source of iron in the presence of superoxide or nitric oxide, as they are able to stimulate release of Fe from storage (Thomas, 1985; Reif, 1992). Superoxide also has the ability to extricate iron from iron-sulphur clusters, releasing iron from aconitase (Winterbourn, 1995; Brand, 2004). This may enhance any iron overload and would affect the IRP/IRE system. If iron is removed from the [4Fe-4S] cluster responsible for maintaining the cytosolic aconitase function, which may also occur from ROS oxidation of cluster cysteine residues, then even in situations of high iron, IRP1 may be free to bind to IREs (Brand, 2004). This would cause upregulation of TfR or DMT1 and downregulation of ferritin or FPN, which would instigate greater iron import, less storage and greater iron sequestration into an already challenged system. Situations of hypoxia are able to induce TfR gene transcription, regardless of IRP/IRE activity (Lok, 1999; Tacchini, 1999), while H_2O_2 has been shown to escalate iron uptake via translational upregulation of TfR (Andriopoulos, 2007). If hypoxia is occurring from an environment of iron overload and high oxidant levels that negatively affect mitochondrial oxidative metabolism, then the addition of extra iron import from upregulated transferrin receptors will only cause further aggravation. IRP2 deletion in mice results in iron dyshomeostasis, axonal degeneration, with bradykinesia and tremor (LaVaute, 2001), substantiating evidence that iron dysregulation aggravates neurodegenerative mechanisms. DMT1 and hepcidin can also be upregulated from exposure to

inflammatory stimuli (Urrutia, 2013), with DMT1 directly affected by IL6 and TNF (Wang, 2013), and hepcidin induced by high iron levels, IL6 and inflammation (Lee, 2004; Nemeth, 2004), culminating in exacerbation of toxic cellular iron sequestration. Tumour necrosis factor (TNF) is released during inflammatory reactions, and is able to downregulate TfR expression, and may be a protective mechanism to reduce intracellular iron (Fahmy, 1993).

While the mechanism of cell death may include mitochondrial-induced apoptosis, other means may be via a distinct, non-apoptotic form of death called ferroptosis. Ferroptosis is an iron-dependent regulated method of cell death, typified by condensed microglia, and compelled by increased endoplasmic reticulum stress and reduced action of glutathione peroxidase 4 (GPX4) (Dixon, 2012; Xie, 2016). GPX4 is a hydroperoxidase that functions in restoring lipid health to protect against ROS-mediated lipid peroxidation, and helps in the decomposition of H_2O_2 and lipid peroxides with the help of GSH (Yang, 2016). Loss of GPX4 function would result in accumulated lipid peroxides of cell membranes, which in combination with toxic free radicals produced from ROS and iron, would lead to ferroptotic death. Uncontrolled ferroptosis has been linked to cytotoxicity in both cancer and PD (Dixon, 2012; Van, 2016), as well as neurotoxicity in other neurodegenerative diseases (Xie, 2016). Moreover, toxicity of the PD MPTP model was repressed by addition of a ferroptosis-specific inhibitor (Van, 2016), signifying an important associative link between ferroptosis dysregulation and parkinsonian neurodegeneration.

Since iron is used in dopamine biosynthesis, dopaminergic neurons would require provision of greater concentrations, while dopamine deamination and auto-oxidation lead to generation of H_2O_2. An additional risk factor is that SN neurons contain neuromelanin pigment, which binds potentially toxic metals such as iron in ferric clusters, making it vulnerable to oxidative damage (Fedorow, 2005). Since the neuromelanin contains high levels of chelated iron and are in neurons targeted in PD, neurodegeneration in cells containing such high concentrations of iron would provide an extra source of iron during overloaded, dysregulated circumstances. This can also occur during conditions of iron overload, as stressed neuromelanin may release stored iron into the LIP upon their core saturation (Faucheux, 2002). Furthermore, melanin is able to reduce ferric iron to the ferrous form, potentially propagating the Fenton reaction (Berg, 2001). These conditions place dopaminergic neurons in the SNpc at greater risk of iron-mediated degeneration.

1.5.3.5 Iron in the Brain

Iron is abundant in the brain as it is utilised for important processes such as oxidative metabolism and myelin synthesis, so the brain maintains large supplies in ferritin (Dayani, 2004). Uptake generally increases with age, while the greatest rate occurrs at birth with the height of myelinogenesis (Jacobson, 1963), this is followed by a two-week decline, and then increases until old age (Hallgren, 1958). Yet cells in the central nervous system are not homogenous in terms of normal iron concentration, with transferrin-mediated distribution dependent on individual cellular requirements (Beard, 1993). Specific brain regions present with high iron concentrations during physiological conditions, particularly components of the basal ganglia including the dorsal striatum, globus pallidus, and SN (Hallgren, 1958; Aoki, 1989). A study utilising spectroscopy measured physiological brain iron, determining that most brain iron is in ferritin, with the amount of iron in the SN over double that in the hippocampus (Galazka-Friedman, 2008). Healthy brains demonstrate a physiological concentration of 3,000-3,830 ng/mg wet weight in the SN (Zecca, 1994), which can be compared with wet liver concentrations of 2,770-16,240 ng/mg (Cumings, 1948). Transferrin levels are comparatively located in areas of high myelin (Connor, 1987), with levels highest in the midbrain (Beard, 1993). Ferritin isoforms are distributed with more H-chain subunits expressed in neurons for swift iron uptake and release, and more L-chain subunits in glia for long-term storage (Connor, 1994). During developmental years, midbrain ferritin levels are greater than other sections, possibly as a protective mechanism, however, this evens out in adults with homogenous ferritin expression across the brain (Beard, 1993). This heterogeneous brain iron regulation is indicative of variations in cellular iron requirements and regulation, which may point to which cells are better able to cope with situations of OS or which are at greater risk of toxicity during a disease state.

1.5.3.6 Iron-Related Disease

Certain diseases and genetic irregularities can lead to loss of iron regulatory functions resulting in toxic accumulation in the periphery and/or the brain. Hereditary hypoceruloplasminemia or aceruloplasminemia is a genetic disorder of iron overload due to a mutation resulting in either complete lack of ceruloplasmin protein production or a reduction in its ferroxidase activity (Brissot, 2010). 95% of systemic iron is recycled from senescent erythrocytes, passing from microglia back into the blood, thus iron oxidation from ferrous to ferric for plasma transferrin binding and transport is crucial for physiological functioning (Xu, 2004). This disorder prevents oxidation of ferrous iron, preventing transferrin binding and increasing the levels of non-transferrin bound iron, which is then free to enter cells and

participate in oxidant-mediated toxicity. It also results in anaemia, from lack of transferrin-bound transport to areas requiring iron. Aceruloplasminemia can cause neurodegenerative iron increases in the brain as well as toxicity in the liver (Miyajima, 1987). Hereditary hemochromatosis results in deficient hepcidin production leading to elevated iron absorption and toxic levels of intracellular iron (Brissot, 2010). Development of genetic disease neuroferritinopathy results in neurodegeneration of the basal ganglia from iron accumulation associated with a mutation in L-chain ferritin protein leading to reduced ferritin expression, elevated iron deposition, and presenting with parkinsonian symptoms (Crompton, 2002; Mancuso, 2005). However, pathology only develops in the brain, proving a separation between the central nervous system and the periphery.

While iron may increase to conditions of iron overload in the periphery, this is not necessarily reflected in similar increases in the brain. This occurs because of the hydrophobic blood brain barrier, which prevents hydrophilic ferric ions from entry, while similarly preventing efflux of non-transferrin bound iron (Hare, 2013). While the periphery may be vulnerable to dietary iron deficiency leading to anaemia, the brain is more resilient due to high regulatory systems. The exception to this is iron deficiency in early life, which can irreversibly affect total brain iron and dopaminergic neuron development (Ben-Shachar, 1986; Youdim, 1989). Similarly, pathological consequences of neurodegenerative diseases tend to remain within the brain until later stages of disease, and disruption to blood brain barrier function.

1.5.3.7 Iron in Neurodegenerative Diseases

Age remains a significant risk factor for neurodegeneration, with age-induced iron increases present in both the SN and striatum (Daugherty, 2013). Deterioration of iron regulatory proteins can lead to dysfunctional iron homeostasis, imbalances in iron levels, and resultant OS and cellular degeneration. Such iron dysregulation and accumulation has been associated with several neurodegenerative diseases, including Alzheimer's, Multiple Scleroses (MS), Huntington's disease (HD), and PD (Loeffler, 1995). Iron has been implicated in Alzheimer's, with cortical and hippocampal accumulation (Andrási, 1995; Antharam, 2012), with iron-induced OS able to increase amyloid beta toxicity (Rival, 2009). Iron and related OS can stimulate tau and amyloid-ß aggregation (Hare, 2013), and it has been associated with Alzheimer's neuropathological plaques and tangles (Smith, 1997). High iron levels are present in oligodendrocytes for myelin synthesis, and MS brains stain positive for iron deposits in white matter (LeVine, 1997). MS patients scanned by MRI also demonstrate correlation between brain lesions and augmented iron levels (Haacke, 2009). MRI in HD patients revealed

elevated iron concentrations in the basal ganglia (Bartzokis, 1999), with HD containing three times more iron compared to control (Chen, 1993). The widespread dysregulation of iron associated with neurodegenerative disease points to a substantial influence on propagating disease pathology. It remains to be determined whether iron accumulation is solely a product of neurodegeneration or whether it is a principal instigator. The ability of iron to catalyse production of neurotoxic free radicals has also placed an emphasis on its possible role in PD pathogenesis.

1.5.3.8 Iron in Parkinson's Disease

Distribution of brain iron changes as a function of age in normal healthy control groups, with older populations showing the greatest concentration of iron within the SNpc (Loeffler, 1995). This could put already vulnerable neurons at greater risk of iron-induced cellular toxicity. Yet, both ferritin subunit (H and L) levels also increase as a normal function of age, as a compensatory adaptation to account for elevations in total cellular iron (Zecca, 2001; Ward, 2013). However, this is not translated to the Parkinson's brain, which exhibits altered iron handling resulting in decreased ferritin in the basal ganglia and SN (Dexter, 1990; Dexter, 1991), as well as significant escalations in total and ferric iron, with extensive nigral iron deposits (Riederer, 1989; Dexter, 1989; Mann, 1994; Ben-Shachar, 2004). Iron levels in the PD SNpc were measured using plasma spectroscopy found 31-35% higher than control, without any marked increases anywhere else in the brain (Dexter, 1989). Magnetic resonance imaging (MRI) confirmed an increase in total PD SN iron (Gorell, 1995; Bartzokis, 1999), while ultrasound experiments determined increased SN echogenicity associated with elevated iron levels (Berg, 1999). Measurements from post-mortem PD SN presented 176% total iron increase, along with a 255% elevation in ferric iron (Sofic, 1988). Amplified iron concentrations have been found specifically within SNpc dopaminergic neurons, as well as Lewy bodies in both PD patients and animal models (Weinreb, 2013). This shift in the amount of iron becoming more readily available to SN cells could trigger cytotoxic elevations in OS.

Iron is present within α-synuclein Lewy bodies in the PD SN, which can bind free iron (Castellani, 2000). It has been postulated that Lewy bodies may act as an iron-binding neuroprotective mechanism (Castellani, 2000), however, toxic properties of α-synuclein aggregates may dispute this claim. Ferric and ferrous iron have been shown to hasten α-synuclein folding and fibril aggregation (Hashimoto, 1999; Li, 2011), with higher iron levels producing dose-dependent aggregation, while greater aggregate concentrations correlate to greater cytotoxicity (Li, 2010). α-synuclein aggregates also have the ability to directly generate

H_2O_2 by three different mechanisms: facilitating dopamine uptake via dopamine transporter grouping with subsequent degradative metabolism (Lee, 2001), α-synuclein aggregation and binding to the inner mitochondrial membrane resulting in mitochondrial defects from reduced Complex I activity (Hsu, 2000), and direct H_2O_2 generation by α-synuclein activation of cytosolic NAPDH oxidase (Nox) (Turnbull, 2001; Junn, 2002; Deas, 2016). This excess H_2O_2 would be exposed to elevated iron and thus lead to a deleterious combination of excess iron and H_2O_2 that can accelerate aggregate formation and potentiate cytotoxicity and disruption to neuronal function via production of free radicals (Turnbull, 2001). Greater OS can in turn instigate further α-synuclein aggregation (Hashimoto, 1999; Li, 2011), creating a neurotoxic feedback loop mechanism. Another study deduced that ferric toxicity increased in the presence of α-synuclein aggregates, via reductions to the mitochondrial membrane potential and concomitant augmented ROS (He, 2011). To encapsulate this data, SN dopaminergic neurons are extremely vulnerable to OS due to naturally elevated iron levels, which helps perpetuate α-synuclein aggregation into Lewy bodies, with a feedback loop to H_2O_2 production and greater OS, along with the additional burden of increased exposure to H_2O_2 from the production and decomposition of dopamine (Loeffler, 1995). PD nigral cells would be exposed to even greater iron concentrations, α-synuclein and OS. Altered iron levels could be attributed to dysregulation of the iron regulatory protein mechanism, excess oxidant production and insufficient clearance by the antioxidant system.

Parkinson's pathology has presented with numerous deviations to homeostatic-control of the iron regulatory proteins. Reductions to ferritin expression (Dexter, 1991) would fail to chelate excess labile iron, allowing further iron released from Lewy bodies and surviving neurons to promote redox reactions contributing to OS and neurodegeneration (Jellinger, 1993). Transgenic mice overexpressing ferritin prove its neuroprotective effects against iron-mediated toxicity following MPTP treatment (Kaur, 2003). DMT1 has also been found to be upregulated in PD SN models (Burdo, 2001; Urrutia, 2013) and in post-mortem PD SN tissue (Jiang, 2010; Salazar, 2008), which can aggravate conditions of iron overload by importing more iron into an already overloaded system. Elevations to DMT1 expression also implicate its involvement in iron-mediated toxicity in the PD brain. A transgenic mouse model void of DMT1 activity demonstrated neuroprotection against MPTP toxicity (Salazar, 2008). Since hepcidin can be induced by inflammation and iron overload, and would result in the observed reductions to serum iron, it was hypothesised that changes to expression during Parkinson's neurodegeneration may also occur. LPS-induced inflammation was able to instigate a

substantial upregulation to hepcidin gene and protein expression specifically within the SN in an animal model (Wang, 2008). PD animal models exhibit hepcidin upregulation followed by a compensatory ferroportin downregulation (Sun, 2012; Zhang, 2013). It was found that reductions in cellular hepcidin expression resulted in a 25% decrease of intracellular iron, improved cellular viability, and lowered 6-OHDA toxicity in a PD model (Xu, 2016). Therefore, augmented hepcidin expression would cause the inverse heightened intracellular iron loading and amplified toxicity.

Another alteration in iron homeostasis occurs in the PD brain from changes to the ferroxidase ceruloplasmin, which triggers parkinsonian symptoms in aceruloplasminemia. Diminutions to cerebrospinal fluid and serum ceruloplasmin are observed in the PD SN (Tórsdóttir, 1999), drawing correlations to increased nigral iron and disease severity (Jin, 2011). A role of ceruloplasmin in PD pathogenesis was determined after discovery of lower serum levels in early-onset PD cases when equated to older-onset patients (Bharucha, 2008). An extremely significant 80% reduction to ceruloplasmin activity was observed in both PD SN tissue and an animal MPTP model (Ayton, 2013). This loss of ferroxidase activity is potentially caused by oxidative damage-mediated ceruloplasmin copper release, which is necessary for function. It has been found that hydrogen-peroxide is directly able to obfuscate ferroxidase activity (Olivieri, 2011). Loss of ferroxidase activity would prevent conversion of ferroportin-released ferrous iron into ferric iron for transferrin binding, leading to iron dysregulation with elevated labile serum iron capable of participating in cytotoxic OS-producing redox reactions. Additionally, loss of extracellular ceruloplasmin function downregulates intracellular ferroportin expression, preventing iron efflux (Jeong, 2003). Absence of ceruloplasmin ferroxidase increases extracellular ferrous iron levels, preventing ferroportin release of its bound iron, and tagging it for ubiquitination (Musci, 2014). In this way, ceruloplasmin is able to initiate ferroportin internalisation and degradation, suggesting an alternative to hepcidin for modulation of ferroportin expression. In support of this, it was also observed that removal of extracellular ferrous iron via addition of chelators prevented ferroportin degradation (Ward, 2012), pointing to a correlation between extracellular iron and regulating ferroportin transcription and expression. Thus, diminished PD SN ferroxidase activity would favour intracellular iron accumulation.

TfR levels were also reduced in PD SN, however, once neuronal loss was taken into account, they were not found to be significantly downregulated as compared to control (Faucheux, 1997). Unaltered TfR in PD brains suggests they are not responsible for instigating intracellular iron elevations or loss of iron homeostasis. Conversely, it was found that levels of systemic

serum iron, ferritin and transferrin saturation were reduced in Parkinson's patients compared to control (Logroscino, 1997), with increased serum transferrin receptor concentrations (Marder, 1998). This systemic dysregulation could function as an additional iron supply shifting iron into the brain, since upregulation of transferrin receptors would increase the amount of iron to be transported across the blood brain barrier. This transport of iron is reflected in the decreased serum iron levels (Logroscino, 1997).

Mitochondrial dysfunction is also implicated in PD pathogenesis (Greenamyre, 2004), with significant decreases to CI activity specifically in the SN of PD patients (Mann, 1994). Reductions to glutathione (GSH) concentrations have been measured in the PD SNpc (Perry, 1982; Kish, 1985; Riederer, 1989), which can lead to failure to scavenge elevated H_2O_2 from DA metabolism (Spina, 1988). Strained neuronal oxidative metabolism, may lead to reduced ATP production, which in turn could account for the declining GSH levels, since ATP is a co-substrate for GSH production (Han, 1999). It has been determined that PD pathology exhibits elevated activity of the antioxidant superoxide dismutase (Saggu, 1989). Superoxide catalyses decomposition of superoxide, with H_2O_2 as a by-product. Excess H_2O_2 build-up can result in iron-induced hydroxyl formation, leading to free radical damage, augmented α-synuclein aggregation, and downstream neurodegeneration. Cumulative inference from this data point to iron as an arbitrating influence, and suggests significant alterations to various components of the iron regulatory mechanisms in Parkinsonian nigral cells, which could place already vulnerable neurons at greater risk of iron and OS-mediated degeneration. The sole initiating factor facilitating such changes to iron homeostasis and perpetuating PD pathogenesis remains to be determined by further investigations.

1.5.3.9 Iron as a Neurodegenerative Link

Evidence provided here proves presence of iron accumulation in several neurodegenerative diseases. While each may present with varying symptoms, disease mechanisms and instigating insults, dysregulation resulting in exposure to toxic concentrations of iron seems to be a common presentation. This common factor suggests that amplified concentrations of iron resulting from changes to iron regulatory protein metabolism may prove to be a neurodegenerative link between several diseases. While it remains elusive as to why cells accumulate iron, neuroinflammation may be a potential cause.

1.5.4 Hydrogen Peroxide

H_2O_2 is a peroxide compound containing a single oxygen-oxygen bond, with a physiological steady-state concentration around 2μM, and about 0.2μM generated per second under healthy conditions (Mueller, 2001). It functions as a cytosolic cell-signalling mediator for various intracellular processes, via oxidation of cysteine residues to regulate protein phosphorylation (Kraft, 2004), and is a strong oxidiser under acidic conditions that participates in redox reactions (Rhee, 2006). H_2O_2 has a role in regulating cellular and mitochondrial function, by inhibiting mitochondrial enzyme function. H_2O_2 and superoxide are both able to directly inactivate mitochondrial aconitase by oxidation of the iron-sulphur cluster complex, thereby releasing both ferrous iron and H_2O_2 (Nulton-Persson, 2001). Additionally, H_2O_2 is also produced for neutralisation of microbes within motile phagocytic neutrophils that migrate via the blood towards inflammatory insults, engulfing them and killing the foreign bodies via generation of H_2O_2 from superoxide (Rhee, 2006). Excess H_2O_2 is able to participate in Fenton chemistry in the presence of labile ferrous iron, or ferric iron and superoxide, to generate cytotoxic hydroxyl radicals (Desagher, 1996). Since H_2O_2 is permeable, it is able to pass freely through cell membranes to exert effects on cytosolic components or extracellular neighbouring cells.

There are several cellular sources capable of H_2O_2 generation, with the principal generators including the mitochondria, dopamine, and NADPH oxidase (Nox). Aerobic metabolism in the mitochondrial electron transport chain is a significant contributor of both superoxide and H_2O_2, as the respiratory chain can prematurely leak electrons. Typically, four electrons released from Complex IV reduce oxygen to generate water necessary for downstream pathways, however premature leakage of one electron produces superoxide, while leakage of two electrons generates H_2O_2 (Brand, 2016). This occurs particularly at mitochondrial complexes I and III, which each contain defined sites of superoxide and H_2O_2 production (St-Pierre, 2002). Mitochondrial matrix superoxide has a short half-life due to the presence of antioxidant manganese linked superoxide dismutases (Mn-SOD), while other metallo-SODs (eg Fe^{2+}, copper (Cu), or zinc (Zn)) intervene in the intermembrane space or cytosol (Adam-Vizi, 2005). Disproportionation of superoxide by SOD gives rise to H_2O_2 by-products, which are easily able to pass through the mitochondrial membrane into the cytosol (Brand, 2016). Another source specifically affecting dopaminergic neurons is the generation of H_2O_2 from dopamine synthesis and degradation (Figure 1.5). Oxidative deamination of dopamine may occur enzymatically by endogenous enzymes such as monoamine oxidase (MAO) or by tyrosine hydroxylase during dopamine synthesis to generate H_2O_2 (Maker, 1981; Sofic, 1992; Haavik, 1997). MAO

generation of H_2O_2 is confirmed in rat brain mitochondria, however was deemed as a secondary source (Sinet, 1980). Production may also occur via nonenzymatic oxidation of dopamine, which can be catalysed by iron ions (Zhou, 2010) (Figure 1.6). Aside from H_2O_2, this oxidation generates highly reactive dopamine quinones, which may either act as precursors for neuromelanin formation, or participate in toxic cellular reactions leading to mitochondrial dysfunction, proteasome inhibition, NADH oxidation, GSH reactivity, microglial activation (Le, 2001), inactivation of complexes I and IV, and mitochondrial permeability transition induction which could eventually cause depolarisation and release of apoptotic factors (Bisaglia, 2010; Zhou, 2010). Lastly, cytosolic production of H_2O_2 may also occur by action of Nox. These NADPH oxidases are both cytoplasmic and membrane-bound catalytic enzymes found in all CNS plasma membranes that reduce oxygen to superoxide, which can then spontaneously disproportionate to generate H_2O_2 (Infanger, 2006). The oxidases remain dormant in microglia until phagocytic activation (Babior, 2000). Nox-produced H_2O_2 may have a role in regulating microglial proliferation (Mander, 2006). Nox is upregulated during neurodegeneration, and is able to activate microglia (Zhang, 2005). Endogenous scavenging mechanisms are in place to regulate cellular H_2O_2 levels.

H_2O_2 decomposition may occur from action by scavenging peroxidases, which are enzymes capable of H_2O_2 decomposition into water. These include catalase, which exerts its effect within cytoplasmic peroxisomes via the equation: $2H_2O_2 \rightarrow 2H_2O + O_2$; and cytosolic or mitochondrial glutathione peroxidase (GPx), which is dependent on GSH and acts via the equation: $2GSH + H_2O_2 \rightarrow 2H_2O + GSSG$ (Armogida, 2012). Cytoplasmic antioxidants peroxiredoxin and thioredoxin also exert regulatory effects, decomposing H_2O_2 unless it reacts with the peroxiredoxin cysteine residue to cause reversible ATP-dependent inactivation (Rhee, 2006). Peroxiredoxin decomposes hydrogen peroxide via the equation: Reduced peroxiredoxin + $H_2O_2 \rightarrow$ Oxidised peroxiredoxin + 2 H_2O. Since the oxidised form has no antioxidant activity, it must be reduced with the help of thioredoxin in the equation: Oxidised peroxiredoxin + Reduced thioredoxin $\rightarrow$ Reduced peroxiredoxin + Oxidised thioredoxin (Rhee, 2001). While mitochondria do not contain catalase, they are able to enzymatically break down mitochondrial-derived H_2O_2 via GPx to prevent initiation of OS (Gluck, 2002). These regulatory mechanisms act to maintain sub-threshold H_2O_2 concentrations in avoidance of cytotoxic accumulation. However, certain disease states lead to loss of homeostatic control.

Antioxidants such as catalase and glutathione peroxidase are essential in scavenging excess H_2O_2, however, the brain tends to have naturally low concentrations (Sinet, 1980), which places cells at risk of radical-mediated OS. Dysfunction to CI, as seen in the PD SN (Mann,

1994), would lead to reduced upstream function, with concomitant elevations to superoxide and H_2O_2 at Complex III. If this dysfunction also affects antioxidant levels, then net superoxide and H_2O_2 would increase (Brand, 2016). H_2O_2 has also been shown to boost MAO-B activity (Konradi, 1986), which would support further dopamine disproportionation and greater H_2O_2 generation. Upregulation of Nox activity in neurons is a mechanism of OS (Gao, 2003), as is elevated SOD activity. Both are observed in the PD brain. Activated microglia have upregulated Nox expression when in the presence of degenerating dopaminergic neurons (Koppula, 2012), and Nox is significantly elevated in SN in human PD patients as well as in MPTP animal models (Wu, 2003). Transgenic mice with knockdown Nox expression displayed dopaminergic neuroprotection after MPTP administration (Wu, 2003), as did treatment with the superoxide inhibitor dextromethorphan in an MPTP model (Zhang, 2004), pointing to the importance of controlling H_2O_2 expression. PD SN demonstrates significantly increased SOD activity (Marttila, 1988; Saggu, 1989), which would catalyse further degradation to H_2O_2, and in turn aggravate iron-mediated toxicity from provision of an adequate H_2O_2 supply to feed the Fenton reaction. H_2O_2 toxicity is confirmed from experimental attenuation of cell death provided by catalase treatment, where cytotoxicity was intensified following SOD treatment (Lin, 1997). While catalase would decompose H_2O_2, SOD would produce it from catalytic decomposition of superoxide, thereby accentuating the significant toxic contribution of H_2O_2. Additionally, studies have reported a specific neuronal vulnerability to H_2O_2 toxicity, demonstrating reduced efficiency at detoxification compared to astrocytes (Dringen, 1999). Alternatively, astrocytes demonstrate potential neuroprotective properties, with the ability to neutralise H_2O_2 equally via both glutathione peroxidase and catalase (Langeveld, 1995; Dringen, 1997). In relation to iron-mediated toxicity, H_2O_2 has also been shown to directly affect expression of several iron regulatory proteins. H_2O_2 can instigate stimulation of IRP1 binding activity, which leads to elevations in intracellular iron via increased TfR influx and decreased ferritin storage (Caltagirone, 2001). H_2O_2 has also been shown to directly upregulate both TfR (Pantopoulos, 1995) and HAMP in hepatocytes (Millonig, 2012). Since elevated iron has been measured in the PD SN, along with decreased glutathione scavengers (Kish, 1985), uncontrolled production of H_2O_2 would upregulate hydroxyl radical production, leading to protein damage, lipid peroxidation and propagation of neurodegenerative pathology.

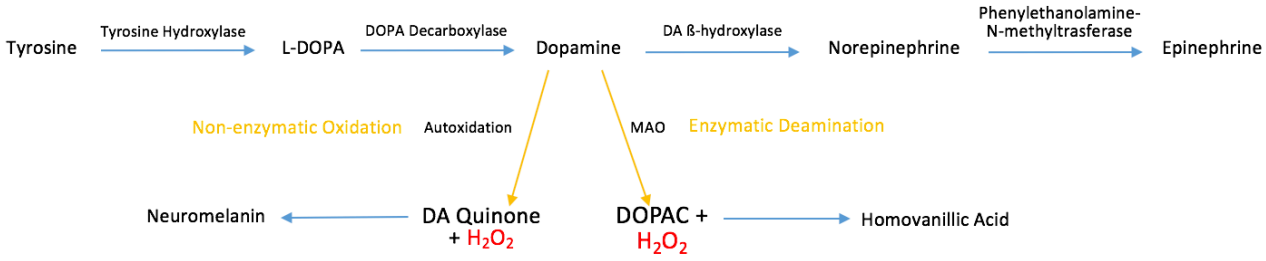

Figure 1.5 Dopamine Pathways for Synthesis, Decomposition, and Formation of Hydrogen Peroxide
Dopamine is a neurotransmitter from the catechol family, with the majority found in the striatum. It is synthesised from tyrosine and L-DOPA precursors with the help of catalytic enzymes by dopaminergic neurons in the nigrostriatal system. This system contains somas within the SNpc, and axons projecting to the striatum. Dopamine itself is a precursor for the epinephrine neurotransmitter. Enzymatic deamination by monoamine oxidase (MAO) generates hydrogen peroxide and the 3,4-dihydroxyphenylacetic acid (DOPAC) metabolite. Non-enzymatic autoxidation by oxygen also generates hydrogen peroxide, as well as a dopamine quinone. These quinones are precursors for neuromelanin formation, and can also participate in toxic reactions leading to mitochondrial dysfunction, permeability transition, and NADH oxidation. *Abbreviations: DA=Dopamine, DOPAC=3,4-dihydroxyphenylacetic acid, H_2O_2=hydrogen peroxide, MAO=Monoamine Oxidase.*

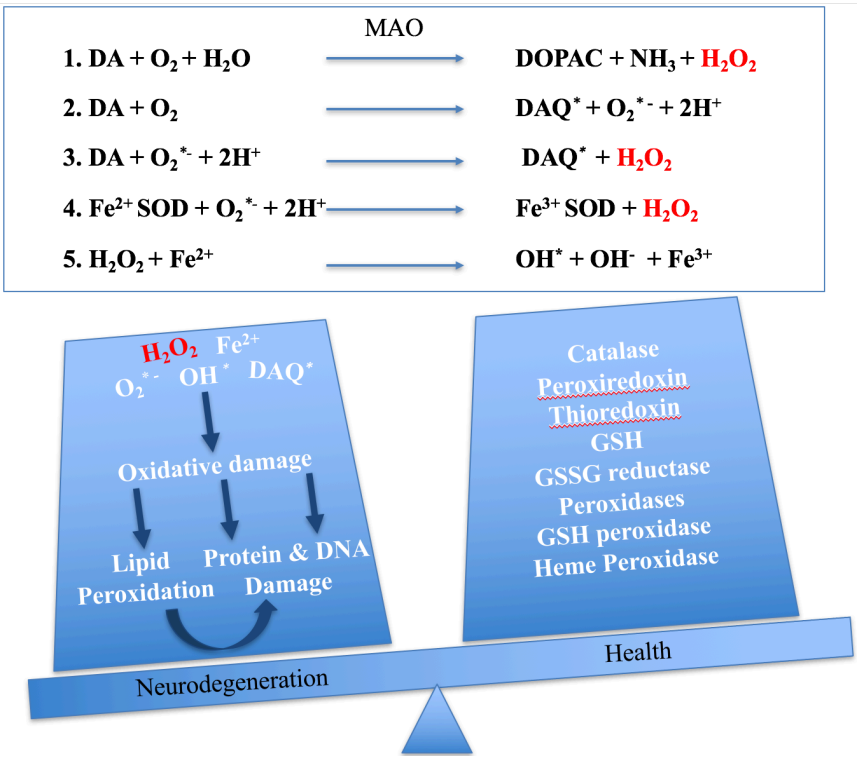

Figure 1.6 Hydrogen Peroxide Formation Equations, Scavengers, and Toxicity in Dopaminergic Neurons
Both enzymatic monoamine oxidase (MAO) deamination and non-enzymatic autoxidation of dopamine result in the formation of hydrogen peroxide species. Enzymatic dopamine deamination is catalysed by MAO (Equation 1) to generate H_2O_2. Dopamine autoxidation (Equations 2 & 3) results in formation of H_2O_2, superoxide (O_2^{*-}), which can be broken down into H_2O_2, and reactive dopamine quinones (DAQ^*), able to inactivate Complex I and IV, and cause mitochondrial permeability transition. Inactivation of CI would increase CIII generation of superoxide and H_2O_2 and affect ATP production. Peroxiredoxin and thioredoxin are cytosolic antioxidants that work together to catalyse H_2O_2 decomposition. Physiological cellular signalling may require above threshold hydrogen peroxide quantities, so its breakdown may be temporarily paused. Peroxiredoxin can be inactivated if their cysteine residues become hyperoxidised by reaction with H_2O_2. They can be reactivated by an ATP-dependent enzyme (Rhee, 2006), however, situations of OS may have high H_2O_2 concentrations but also low ATP. This may have deleterious consequences if the feedback loop halts H_2O_2 antioxidant activity in situations that would require it. H_2O_2 is also formed as a product of superoxide decomposition by superoxide dismutase (SOD) bound to metal ions (Fe^{2+}-SOD) (Equation 4), and is able to alter regulation of proteins involved in iron homeostasis, as well as react with ferrous iron to generate hydroxyl radicals in the Fenton reaction (Equation 5). PD SN has increased SOD, which would generate copious hydrogen peroxide concentrations, as well as increased iron, which reacts with H_2O_2 and can accelerate α-synuclein folding and aggregation. α-synuclein aggregations can generate further H_2O_2. Dopamine deamination pathways generate additional quantities of H_2O_2. Thus a combination of these factors leaves dopaminergic neurons at much greater risk of H_2O_2 accumulation, with oxidative damage to cellular lipids, proteins and DNA, and with subsequent H_2O_2/iron/OS-mediated neurotoxicity. The elevated OS can negatively affect iron homeostasis, causing even further devastation to naturally susceptible SN neurons, and tipping the scale away from healthy function towards neurodegeneration.
Abbreviations: DA=Dopamine, DAQ^*=Dopamine Quinone, DOPAC=3,4,Dihydroxyphenylacetic acid, H_2O_2=Hydrogen Peroxide, NH_3=Ammonia, O_2=Oxygen, O_2^{*-}=Superoxide, OH^*=Hydroxyl radical, MAO=Monoamine Oxidase, SOD=Superoxide Dismutase.

1.6 Neuroinflammation

1.6.1 Physiological Inflammation

Inflammation may be defined as a beneficial, localised response to neutralise injury, pathogens or inflammatory factors, with the intention of issue resolution by tissue repair or removal of the injurious agent. The principal facilitators of neuroinflammation in the brain are activated microglia (Wyss-Coray, 2012). These cells are able to release inflammatory factors crucial for cellular functioning, or assist by phagocytic removal of debris and toxic compounds, as well as myelin reparation (Glezer, 2007). Microglia can release a host of various factors, some of which may be anti-inflammatory to support neuronal survival (Lull, 2010). Astrocytes are also involved in inflammation. These cells are normally neuro-supportive, providing essential nutrients to neurons, aiding in neurotransmitter recycling and synaptic regulation, as well as homeostasis of ions and OS (Wyss-Coray, 2012). Akin to microglia, astroglia are able to patrol the microenvironment and become activated in response to insult or injury, leading to reactive astrogliosis of astrocytic activation and proliferation (Liu, 2003).

Moderate levels of certain reactive species such as nitric oxide, peroxynitrite, H_2O_2, hydroxyl radicals or superoxide play a functional, physiological role. They mediate cellular signalling (Das, 2014), whereby increased oxidant presence provokes a change in function (Dröge, 2002). Radicals including superoxide and H_2O_2 maintain beneficial function by acting as secondary messengers. Alterations in cellular conditions leads to radical-mediated stimulation of signalling pathways (Wyss-Coray, 2012). Nitric oxide also regulates cellular signalling by aiding in neurotransmission and vasodilation (Weiss, 1993). Controlled levels of free radicals even have significant roles in membrane function, ATP generation during oxidative phosphorylation, aiding in apoptotic removal of malfunctioning cells, elimination of malignant cells and exogenous microorganisms (Devasagayam, 2004). As these oxidants are typical products of oxidative metabolism with useful biological functions, antioxidant safeguards are in place, restraining radical levels to ensure prevention of toxic accumulation.

Free radical neutralising protective mechanisms include superoxide dismutase (SOD), catalase, glutathione (GSH), glutathione peroxidase (GPx), glutathione reductase (GR), and ascorbic acid. Antioxidants help prevent ROS formation, and ensuing OS, by scavenging for free radicals then catalysing their decomposition into nontoxic products (Devasagayam, 2004). For example, the metalloenzyme SOD combined with ferrous iron, dismutates superoxide to form H_2O_2, which in turn, is decomposed by catalase into water and oxygen (Hopkin, 1992). OS only occurs when a persisting environmental or pathological insult creates toxic levels of reactive metabolites or free radicals that surpasses the neutralising abilities of antioxidants.

While microglial activation of pro-inflammatory mechanisms is important in maintaining host defence, chronic inflammation has been linked to the risk of neurodegenerative diseases (Koppula, 2012).

1.6.2 Pathological Role of Neuroinflammation

Idiopathic PD may have a multifaceted derivation, resulting from interaction between genetic mutational defects, toxic environmental exposures, as well as inherent vulnerabilities of the SN physiology that may result in inflammatory dysregulation. Absence of consistent neuronal regeneration, high energy requirements, and large microglial populations leave dopaminergic neurons vulnerable to damage from components of the inflammatory orchestra. This excessive neuroinflammation has led to formation of the OS-mediated hypothesis of neurodegeneration. Uncontrolled inflammation in the brain is able to perpetuate neurodegeneration in different diseases, with chronic microglial activation a primary contributing factor to neuroinflammation (Tang, 2016). Akin to microglia, astrocytes also modulate their activity in response to inflammatory states to help mediate the inflammatory response, although to a lesser degree than microglia (Liu, 2003). Additionally, astrocytes can become activated by microglial-released factors such as TNF, to release further pro-inflammatory cytokines and nitric oxide (Tacconi, 1998). Dopaminergic neurons are particularly sensitive to inflammatory effects of activated microglia due to their increased iron and H_2O_2 concentrations, which increases vulnerability of SN neurons to ROS and iron-mediated toxicity (Gao, 2002; Block, 2007). While the SN is naturally high in microglial concentrations (Lawson, 1990), which have been shown to demonstrate morphological abnormalities and conformational dystrophy that may potentially lead to loss of neuroprotection during microglial senescence in normal ageing (Streit, 2004; Conde, 2006; Yokokura, 2016), even higher concentrations of microglia and astrocytes are found within regions of neurodegeneration, contributing to inflammation by release of reactive oxygen species (ROS), nitrogen species (RNS), and cytokines (Teismann, 2004). Neurons have demonstrated loss of viability from pro-inflammatory cytokines (Gadient, 1997; Frankola, 2011), ROS including H_2O_2 and hydroxyl radicals (Fahn, 1992; Koutsilieri, 2002), and RNS such as nitric oxide and peroxynitrite (Bonfoco, 1995; Troy, 1996). This is supported by the ability of LPS to sufficiently activate microglia into causing targeted degeneration of dopaminergic neurons (Gao, 2002), and since LPS does not directly affect neurons, the mechanism of cell death must be as a result of microglial action through inflammation. From the negative effects of chronic inflammation on neuronal viability, and the increased presence

of activated microglia in the PD SN, it can be deduced that inflammation is a contributing factor to Parkinson's pathology. Pro-inflammatory cytokines can alter intracellular iron handling (Fahmy, 1993), whereby the enhanced innate inflammatory response can induce an increase in neuronal iron uptake leading to neurotoxicity. Once a cell is exposed to OS, they become hypersensitive to further insult by a secondary exposure (Lin, 1997). This sensitivity may occur from depletion of antioxidant defence mechanisms, and cellular damage that may no longer be remedied. Continuous cytotoxic events and excessive oxidative attacks may irreversibly compromise cellular viability, triggering neuronal demise via propagation of cell death mechanisms.

Apoptosis is a form of controlled, regulated cell death, coordinated by changes to mitochondrial permeability transition (PT) (Kroemer, 1997). Mitochondrial transmembrane potential (MTP) is created by functional ionic dispersion across the inner membrane to form a gradient necessary to maintain physiological activity (Kroemer, 1997). Decreased MTP would disrupt mitochondrial capacity, and is an indicator of early apoptosis (Zoratti, 1995). Opening of the mitochondrial permeability transition pore resulting in apoptosis is affected by changes such as increased mitochondrial matrix pH, oxidation of nicotinamide adenine dinucleotide (NAD) pools, reductions to metabolic supply, or presence of ROS such as H_2O_2 or nitric oxide (Hortelano, 1997; Kroemer, 1997). NAD exists as either the oxidised (NAD^+) or reduced (NADH) forms, and participates in redox activity for electron transfer within mitochondria. Once triggered, apoptogenic factors are released from mitochondria, causing condensed cellular compartments and abated mitochondrial function. This leads to altered mitochondrial membrane potential, extreme ROS production, nuclear DNA fragmentation, and translocation of phosphatidyl serine (PS). PS is a cell membrane component able to translocate from the internal cytosolic surface to the extracellular surface membrane, thus targeting the cell for phagocytosis by macrophages (Huynh, 2002). Cell contents are not released to surrounding cells, avoiding an inflammatory response and secondary necrosis caused by proinflammatory substances, but are instead sequestered into phagocytes for lysosomal decomposition within apoptotic bodies (Jabs, 1999). Necrotic death occurs as a result of severe injury, which may include lack of oxygen, ischemic damage, physical trauma, and exposure to cytotoxic mediators or chemicals. This damage results in swelling of cellular compartments, eventual mitochondrial rupture, and release of cellular constituents to the extracellular space (Jabs, 1999). Exposure causes local inflammation, that may perpetuate a detrimental response in neighbouring cells (Bonfoco, 1995).

The microglial inflammatory response has been shown to be long-lasting, with reactive microglia and loss of dopaminergic SN neurons observed years after the inflicting insult (Langston, 1999; McGeer, 2003). Since persistent glial activation can inflict degenerative toxicity, the question remains what is causing this aberrant reactive microgliosis in PD. Microglia are activated by various mechanisms, including pathogenic detection, environmental toxins, neuronal death, and mutated proteins, (Block, 2005). Upon activation, they can release damaging factors to kill offending particles. However, these factors may also diffuse to cells in close proximity (Blaylock, 2004). If the glial response is terminated, these factors should not exert significant damage to surrounding neurons. However, chronic microglial activation would result in much more extensive damage, that may cause neuronal death, which in turn is able to instigate further microglial activation. One such toxic factor resulting from microglial phagocytic action is Nox-generated superoxide. If microglia encounter offending toxins, phagocytosis is initiated, resulting in activation of microglial Nox and the subsequent respiratory burst of superoxide (Block, 2005). In the presence of SOD, this may be dismutated to form H_2O_2, which has been shown to enhance OS and neuronal toxicity. If microglia perform this action in a region of low toxin concentration, this may dissipate the respiratory burst amongst surrounding cells. However, in the presence of protein aggregates, such as with α-synuclein in the PD SN, numerous microglia performing simultaneous and repeated phagocytosis would prove deleterious by generation of toxic superoxide concentrations, thereby amplifying glial activation over time. The α-synuclein instigation of microglial activation and its phagocytic release of superoxide has been demonstrated in an *in vitro* study (Zhang, 2005). A positive feedback mechanism exists for microglial ROS production, as Nox-mediated superoxide production can instigate further inflammation by signalling production and release of microglial pro-inflammatory cytokines (Qin, 2004). Additionally, genetic Nox depletion was able to subdue microglial activation, which then inhibited astrocyte activation, thus H_2O_2 generated from Nox superoxide has a role in regulating both microglia and astrogliosis directly (Hou, 2017). This was confirmed by extracellular addition of H_2O_2, which served to activate glia (Hou, 2017). Furthermore, degenerating neurons can promote microglial activation by release of neuromelanin (Zhang, 2011). The PD brain demonstrates a substantial reduction in SN neuromelanin from loss of dopaminergic neurons, which is released into the extracellular space (Calabrese, 1991), potentially further over-activating microglia. As more neurons die, this would feed the self-propelling disease progression, perpetuating microglial gliosis and driving the degenerative neuroinflammation.

This pro-inflammatory environment characterised by elevated glial activation and persistent release of toxic factors is supported by various studies. *In vivo* studies monitored the effects of LPS infusions on rat dopaminergic neurons, which resulted in inflammation and eventual degeneration of dopaminergic nigral neurons (Gao, 2002; Machado, 2011). *In vitro* examination corroborated the critical role of microglia in propagating inflammatory reactions when their inhibited activation and reduced ROS release assuaged neuronal degeneration (Liu, 2000). Postmortem tissue analysis from PD, AD, HD and amyotrophic lateral sclerosis patients exhibited higher ROS concentrations and pro-inflammatory cytokines within individual areas pertaining to neurodegeneration (Greenamyre, 1999; Koppula, 2012), as well as elevated concentrations of activated astrocytes and microglia (Glezer, 2007). In the Parkinson's brain, there is evidence of greater innate inflammation compared to healthy individuals, with elevated nigral concentrations of activated microglia and pro-inflammatory cytokines, including IL1, IL6 and TNF (Hunot, 1999; Nagatsu, 2000; Barcia, 2003). Corroboration of inflammation as a contributing or instigating factor of neurodegeneration in PD pathology is supported by the beneficial effects of anti-inflammatory treatments on slowing disease progression. Treatment with nonsteroidal anti-inflammatory drugs (NSAID) was able to attenuate dopaminergic cell death in PD animal models, as well as slow disease onset in human patients (Chen, 2003).

The role of inflammation in PD is further substantiated by the positive correlation between mechanical brain injury and disease development (McGeer, 1988). Exposure to severe brain inflammation from head injuries in early adulthood may prompt a self-propelling inflammatory cycle that can progress to development of neurodegenerative disease later on, as seen in World War II veterans with increased dementia risk (Plassman, 2000), boxers exhibiting loss of melanin pigment in the SN (Unterharnscheidt, 1995), a correlation between trauma with concussion and PD development, and greater PD incidence in head trauma cases occurring before age 30 (Jafari, 2013). Severe injury from a skull fracture was also able to induce progressing parkinsonian symptoms after 6 weeks (Doder, 1999). This correlation with timing in early adulthood suggests that the inflammatory propagation is a long-lasting event, beginning with the initial traumatic insult causing neuronal death that propels down an inflammatory pathway of continuous glial activation leading to eventual neurodegeneration associated with disease. More significantly, this association between sudden induction of the inflammatory response and development of Parkinson's pathology elucidates a possible causative factor to either PD instigation or development.

1.7 Microglia

1.7.1 Physiological Function

Microglial cells are resident brain macrophages, derived from monocytic cells in the bone marrow. They arrive into the brain at early stages of embryogenesis from embryonic day 7-9, and are then able to mature and differentiate alongside the rest of the CNS cells (Lee Mosley, 2006). These glial cells represent between 5-20% of total brain cells (Arcuri, 2017). Microglia are highly dynamic cells constantly patrolling the microenvironment for foreign bodies, and they exist in various stages of activation and according morphologies (Nimmerjahn, 2005) (Figure 1.5). The dominant microglial state is the resting morphology. This consists of ramified cells, with actively scanning, extending and retracting processes, and arborisations that can be rebuilt if necessary to avoid neuronal disruption (Nimmerjahn, 2005). These branches extend out in different directions from the small cellular soma, which measures about 8-12μm (Glenn, 1992) (Figure 1.7A), and favour direction towards the synaptic cleft where they can help regulate activity (Wake, 2009). Upon detection of neuronal or tissue injury, inflammatory factors such as cytokines and free radicals, or foreign entities, microglia undergo morphological changes, initiate mitotic proliferation, and move to areas of injury (Glenn, 1992). The first transitional phase moves from resting to reactive morphology (Figure 1.7B), typified by withdrawing and thickening processes (Beynon, 2012). Transition progresses to the final morphological form of reactive, phagocytic amoeboid microglia (Figure 1.7C), characterised by almost complete lack of cellular processes, with a remaining process branch to enable motility (Beynon, 2012).

Microglia maintain important neuroprotective biological functions, including immune patrol and scavenging macrophage action, neuronal support, phagocytic clearance of cellular debris and apoptotic cells, secretion of tissue rebuilding mediators (Wyss-Coray, 2006), or synaptic pruning necessary for efficient maturation, homeostasis, and development of synaptic circuits (Paolicelli, 2011; Stephan, 2012). Additionally, they participate in the quad-partite synapse, with close proximity to pre and post-synaptic neurons, where they serve as synaptic sensors to help monitor and maintain efficient neurotransmission (Schafer, 2013). As macrophages, microglia are able to release a variety of pro and anti-inflammatory growth factors, chemokines, and cytokines, allowing for promotion of regulated apoptotic cell death. This process consists of pro-apoptotic occurrences recognising cells tagged for phagocytosis by receptor activity. Certain receptors, such as the Toll-like receptors (TLR), have great binding affinity for microbial pathogens (Fu, 2014), while others recognise apoptotic factors, such as presentation of phosphatidylserine or neuronal release of ATP (Wake, 2011). Thus, microglia

are able to patrol the brain for any offending factors, and exert macrophagic activity as a neuroprotective mechanism.

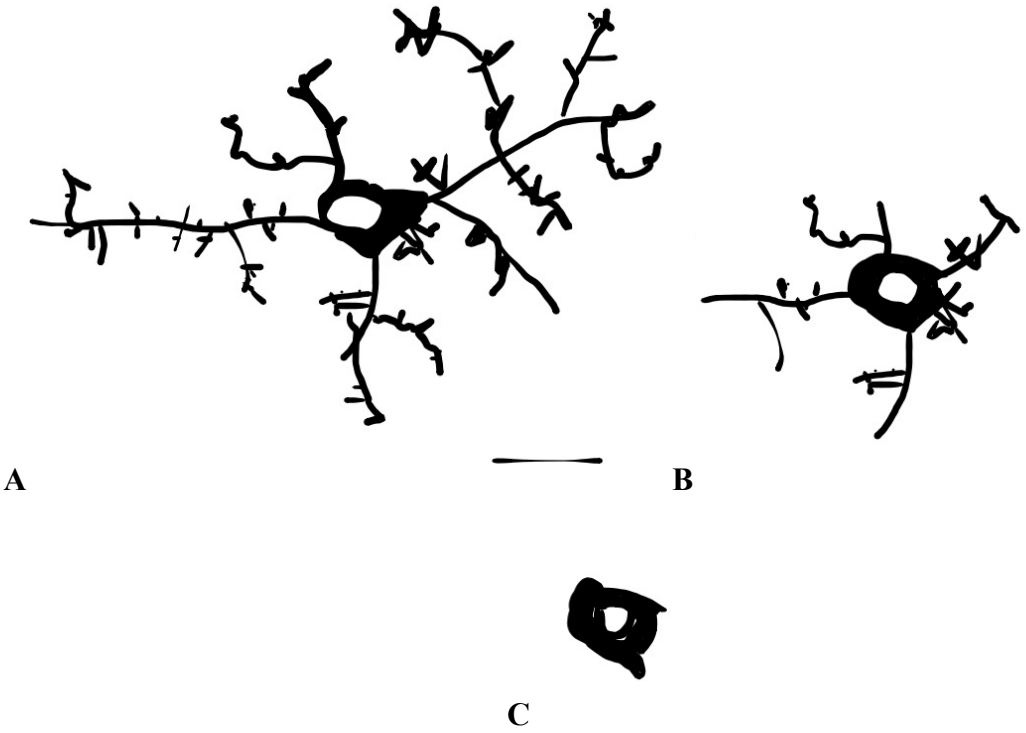

Figure 1.7 Microglial Morphological Changes
This drawing represents an individual microglia as observed *in situ* with resting morphology of extended, branching processes (A), reactive morphology showing withdrawing processes (B), and fully activated phagocytic amoeboid morphology (C). The scale bar represents 20µm (Adapted from Glenn, 1992 and Beynon, 2012).

1.7.2 Pathological Role

Under normal conditions, a regulatory system is initiated immediately following an immune response, whereby microglial activity is either activated or the issue is quietly resolved (Tang, 2016). However, diseased conditions result in the uncontrolled immune responses observed during chronic neuroinflammation. While microglia can be neuroprotective, they can also be neurotoxic by releasing pro-inflammatory cytotoxic substances to mediate these inflammatory responses. Two dynamic and reversible microglial phenotypes are associated with neurodegeneration: M1 and M2 (Figure 1.8). M1 microglia express what may be termed as classical activation, characterised by the typical release of destructive inflammatory factors, such as tumour necrosis factor, interleukin-1ß, interleukin-6, and nitric oxide, amongst various others (Tang, 2016). Aside from morphological changes, these microglia also alter function to become more pro-inflammatory, and can be induced by administration of lipopolysaccharide to trigger neurodegeneration (Gao, 2002). They increase similarity to macrophages and exhibit upregulated expression of cell surface complexes for antigen-binding (Peterson, 2014). An example of this is upregulation of major histocompatibility complexes (MHC), which bind pathogen antigens for presentation to peripheral immune T-cells invading the brain to neutralise pathogens (Lull, 2010). This is supported by the ability of LPS activation of the inflammatory response to induce significant MHC expression (Xu, 1994). Chronic activation of this M1 phenotype can lead to cytotoxicity by action of a positive feedback loop from initial elevated inflammation causing release of apoptotic factors and neuronal death, which releases further apoptotic factors and induces greater microglial activation. On the other hand, M2 is immunosuppressive, promoting repair and inflammatory alleviation to provide resolution to the evoked immune response (Le, 2001; Wang, 2014). Anti-inflammatory cytokines are used to suppress M1 production of pro-inflammatory cytokines, with M2-released IL4 and IL10 known to inhibit M1 release of IL6, TNF, and NO after LPS activation (Ledeboer, 2000). Microglial activation can persist through a positive feedback loop, where prolonged activation can damage viable neurons, resulting in reactive microgliosis. This function is to destroy infected neurons, viruses & bacteria, but in chronic inflammation, this response can also cause large amounts of collateral neural damage. Microglial polarisation to both M1 and M2 phenotypes has been reported to demonstrate impaired activity with suppressed reactions correlated to an ageing microenvironment (Mahbub, 2012). This muted immune response may cause further detriment by placing the elderly brain at greater risk of insult.

Microglia-neuron interactions occur as part of a healthy microenvironment. To avoid the cytotoxic effects of prolonged microglial activation, microglia maintain an inhibitory

signalling with neurons to modulate their immune response (Barclay, 2002). Age and chronic exposure to stressors can place strain on this intercellular communication, creating transferal towards an inflammatory environment (Jurgens, 2012). Neuronal-released molecules such as the glycoprotein CD200 are able to signal microglia by action on microglial CD200 receptors to help preserve their resting state (Wright, 2003). Malfunction in this signalling pathway, and disruption to CD200 communication, can induce the M1 phenotype to perpetuate inflammation (Meuth, 2008). Disruption to this CD200 signalling *in vitro* has demonstrated IL6 release, neuroinflammation and neuronal death (Meuth, 2008). Neurons also have a role in activating microglial polarisation via their release of matrix metalloproteinases (MMP) or ATP. MMP-3 is released by apoptotic neurons, and is able to selectively stimulate pro-inflammatory M1 microglial activity (Kim, 2005). Furthermore, neuronal damage can result in the extracellular dumping of ATP, which serves as a triggering mechanism to activate microglia towards the pro-inflammatory phenotype (Fields, 2000; Zhang, 2007). While microglial activation to either phenotype is a beneficial and essential instigating factor for the immune response, chronic activation can skew microglial polarisation towards the pro-inflammatory phenotype with injurious cytotoxic effects. This data implies that neuronal apoptotic cell death as seen in neurodegenerative disease, with release of pro-inflammatory signals and disturbance to anti-inflammatory pathways, helps to further propagate pro-inflammatory microglial activation, which would serve to exacerbate neurodegeneration.

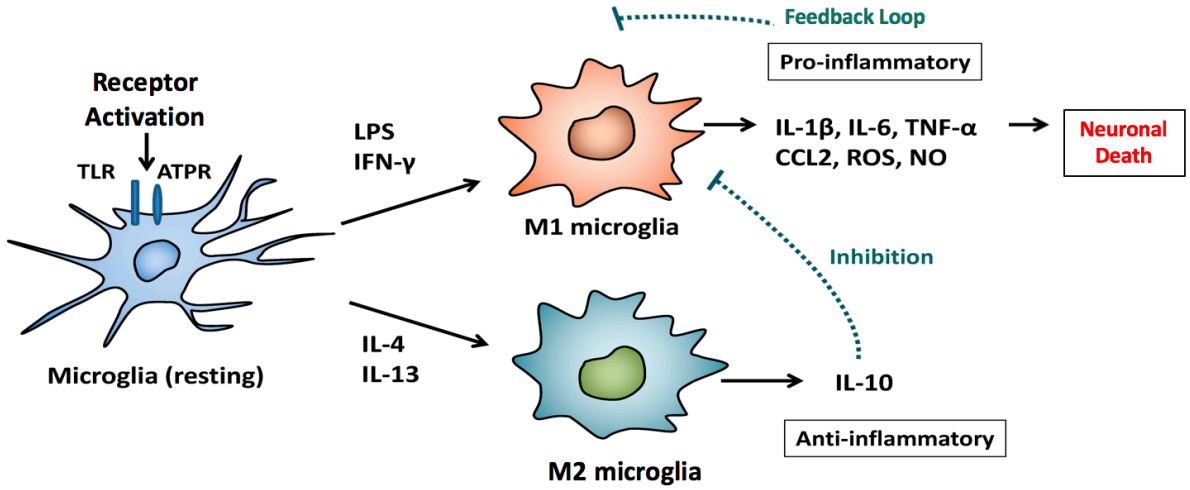

Figure 1.8 Microglial Polarisation to M1 or M2 Phenotypes
Resting microglial receptors, such as toll-like receptors (TLR) or ATP receptors (ATPR), can be stimulated to instigate expression of either microglial phenotype M1 or M2. LPS and IFNγ can skew microglial activity towards the M1 phenotype, resulting in release of pro-inflammatory cytokines, chemokines, reactive oxygen species and nitric oxide. Chronic production of these pro-inflammatory products can further activate M1 phenotype expression, leading a cascade towards neuronal death. Alternatively, IL4 and IL13 signalling pathways can skew microglial activity towards the M2 phenotype, which can release anti-inflammatory IL10 able to downregulate M1 activity. *(Image adapted from Nakagawa, 2014).*

1.7.3 Microglia in Parkinson's Disease

The SN has 4.5 times more microglia compared to other areas of the brain, leaving these neurons particularly vulnerable to deleterious effects of microglial inflammation (Kim, 2000). The initial mechanism triggering the PD microglial activation remains unknown, but PD pathology has been proven to contain high levels of iron-containing reactive microglia in nigral cells (Barcia, 2004; Ouchi, 2005; Gerhard, 2006). Elevated microglial activation and increased release of pro-inflammatory cytokines have been shown in PD, as well as in other neurodegenerative diseases including AD, HD, ALS and MS (Glezer, 2007). Pathological chronic activation of microglia can culminate in degeneration of dopaminergic neurons. The M1 phenotype for pro-inflammatory activated microglia are found surrounding dopaminergic neurons in the PD midbrain, with a positive correlation of increased M1 presence to both increased neuronal death and symptom severity (Ouchi, 2005). Aggregated α-synuclein existing as part of PD pathology are capable of promoting microglial activation, thereby enhancing toxicity to dopaminergic neurons. Furthermore, these activated microglia phagocytose α-synuclein, which then activates microglial NADPH oxidases to generate superoxide and H_2O_2 proven to mediate dopaminergic toxicity (Zhang, 2005). Oxidative bursts by microglia are also able to instigate release of Nox (Twig, 2001), providing two different mechanisms for microglia to enhance H_2O_2 production. Nox remains the prevailing source for extracellular ROS generated by microglia (Qin, 2004). H_2O_2 has been shown to mediate further microglial activation (Mander, 2006). Similarly, LPS treatment of microglia successfully activated them into releasing various inflammatory factors, but only induced dopaminergic cell death after release of H_2O_2 or NO in an *in vitro* PD model (Le, 2001). This infers a causal link between microglial activation and neuroinflammation-mediated degeneration of dopaminergic neurons.

A combination of elevated iron, ROS, α-synuclein aggregation, and factors released from traumatised neurons would cause microglial activation, which in turn would release ROS and pro-inflammatory factors. This milieu can result in dysregulation of iron regulatory proteins, leading to uncontrolled elevation in iron, which again instigates free radical generation. All enzymes affected by microglia have catalytically active iron within their ISC (Moncada, 1991), providing an additional source of intracellular iron as oxidative inhibition of enzyme activity releases this iron. The PD SN demonstrates high iron levels and downregulated ferritin storage. Neuromelanin is present in nigral cells, providing an additional iron source. High iron facilitates α-synuclein folding and aggregation, which can release H_2O_2, cause greater microglial activation and activate Nox to create more superoxide and H_2O_2. Dopaminergic

neurons generate reactive quinones and H_2O_2 during dopamine deamination, which places DA neurons in the SN at much greater vulnerability. Deamination is catalysed by iron, while MAO-B activity is enhanced by H_2O_2, causing further H_2O_2 production. ROS production correlates to disease progression as PD patients have higher OS evidence in the SN. Such high oxidant generation overrides naturally low SN antioxidant defences, causing cellular stress and mitochondrial dysfunction. There is evidence of reduced GSH and catalase activity in the PD SN. This in turn creates further ROS/RNS, while now also negatively affecting energy metabolism. Deficiencies to mitochondrial function are also accompanied by CI defects as seen in PD. Loss of ATP prevents peroxiredoxin scavenging of H_2O_2, thereby increasing its toxicity. Loss of dopaminergic neurons would initiate decomposition of dopamine with subsequent induction of additional microglial activation. Chronic positive feedback in this manner may lead to induction of apoptotic factors and demise of dopaminergic neurons, as seen in PD pathology.

1.8 Modelling Parkinson's Disease with Cell Culture

PD is a multifactorial disease with a plethora of elements contributing to its pathogenesis. *In vitro* cell culture models of disease provide an effective method to observe one or two particular factors, without any obscuring effects from others. This advantageous environment allows for controlled manipulation of specific facets of disease in order to observe the cellular response. Cell culture models also permit exploration of a particular gene or protein that may be differentially expressed during disease, or allow for investigation to follow one particular disease pathway. This is a cost-effective, robust method that provides a large number of cells at minimal cost to animal lives. As established cell lines are deprived of senescence via viral transfection, they do not fully represent parkinsonian cells, but only provide a useful model of cellular systems. Result replication using primary cell cultures accounts for this transgression, to mimic cellular behaviour and provide further understanding of their biochemical conduct in a system as close as possible to that in the brain. An advantage for control and model implementation, but an impediment to fully characterising disease pathology, is the lack of the brain microenvironment. Observation of one aspect of inflammation on one cell type may allow for efficient determination of inflammatory effects on cell behaviour, however, results cannot be fully extrapolated to explain disease progression. Co-cultures take this into account by trying to provide a more biological environment. Once certain cellular reactions and behaviours have been acquired, the cell culture model may be developed further by transference to animal models in order to provide an equivalent microenvironment. In this instance, there remains the limitations of disease instigation methods, as well as variations to animal verses human conditions.

Various models for PD are implemented via toxin or genetic manipulation according to which is more appropriate for a given experiment. Unique model systems may employ different cell types, from use of established cell lines, such as use of dopaminergic N27 cells in this thesis or alternatively, SH-SY5Y bone marrow cells expressing dopaminergic markers (Alberio, 2012), or primary cell lines as well as full animal model replications. Different mechanisms of disease instigation may also be applied to trigger PD pathology, such as LPS to observe the inflammatory response, 6-OHDA for OS, or MPTP/MPP+ administration for disruption to mitochondrial function, all leading to eventual dopaminergic neurodegeneration (Porras, 2012). *In vivo* bacterial lactacystin, PSI or MG-132 may be employed by microinjection to inhibit proteasomal activity (Bové, 2006; Xie, 2010) and induce degeneration of SN dopaminergic neurons. Such a platform allows for examination of both neuroprotective

treatments or neurotoxic consequences. Animal models may employ intracerebral or peripheral toxin injections, depending on their capacity to penetrate the blood brain barrier. Since one-time toxin exposure differs to repeated exposure in the PD brain, a design limitation here would include the requirement for repeated neurotoxin treatment. This may also be necessary due to lack of a progressive nature from toxin exposure compared to advancing disease progression seen in PD.

A second method of disease induction utilises genetic manipulation in the form of transgenic models to observe the effects of varying gene expression on disease progression. This involves overexpressing autosomal-dominant genes or using knockout genes in those that have autosomal recessive expression. For example, one such model developed α-synuclein knock-out mice to investigate the protein's role in PD pathogenesis (Lo Bianco, 2002), while another explored the neuroprotective effects of ferritin overexpression in mice dopaminergic neurons exposed to MPTP (Kaur, 2003). Familial PD has been examined via alterations to genes found with mutations in PD, including LRRK2, SYNCA, parkin, PINK1 and DJ-1 in both animal and cellular models (Dawson, 2010). These models may differ in terms of full parity with PD pathology, yet do instigate dopaminergic neurodegeneration.

Each of these disease models would differ in terms of method, time-scale, location and concentration of toxin administration, and would not provide the full scope of pathological expression seen in the PD brain. Ideally, PD models would be progressive, reliant on age, with α-synuclein deposits into Lewy bodies, and have significant dopaminergic neurons degeneration with ensuing motor dysfunction symptoms (Dawson, 2010). This is not the case with *in vitro* or *in vivo* PD models. However, they do allow for observation at various disease stages, with understanding of effects from presence or removal of certain genes, or for determination of beneficial therapeutic targets. As long as cell culture and animal model results are interpreted with attention to these shortcomings, they can prove extremely valuable. Thus, the benefits of investigating disease models outweigh the disadvantages, providing the means to deduce certain implications and correlations between pathogenetic factors that can then be translated to more advanced models from which to infer crucial informative understanding of PD pathology.

1.9 Hypothesis

The enhanced innate inflammatory response and chronic microglial activation can instigate release of pro-inflammatory factors that can trigger an increase in dopaminergic neuronal iron uptake, ultimately leading to the death of dopaminergic neurons as seen in the Parkinson's disease substantia nigra.

1.10 Aims

1.10.1 Goals

This project aims to investigate the effects of microglial activation on iron handling in mesencephalic dopaminergic neurons, and whether addition of astrocyte presence may modulate these effects. Investigation will be performed by assessment of fluctuations in iron regulatory proteins, including hepcidin, ferroportin, ferritin, transferrin receptors, divalent metal transporter 1, aconitase 1, and iron responsive element-binding protein 2, in microglia, dopaminergic neuron and astrocyte cell cultures following exposure to LPS-activated microglia-released inflammatory factors.

The methodology employed to investigate these goals includes quantification of microglial-released inflammatory factors by Griess assay, H_2O_2 assay or enzyme-linked immunosorbent assay (ELISA). Three murine cell lines were utilised, including astrocytes (C6), microglia (N9), and dopaminergic neurons (N27). N27 culture results were replicated using primary neuronal cultures. Cells were treated with either LPS, activated microglial-released inflammatory factors in conditioned medium, pro-inflammatory cytokines, H_2O_2, or catalase. Determination of changes to intracellular iron levels was performed via the ferrocene assay, while gene expression of iron regulatory proteins was determined via polymerase chain reaction (PCR) DNA amplification. After individual examination in mono-culture, experiments were conducted on co-cultures and tri-cultures using Transwell plates to detect any variations to preceding results. Lastly, downstream effects of altered iron metabolism were examined to investigate changes to neuronal OS, mitochondrial membrane potential or apoptosis and necrosis initiation using fluorescent microscopy or flow cytometry.

Any observed changes may result from inflammation-triggered alterations in gene expression of these iron regulatory proteins, with downstream pathways that may eventually lead to neuronal degeneration. Since dopaminergic neurons in PD are particularly susceptible to iron overload and inflammatory exposure, it is vital to determine what is causing the observed increases in iron, and which specific regulatory proteins are being affected by the inflammation. Such discoveries could lead to significant improvements in therapeutic strategies for PD.

CHAPTER 2:

Materials and Methods

2. Materials and Methods

This chapter outlines the various materials and methods utilised to examine the microglial inflammatory response and its effects on dopaminergic neuron iron metabolism. This includes *in vitro* microglial, astrocytic and neuronal cell culture experimental protocols. Detailed methods for the cellular assays employed to investigate inflammatory effects following microglial activation are also included, such as cytokine production and cell viability. Similarly included are the materials and methods pertaining to direct cytokine treatments, H_2O_2 assays, iron detection and determination of iron regulatory protein gene expression. Lastly, downstream effects of changes in neuronal iron handling were determined via fluorescent probes, with comprehensive descriptions of determination of cellular OS, mitochondrial membrane potential, and apoptosis and necrosis.

2.1 *In Vitro* Cell Culture Experiments

2.1.1. Introduction

In vitro cell culture is used as a model system to study cell physiology. Immortalised cell lines have been isolated from cancers or altered by retroviral transfection to inhibit genes that initiate senescence, thus becoming able to allow the cell cycle to continue with growth and multiplication. Continuous cell division provides a large number of cells without the need for large numbers of animals, thus leading to more cost-effective experimentation on identical phenotype replicates, allowing for reproducible results in a short period of time. Cultures provide samples consisting of cells with equal purity, which therefore provide a standard quality to allow for greater consistency and reproducibility. In order to determine the effects of microglial inflammatory factors on iron handling, a model observing aspects of Parkinsonian physiology was implemented *in vitro*, utilising three distinct cell lines to represent astrocytes, microglia and neurons. This allowed for individual investigations into changes in neuronal behaviour, neuroinflammation after microglial activation, and co-culturing with potentially neuroprotective astrocytes. Optimisation of exposure times and toxin concentrations was determined in order to provide the greatest microglial activation without sacrificing cell viability or leading to overstimulation or cytotoxicity. This elicited microglial activation was then used to simulate neuronal inflammation, whereupon a variety of assays was executed to monitor for changes in iron levels and gene expression. Distinct treatments in this cell culture model allowed for examination of specific mechanisms of cellular iron regulatory processes, removing the added complication of studying entire brain physiology. Pure *in vitro* cultures permits any significant results to be indubitably attributed to a specific cell type, as opposed to the intact brain. Such individualised observations coupled with co-culture and primary culture experimentation provide a more complete view of cellular interactions during iron metabolism within a diseased system, which could be tied to physiological processes occurring during PD neurodegeneration in the brain.

2.1.2 Cell Culture Methods and Consumables

All cell culture experiments were conducted under sterile conditions, using ultraviolet-irradiated ventilation hoods, treated with 70% ethanol before and after each use, and with monthly Virkon sterilisation so as to minimise the risk of culture contamination. Equipment was either purchased as sterile, or autoclaved or disinfected with 70% ethanol prior to use, in order to ensure an aseptic environment.

Cells were incubated at 37ºC in a humidified environment under slightly acidic conditions to maintain optimum pH levels by means of supplementation with 5% carbon dioxide throughout all cell culture work. All media was warmed to 37ºC prior to use in a water reservoir containing autoclaved water treated with Aqua-Stabil water bath protective media (Sigma), to avoid any shock on the cells. Microglia were passaged after reaching ~70% confluency, while neurons and astrocytes were passaged closer to full confluency. Cell culture flasks ($25cm^3$, $75cm^3$, $150cm^3$), scrapers, pipette tips (10/20µl, 200µl, 1ml), eppendorf tubes (2.5ml & 500µl), plates (6, 12, 96 well plates), serological pipettes, and glass Pasteur pipettes were ordered from VWR (UK). Other consumables include Falcon centrifuge tubes (15ml & 50ml) (Scientific Labs, UK), cryogenic vials (Thermo Scientific), lipopolysaccharide (LPS) from Salmonella Minnesota (Enzo Life Sciences), Roswell Park Memorial Institute neuronal medium (RPMI) (Lonza), Distritips (Gilson), and transwell inserts (Appleton Woods). Trizma Base, weighing boats, protease inhibitor cocktail, RIPA buffer, heat-inactivated fetal bovine serum (FBS), L-glutamine, penicillin-streptomycin, Dulbecco's Phosphate Buffered Saline (PBS), Dulbecco's Modified Eagle's Medium (DMEM), Hank's Balanced Salt Solution (HBSS), M199 medium, Griess reagent, syringe filters, syringe luer lock tips, toluidine blue, Trypsin-EDTA were all purchased from Sigma (UK).

2.1.3 N9 Cell Line

Microglial N9 cells, originating from oncogenic retroviral transformation of murine embryonic 13-day primary microglial cells (Righi, 1989). N9 cells were gifted to the laboratory, with a frozen stock that was maintained after use and stored in liquid nitrogen, while short-term stock was stored in -80ºC. These cells were utilised in all microglial experiments. N9 cells were utilised for cell model experiments after first demonstrating evidence of certain microglial characteristics, including presentation of phenotypic microglial markers detailed below, as well as the ability to produce and release pro-inflammatory cytokines (IL1ß, IL6, TNF). Use of N9 cells allows for initiation of the microglial inflammatory response, in order to expose dopaminergic neurons to this inflammation for determination of its effects on iron metabolism. Cells were grown and cultured in DMEM (Sigma, D5796), supplemented with 5% heat-inactivated sterile-filtered FBS (BioSera, F1000), 8mM L-glutamine (Sigma, G7513), and 50 U/ml penicillin and 50 µg/ml streptomycin (Sigma, P4333). This supplemented solution, referred to as complete microglial medium, was used in conjunction with all N9 cell work. Microglial activation was achieved via treatment with LPS.

N9 cells maintain a microglial phenotype, as established by selective expression of Iba1 protein as detected by Western Blot analysis. Iba1, or ionised calcium-binding adaptor molecule 1, is a macrophage-specific cytoplasmic protein expressed in microglia within the brain, however not in neurons or astrocytes, and is involved in regulation of microglial activation (Ito, 1998). Immunoblotting results demonstrated no Iba1 in neuronal cells and an increasing Iba1 concentration proportional to an increasing cell density of N9 cells (Figure 2.1). Microglia have varying morphologies, reliant on their present activation state. Resting microglia have larger cell bodies and extended, ramified processes to allow for detection of any alterations in their surrounding microenvironment (Torres-Platas, 2014). Detection of any such changes results in instigation of cellular activation, and corresponding reversible changes in morphological stages from primed, to reactive and finally leading to smaller, more dynamic, amoeboid cells with significantly fewer and shorter processes, allowing for faster movement to carry out phagocytosis of any offending substances (Torres-Platas, 2014). Microscopic examination of N9 cells revealed a ramified phenotype, as would be expected of resting microglia.

Microglial cells can be activated by various mechanisms. N9s also display activation after treatment with lipopolysaccharide (LPS), an endotoxin derived from gram-negative bacterial cell membranes. Its ability to powerfully activate an innate microglial inflammatory response makes LPS usage common in animal model experiments. LPS treatment initiates inflammation upon binding microglia-expressed toll-like receptor 4 (TLR4) (Zhang, 2014), which instigates a TLR4-dependent degenerative pathway with a signalling cascade inducing activation of nuclear factor kappa-light-chain-enhancer of activated B cells (NFκB), which can in turn lead to neuronal degeneration (Castaño, 1998; Jung 2005),

The resultant microglial inflammation is evidenced by an LPS-induced cellular activation with a change in morphology to an M1 microglial phenotype (Orihuela, 2016) presenting an activated amoeboid state with withdrawn processes, release of pro-inflammatory cytokines including IL1, IL6 and TNF, and initiation of nitric oxide production (as demonstrated in Figure 2.8). This property makes the N9 cells ideally suited to monitor the physiological effects of microglial stimulation, activation, and resultant inflammation *in vitro*.

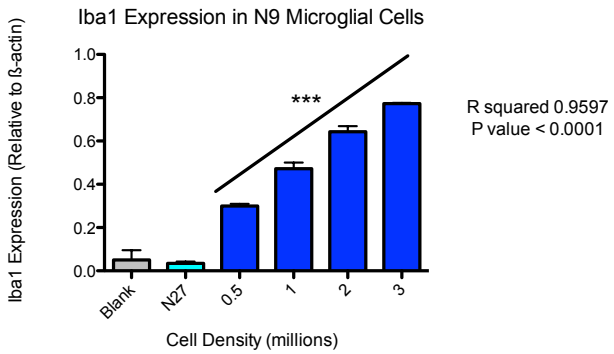

Figure 2.1 Iba1 Protein Expression in N9 Microglial Cells and N27 Dopaminergic Neurons as Determined by Western Blot Analysis. Microglial marker Iba1 protein expression was confirmed via Western blot immunolabelling of N9 and N27 lysates incubated with the anti-Iba1 antibody at 4ºC overnight. The N27 lysates, seeded at a density of 2 x 10^6 cells/well, served as the negative control. The antibody for ßactin, which has ubiquitous cellular expression, was used as a loading control to ensure equal sample loading within all wells and successful protein transfer. With a molecular weight ~42kDa, this is sufficiently different from that of Iba1, and therefore a decent target to act as loading control. All cell lysates were added at an equal volume of 14µl per immunoblot well. The graph depicts the mean ± SEM from densitometry analysis of Iba1 protein normalised to the ßactin loading control. Immunoreactivity was observed exclusively on N9 cell lysates at around 17kDa, which is the predicted molecular weight for Iba1. Increasing Iba1 expression along with increasing N9 cell density proves a microglial phenotype in N9 cells, with no evidence of Iba1 expression in the N27 neuronal cell line. The linear regression p value is < 0.0001, with a line of best fit having an r^2 value of 0.9597. *Statistical significance is denoted via asterisks: ***p<0.05. n=3 for all experimental conditions.*

2.1.4 N27 Cell Line

N27 neuronal cells were derived from immortalised foetal rat mesencephalic cells (a kind gift from Dr Nabil Hajji, Imperial College London). Cloned dopaminergic cells were prepared by transfection, and were shown to generate homovanillic acid after several periods of growth (Prasad, 1994). Homovanillic acid is a dopamine metabolite, so its presence helps affirm that this cell line has a dopaminergic physiology. N27 cells also preserve expression of dopaminergic markers, including tyrosine hydroxylase (TH) and neuronal nuclei (NeuN), as confirmed via Western Blot (Figure 2.2). TH is the rate-limiting enzyme that catalyses hydroxylation of L-tyrosine to L-DOPA during dopamine synthesis. NeuN is a neuronal marker found in most neuronal cells, excluding Purkinje and mitral cells in the cerebellum and olfactory bulb, respectively, with a higher immunoreactivity found in mature neurons (Mullen, 1992). Western Blot analysis demonstrated the absence of either TH or NeuN protein in N9 microglial cells, whilst TH and NeuN (46 and 48kDa) protein levels increased relative to N27 cell density. Since iron accumulates within nigrostriatal dopaminergic neurons in PD (Dexter, 1989), these N27 mesencephalic dopaminergic neurons are ideally suited to serve as an appropriate cell line to investigate iron metabolism. Specifically defined parameters allow for valid comparisons to be drawn between N27 cells and normal dopaminergic neurons, without added complications from various influences present within the intact brain. Usage of N27 cells allowed for the study of the effects of microglial inflammation on iron metabolism in

dopaminergic neurons via treatment with microglial conditioned medium, an established method of studying effects of inflammation on a single culture *in vitro* (Röhl, 2008; Zhu, 2010).

Cells were cultured in Roswell Park Memorial Institute (RPMI)-1640 medium (Sigma, BE), supplemented with 5% filter-sterilised FBS, 8mM L-glutamine, and 50 U/ml penicillin and 50µg/ml streptomycin (Sigma, P4333), referred to as complete N27 medium. This medium was utilised throughout for any N27 cell work. N27 cells were used for all immortalised neuronal cell culture experiments.

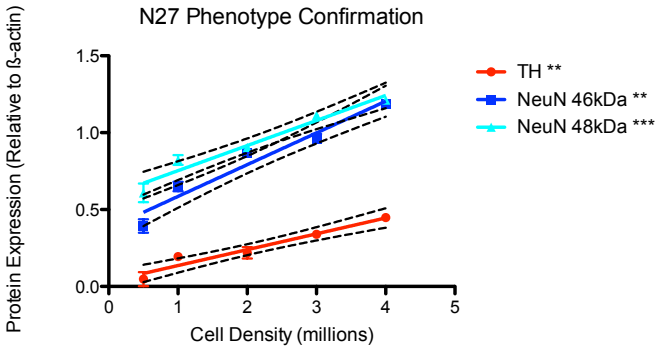

Figure 2.2 NeuN and Tyrosine Hydroxylase Protein Expression in N27 Dopaminergic Neurons and N9 Microglia as Determined by Western Blot Analysis. Expression of TH, NeuN 46kDa and NeuN 48kDa proteins was determined via Western blot immunolabelling of N9 and N27 lysates incubated with an anti-TH antibody and an anti-NeuN antibody, along with 0.01% sodium azide and 1% BSA at room temperature overnight. ßactin antibody was used as a loading control to ensure equal sample loading across all wells and successful protein transfer. N9 lysates served as the negative control. The graph depicts the linear regression analysis with dotted lines representing ± 95% confidence intervals for all three dopaminergic markers. NeuN antibody immunoreactivity established a neuronal phenotype, with linear regression analysis resulting in 48kDa= $p<0.0003$***, $r^2=0.797$, and 46kDa= $p<0.002$**, $r^2=0.804$. The TH marker confirmed the presence of catecholaminergic neurons, by displaying increasing expression proportional to increasing N27 cell density, with linear regression p value=0.0012, $r^2=0.85$. Immunoreactivity was observed exclusively on N27 cell lysates at around 60kDa, which is the predicted molecular weight for TH, and two bands at 46kDa and 48kDa for NeuN. As expected, no expression of either NeuN or TH proteins were observed in the N9 microglial cell line. *Statistical significance is denoted by asterisks: **p<0.01, ***p<0.001. n=3 for all experimental conditions.*

2.1.5 C6 Cell Line

The C6 astrocytic clonal cell line derived from cultured rat astrogliomas (Benda, 1968), acquired from the European Collection of Cell Cultures (ECACC) (Porton Down, Wiltshire), is used as a model of *in vitro* glial physiology. This cell line has been useful in the observations of various astrocytic cellular properties, from the consequences of LPS (Galea, 1992; Xu, 2000; Kim, 2006), inflammatory cytokines and H_2O_2 treatmemts (Feinstein, 1994; Simmons, 1993; Das, 2008), to neuroprotective effects (Flier, 2009; Quincozes-Santos, 2008). C6 maintain glial fibrillary acidic protein (GFAP) expression, which is a useful astrocytic identifier as it is the main cytoskeletal filament protein found in astrocytes within the central nervous system, and is involved in astrocytic activation (Eng, 2000; Min, 2013; Goswami, 2015). GFAP expression

was confirmed via immunoblotting (Figure 2.3). C6 have also been shown to express other astrocytic markers, and one study completed a thorough profile of C6 gene expression compared to that in untransformed primary rat astrocytes (Gunnersen, 2000). While there were a few genes with either higher or reduced expression levels in C6, this study confirms a great similarity in gene expression between the C6 cell line and normal astrocytes. Thus, C6 were determined to be a suitable cell line for use in this project.

Cells were grown in a separate growth medium from other cell lines for continuity with previous lab work. C6 were cultured in Medium 199 (M199) with Earle's salts (Sigma, M4530), supplemented with 10% sterile filtered FBS, 2% L-glutamine, and 50 U/ml penicillin and 50µg/ml streptomycin, hereafter referred to as complete C6 medium, and applied for any further C6 cell work.

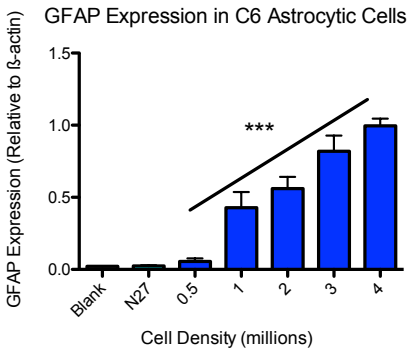

Figure 2.3 GFAP Protein Expression in C6 Astrocytes and N27 Dopaminergic Neurons as Determined by Western Blot Analysis. Expression of GFAP protein was determined via Western blot immunolabelling of C6 and N27 lysates incubated with an anti-GFAP antibody at 4ºC overnight. N27 lysates served as the negative control, while results were normalised to a ßactin loading control. Immunoreactivity was observed exclusively on C6 cell lysates at around 55kDa, which is the predicted molecular weight for GFAP. GFAP immunoreactivity was observed in C6 astrocytes only, with a directly proportional increase in reactivity to cellular concentration. The graph depicts the mean ± SEM for all data, with linear regression trend having a p value <0.0001***, and r^2=0.867, establishing the evidence for a significantly increasing GFAP presence proportional to increasing cell density. *Statistical significance is denoted via asterisks: ***p<0.001. n=3 for all experimental conditions.*

2.1.6 Primary Hippocampal Neuronal Culture

Once experiments have been optimised and results replicated consistently in secondary cultures, it is useful to next monitor behaviour in primary cultures. Primary cultures are less time and cost effective than immortalised cells, with a limited number of cells, however provide a closer representation of the original phenotype. While work for this thesis was previously done utilising the dopaminergic N27 cell line, primary cultures were performed using hippocampal cells. This was partly due to the fact that hippocampal neurons have a higher yield, maintaining a percentage of about 2-3% glial cells compared to neurons, while dopaminergic neurons retain about 70-80% glia depending on isolation methods. Since glial

presence may have neuroprotective effects, it was deemed more effective to duplicate results in a more isolated neuronal population.

Primary hippocampal neurons were isolated from Wistar rat pups at embryonic day 18-19 (E18-19). All equipment was sterilised and sprayed with ethanol. A sacrificed pregnant rat was sprayed with ethanol, and the abdominal cavity sliced open. The amniotic sac was removed and cut open. Each fetus, total number depending on the rat and viability, was fully decapitated. The brains were excised and placed in a petri dish with ice cold fluid, containing freshly prepared, sterile-filtered solution containing standard Krebs buffer, 20mM HEPES and 0.03% $MgSO_4$ at pH 7.2. Using a microscope, hippocampi were removed and cleaned from excess brain matter and blood vessels. The isolated tissue was mechanically broken down with a sterile blade. 1ml warmed trypsin was added to tissue, and cells collected into a clean 15ml falcon tube. Cells were incubated 4 minutes in the trypsin, after which ~4ml of a mild trypsin inhibitor was added. The tube was centrifuged (1100rpm, 3m), whereupon as much liquid as possible was removed by pipetting, with care to not disturb cells. The pellet was gently resuspended in 1ml of trypsin inhibitor, at double the concentration of the first one. This was repeated for a total of 3ml, and incubated 1 minute to allow tissue fragments to sediment at the bottom of the tube. The top layer of cells was gently transferred via pipette to a clean falcon tube, with 7ml neurobasal medium, and centrifuged (1000rpm, 5m). The supernatant was carefully pipetted out, without disturbing the cell pellet, which was then resuspended very gently in 1ml neurobasal medium. This was repeated 1-2 more times. This portion of the primary culture preparation was performed by Darya Kiryushko, who had acquired the appropriate licencing to execute such work. Cells were counted on a haemocytometer and appropriate dilutions made for plating, using warmed sterile-filtered complete primary neuronal medium as described below. Higher cellular densities were plated than with immortalised cell lines since primary cells do not proliferate and a higher percentage may die. Roughly 650,000 cells were seeded, to compensate for any cells that may die after plating.

Primary neurons were grown in a special medium made fresh before each extraction, consisting of 46ml Neurobasal-A medium (Life Technologies, A1371001), 1ml B27 supplement (ThermoFisher, 17504-044), 0.5ml penicillin/streptomycin, 0.5ml GlutaMAX supplement (ThermoFisher, 35050038), and 2ml 1M HEPES buffer (Sigma, H3537), henceforth referred to as complete primary neuronal medium. The medium was adjusted to a pH of 7.2, then filtered to ensure sterility. As primary cultures will not adhere directly to plastic, plates had to first be coated with a natural substrate. First, 15% poly-L-ornithine solution (Sigma, P4957) diluted in sterile-filtered PBS (6wp=1ml, 12wp=0.5ml) was added to wells and

incubated for 2 hours at 37ºC. Plates were then thoroughly washed three times with sterile-filtered PBS to ensure any unbound ornithine was washed off. Immediately after washing, 1ml laminin from Engelbreth-Holm-Swarm murine sarcoma basement membrane (Sigma, L2020) (diluted to 4.16µg/ml in PBS) was added to each well, and the plates were incubated overnight. Solutions were discarded just before plating to ensure the laminin did not dry out. Once primary cells were plated, they were allowed to rest 24h to ensure treatment was not affected by stress from the plating procedure. Treatment procedures were consistent with those of the immortalised cell lines.

2.2 Cellular Protocols

2.2.1 Cell Freezing

Once N27 and C6 reach full confluency, and N9 reach ~70% confluency, cells were detached according to their specific methods, then transferred to a 50ml Falcon tube and pelleted by centrifugation (1200rpm, 5min). The cellular pellet was resuspended in 1ml warmed freezing medium, containing the appropriate cellular medium along with 2% L-Glutamine, 10% FBS, and 10% DMSO added dropwise to avoid osmotic shock. Cells were then counted and diluted appropriately to achieve a density of ~200,000 cells/ml, and transferred to cryovials in 1ml aliquots. Cryovials were frozen at -20ºC for 1 hour in a Mr Frosty freezing container, which maintains a measured 1ºC/min cryopreservation cooling speed. Vials were then moved to -80ºC for short term or into liquid nitrogen for long term cold storage.

2.2.2 Cell Thawing

Frozen cell line aliquots were removed from cold storage and rapidly thawed using 1ml warmed complete medium according to cell type added directly to the cryovial. This solution was then warmed in the 37ºC water bath until fully thawed, at which point, cells were pipetted into a 50ml Falcon tube with the addition of 10ml complete medium and centrifuged (1200rpm, 5min). The supernatant containing dimethyl sulfoxide (DMSO) was discarded, and pelleted cells were resuspended in warmed complete medium. This solution was then carefully transferred to a $25cm^3$ sterile cell culture flask (VWR, 734-0044) with an additional 5ml medium and incubated at 37ºC for cells to become confluent, whereupon cells were appropriately detached and passaged to a $75cm^2$ flask to continue subcultivation.

2.2.3 Cell Passaging

Every couple days, once cells have reached confluency (~70% for N9, ~90% for N27 and C6), they were passaged for plating or for transfer into fresh flasks. The maximum passage number used was up to 40, after which cells were discarded and a fresh aliquot defrosted. N9 passaging involved discarding old medium and washing cells with warmed fresh complete microglial medium to remove any floating dead cells. Flasks were scraped thoroughly with a sterile rubber policeman cell scraper (VWR, 734-0386), and cells were collected twice into a 50ml Falcon using complete medium.

N27 and C6 had a different passaging technique, as mechanical removal may overstress these cell types. Once the old medium was discarded, cells were gently washed twice with warmed phosphate buffered saline (PBS) in N27 and Hank's Balanced Salt Solution (HBSS)

in C6. Both are saline solutions added to ensure removal of any remaining medium, which contains trypsin inhibiting serum. Next, a minimal volume, depending on flask size, of warmed trypsin-EDTA (Sigma, T4049) was added for about 2 minutes. After trypsin incubation, flasks were tapped gently on the sides to dislodge cells. Cells were checked briefly under the inverted microscope to confirm loss of adhesion and dispersal of the cell layer, then transferred to a fresh 50cm^3 falcon tube via two collections with warmed complete appropriate growth medium. The falcon containing suspended cells was then centrifuged (1200rpm, 5min), after which the supernatant was discarded and the cell pellet was resuspended with 1ml fresh appropriate medium. A suitable amount of medium was added as dilution according to pellet size. Cells were then transferred to a fresh sterile cell culture vessel for incubation or counted and plated for direct use. Primary neurons were not passaged.

2.2.4 Cell Counting and Plating

Viable cells were counted using a haemocytometer. 10µl of cell suspension was added to 10µl Trypan blue solution (Sigma, T8154). Since the stain can only be absorbed by damaged or dead cells, it is a useful method in determining cell viability. The cell suspension stain solution was mixed thoroughly by pipetting, to allow the stain to be taken up by damaged cells, then 10µl loaded onto the haemocytometer with a glass coverslip. Unstained cells were counted under the microscope within a 4 x 4 quadrant within a 0.1mm^3 area, using the same counting methods each time. Dilutions were then calculated based on total volume and the desired cell density, the appropriate complete medium was added, whereupon cells were seeded into 6, 12, or 96 well plates at a density depending on the individual experiment and incubation time. After seeding, cells were left to rest 24h to ensure they returned to resting morphology, thus avoiding experimentation on stressed cells.

2.2.5 Transwell Co-Culture Systems

Once cells were incubated and examined individually in mono-cultures, a permeable Transwell co-culture system was implemented to observe any changes in cellular behaviour within a more realistic environment. Mono-culture experiments involved treatment of neuronal and astrocytic cultures with a one-time exposure to pro-inflammatory supernatant from activated microglia for varying time periods. However, short lived inflammatory mediators such as free radicals (Li, 2005) may be lost during the longer microglial incubation periods or in the transfer of conditioned media. Co-culture systems deliver exposure for extended periods of time, thus providing a more realistic framework representative of the PD brain. Transwell inserts used (Appleton Woods, 3450) had a larger surface area (6wp) to ensure adequate protein

extraction in consequent assays, with a 0.4µm porous semi-permeable filter membrane to ensure sufficient permeability for any soluble and secreted factors, whilst maintaining cell separation.

2.2.5.1 Co-Culture

N27 cells were plated at the bottom of the cell plate at a density of 300,000c/w in complete N27 medium. Once cells had adhered (after ~1h), the Transwell insert was placed on top of N27s, and N9 cells were seeded within the insert at a lower density ~250,000c/w, and left to rest overnight (Figure 2.4). Equilibrium, reached with a volume of 2.6ml below and 1.5ml within the Transwell insert, must be monitored and maintained throughout experimentation. Once N27 and N9 cultures were established on opposite sides of the Transwell semi-permeable membrane, cells were ready for treatment exposure.

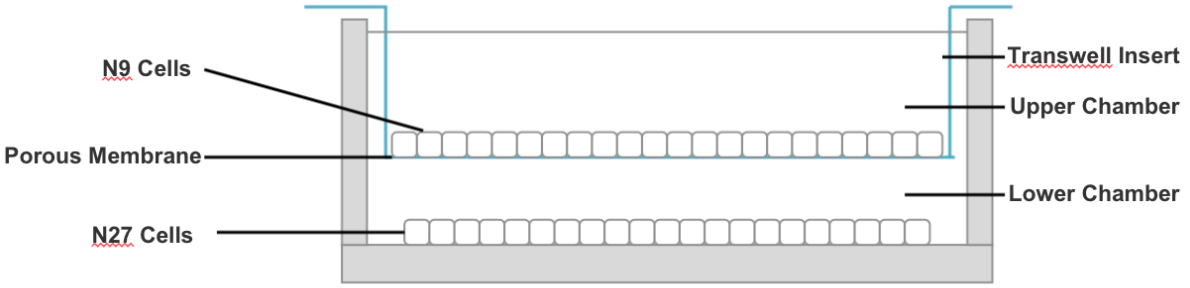

Figure 2.4 2-Transwell Co-Culture System
A schematic representation of the 2-Transwell co-culture system. N9 cells were seeded (250,000c/w) into the upper chamber of the Transwell insert, after N27 cells had been seeded (300,000c/w) in the lower chamber. After resting (24h), N9 cells were treated with LPS (0.25µg/ml 24h).

2.2.5.2 Tri-Culture

In order to observe a more complete model structure, a tri-culture system was created where C6 cells were seeded onto the underside of the Transwell insert. First, the incubator was thoroughly cleaned and humidity levels carefully monitored. Then N9 cells were seeded to the base of a 6wp (300,000c/w), covered and left to rest overnight. Meanwhile, Transwell inserts were carefully turned upside down using sterile forceps onto the inside of a sterile plate lid. C6 cells were carefully seeded onto the centre of the upside down inserts (125,000c/w in 200µl) and incubated (3h), during which time the liquid level was monitored and topped up with fresh warmed complete C6 medium (Figure 2.5A). After incubation and cell adhesion, the inserts were flipped back upright into a 6 well plate and N27 cells were seeded into the top of the insert (200,000c/w). The medium used henceforth was complete N27 medium. Cells were left to incubate overnight, whereupon the tri-culture system was ready for treatment (Figure 2.5B).

A

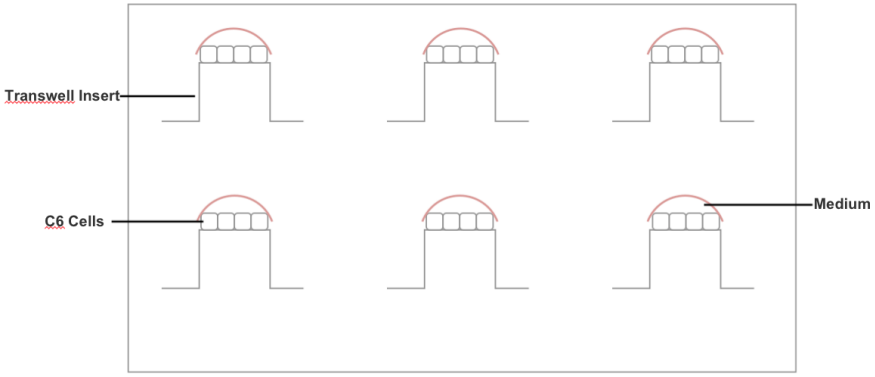

B

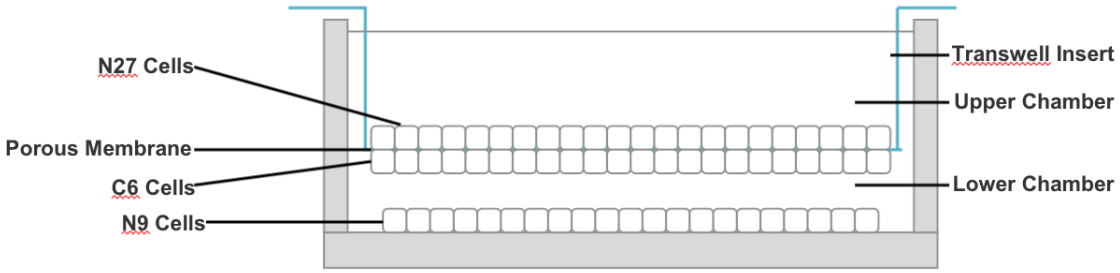

Figure 2.5 3-Transwell Tri-Culture System
A schematic representation of the 3-Transwell tri-culture system. N9 cells were seeded (300,000c/w) into 6 well plates. Separately, C6 cells were carefully seeded (125,000c/w in 200µl) onto upturned Transwell inserts (A) for 3h to ensure cell adhesion. They were then inserted into blank wells with 2.6ml cRPMI, whereupon N27 cells were seeded (200,000c/w) into the upper Transwell chamber (B) with 1.5ml cRPMI. After resting 24h, N9 cells were pulse activated with LPS (2h), subsequently washed twice with warm cRPMI to remove any residual LPS traces and then the N27/C6 insert was placed gently on top of the activated N9 cells.

2.3 Cellular Treatments

2.3.1 LPS and Conditioned Medium Treatments

2.3.1.1 LPS

PD pathology includes prolonged stimulation of the CNS innate immune response, with continued microglial activation, that eventually contributes to neuronal damage and degeneration. To mimic this reaction in a cell culture model, administration of the bacterial endotoxin LPS was used to induce the immune response and thus activate the microglial cells into releasing pro-inflammatory factors. LPS is known to instigate a strong microglial response *in vivo* via the Toll-Like Receptor 4 signalling pathway (Carvey, 2003; Qin, 2005). Rough-form lipopolysaccharide for *in vitro* activation, purified from *Salmonella minnesota* (Enzo Life Sciences, ALX-581-008-L002), was diluted from stock concentration (1mg/ml) with deionised H_2O to the appropriate dosages for cellular treatment.

2.3.1.2 Microglial Treatment with LPS in Mono-Culture

Once N9 microglial cells were seeded (350,000c/w in a 6wp) and rested (24h), LPS dilutions were added directly to the well plates. The corresponding volume to be added was first carefully removed from the cell culture medium without disrupting any cells, to ensure a constant volume throughout experimentation. After the desired incubation periods (0-24h), the microglial supernatant was collected into eppendorfs for quantifiable assessment of released inflammatory factors via ELISA (IL1ß, IL6, TNF) or Griess assay (nitrite ions) (Figure 2.6). Once the optimum LPS concentration was established, N9 cells were also analysed for changes in gene expression and iron concentrations, respectively via RT-PCR and ferrocene assays.

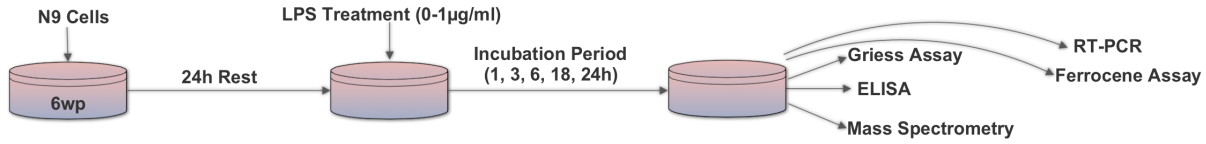

Figure 2.6 Schematic Representation of Microglial LPS Treatment Protocol
N9 microglial cells were seeded (350,000c/w) and then left overnight to return to their resting morphology. Cells were then treated with varying LPS concentrations, and left to incubate for 1-24h. The culture supernatant was collected, and used to quantify levels of released microglial factors. After optimising the LPS dosage (*Section 2.3.1.4*) to elicit a robust inflammatory response, microglial cells were lysed after treatment for analysis of any changes to iron metabolism via RT-PCR or ferrocene assays.

2.3.1.3 Exposure to Conditioned Medium

Once an optimised LPS concentration and exposure time to elicit the greatest inflammatory response was determined, microglial cells were accordingly activated to release inflammatory factors into the cell culture supernatant. This microglial conditioned medium (MCM) was collected and used to expose N27 and C6 cells to the inflammatory elements, after which the cells were monitored for any changes in iron levels and gene expression of iron regulatory proteins.

First, N9 cells were plated (350,000 c/w 6wp) and left to rest (24h). The optimum LPS dosage (0.25µg/ml) was used to treat cells for the optimum exposure time (24h), in an attempt to induce the most robust inflammatory response. Meanwhile, N27 or C6 were seeded (respectively 500,000 and 300,000 c/w) in 6wp, then left to rest (24h). Wells were aspirated and washed in warm PBS to ensure removal of any cellular debris or dead cells if present, then 1.5ml of the collected MCM was transferred to the wells with 0.5ml of fresh complete medium according to cell type. Cells were left to incubate for a range of times, after which cells were lysed for use in various assays (Figure 2.7).

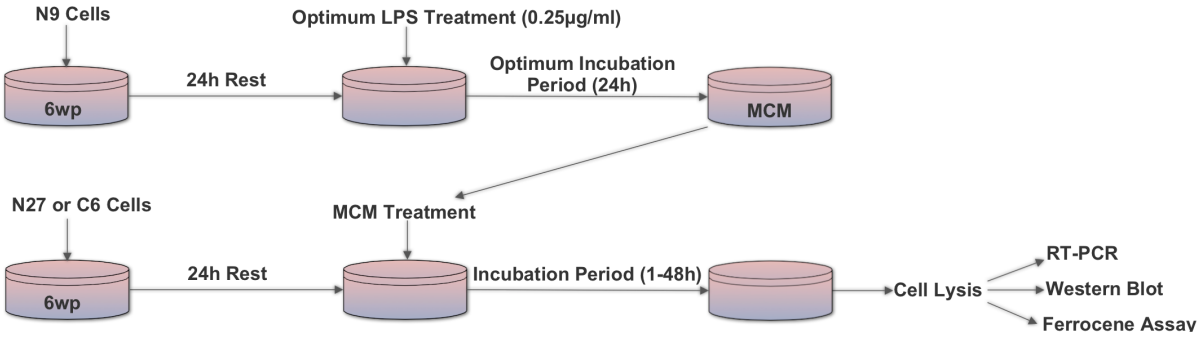

Figure 2.7 Schematic Representation of Microglial Conditioned Media Protocol
N9 microglial cells were seeded (350,000 c/w) and then left to rest (24h) to return to their resting morphology. After optimisation, they were then treated with LPS (0.25µg/ml) and left to incubate (24h). This conditioned medium was collected from wells, and transferred to wells containing various other cell types (N27 and C6) that were previously seeded (respectively 500,000 and 300,000 c/w) and rested (24h). Cells were exposed to MCM for a range of times, and then lysed for assessment via different assays.

2.3.1.4 Optimisation of LPS Concentrations for MCM Treatments

N9 microglial cells were treated with a range of LPS concentrations or a vehicle control for various exposure time points, after which culture supernatant was collected in order to create a time-dose response via assessment of microglial activation and their release of inflammatory factors from different cellular assays. This included information from ELISA assays to determine microglial release of pro-inflammatory cytokines, including IL1ß, IL6 and TNF, as well as nitric oxide quantification via determination of nitrite ion concentration using the Griess assay (Figure 2.8 A-D). Results display an increasing level of cytokines released into the cell culture medium, with significance beginning at 3h of LPS exposure and increasing up to 24h. Levels of cytokines concur with previous studies (Nakamura, 1999; Lund, 2006), with the greatest and fastest increase first from TNF, followed by IL6, NO and lastly IL1ß. Regarding Nakamura's study, they similarly found that IL6 peaked around 24h, while IL1ß peaked just before that at around 15h. Contrarily, they report that TNF began to drop after 6h, however, this study's TNF results continually increase up to 24h. It is possible that the slight differences can be due to species variations since their studies were conducted using primary rat cultures, as opposed to retrovirally transformed murine cells. In this study, IL6, TNF and NO showed significant increases with all LPS concentrations ranging from 0.0625-1µg/ml, while IL1ß only exhibited greater significance for the higher doses of 1 and 0.25µg/ml. So to ensure sufficient cytokine expression, either a dose of 1 or 0.25µg/ml must be chosen. Analysis of LPS treatment data led to determination that 24h incubation presented the greatest inflammatory reaction, and 0.25µg/ml LPS was selected as sufficient to elicit a microglial inflammatory response at a sub-maximal dosage. Thus, 0.25µg/ml was the nominated optimal LPS concentration for use in all ensuing experimentation to elicit a strong inflammatory response whilst maintaining a sub-maximal dosage to conserve cell viability. Since the longest incubation period was 24h, cell viability tests were next performed at that exposure time.

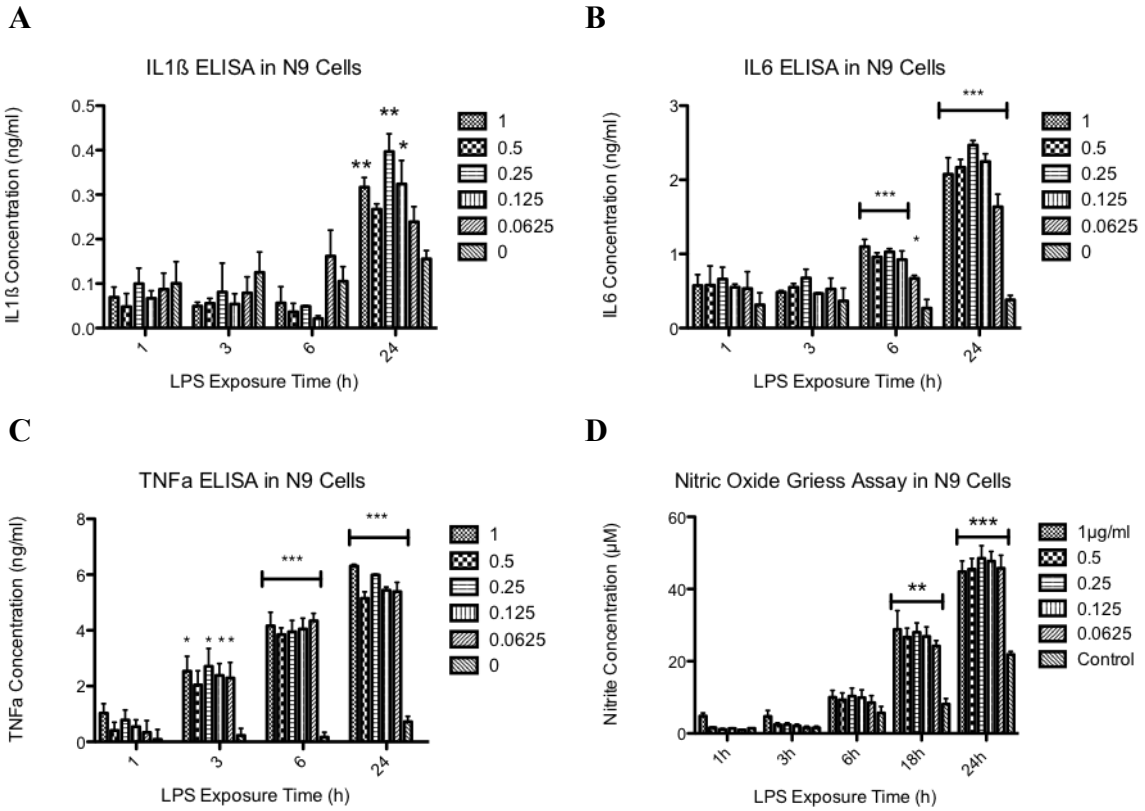

Figure 2.8 Optimising Release of Microglial Inflammatory Factors in N9 Cells for Successive Treatments with ELISA and Griess Assays N9 cells were treated with a range of LPS concentrations for various incubation periods in order to observe the inflammatory response. Following LPS incubation, the cell culture supernatant was removed for testing. ELISA assays were carried out to determine the levels of pro-inflammatory cytokines (IL1ß, IL6, TNF; respectively A, B, C) released by activated microglia, while the Griess assay allowed for the determination of nitric oxide in the supernatant (D). Results reveal significance compared to control at higher incubation periods. *Asterisks denote a statistical significance from control: *p<0.05, **p<0.01, ***p<0.001. n=3.*

2.3.1.5 Optimisation of LPS Exposure Times

According to the above results, microglial N9 cells treated with a range of LPS concentrations demonstrated the greatest levels of reaction at the 24h incubation period. In order to determine if this time point negatively affected cell viability, N9 cells were plated (10,000 c/w in 96wp) and incubated (24h). Subsequently, three viability assays comprising of MTS, Neutral Red and Bradford, were conducted in order to determine toxicity to the cells at the treated doses of LPS. There was no statistically significant loss of cell viability compared to control in any of the three assays (Figure 2.9 A-C), with the exception of a slight loss after 0.5µg/ml LPS in the Bradford assay. This infers that treatment with any of the measured LPS concentrations would not negatively affect microglial viability. The optimal dosage previously selected for subsequent studies was 0.25µg/ml LPS, which did not demonstrate any change in cell viability after LPS treatment. Since the 24h LPS incubation period appears to stimulate the greatest inflammatory response without any significant toxicity to microglial cell cultures at the chosen optimal concentration, it was henceforth utilised for all subsequent studies to activate microglial N9 cells.

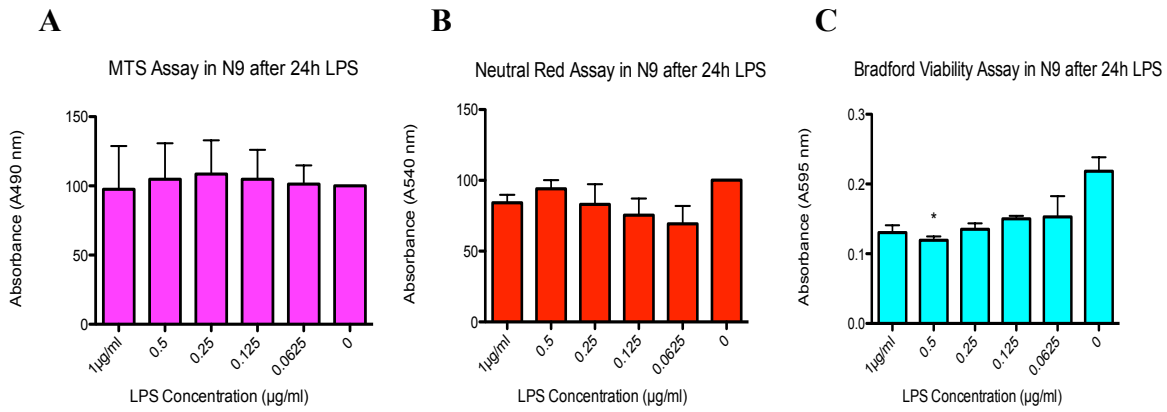

Figure 2.9 Optimising LPS Exposure Time in N9 Cells for Successive Treatments With Viability Assays
N9 cells were seeded and treated with various LPS concentrations for 24 hours, after which three viability assays were performed: MTS, Neutral Red and Bradford (A, B, and C, respectively). The dose responses showed no statistically significant loss of cell viability, except with 0.5µg/ml in the Bradford assay. 0.25µg/ml dosage was selected as the optimum sub-maximal LPS concentration, with 24h chosen as the optimal exposure time to elicit a robust inflammatory response. *Statistical significance as compared to control is indicated by asterisks*: *$p<0.05$. *n=3.*

2.3.1.6 Microglial Treatment with LPS in Transwell Plates

Following N9 activation in mono-culture, and treatment of N27 neurons with microglial conditioned media, cellular iron metabolism was observed using Transwell plates. For the co-culture setup of plating N27 and N9 cells on opposite sides of the permeable Transwell membrane *(Section 2.2.5.1)*, N9s were activated with LPS at the previously determined optimum concentration of 0.25µg/ml. After the incubation period of 24h, which was the most robust time observed in mono-culture exposure to conditioned medium, cells were collected according to the assay protocol.

For tri-culture treatment, 24h after the Transwell setup *(Section 2.2.5.2)*, N9 cells were separately pulse treated with LPS (0.5µg/ml, 2h). While N27 remain unaffected by direct LPS treatment, astrocytes express the toll-like receptor TLR4 necessary for LPS signalling (Chow, 1999; Bowman, 2003; Niranjan, 2012) and can contribute to the inflammatory response. Since C6 cells are directly affected by LPS treatment, to ensure that any observed affects were a direct result of microglial activation and not astrogliosis, N9 cells were gently washed twice in warm medium to remove any residual traces of LPS. Next, 2.6ml fresh complete N27 medium was added to N9 wells, and freshly prepared Transwell inserts containing both C6 and N27 cells were gently transferred into the wells and left to incubate for varying time points (1, 3, 6, 18, 24h).

2.3.2 Cytokine Treatment

After neuronal cell treatment with MCM from activated microglial cells elicited certain changes in iron metabolism, the specific inflammatory mediator triggering these changes needed to be determined. Since microglia release various pro-inflammatory factors, the first to be examined were certain key cytokines. Thus, N27 were treated with accumulating concentrations of three inflammatory cytokines: IL1ß, IL6, and TNF. In order to determine which concentrations to use, formerly published protocols were compared for various physiological levels of such cytokines used to treat cells in culture (Liu, 1994; Akaneya, 1995; Schäfer, 1999; Smirnov, 1999), as well as observing the physiological concentrations released by the activated N9 cells from ELISA results.

For treatment, N27 cells were seeded (500,000 c/w in 6wp) and left to rest overnight. After 24 hours, wells were directly treated with increasing concentrations (1-100ng/ml) of either IL1ß (PRC0814, ThermoFisher), IL6 (400-06, Peprotech), TNF (400-14, Peprotech) or a vehicle control. Cells were incubated for either 3h or 24h, after which cells were lysed for determination of iron regulatory protein gene expression and ferrocene analysis.

2.3.2.1 Cytokine Neutralisation

To investigate whether MCM-induced changes in N27 iron metabolism could be attributed to the presence of inflammatory cytokines, certain cytokines were neutralised in the MCM before exposure to neuronal cells. N9 cells were seeded as normal (350,000 c/w in 6wp), and left to rest overnight. After LPS treatment, the MCM supernatant was transferred to a fresh 6wp, whereupon cytokine antibodies were added at concentrations deemed to be sufficient for neutralising (IL6= 0.36µg/ml; TNF=5µg/ml). This conditioned medium was then left to incubate under standard conditions (1h) to ensure adequate protein binding by the antibodies. After this cytokine neutralisation, the new MCM without antibodies was used to treat the N27 cells as normal (Figure 2.10).

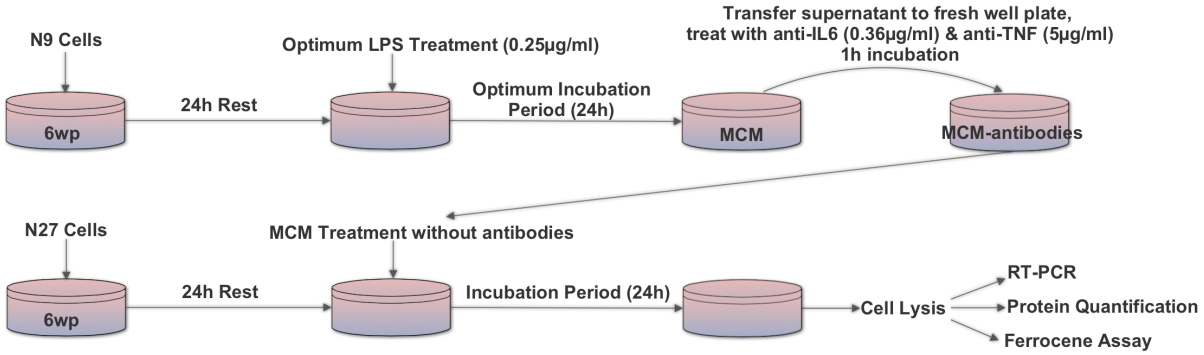

Figure 2.10 Schematic Representation of Protocol for Cytokine Neutralisation
N9 microglial cells were seeded (350,000 c/w) and left to rest (24h) to return to their resting morphology. After optimisation, microglia were activated with LPS (0.25µg/ml) and left to incubate (24h). This conditioned medium was transferred to fresh wells and incubated (1h) with antibodies to neutralise any potential inflammatory effects of cytokines (IL6 & TNF) in the conditioned media. This new MCM (-IL6 & -TNF) was transferred to already established and rested (24h) neuronal N27 cultures (500,000 c/w). After incubation (24h), cells were lysed for assessment via different assays.

2.3.3 Hydrogen Peroxide Treatment

Activated microglia also release ROS, which help perpetuate an inflammatory state. Results from neurons treated with MCM showed significant alterations in iron levels and IRP gene expression, so it was left to be determined what particular inflammatory factor within the activated microglial MCM was effecting these observed changes. It was originally believed to be caused by pro-inflammatory cytokines, such as the interleukins 1ß or 6, or tumour necrosis factor. However, direct treatment with these factors did not elicit the same observed changes as with MCM treatment. Thus, it was deduced that another microglial-released factor must be responsible. H_2O_2 is one such ROS that may affect levels of iron regulatory proteins. To determine the consequences of direct H_2O_2 treatment on neuronal cultures, both N27 and primary neuronal cells were exposed to increasing concentrations (0-200µM) of hydrogen peroxide solution (Sigma, H1009).

First, N27s were seeded (500,000 c/w in 6wp), and treated to various H_2O_2 doses (0, 5, 25, 50, 100, 200 μM) for 3 and 24 hours. After performing the ferrocene assay to discern any altered levels of iron expression, RT-PCR was then executed applying the concentrations found to be significantly different in the ferrocene assay. Results were duplicated using primary neuronal cultures (750,000 c/w).

2.3.3.1 Decomposed Treatment

If a significant effect was observed during the cytokine neutralisation, but no effects were observed with direct cytokine treatment, then to prove that this experimental consequence was correlated to H_2O_2, dissipating the H_2O_2 signal should result in quenching of any detected effects. Thus, 100μM H_2O_2 in complete RPMI was added to a fresh empty 6wp. This was allowed to incubate for one hour, as was the previous conditioned medium with the antibodies. After this time, previously seeded N27 cells (500,000 c/w in 6wp) were washed twice with warmed RPMI and fully aspirated, after which this decomposed H_2O_2 media was immediately transferred to the wells. Cells were incubated 24h as normal, after which gene expression and iron levels were measured for comparison with previous results.

2.3.3.2 Treatment +/- Catalase

A consequence of chronic ROS presence includes cellular damage and eventually neuronal cell death. Accordingly, an endogenous cellular antioxidant system is present to defend against such oxidative insults. Catalase is an enzyme crucial for protecting cells from the oxidative damage associated with H_2O_2 by catalysing its decomposition to water and oxygen. If H_2O_2 treatment was able to induce a change in iron metabolism as represented by iron levels and gene expression of iron regulatory proteins, then disproportionation of H_2O_2 by catalase should quench any observed changes.

N27 cells were established (500,000 c/w in 6wp), whereupon cells were treated with either 100μM H_2O_2, 100μM H_2O_2 + 100U/ml catalase, or just 100U/ml catalase (Sigma, C30). This was replicated using 200μM H_2O_2 with catalase as above. In order to compare results with those from the conditioned media treatments, cells were also treated with MCM or MCM + 100U/ml catalase. Control wells were treated with an equal volume of water. Following incubation (24h), cells were gathered for quantification of gene expression and intracellular iron levels.

2.4 Cellular Assays

PD has demonstrated dysregulation of iron under inflammatory conditions. These conditions were mimicked in cultures to help determine which inflammatory factors were potentially responsible for causing such changes. The culture model involved microglial cell cultures which were activated with LPS to release inflammatory factors. Neuronal cell cultures were then exposed to the MCM or individual factors in order to determine the specific effects of inflammation on iron regulation in neurons. To pinpoint such molecular changes, a range of cellular assays and lab techniques were carried out. This included determining levels of certain key inflammatory factors released by microglia via Griess, H_2O_2 and ELISA assays, quantifying intracellular iron levels using the ferrocene assay, quantifying proteins for cellular verification or extracting mRNA to calculate gene expression of iron regulatory proteins.

2.4.1 Cellular Viability

Microglial cells were activated with LPS, while neurons and astrocytes were exposed to microglial inflammatory factors. To ensure cell viability was not affected by these treatments, and any observed outcomes were attributed to effects of treatment rather than any cytotoxic effects and a loss of cells, three different cellular viability assays were performed. Cells were seeded (10,000c/w 96wp, in 100µl complete media) and left to rest overnight. After which microglial cells were treated with a range of LPS concentrations (0.0625-1µg/ml) or an equal volume of control (dH_2O) for a 24h incubation period. Assays were then performed directly on N9 cells, or on N27s or C6s after 24h MCM treatment at these concentrations, by incubating a specific reagent in a culture population containing enough viable cells with enzymatic activity to transform the substrate into a coloured product detectable by spectrophotometer. This product is thus directly proportional to the quantity of viable cells, as dead cells lose any enzymatic activity. All wells were run in triplicates. Absorbance was measured using VersaMax Microplate Reader (Molecular Devices), and data represented as a percentage of the control, conveyed as mean ± standard error mean.

2.4.1.1 MTS

A colourimetric cell viability assay was run using soluble CellTiter 96 AQ_{ueous} One Solution Reagent (Promega, G3580), which contains tetrazolium compound MTS (3-(4,5-dimethylthiazol-2-yl)-5-(3-carboxymethoxyphenyl)-2-(4-sulfophenyl)-2H-tetrazolium, inner salt) coupled with phenazine ethosulfate (PES), a stabling electron coupling reagent. PES is able to penetrate viable cells, whereupon cytoplasmic NADH from mitochondrial

dehydrogenase enzymes is reduced, so that once PES exits cells to the culture medium, it can reduce MTS tetrazolium to the soluble formazan product for colourimetric detection (Buttke, 1993; Berg, 1999; Goodwin, 1995). Nonviable and dead cells lack the enzyme activity required to instigate tetrazolium reduction, thus any coloured product is directly proportional to the number of viable cells. As per manufacturer's instructions, cells were directly treated with 20µl CellTiter 96 AQ_{ueous} One Solution Reagent, and incubated at 37ºC (3h) under humidified cell culture conditions. Upon completion of the incubation period, plates were measured on a spectrophotometer with absorbance 490nm.

2.4.1.2 Neutral Red

The Neutral Red (NR) assay is centred upon the mildly cationic NR dye uptake into viable cell lysosomes based on their ability for non-ionic diffusion past cell membranes (Nemes, 1979). At a physiological pH level, the dye has little charge, allowing passive diffusion. Lysosomes maintain a more acidified environment, thus ionising the dye upon entrance and retaining it within by anionic group binding (Repetto, 2008). This dye can be extricated and quantified by addition of an acidified ethanol destain solution, producing a coloured solution ready for colourimetric quantification by spectrophotometry. Since a dead or dying cell loses the capacity to maintain a physiological pH gradient (Repetto, 2008), reduced lysosomal integrity means an inability to retain NR dye, thus ensuring that any observed dye is directly proportional to the amount of viable cells. Accordingly, neutral red is a useful screening tool for quantitative determination of cell viability.

NR dye (Sigma, N4638) was first solubilised and stored in DPBS to a concentration of 4mg/ml. For treatment, this stock solution was prepared to a concentration of 40µg/ml in complete appropriate culture media, referred to as NR medium, and left to incubate 24h at 37ºC under cell culture conditions. This pre-incubation period brings the dye to comparable conditions to avoid shock when coating cells, as well as avoiding crystal formation with dye mixture in culture medium (Borenfreund, 1985). NR destain was also prepared, consisting of 50% ethanol, 49% water, 1% glacial acetic acid. After cell incubation with LPS or MCM treatment (24h), the medium was aspirated and replaced with 100µl NR medium. Cells were incubated under normal cell conditions at a humidified 37ºC for 3h. Cells were then inspected under the microscope to ensure NR precipitation into live cells. This NR medium was then aspirated, and cells were washed with 150µl DPBS. This was then aspirated, and 150µl NR destain added to wells. Plates were placed on a plate shaker for 10 minutes to solubilise the dye, and absorbance measured at 540nm.

2.4.1.3 Bradford

Total protein concentrations were measured via Bradford assay immediately following the NR absorbance measurements, within the same cell wells. This involves Coomassie Brilliant Blue G-250 binding to any protein present, resulting in an absorption shift from A_{465} nm to A_{595} nm (Bradford, 1976). The increase in absorption should therefore represent a concomitant increase in protein levels. In this instance, several washes with PBS ensured sufficient removal of any floating dead cells, to verify that any quantified protein was from living cells. Lysed cells and prepared standard concentrations were then treated with Bradford reagent for colourimetric reading.

NR stain was aspirated and wells washed three times with 150µl DPBS. Cells were then lysed by addition of 50µl 0.1M sodium hydroxide (NaOH). Bovine serum albumin (BSA) (Sigma, A9647) standards were made in dH_2O with concentrations from 0-1.4mg/ml. 5µl standards were added to blank wells, with the addition of 50µl NaOH. Next, 200µl Bradford reagent (Sigma, B6916) was pipetted into each well, including standards. Plates were placed on a plate shaker (20m), and absorbance measured at 595nm using a plate reader (VersaMax Microplate Reader, Molecular Devices). Standard results were used to plot a standard curve, whose line of best fit was applied to calculate total lysate protein concentrations. Briefly, this was computed by averaging triplicate standard results. The net values were calculated by subtracting the mean value at the 0mg/ml concentration. Finally, the mean net values were plotted, and a line of best fit created. Figure 2.11 depicts an example of a Bradford standard curve. Sample concentrations were determined by substituting the sample net mean values, calculated as above, for the x value within the line of best fit gradient equation. All future calculations involving use of standards and lines of best fit were calculated in this way.

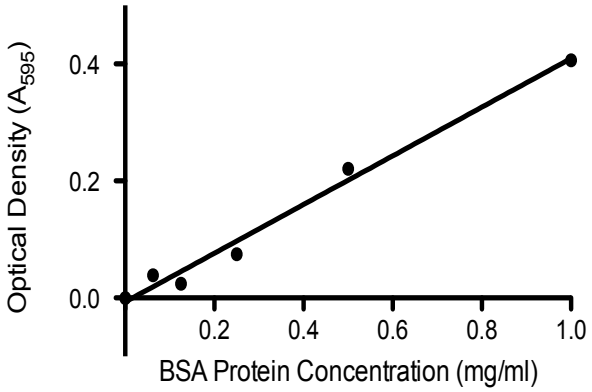

Figure 2.11 Bradford Assay Standard Curve
Bovine serum albumin at known protein concentrations (0-1.4mg/ml in dH_2O) was used for standards in the Bradford assay. Wells run in triplicate were treated with NaOH and Bradford reagent, incubated (20m on microplate shaker), with absorbance read at A_{595} nm. The resultant standard plot of replicate mean net values was given a line of best fit, an example of which is depicted above, whose gradient was applied to determine protein concentrations for each sample. Fresh standards were prepared for each 96wp run. *n=3.*

2.4.2 Griess Assay

Nitric oxide (NO) is a freely diffusible messenger crucial to physiological systems, with roles such as vasodilation or neuronal second messenger (Dawson, 1992). However, it can also have cytotoxic effects when released for longer periods of time by activated microglia. NO production is a result of oxidising the guanidine nitrogen atom of L-arginine by the enzyme NO synthase (NOS) (Moncada, 1991). There are several isoforms of this enzyme, one of which is iNOS, an inducible isoform that can be triggered by cytokines and inflammation to release NO for longer periods of time (Moncada, 1991). As it is a reactive free radical, NO can mediate cellular damage and participate in reactions that contribute to nitrosative and oxidative stress. For the purposes of this research, the LPS-activated microglial inflammatory response causes a cytokine release that can trigger iNOS, and result in long periods of NO production that may have a role in the pathophysiology leading to changes in neuronal iron metabolism. Thus, it is important to be able to measure NO release from activated microglia into the supernatant. The quantification method applied here was the highly sensitive Griess reaction, first described by Johann Peter Griess in 1879, which has been employed to study iNOS activity and its nitrite quantification in *in vitro* culture systems (Granger, 1996; Haas, 2002; Shirwaikar, 2004).

Nitrite is a metabolite by-product of nitric oxide metabolism, which is accordingly directly proportional to NO levels. As NO is difficult to measure directly due to its quick oxidation to nitrate or nitrite, and its short half-life ranging from ~30-130s (Ford, 1993; Sun, 2003), the more stable nitrite levels must be quantified instead as an index to deduce NO concentrations. Griess chemistry involves nitrite diazotization of sulphanilic acid, which in turn binds with diamine to produce a diazonium salt. This binds the Griess reagent or N-(1-

naphthyl)ethylenediamine to generate a pink end-product measurable by colourimetric detection (Granger, 1996; Guevara, 1998).

Nitrite concentrations in the supernatant were determined via the Griess reaction using the following protocol. Sodium nitrite standards ranging from 3.125µM-100µM were prepared from a 10mM stock solution diluted in the same DMEM as N9 cells to be tested, to correct for any colour variances between medium batches. Microglial LPS-activated supernatant at various time points and LPS concentrations was collected from N9 6wp, and centrifuged (5m, 1200g) to pellet any dead or remaining cells. 100µl either supernatant samples or standard was pipetted in triplicates into a 96wp. 100µl Griess reagent (Sigma, 03553) was added to each well, and plates incubated 10m on a microtitre shaker at RTP. Absorbance was measured at a wavelength of 540nm using a microplate reader (Molecular Devices). Readings were used to plot a standard curve with plotted mean net values, whose line of best fit was then used to calculate sample nitrite concentrations (Figure 2.12).

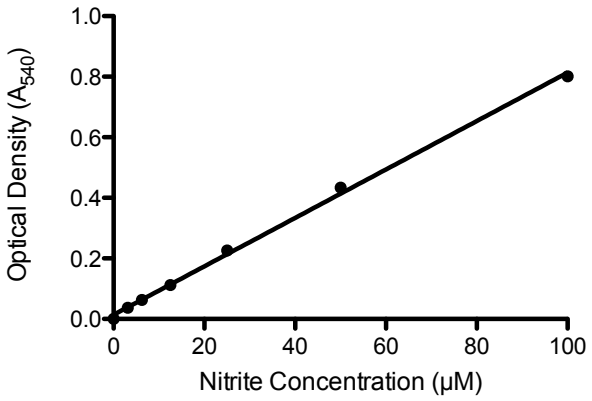

Figure 2.12 Griess Assay Standard Curve
A range of sodium nitrite concentrations (3.125-100µM diluted in cell medium) was freshly prepared each time for use as the standard range in the Griess assay. 100µl of each sample was added in triplicate to a 96wp, followed by an equal volume of Griess Reagent. After a 10m incubation period on a microplate shaker, plates were read on a spectrophotometer at an absorbance of A_{540} nm. The mean standard results normalised to the 0µM nitrite reading were used to create a standard curve, an example of which is depicted here. A line of best fit was created, whereby its gradient was utilised to calculate the remaining sample nitrite concentrations. *n=3, each run in triplicate.*

2.4.3 ELISA

Enzyme linked immunosorbent assays (ELISAs) employs a plate-based system using antigen detection for protein quantification and detection via spectrophotometer. The sensitive sandwich assay involves fixing a capture antibody to the bottom of a plate, adding samples with the antigens for measurement, which are then specifically immobilised by capture antibody binding on the plate surface. Next, addition of a biotinylated detection antibody binds the antigen, creating a sandwich complex. Subsequently, an avidin-horseradish peroxidase (HRP) conjugate is added, where the avidin binds with biotin on the biotinylated detection

antibody. A wash step was added in between each step to ensure removal of any unbound antigens or antibodies that may skew the final readings. When the 2,2'-azino-bis(3-ethylbenzthiazoline-6-sulphonic acid) (ABTS) liquid substrate was finally added, it catalysed the HRP enzyme to create a product emitting a visible signal. This signal is detectable by spectrophotometry, and signal intensity is relative to the number of bound detection antibodies, which are indicative of the number of antigens present within the sample, thus quantifying them (Figure 2.13). Standards were run in parallel with samples, and final results were enumerated by comparison against a standard curve. Applying this technique allows determination of key pro-inflammatory cytokines, including IL1ß, IL6 and TNF, released by LPS-activated microglia into the cell culture supernatant.

Pro-inflammatory cytokines of interest were quantified using murine sandwich ELISA development kits (Peprotech, USA) for IL1ß (900-K47), IL6 (900-M50), and TNF (900-K54), following the protocol as per the manufacturer instructions. Capture antibodies provided were diluted with PBS to 1µg/ml (TNF) or 2µg/ml (IL1ß & IL6), and 100µl pipetted to each well of a flat bottom high-binding polystyrene EIA/RIA plate (Fisher Scientific, 10544522). Each individual plate run contained only one cytokine to avoid any confusion or contamination. Plates were sealed (Sigma, CLS3095), and incubated (ON at RTP). Following incubation, plates were washed with wash buffer (0.05% Tween-20 in PBS) (300µl x4). To block any unused protein-binding sites, plates were incubated with blocking buffer (1% BSA in PBS) (300µl/w, 1h RTP), then washed (300µl x4), and incubated with samples or standards in triplicates (100µl/w, 2h RTP). Standards were prepared by dilution in diluent (0.05% Tween-20 + 0.1% BSA in PBS) to a concentration of 2ng/ml (TNF) or 4ng/ml (IL1ß & IL6), then serially diluted down five times. After incubation, plates were washed (300µl x4), and incubated with detection antibodies diluted in diluent to concentrations of 0.25µg/ml (TNF) or 0.5µg/ml (IL1ß & IL6) (100µl/w, 2h RTP). Wells were washed (300µl x4), then incubated in avidin-HRP conjugate (100µl/w, 30m RTP), diluted in diluent to 1:2000. Following the last wash step (300µl x4), ABTS liquid substrate was added to wells (100µl/w) and plates incubated at RTP for colour development. Plates were read at 5 minute intervals for ~45m at A_{405} nm, with a wavelength correction at A_{650} nm to monitor colour change (VersaMax Microplate Reader, Molecular Devices). Once the standard curve optical density readings neared 1.4 units at the highest concentration and remained ≤ 0.2 units for the 0ng/ml standard, measurements were stopped and results were taken from an average of 2 readings. Results from the standard measurements of A_{650} subtracted from those at A_{405} were mapped against the known standard concentrations to create a standard curve (Figure 2.14), the equation of which was used to

create a line of best fit in order to estimate sample protein concentrations. Data was normalised and expressed as mean percentage of control.

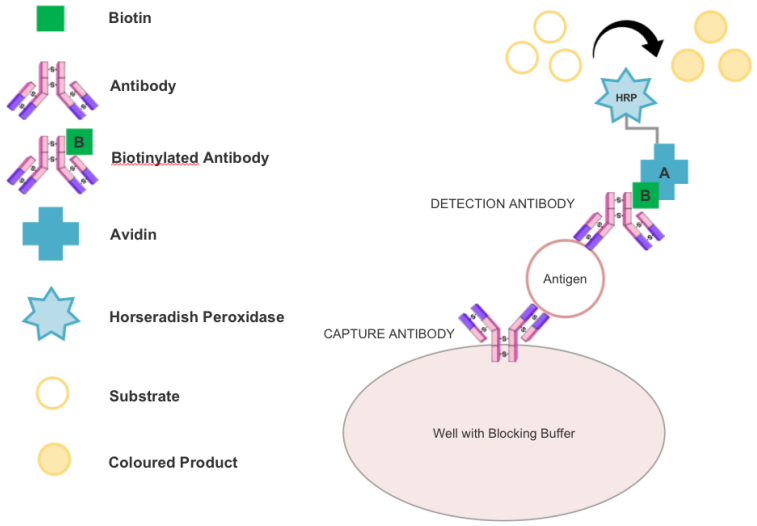

Figure 2.13 Sandwich ELISA Diagram
Cell plates (96wp) were pre-coated and incubated with a specific capture antibody for the protein to be quantified (ON RTP). Blocking buffer was added to block any unused protein-binding sites on the plate. Samples and standards were added to plates, whereupon any antigen of interest present were able to bind the capture antibodies. Next, a biotinylated detection antibody was added, also specific to the antigen, binding them from another epitope to close the sandwich. Addition of the enzyme-linked Avidin-HRP conjugate allows the avidin to bind biotin on the detection antibody, resulting in a number of HRP labelled complexes relative to the number of antigens bound to capture antibodies. Upon addition of the substrate 2,2'-azino-bis(3-ethylbenzthiazoline-6-sulphonic acid) (ABTS), the colourless solution reacts with HRP enzymes to create a coloured product quantified at an absorbance of A_{405}.

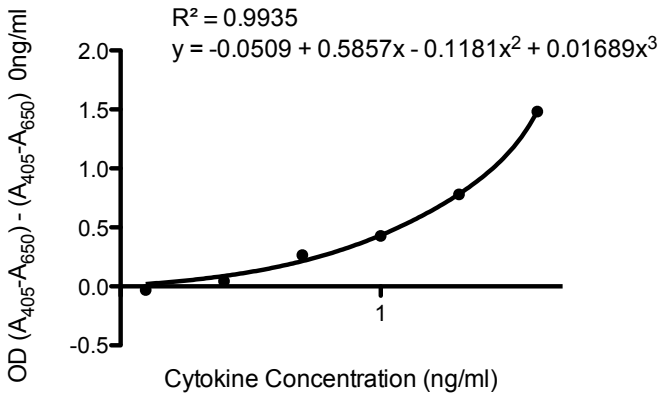

Figure 2.14 ELISA Standard Curve
This graph is representative of an example standard curve utilised for protein determination via ELISA assay. Results from an averaged reading of $A_{405} - A_{650}$ were used to plot the curve, whose polynomial regression line of best fit equation was used for sample protein concentration calculations. Fresh standards were run in parallel with samples for each new assay. Data is expressed as mean net values. *n=3*.

2.4.4 Ferrocene Assay

Iron is a crucial element for physiological functioning of cells. It is an indispensable part of mitochondrial respiration and oxygen transport in haemoglobin, acts as enzyme cofactors such as with tyrosine hydroxylase in neurons, and participates in crucial redox reactions (Zecca, 2004). However, since free iron is very reactive, abnormal iron regulation aggravates the neuronal environment by causing an escalation in OS, which may eventually lead to toxicity and cell death. Excess iron concentrations have been linked with cellular damage in neurodegeneration (Dexter 1987; Riederer, 1989; Ben Shachar, 2004), so determining the source that instigates such iron dyshomeostasis would be a novel therapeutic target in several neurodegenerative conditions. For the purposes of this study, intracellular iron levels after cellular incubation with pro-inflammatory stimuli were determined by means of the ferrocene assay.

This simple, inexpensive and robust colourimetric assay is able to quantify iron levels by spectrophotometric detection. Cell cultures were first incubated with ferric ammonium citrate (FAC) to be taken up into cells, thereby increasing assay sensitivity by providing significant iron levels for detection. Before lysis, cells were washed twice with PBS to stop iron uptake. This also ensures that any detected iron was intracellular, and not from any surface-bound iron or residual FAC within cell wells. Lysates were then treated with an iron releasing reagent, containing potassium permanganate ($KMnO_4$) to release any complexed iron at RTP, including any stored within ferritin or haem proteins (Tennant, 1969). Finally, the Fe^{2+} chelator ferrocene was added to adhere to any released, unbound ferrous iron, forming a highly-stable, intensely-coloured complex measurable at A_{550} nm. The ammonium acetate buffers the complex solution to ensure its formation is maintained stable, while the ascorbic acid serves to reduce any leftover $KMnO_4$ (Fish, 1988). It has been shown previously that cellular incubation with 100µM FAC for iron loading did not affect cellular viability compared to control (Riemer, 2004).

The following protocol was applied to determine iron levels within all collected samples. Cells were seeded (300,000c/w in 24wp) and left to rest overnight. Wells were washed (x2) with 1ml complete warmed medium to remove any dead cells. N9 cells were aspirated, and the medium was changed for the same complete media with the addition of FAC (Sigma, F5879) at a final concentration of 100µM. This was the same protocol for N27 with the addition of direct cytokine or H_2O_2 treatments. Inflammatory stimuli were then added as normal to this FAC-enriched media. N27 cells for MCM treatment were also aspirated, then changed for 1.5ml MCM with 200µl 1mM FAC and 300µl fresh complete RPMI. Upon completion of the

appropriate incubation periods, media was completely aspirated and wells washed (x2) with ice-cold PBS to terminate iron uptake into cells. The PBS was fully aspirated, and plates were sealed and frozen (-20ºC, ON) to lyse cells. The following morning, frozen cells were further lysed with addition of 200µl 50mM sodium hydroxide (NaOH) (Sigma, 221465), and left to incubate on a plate shaker in a humidified atmosphere (2h). Cells were then scraped using a rubber policeman into pre-prepared eppendorfs. Each sample eppendorf contained: 100µl scraped sample cells, 100µl 10mM hydrochloric acid (HCl) (Sigma, 258148), and 100µl freshly prepared iron releasing reagent (1.4M HCl + 4.5% $KMnO_4$) (Sigma, 223468). This acidic permanganate solution facilitated the release of any complexed iron, including that in ferritin storage or haem complexes (Fish, 1988). A duplicate set of fresh standards were run in parallel with samples for each assay, made from 30mM ferric chloride ($FeCl_3$) stock in 10mM HCl. On the day of the assay, the 30mM stock was diluted down to 1mM in 10mM HCl, which was then serially diluted for a range of $FeCl_3$ concentrations from 300µM-0µM. After thorough vortexing, each sample eppendorf contained freshly prepared 100µl standard dilution, 100µl 50mM NaOH and 100µl iron releasing reagent. All eppendorfs were then incubated in a fume hood at 60ºC for 2 hours. After incubation, tubes were removed from hot plates and left to cool to RTP, then centrifuged briefly to condense any evaporated solution, whereupon 30µl iron detection reagent (6.5mM ferrozine + 2.5mM ammonium acetate + 1M ascorbic acid + 6.5mM neocuproine solubilised in methanol) (respectively: 82940, 221465, A7631, N1501, all from Sigma) was added to each tube for 30m (covered at RTP). This iron detection solution contained ascorbic acid, capable of reducing any ferric iron to ferrous iron. Ferrozine within the solution was then free to bind all ferrous iron for formation of a highly stable ferrous iron complex, forming a concentrated purple colour for spectrophotometric detection. Upon completion, tubes were very thoroughly vortexed, and 280µl solution transferred to a 96wp for spectophotmetric analysis at A_{550} nm. An average of two readings was taken to create a standard curve, which was used to deduce net iron concentrations within sample lysates. Iron contamination was avoided by using sterile glassware and pipette tips, as wells as ultrapure MilliQ water.

2.4.4.1 Ferrocene Assay Optimisation

It was determined after running several unsuccessful assays that intracellular levels of iron after certain treatments were not sufficient enough to show up on the ferrocene assay as per the protocol. Thus, the need for addition of 100µM FAC within the culture media, as per the protocol tested in Riemer (2004). This allowed for iron loading sufficient for detection.

Another problem encountered during assay optimisation was the insolubility of neocuproine, which is only slightly soluble in water (Nilsson, 2012). The assay was successful only after first dissolving neocuproine in methanol at a dilution of 1:100 in water, then adding this to the rest of the iron detection reagent.

2.4.5 Hydrogen Peroxide Assay

H_2O_2 generation can occur as a by-product of aerobic metabolism, from the breakdown of superoxide by superoxide dismutase (SOD). If free iron is also present, this can lead to hydroxyl radical formation by means of the Fenton reaction. Detoxification mechanisms are in place to protect cells by preventing the onset of OS with antioxidants catalase and glutathione peroxidase (Kish, 1985). However, uncontrolled levels of H_2O_2 result in greater radical formation and OS which eventually affect neuronal survival. Experiments run here led to the hypothesis that H_2O_2 present in microglial supernatant was having an effect on the IRP expression in N27 cells after MCM treatment. In order to determine if this was indeed the case and to confirm H_2O_2 presence, the amount of H_2O_2 in microglial supernatant needed to be quantified. This was performed using a specific H_2O_2 assay.

For quantification of H_2O_2 in solution, an analysis kit (Abcam, ab102500) was utilised and followed as per the manufacturer's instructions. This quick assay is sensitive enough to detect H_2O_2 levels over 0.04µM in samples. The OxiRed probe, along with horse radish peroxidase (HRP), oxidises the H_2O_2 present in sample supernatant to generate a product visible by colourimetric detection at A_{570} nm. Briefly, all buffers and reagents were equilibrated to RTP before use, and the OxiRed probe was warmed for a few minutes in a 37ºC water bath to thaw DMSO. HRP was dissolved in 220µl Assay Buffer, and kept on ice. N9 cells were seeded and treated with 0.25µg/ml LPS or control as usual, then cells were washed with cold PBS and resuspended in 500µl assay buffer provided in the kit. Supernatants were collected into eppendorf tubes, mixed thoroughly by pipetting, and centrifuged (1000g x 15m). Pellets were discarded by transferring supernatant samples to fresh eppendorf tubes on ice. 500µl was added to 10kDa spin columns (10,000g x 5m) to deproteinise samples. A fresh set of standards was prepared each time by diluting 10µl 0.88M Standard in 870µl dH_2O to produce 10mM H_2O_2. This was further diluted to 0.1mM, which was then serially diluted for standard curve dilutions, ranging from 0-5nM. Samples and standards were run in duplicates in 96wp by pipetting 50µl into each well. 50µl of reaction mixture (46µl Assay Buffer, 2µl thawed OxiRed Probe, 2µl HRP) was added to each well. Plates were sealed and protected from light for an incubation period of 10m at RTP. Absorbance was measured on a plate reader (Molecular Devices) at A_{570}

nm. H_2O_2 concentrations in samples were calculated based on the standard curve line of best fit (Figure 2.15), with data representing mean ± SEM.

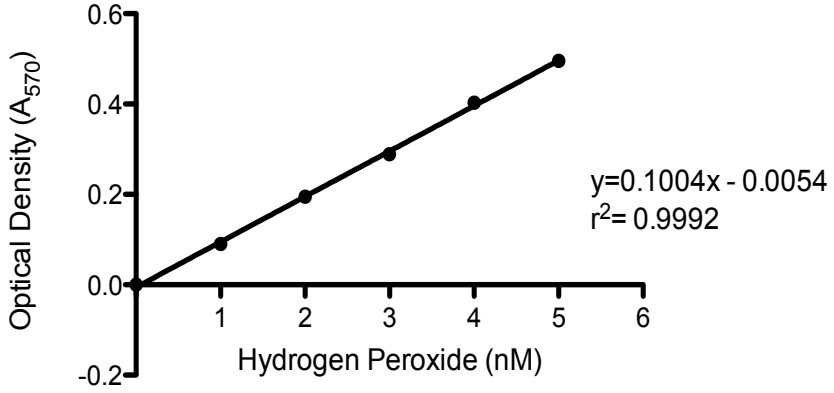

Figure 2.15 Hydrogen Peroxide Assay Standard Curve
Hydrogen peroxide standards were freshly prepared (0-5nM, diluted in dH_2O) for use in the H_2O_2 assay. Microglial N9 cells were harvested and treated with LPS as normal, after which cells were washed in cold PBS, and treated with the kit H_2O_2 assay buffer. After a centrifugation step, supernatants were collected and deproteinised using 10kDa spin columns. Standards and samples were then treated with 50µl reaction mix containing assay buffer, OxiRed Probe, and horse radish peroxidase. Plates were incubated (RTP, 10m), protected from light. The OxiRed Probe is able to react with H_2O_2 in the presence of HRP to form a coloured product measurable on a spectrophotometer at an absorbance A_{570} nm to complete the colorimetric assay. Mean standard results normalised to the 0nM reading were used to create a standard curve, as shown here. A line of best fit was created, whereby its gradient was utilised to deduce sample H_2O_2 concentrations. *n=3, each run in duplicate.*

2.5 Protein Expression

2.5.1 Protein Extraction for Quantification

Protein levels in samples required quantification for either cell culture validation experiments or to determine if the microglial inflammatory response effect on IRP gene expression translated to changes in protein levels. In order to accomplish this, after cell seeding and incubation with the appropriate stimuli, wells were washed (x2 cold PBS), aspirated and lysed on ice with 70µl Radio-Immunoprecipitation Assay (RIPA) buffer (Sigma, R0278) mixed with 1% protease inhibitor (PI) cocktail (Sigma, P8340). After 5m, cells were thoroughly scraped using a rubber policeman, and collected into mini eppendorf tubes. These were cooled at 4ºC 45m to help ensure cell lysis, and then centrifuged (11,000rpm 25m @ 4ºC) to remove cell particulates. Resultant pellets were discarded, while the supernatant containing proteins were transferred to fresh tubes for storage at -20ºC until time for use.

2.5.2 Western Blotting

Western Blot chemiluminescence was used to determine protein presence to validate the use of the 3 cell lines within this project. After running samples through the Bradford assay (Section 2.4.1.3) to determine protein concentration against a standard curve, volumes were corrected for protein concentration to normalise all samples. Hand-cast 1mm thickness 15 well glycine gels were pre-prepared using a 15% running gel (30% acrylamide, 0.375M running gel buffer, dH2O, 10% SDS, 10% ammonium persulfate, and TEMED), any bubbles evened out by addition of 2-propanol along the top, gels left to set, and then topped with a stacking gel (10% APS, 10% SDS, 0.125M stacking gel buffer, 30% acrylamide, 0.01% TEMED, dH2O), and left at 4ºC ON. Once all samples were ready and protein concentrations determined via Bradford, samples were thawed on ice and diluted to normalise protein levels at 10µg in a solution of sample with dH_2O plus an equal volume of 6µl Laemmli buffer (Sigma, S3401) to help denature proteins. To further ensure protein structure denaturation, samples were then placed in a hot plate at 95ºC (10m), and centrifuged afterwards to resuspend any evaporated liquid. After denaturation, 12µl of samples and a pre-stained protein standard ladder (ThermoFisher, LC5925) were carefully pipetted into wells for sodium dodecyl sulphate (SDS) polyacrylamide gel electrophoresis (PAGE). This method involves denaturing the protein molecular structure with SDS to provide linear, negatively charged polypeptides ready for separation by molecular weight along the gels. An applied electrical field at a constant current of 25mA (12m), followed by 70mA (40-45m), forces negatively charged polypeptide SDS-bound chains to travel towards the anode, with mobility dependent on size or molecular weight.

Upon completion of protein separation with SDS-PAGE, proteins were then transferred to polyvinylidene difluoride (PVDF) membranes (Sigma, P2938) for western immunoblotting. Proteins are transferred in the same formation from gels to PVDF membranes, in order to allow for antibody binding and detection. Gels are placed onto membranes sandwiched between filter papers (Invitrogen, LC2008_ 3626081607), for a semi-dry transfer set at a constant voltage of 20V (45m).

Membranes could then be blocked with 5% bovine serum albumin (BSA) or nonfat milk diluted in tris-buffered saline with 0.2% Tween-20 (TBST) (1h) to ensure blockage of any non-specific binding in areas of the membranes not attached by target proteins. This prevents antibodies from binding to random areas of the membrane, ensuring they only bind to sample proteins, thereby reducing background noise and providing a sharper blot result. Any excess unbound blocking proteins are washed away (TBST 10m, x3 on plate shaker), then blots are incubated in primary antibody overnight (1:1000 in TBST, 4ºC). Blots were then washed (TBST 10m, x3), and incubated with a ßactin (Abcam, ab6276) loading control (1:20,000 in TBST, 1h RTP), followed by another wash (TBST 10m, x3) then HRP-conjugated secondary antibody (Vector Laboratories, X0126 PI-1000) incubation (1:4000 in TBST, 1h RTP). Residual antibodies were washed off (TBST 10m, x3), incubated in solution of dH_2O with chemiluminescent 0.05% clear and brown clarity western developing substrates (Bio-Rad, 1705060) (1m) (Figure 2.16). Immediately afterwards, blots were placed in between saran wrap on a Hypercassette (GE Healthcare Life Sciences, RPN11629) and read on a darkroom developing machine (Konica, SRX-101A) using chemiluminescent hyperfilm (VWR, 28-9068-36). Since antibodies should only bind to target proteins, this should result in a visible band detected on film. Blots were digitally scanned to quantify bands via ImageJ software densitometry analysis, corrected with loading control results.

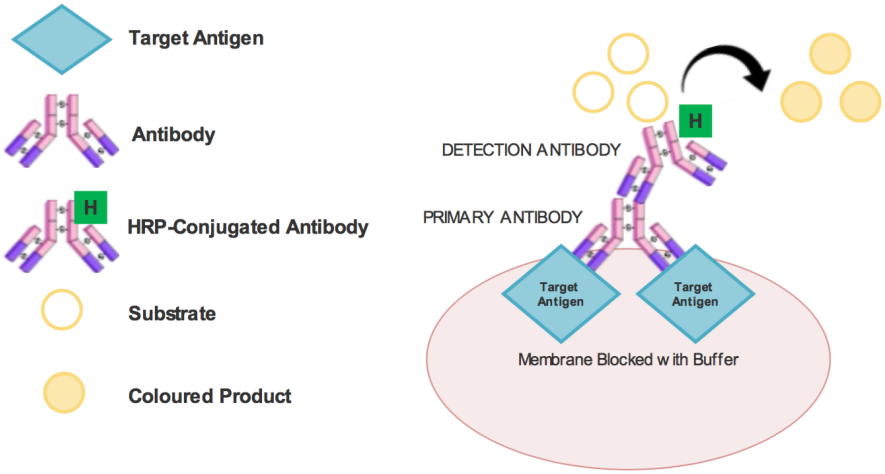

Figure 2.16 Western Blot Diagram
Membranes are first blocked with milk protein to prevent any non-specific antibody binding (5% nonfat milk, 1h RTP). Next, primary antibody incubation (1:1000 TBST, 4ºC ON) allows for antibody binding specifically on target antigens within sample bands. Next, an HRP-conjugated secondary antibody incubation (1:4000-1:10,000 in TBST, 1h RTP) allows for binding to primary antibodies. Any unbound antibodies are thoroughly removed in washing steps between each incubation period (TBST 10m, x3 on shaker). The number of remaining HRP-bound complex structures is thus relative to the amount of target antigens present in samples. Addition of ECL chemiluminescent western developing substrates results in their catalysis by HRP enzymes, to produce a measurable light emission captured on chemiluminescent film relative to the amount of target antigens.

Table 2.1 Western Blot Antibodies
Information on antibodies applied to Western Blots. *Abbreviations: BSA=Bovine Serum Albumin, GFAP=Glial Fibrillary Acidic Protein, Iba1=Ionised Calcium-Binding Adapter Molecule 1, MC=Monoclonal, NeuN=Neuronal Nuclei, NGS=Normal Goat Serum, ON=Overnight, PC=Polyclonal, RTP=Room Temperature, 1º=Primary, 2º=Secondary.*

Antigen	Molecular Weight (kDa)	Blocking Buffers	1º Antibody	1º Incubation	2º Antibody (HRP Conjugated)	2º Incubation
Tyrosine Hydroxylase	~ 62	5% BSA in TBST, 1h RTP	Rabbit PC (Millipore, AB152)	1:1000 in 1% BSA + 0.01% Sodium Azide, ON RTP	Goat anti-rabbit (Vector Labs, X0126 PI-1000)	1:10,000 in TBST, 1h RTP
NeuN	~ 46 & 48	5% BSA in TBST, 1h RTP	Mouse PC (Millipore, MAB377)	1:1000 in 1% BSA + 0.01% Sodium Azide, ON RTP	Horse anti-mouse (Vector Labs, X0328 PI-2000)	1:10,000 in TBST, 1h RTP
Iba1	~17	3% NGS in TBST, 1h RTP	Rabbit PC (Wako Lab, 016-20001)	1:1000 in 3% NGS TBST, ON 4ºC	Goat anti-rabbit (Vector Labs, X0126 PI-1000)	1:2000 in 3% NGS TBST, 1h RTP
GFAP	~50	5% nonfat milk in TBST, 1h RTP	Rabbit MC (Abcam, ab33922)	1:2000 in TBST, ON 4ºC	Goat anti-rabbit (Vector Labs, X0126 PI-1000)	1:4000 in TBST, 1h RTP

2.5.3 U-PLEX Custom Immunoassay

One of this project's goals was to measure the changes afflicted on neuronal IRP expression under conditions of microglial inflammation. Once iron levels and gene expression after LPS, MCM or direct inflammatory factor exposure had been measured via ferrocene and RT-PCR, it remained to see if protein levels were affected by the changes in gene expression. Western Blots were first attempted, however did not produce consistent or quantifiable results, even after various protocol attempts using both film and an automated immunoblot processor. In addition, 7 distinct proteins were being examined in this study (HAMP, FPN, FtH1, TfR, DMT1, Aco1, IREb2), which would be impossible to measure from one immunoblot stripped seven times. In order to properly quantify significant changes in these protein concentrations, a custom multiplex panel was created using Mesoscale Discovery (MSD) U-PLEX immunoassays. This technique allows for precise, quantifiable determination of up to 10 separate proteins from the same sample. As gene expression levels were significantly affected in 5 key iron regulatory proteins, these same 5 proteins were analysed via MSD. 5-spot U-PLEX plates (MSD, K15230N-2) and MSD GOLD SULFO-TAG NHS-Ester 2µM (MSD, R91AO-2) were ordered for these measurements, and assays carried out as per the manufacturer's protocols.

The first step to this custom assay was to locate and source 5 biotinylated monoclonal antibodies tested in ELISA, with reactivity in mouse and rat, and conjugated from a whole native protein or from as long a peptide as possible (Bioss, HAMP=BS-8870R-B, DMT1=BS-3577R-B, FPN=BS-4906R-B, TfR=BS-0988R-B, FtH1=BS-5907R-B). Secondly, the same 5 proteins had to be ordered as detection antibodies, with the specifications that they were unconjugated, ELISA tested, with a concentration of at least 1mg/ml, reactivity in mouse and rat, and provided in carrier-free/PBS-only buffer (ProteinTech, TfR=10084-2-AP; Biorbyt, HAMP=orb315547, FPN=orb6975, FtH1=orb1795, DMT1=orb5976). Once all products and reagents had arrived, biotinylated capture antibodies were coupled to U-PLEX linkers (Figure 2.17A). Each antibody was diluted to 10µg/ml in coating diluent (PBS + 0.5% BSA), whereupon 200µl was added to 300µl of its specifically assigned linker (where HAMP=1, FPN=2, TfR=3, DMT1=8, FtH1=10). Tubes were vortexed and incubated 30m RTP. Then 200µl biotin-containing Stop Solution buffer was added (30m RTP) to end the linker-antibody coupling reaction. It is at this point that up to 10 U-PLEX-coupled antibodies may be pooled upon completion of assay optimisation. If they are not pooled, then each well would contain only one protein reading corresponding to the specific linker added to that well. This multiplex coating solution was then diluted to 1X concentration ready for plate coating.

Unconjugated detection antibodies were conjugated to electrochemiluminesent (ECL) MSD GOLD SULFO-TAG NHS-Ester before use according to the MSD protocol. A 1mg/ml solution of preservative-free detection antibodies was prepared using the supplied Conjugation Buffer. Then the required SULFO-TAG solution necessary was calculated according to the following equations, and added to the detection antibody solution. The tubes were vortexed, and incubated (2h RTP), protected from light. The conjugates were then placed in Zeba Spin Columns (Fisher Scientific, 11706446) for purification, and eluates stored for future use with the MSD protocol.

$$1{,}000 \times \frac{\text{Protein conc (mg/ml)}}{\text{Protein MW (Da)}} \times \text{Challenge Ratio} \times \text{Vol of protein solution}(\mu l) = \text{nmol required}$$

$$\frac{\text{nmol of SULFO-TAG required}}{\text{Conc of SULFO-TAG stock (nmol/}\mu l)} = \mu l \text{ of SULFO-TAG stock solution for conjugation}$$

Where: Challenge Ratio= ~20 Sulfo-tags per protein so that ~10 are actually coupled to provide a decent signal. Volume of Protein Solution= 250µl.
Concentration of SULFO-TAG stock= 2000nM.

50µl multiplex coating solution was added to each well, plates were sealed and incubated on a microtitre plate shaker (4ºC ON) to allow the biotin-antibody-linker complexes to bind to their specific spots in U-PLEX wells (Figure 2.17B). Plates were washed (150µl/w PBST, x3) to remove any unbound linkers, and samples or controls added to wells (25µl/w). Plates were sealed and incubated with samples (1h RTP, with shaking). Any unbound sample was washed off (150µl/w PBST, x3), followed by addition of 25µl SULFO-TAGged detection antibodies (1h RTP, with shaking) to create a sandwich complex. A final washing step removed any unbound detection antibodies (150µl/w PBST, x3), and 150µl 2X Read Buffer added per well to catalyse the electrochemiluminescence reaction. Plates were immediately read on an MSD instrument (MSD, SECTOR Imager), where voltage to U-PLEX plate electrodes initiates SULFO-TAG labels to emit a visible ECL signal relative to the amount of analyte within samples. Data was analysed using MSD Discovery Workbench software.

Ideally, U-PLEX plates work by first linking a biotinylated capture antibody to a specific linker that codes for one spot on a 10-spot U-PLEX plate. Once the assay is optimised individually, up to 10 different antibodies can be pooled together to quantify multiple analytes within the same well of a 96wp. This is a very efficient and robust method at determining up to 10 different protein concentrations in large numbers of samples. Unfortunately, the assay was never properly optimised for as yet unknown reasons, even after hours of assistance from

an MSD representative, leaving protein concentrations for these samples as yet unquantified. Western Blotting is only semi-quantitative, and multiplexing for 5 different proteins would require extensive stripping and reprobing, which would compromise result accuracy. Thus, future work could involve determining where the U-PLEX assay went wrong to efficiently complete the protein quantification, as it would be useful to observe whether the detected gene expression changes translated to increased IRP protein levels.

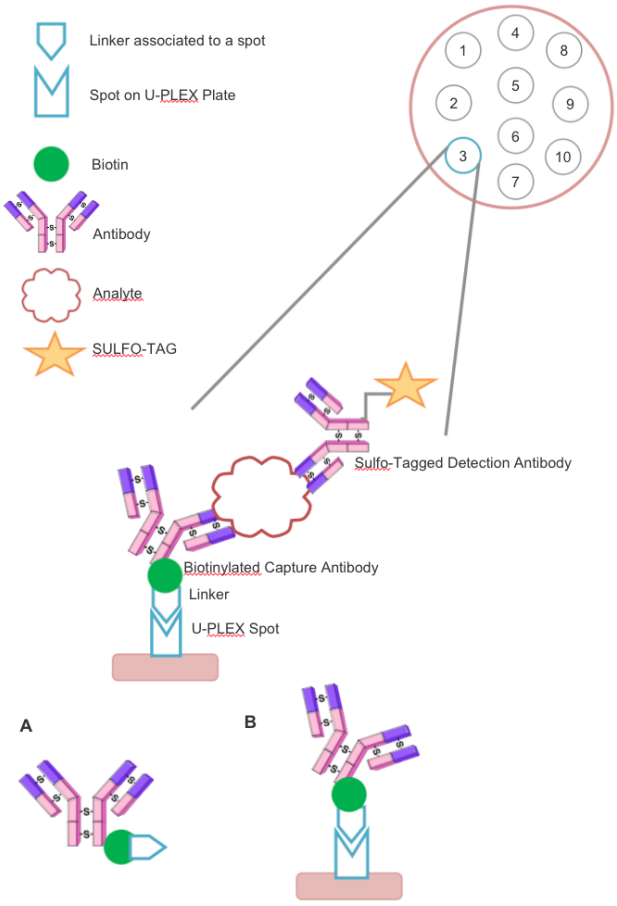

Figure 2.17 U-PLEX Mechanics
5 biotinylated primary capture antibodies (HAMP, FPN, TfR, DMT1, FtH1) were individually coupled to 5 unique U-PLEX linkers (A), where each linker then assembles onto its specifically corresponding spot on a U-PLEX plate (B). This solution was then coated onto a 5-spot U-PLEX immunoassay plate (4ºC ON). Protein samples and controls were added to each well (1h RTP), washed (PBST x3), and incubated with pre-tagged SULFO-TAG NHS-Ester detection antibodies to complete the sandwich immunoassay. Addition of a Read Buffer to catalyse the reaction, coupled with an applied voltage to U-PLEX plates, lead to emission of an ECL signal directly proportional to the amount of analyte within samples.

2.6 Gene Expression via qRT-PCR

To help determine the effects of inflammation on iron regulation, key IRPs were monitored for changes to gene expression using quantitative real-time polymerase chain reaction (qRT-PCR). Expression was measured after all treatments, in N9, C6 and N27 cells. Each step was performed as per product manufacturer's instructions.

2.6.1 mRNA Extraction

The first step for the PCR protocol involved mRNA extraction using the RNeasy Plus Mini Kit (Qiagen, 74134). After cell incubation in the appropriate stimuli as per usual protocol in 6wp, medium was fully aspirated, and 350µl Buffer RLT Plus with ß-mercaptoethanol (ß-ME) (Sigma, M6250) added (ratio 100:1). Plates were placed on ice to lyse cells (5m), followed by cell collection with rubber policeman into labelled eppendorf tubes. After a thorough vortex to remove any cell clumps, lysates were homogenised by pipetting ~20 times each, and then transferred to gDNA eliminator spin columns. These were centrifuged (10,000rpm, 30s), and 350µl 70% ethanol (made with RNase free water) added to the flow-through. This was mixed thoroughly by pipetting, and 700µl transferred to an RNeasy spin column for centrifuging (10,000rpm, 15s). The flow-through was discarded and 700µl Buffer RW1 added to the RNeasy spin column for centrifuging (10,000rpm, 15s). The flow-through was discarded and 500µl Buffer RPE added to the RNeasy spin column for centrifuging (10,000rpm, 15s). The flow-through was discarded, followed by another addition of 500µl Buffer RPE to the RNeasy spin column for centrifuging (10,000rpm, 2m) to dry out the spin column membrane and remove any residual ethanol. The RNeasy spin column was carefully removed from the collection tube and moved into a new 1.5ml collection tube. 40µl RNase-free water was added to the spin column, which was then centrifuged (10,000rpm, 1m). Since nucleic acids can absorb UV light, the RNA eluate concentration could then be measured on a NanoDrop spectrophotometer (Labtech, ND-1000). These readings were used to convert all RNA samples to an equal concentration for reverse transcription. Sample purity was also calculated with the NanoDrop at an absorbance of 260/280nm, ideally falling at a ratio around 2. This ensured adequately pure samples before proceeding with the PCR protocol (Figure 2.18). All mRNA samples were stored at -80ºC until required for the proceeding reverse transcription step.

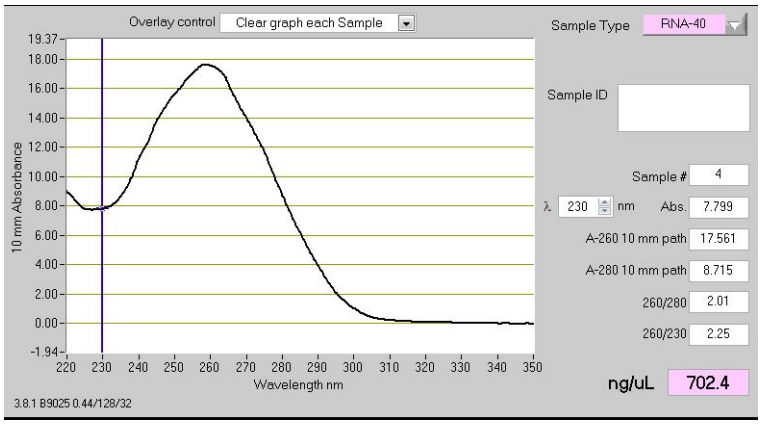

Figure 2.18 RNA Quantification and Purity via Spectrophotometry
A graphical representation of the absorbance against wavelength from an RNA eluate after mRNA extraction as measured by a NanoDrop spectrophotometer. Concentration (ng/µl) is calculated using sample and control (RNase-free water) absorbance at A_{260} and the RNA extinction coefficient ($0.025(ng/\mu l^{-1})cm^{-1}$), while RNA purity is estimated by dividing A_{260} by A_{280} for an ideal 260/280 ratio around 2.

2.6.2 cDNA Synthesis

RNA samples were next converted to complementary DNA (cDNA) using reverse transcription (RT) with the QuantiTect Reverse Transcription Kit (Qiagen, 205-313). RNA concentrations as previously determined by NanoDrop spectrophotometry were used to calculate volumes necessary to equalise all samples to 500ng. To ensure removal of genomic DNA (gDNA) contamination from samples, 2µl Qiagen gDNA Eliminator was added to the 500ng RNA (diluted in RNase-free water) in RNase-free tubes (Life Technologies, AM12400) for a total volume of 14µl, incubated at 42ºC (2m). Samples were removed to ice, while an RT mixture was prepared containing 1µl QuantiTect RT Primer Mix, 4µl QuantiTect RT Buffer, 1µl QuantiTect Reverse Transcriptase for each sample. 6µl of the RT mix was added to each RNA sample, for a final volume of 20µl. Tubes were then incubated in hot plates at 42ºC (15m), followed by an incubation at 95ºC (3m) to inactivate the RT enzyme. Samples were then diluted in RNase-free water to 2.5ng/µl. The ensuing cDNA samples ready for qRT-PCR were stored at -20ºC until use.

2.6.3 qRT-PCR

RT-PCR is a gene expansion technique used to quantify relative gene expression after thermal cycling. Its ability to accurately enumerate nucleic acid sequences has made it a popular lab-based practice. The technique commences with few copies of a specific DNA sequence, creating a twofold expression after every cycle, resulting in numerous duplicates of that particular DNA sequence. It does so by repeated exponential amplification of a specific DNA portion. First, cells are lysed for RNA extraction. Once total mRNA has been isolated via the RNeasy Kit, it is then converted to cDNA using reverse transcriptase enzymes, with

gDNA contamination reduced via use of gDNA eliminator columns in a centrifugation step. This is a crucial step, since RT-PCR cannot distinguish between cDNA and gDNA, thus gDNA amplification may lead to false positives. Once pure DNA is obtained from samples, RT-PCR may be performed.

Custom probes, small DNA fragments matching the specific template for the protein of interest, are added along with a master mix containing nucleotide bases and heat resistant Taq polymerase. This experiment utilised TaqMan probes to enhance PCR specificity, as they are specific to the gene of interest. A reporter fluorophore, either 6-carboxyfluorescein (FAM) or hexachlorofluorescein (HEX), and quencher are attached to opposite ends of the probe. The quencher serves to extinguish fluorescence until the primer anneals the DNA template and is extended by polymerase, separating the reporter from the quencher activity. Heating disrupts the hydrogen bonds, denaturing and unfolding the DNA double helix. Cooling allows for primer annealing to the single stranded DNA. DNA polymerase adds on extra complementary nucleotides to elongate and complete the new DNA strands. A complementary strand is created, with a resultant two identical DNA strands that are detected by the fluorescent reporter, now no longer quenched. The process repeats, with the assumption that there is a twofold exponential growth for each new synthesised DNA strand. PCR results are thus based on presence of the fluorescent reporters, since the amount of released fluorophores are relative to the amount of DNA template. Amplification of DNA is monitored with each PCR cycle, whereupon fluorescence becomes quantifiable after surpassing the threshold cycle (C_T). A lower C_T value infers a higher presence of the gene of interest, as less time was taken for it to be amplified.

qRT-PCR experiments here were performed by first preparing a master mix solution containing 10µl Brilliant II QPCR Low ROX Master Mix (Agilent, 600806), 7µl RNase-free water, and 1µl custom ordered IRP probe (see Table 2.2) per sample. 2µl cDNA samples were pipetted into MicroAmp Optical 96 well reaction plates (Life Technologies, 4306737), followed by 18µl of the prepared master mix. The 20µl reactions were run in triplicate with 2µl of sample cDNA for a final 5ng reaction per well, with a ßactin housekeeping gene run in parallel. Housekeeping genes are necessary to normalise data. To ensure the greatest accuracy, ßactin was specifically chosen as the reference gene according to results from a geNorm Reference gene selection analysis (see Section 2.6.4.3). Wells were sealed with MicroAmp Optical 8-Cap strips (Life Technologies, 4323032) and cDNA samples were analysed by qRT-PCR using an Mx3000P system with MxPro qPCR software (Stratagene, v4.1). Each plate included a negative control of only RNase-free water, and a positive control calibrator made

up of pooled cDNA samples from control treatment conditions. All PCRs were run according to the following denature, anneal, extension optimised thermal cycle set-up: 1 cycle at 95ºC 10m, 50 cycles at 95ºC 30s, 55ºC 60s, 72ºC 30s. Gene expression was normalised to the ßactin housekeeping gene. Upon completion of RT-PCR, data analysis was performed utilising the $2^{-\Delta\Delta CT}$ method, as explained in Section 2.6.4.

Table 2.2 Gene Information and Primer Sequences for PCR Assays
All qRT-PCR primer/probe taqman assays listed in this table were custom developed by PrimerDesign Ltd. IRP genes of interest were supplied with a FAM reporter, while the housekeeping gene ßactin was made with a HEX reporter for duplexing. The primer sequencing information for ßactin was not provided by the manufacturer. All assays were specific for both *mus musculus* (mouse) and *rattus norvegicus* (rat), with the exception of hepcidin (HAMP) which had a separate probe for each species. *Abbreviations: FAM=6-carboxyfluorescein, HEX=hexachlorofluorescein, A= adenine, C= cytosine, G=guanine, T=thymine.*

Name	Gene	Reporter	Sense Primer	Antisense Primer	Amplicon Product Length	Amplicon Distance from 3' end of sequence
DMT1 Solute carrier family 11, member 2, transcript variant 1	Slc11a2	FAM	TTGGCGCC ATCAACCC T	GGGGATTTT CTCATCAAA GTAGGT	98	4170
Ferritin Heavy Chain Ferritin heavy chain 1, transcript variant 1	Fth1	FAM	GCCAGAAC TACCACCA GGA	TCAAAATAA CAAGACATA GACAGATA GA	100	689
Transferrin Receptor	Tfrc	FAM	TTTAATGG AAGACTCT GCTTTGC	CCGTTTCAG CCAGTTTCA CA	130	4572
Ferroportin Solute carrier family 40 member 1	Slc40a1	FAM	AACTACCT TCTTGACC TTCTGC	GGGCAAATC GGAAATAC ATAAGAT	130	1554
Hepcidin Mus musculus hepcidin antimicrobial peptide	HAMP	FAM	CACAGCAG AACAGAAG GCA	AAGGAGGA GAAGCAGG AGAC	72	396
Hepcidin Rattus norvegicus hepcidin antimicrobial peptide	HAMP	FAM	TGGGGCAG AAAGCAAG ACT	AACAGAGA CCACAGGA GGAAT	125	223
Iron Regulatory Protein 1 Aconitase 1	Aco1	FAM	GCCTGGGA GTTCTTGG TT	CAATCACCT GGGGAAGC A	95	3374
Iron Responsive Element Binding Protein 2	Ireb2	FAM	CTTGGCAT TACAAAGC ACCTC	AACTCCACT TCCAAAGAA CTCAA	72	4673
ßactin	Actb	HEX	Housekeeping	-		

2.6.4 PCR Data Analysis

2.6.4.1 Comparative C_T Method

Collected PCR data was analysed on MxPro and Excel software. Relative gene quantification was calculated by application of Livak's (2001) comparative C_T ($\Delta\Delta C_T$) technique, which compares treated target gene signals with those of a control group for an expedient qRT-PCR analysis. Data was represented on graphs with fluorescence versus the number of cycles. A pre-determined threshold was set at a uniform value per experiment for each gene of interest, to maintain consistency throughout and to allow comparison between PCR plates. A final PCR reading for each reaction was denoted by the number of cycles required for the measured fluorescence to cross the assigned threshold for that particular gene. This number may be referred to as a threshold cycle (C_T) value. Once all readings were measured, relative gene expression of treated verses control were calculated using the C_T values in the following equations:

1. $\mathbf{\Delta C_T} = C_T$ (gene of interest) – C_T (housekeeping gene)

This resultant value for each treated condition was normalised to that of its parallel control, after triplicates were averaged, by applying equation 2:

2. $\mathbf{\Delta\Delta C_T}$ = Mean ΔC_T (treated sample) – Mean ΔC_T (corresponding control)

Upon completion of housekeeping normalisation, followed by calculation of average treated values relative to their equivalent average control values, true fold-change was computed to quantify target gene expression values by employing the following $\Delta\Delta C_T$ algorithm:

3. $\mathbf{2^{-\Delta\Delta C_T}}$

2.6.4.2 PCR Validation Experiments

Accurate PCR data relies on precision in pure sample quality, optimised experimental set-up, and PCR amplification efficiency. If it may be assumed that mRNA extraction was successful from NanoDrop 260/280 purity quantification, cDNA was decontaminated from any remaining gDNA, and experimental set-up was successfully optimised with consistent conditions between runs, precise pipetting using calibrated instruments, and an accurate thermal cycle, then there is one remaining factor that requires deliberation. The premise of a successful PCR run hinges on the assumption that amplification efficiency is equal between all probes being studied (Livak, 2001), at a consistent rate where there is a twofold amplicon increase within its geometric amplification phase. This equates to an efficiency rate of 100%.

To validate PCR efficiency, cDNA calibrator from samples revealed to express all genes of interest was prepared from a concentration of 1000ng and pooled together. An 8-fold serial dilution was performed and samples plated in triplicate with each experimental probe for analysis by qRT-PCR. Resultant C_T values were plotted against the log of input dilution amounts in a semi-log regression curve (Figure 2.19A), where the gradients for each slope were determined. Inputting these values into the following equation allowed for determination of the overall amplification efficiency of the PCR reaction for each individual amplicon:

$$\mathbf{E\ (\%)} = (10^{-1/\text{gradient}} - 1) \times 100$$

The standard curve slope estimates amplification efficiency, where 100% efficiency should have a corresponding curve slope of -3.33, with values ~± 0.3 falling at an acceptable 90% efficiency. All graphs, with the exception of GAPDH passed the efficiency test, with a range from 89.29-97.73%. Upon completion of the efficiency test, C_T values were then normalised to housekeeping genes, and ΔC_T data was graphed against log input in another regression curve for probe validation (Figure 2.19B). The resulting gradient served as a passing criteria for the validation experiment, where a gradient < 0.1 represented equivalent efficiencies for both the target and housekeeping genes. All probes, excluding GAPDH, had validation values less than 0.1 (ranging from 0.0013-0.0983). These results validate the $\Delta\Delta C_T$ method to be applied for qRT-PCR analysis, confirming similar amplification efficiencies between target and reference genes.

A

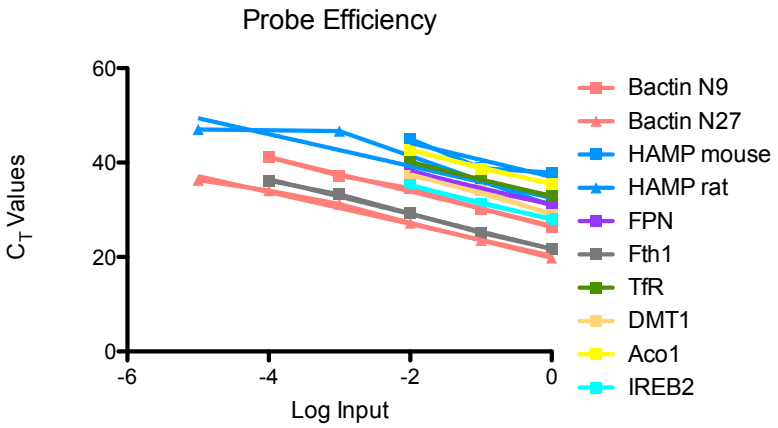

B

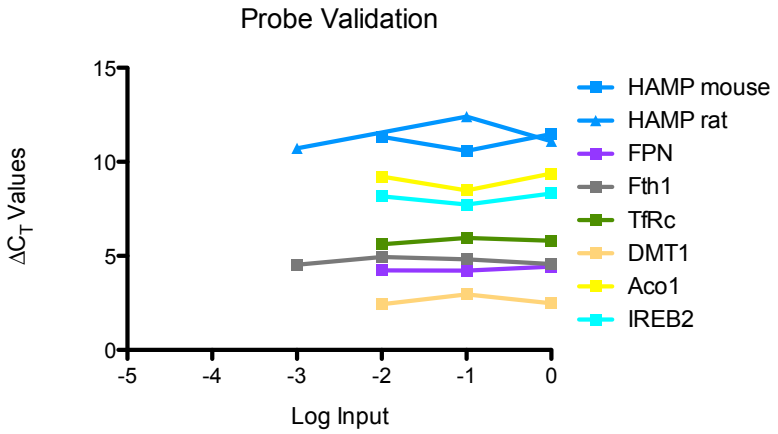

Figure 2.19 Validation Experiments
qRT-PCR probe efficiency (A) and validation (B) experiments using C_T and ΔC_T results, respectively, from genes of interest plotted against log input amounts in semi-log regression curves. All genes had an efficiency greater than 89.28% and a validity slope less than 0.1. This validates the comparative C_T method for use in this experiment, proving comparable amplification efficiencies between target and reference genes.

2.6.4.3 Housekeeping Validation

A reference gene was run in parallel with all samples to normalise results during analysis. To ensure that the chosen housekeeper was unaffected by treatment conditions, a geNorm analysis was conducted to test 6 different candidate reference genes (*ACTB, UBC, GAPD, Cyc1, ATP5b, 18s*) according to their expression stability using the 6 Double Dye Probe geNorm Reference Gene Detection kit (Primer Design, ge-DD-6-ra). GeNorm selection occurs by first measuring the sample expression in the provided panel of reference genes. PCR plates with 2µl/well were plated as per usual, using N9, N27 and C6 cells treated, respectively, with LPS or MCM (3h & 24h). All samples were measured in the same run for a given reference target, according to Hellemans' (2007) sample maximisation strategy. The kit was used in conjunction with the Qbase statistical analysis software involving geometric averaging of various control genes to select the optimum reference gene for this particular experiment. This software ranked the reference gene results in order of their stability after cellular treatment, providing several output graphs to ascertain which genes would serve as the best housekeepers (Figure 2.20), as well as the optimum number that should be run in tandem to calculate a geometric mean for the most accurate gene expression normalisation.

Qbase results determined a difference in stability between rat and mouse cell lines. Analysis employed a stepwise elimination beginning with the least stable gene, followed by a ranking with increasing expression stability. GeNorm (M) represents the average expression stability value. Table 2.3 depicts the stability ranking as determined by Qbase analysis for all three cell lines together, as well as individually. Next, the ideal number of housekeepers to run in duplex was calculated via the variation in mean housekeeper stability. The pairwise variation is defined by geNorm (V) (data not shown). These results have determined that the top two housekeeping genes with the most stable expression following treatment with experimental stimuli (barring ATP5b, which demonstrated no expression in N9 cells) were Cyc1 and ACTB. GeNorm (V) results were unable to determine an optimal number of reference targets due to the small n number with the removal of ATP5b, which led to a relatively high variability between sequential normalisation factors. Thus the system suggested either using 3 reference targets for normalisation with genes of interest or to attempt evaluating another potential reference candidate, which were both financially unfeasible or time constrictive. GAPD was also ordered for a duplexing housekeeper gene along with ACTB, however, it failed to pass the probe efficiency test as determined in Section 2.6.4.2 in comparison to the other validated amplicons. To avoid negatively affecting absolute quantification of the relative fold-change of gene expression because of lack of probe efficiency, GAPD was excluded from future study.

Since ßactin (ACTB) has been widely used as a housekeeping gene, and the geNome (M) analysis confirmed a relatively stable ACTB position within the ranking for all cell lines under experimental conditions, it was thus selected as a suitable housekeeping gene of choice implemented for all PCR experimentation within this project. However, any future studies under similar experimental conditions may want to consider using only rat cell lines so that ATP5b and/or Cyc1 may be used as housekeepers instead.

Table 2.3 GeNorm Stability Classification Results
This table represents the ranking of key reference genes for qRT-PCR for each individual cell line as well as the three together, as determined by the PrimerDesign geNorm reference gene detection kit. GeNorm selection is employed to gauge whether experimental conditions may significantly affect housekeeping genes, thereby affecting normalisation and decreasing validity of results. Genes are listed according to stability of expression after cell treatment with their corresponding stimuli.

Cell Line	Stability Ranking (least to most stable)
N9 + N27 + C6	UBC, 18s, GAPD, ACTB, Cyc1
N9 (mouse)	18s, UBC, GAPD, ACTB, Cyc1
N27 (rat)	18s, UBC, ACTB, GAPD, Cyc1, ATP5b
C6 (rat)	18s, ACTB, GAPD, UBC, Cyc1, ATP5b

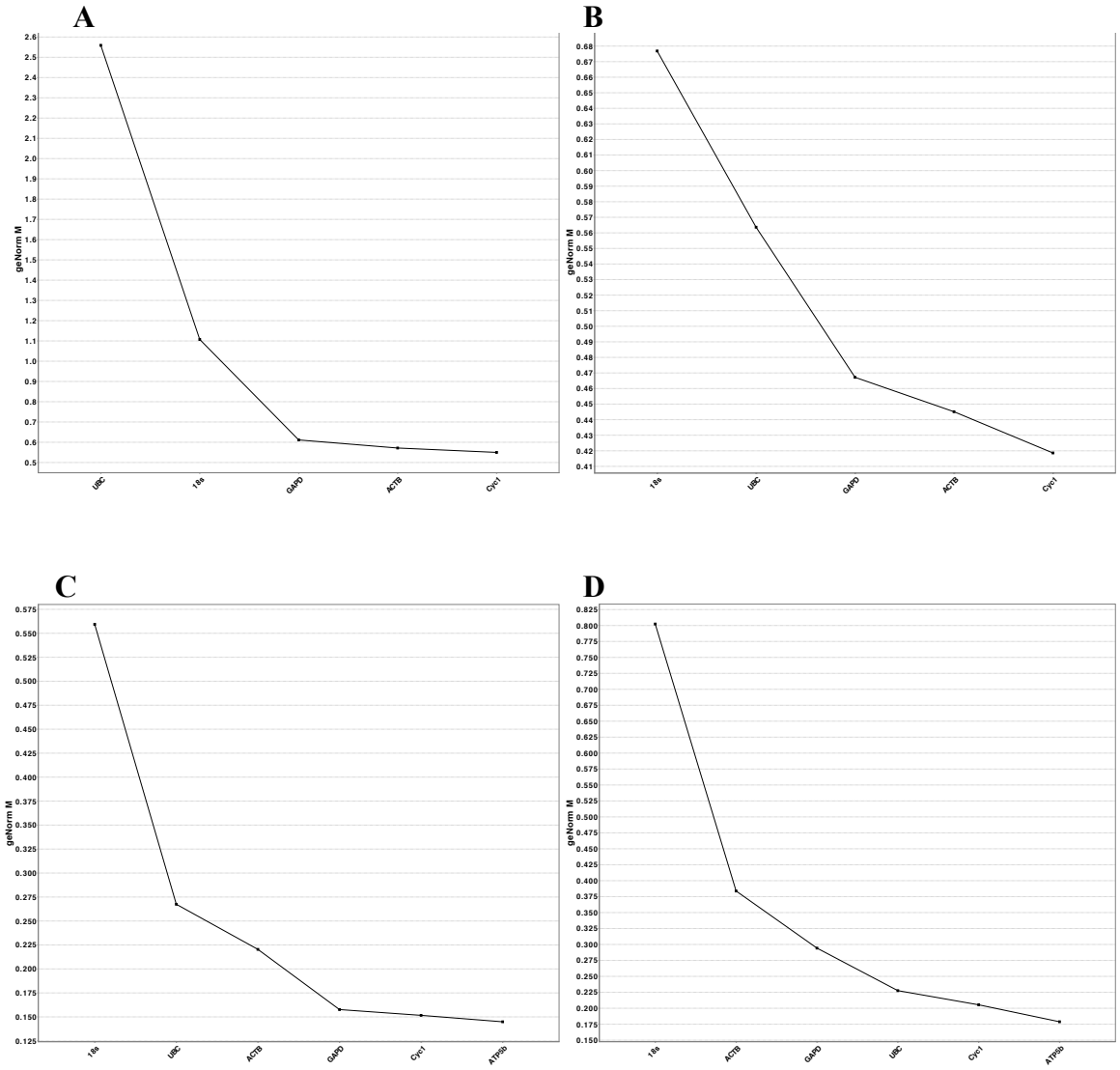

Figure 2.20 Housekeeping Validation via GeNorm Analysis
These graphs represent the average expression stability of several key reference targets (18s, GAPD, ACTB, UBC, Cyc1, ATP5b), with genes plotted against the geNorm (M) (average expression stability value). The least stable gene can be seen on the leftmost side of the x-axis, with an increasing stability of expression moving towards the right. Expression was examined in all three cell culture lines (A), N9 only (B), N27 only (C), and C6 only (D). Microglial N9 cells did not express any ATP5b, so was not represented in the data for graphs A and B.

2.7 Hepcidin Quantification with Mass Spectrometry

Hepcidin is a master regulator of iron metabolism, capable of binding the iron exporter ferroportin and initiating its degradation. As hepcidin is shown to affect systemic iron levels when upregulated in response to inflammation and excess iron, and unregulated increases in iron can be neurotoxic (Oestreicher, 1994; Jiang, 2006), the unknown source of hepcidin release remains of vital discovery. It was postulated that microglia could be one such source of hepcidin, releasing it following an inflammatory response. To determine whether or not this was the case, N9 cells were seeded for LPS stimulation as usual (24h). Upon completion of this treatment, supernatants were collected, centrifuged (10,000rpm, 5m) and pellets discarded. The remaining supernatants for 0.25μg/ml LPS treatment and control were frozen at -20ºC for analysis to determine hepcidin levels in the culture media by mass spectrometry at a laboratory in King's College London, as per the protocol in their paper (Pechlaner, 2016). Mass spectrometry involves separating ions according to mass-charge ratios. Hepcidin ions would have the same ratio, causing the same deflection, and thus becoming visible for quantitative detection by a mass spectrometer (Acquity UPLC coupled to Waters Xevo TQ triple quadrupole), with data acquired on MassLynx version 4.1. Results would be compared to those of known standard concentrations using a synthesised internal standard [$^{13}C_9$, $^{15}N_1$]Phe^{4,9}-hepcidin, allowing for precise determination of the amount of hepcidin present within supernatant samples.

2.8 Fluorescent Probes Measuring Downstream Effects

Experiments thus far have considered the effects of microglial inflammation on the regulation of neuronal iron after short term and co-culture treatments. Dysregulated IRPs and intracellular iron levels could have latent effects on downstream pathways towards cell death. Therefore, it must be determined whether abnormalities in neuronal iron metabolism trigger further long-term changes. Several factors were examined to accomplish this, including OS, mitochondrial dysfunction, apoptosis and necrosis. Results were measured and quantified using fluorescent microscopy and flow cytometry.

Fluorescent microscopy involves illumination of samples containing fluorescent dyes with specific light wavelengths absorbed by fluorophores. This results in weaker light emissions filtered to a detector that creates a superimposed image. The fluorescent microscope (Nikon TS) was used with the 4-channel experiment protocol and filters A DAPI, B488, C555, D Far Red. Images were analysed using the MicroManager software. Single-cell flow cytometry is based on cell suspension separated for passage through an electronic light sensor. Thousands of measurements are processed and acquired within set parameter gates. Data was quantified and analysed using FlowJo software.

2.8.1 Oxidative Stress

2.8.1.1 Cell Rox Deep Red Reagent

Loss of equilibrium between ROS production and antioxidant scavengers leads to cellular OS. CellRox Deep Red Reagent (ThermoFisher, C10422) involves the use of fluorogenic probes to measure ROS in live or fixed cells (Ma, 2013). The reduced state CellRox OS reagents added to seeded cultures are non-fluorescent. Upon cell permeation, reagents localise to the cytoplasm where they can be oxidised to display bright fluorescence at an absorption/emission of ~644/665nm. The greater the cellular OS (and the concomitant presence of oxidants), then the greater the observed fluorescence, thus allowing for determination of cellular OS. Protocols performed were followed as per manufacturer's precise instructions.

N27 neuronal cultures were seeded and treated with MCM as per usual. Upon completion of the 24h incubation period, CellRox reagent was added directly to wells at a final concentration of 5µM. Cells were incubated under normal conditions (37ºC in humidified atmosphere) for 30m to allow for reagent to permeate cells. After incubation, medium was fully aspirated, and wells washed with PBS (x3). Cells were then fixed with 2ml 3.7% paraformaldehyde (PFA) for 15m, and then analysed under the fluorescent microscope. Cells treated with the neurotoxin 6-Hydroxydopamine (6-OHDA) at a concentration of 15µM for the same 24h incubation

period were used as positive controls for OS. Results obtained were from both treated and control conditions within 9 random fields per well under x200 magnification.

2.8.2 Mitochondrial Membrane Potential

2.8.2.1 MitoTracker Red

MitoTracker (MT) Red is a cell membrane permeable probe that functions by diffusion through the plasma membrane, where it is oxidised to a fluorescent stain and accumulates within actively respiring mitochondria. This mitochondrial accumulation depends on an active negative membrane potential, so that labelling occurs only in healthy mitochondria. The stain is retained even after lost membrane potential with aldehyde fixation, unlike other dyes, as it binds with mitochondrial thiols to form a permanently-bound fixable fluorescent conjugate.

All products were equilibrated to RTP before use. The lyophilised MitoTracker Red probe was first dissolved to a concentration of 1mM in DMSO, then aliquoted and stored at -20ºC protected from light. N27 cells were seeded and incubated with MCM (24h and 48h) as per usual, however, were grown on coverslips within wells. A negative control was run in parallel, with N27 cells incubated the same amount of time and under the same conditions, without the addition of the MT dye. When cells were ready, the 1mM stock was then further diluted to a working concentration of 100nM in serum-free growth media. The dilution was wrapped in foil to protect from light, and warmed to 37ºC in a water bath. Growth media was fully aspirated from cell wells, cells washed in warmed serum-free RPMI (x1), and the pre-warmed 37ºC MT stain was added at a final concentration of 200nM. Cells were then incubated at 37ºC for stain permeation (25m), after which the stain solution was aspirated and replaced with warmed serum-free RPMI. This was aspirated and replaced with pre-warmed 4% PFA in PBS (15m). Following fixation, wells were rinsed with PBS (x2), and cells observed under the fluorescence microscope (Nikon TS) with excitation/emission set to ~579/599 in order to look for live cells and the downstream effects of MCM incubation on neuronal mitochondrial membrane potential. Images were analysed using ImageJ Quantification, with 9 averaged random field images per well normalised to background.

2.8.3 Apoptosis & Necrosis

The dead cell apoptosis kit with Annexin V Alexa Fluor 488 and propidium iodide (Invitrogen, V13241_3636530485) protocol was followed as per the manufacturer's instructions. Cells are differentiated based on the fact that live cells contain phosphatidylserine (PS) on their inner cytoplasmic surface. However, PS is translocated and exposed to the external environment in apoptotic cells. Annexin V is a protein with high PS affinity, and is

able to bind PS only when it is exposed on the outer cell membrane. Alexa Fluor dye conjugated to Annexin V thus labels it with a fluorophore that can help distinguish live from apoptotic cells via fluorescent detection, where apoptotic cells demonstrate membrane staining. Propidium iodide (PI) can only permeate dead cells, binding to nucleic acids and producing a red fluorescence. Thus, addition of PI to cell populations can help differentiate between apoptotic and necrotic cells. Upon completion of the protocol, the populations should separate into 4 groups, where live cells have weak Annexin V staining and low level fluorescence, early apoptotic cells have high surface labelling with green fluorescence, late apoptotic cells demonstrate both membrane staining by Annexin V (green fluorescence) and strong PI nuclear staining (red fluorescence), while dead necrotic cells only show PI staining (red).

2.8.3.1 Alexa Fluor Annexin V & PI

The flow cytometry protocol involved treatment of N27 cells with MCM as per usual, with a negative control run in parallel without MCM treatment, and a positive control for apoptosis where N27 cells were incubated with 1µM staurosporine. A 1x annexin-binding buffer (abb) was prepared from the provided 5x buffer, diluted in dH_2O. Next, 100µg/ml working solution of PI was made by dilution in the 1x annexin-binding buffer. Upon completion of the incubation period, media was aspirated and cells were washed in warmed PBS (x2). 1ml warmed complete RPMI was added per well, and cells scraped and collected to eppendorfs. Tubes were centrifuged (200g, 5m), and the media very carefully aspirated to discard the supernatant. Each tube was resuspended in 500µl 1x abb, briefly vortexed and cell density determined by Trypan Blue counting on a haemocytometer. Cell density was then diluted in 1x abb to a final concentration of ~1 x 10^6 cells/ml. After dilution, tubes were vortexed, and 100µl of each was added to a fresh tube. Using the staurosporine positive control cells, they were split into 4 separate tubes: unstained, Annexin V, PI, Annexin V + PI. The rest of the samples were double stained with 5µl Annexin V and 1µl 100µg/ml PI working solution. Tubes were incubated in the dark (15m, RTP), covered with foil, after which 200µl 1x abb was added per tube, and they were placed on ice. Stained cells were analysed as soon as possible by flow cytometry (FACScalibur), with fluorescence measured at an emission of 530-575nm.

2.9 Statistical Analysis

Data was expressed as mean ± standard error mean (SEM) from a minimum of 3 independent experiments, performed in triplicate where possible. Using GraphPad Prism (Version 5.0a for Mac OS X), data was tested for statistical significance via the analysis of variance (ANOVA) statistical test with Dunnett's post-test to compare multiple means against the control group. A 2-tailed unpaired student's t-test was used for individual comparisons. A p value <0.05 was considered as statistically significant, with significance indicated by the following asterisks: *=$p<0.05$, **=$p<0.01$, ***=$p<0.001$.

CHAPTER 3:

Investigation into the time course of inflammatory factor effects released by activated microglia on iron regulatory proteins in *in vitro* dopaminergic neurons

3. Investigation into the time course of inflammatory factor effects released by activated microglia on iron uptake and gene expression of iron regulatory proteins in *in vitro* dopaminergic neurons

This chapter aims to define the time course of the LPS-activated microglial inflammatory response in order to determine an appropriate LPS concentration and exposure time for subsequent treatment to dopaminergic neurons. This was executed by analysis of microglial-released pro-inflammatory factors. Microglia were then examined for any inflammation-induced alterations in their iron metabolism, by examination of total intracellular iron levels along with gene expression of several key iron regulatory proteins. The examined proteins included hepcidin, ferroportin, ferritin, transferrin receptors, divalent metal transporter 1, aconitase 1, and iron responsive element binding protein 2 (respectively, HAMP, FPN, FtH1, TfR, DMT1, Aco1, IREb2). Next, N27 dopaminergic neurons were treated with the microglial supernatant containing their released inflammatory factors, referred to as microglial conditioned medium (MCM). A time course of inflammatory factor exposure to N27s was measured, in order to define the optimum time for use in subsequent experimentation. Total intracellular iron in N27s was measured, as was their gene expression for the same iron regulatory proteins as above.

3.1 Introduction

Microglia are known to release an array of inflammatory factors upon activation, however their direct effects on iron metabolism in dopaminergic neurons are yet to be fully investigated. Since PD has exhibited augmented numbers of activated microglia, accompanied by high levels of inflammatory factors and increased iron concentrations, it is theorised that these microglial inflammatory factors are affecting changes to neuronal iron metabolism. Such changes may occur from altered levels of iron regulatory proteins, with those chosen for study including HAMP, FPN, FtH1, TfR, DMT1, Aco1, and IREb2 (Table 3.1). These proteins very carefully monitor intracellular iron levels, so any fluctuations may lead to iron overload. Excess iron is known to contribute to neurodegeneration by stimulating free radical formation (Olanow, 1994), whereby the resultant OS initiates downstream effects with consequential neuronal degeneration (Brown, 2003).

Hepcidin is known as the master iron regulator, preventing cellular iron export, and thus having a direct effect on intracellular and extracellular iron levels. It is upregulated in response to inflammation and excess iron (Nemeth, 2003). While hepcidin is a crucial protein in iron distribution and regulation necessary for physiological iron homeostasis (Ganz, 2011), the source of its synthesis and release during inflammation remains to be elucidated. It is postulated that microglia may be a potential source upon activation.

Representing an *in vitro* model of inflammation in PD, microglial cells activated by the gram-negative bacteria LPS induce release of inflammatory factors, such as IL1ß, IL6 and TNF, into the culture media. Irrespective of which specific inflammatory factors cause the observed neurodegeneration, inflammation instigated by activated microglia has been shown to trigger the neurodegenerative pathway in various *in vitro* and *in vivo* PD models. Thus, aiming at reducing inflammation and the ensuing iron accumulation offers a curative target. However, since the exact source of iron dysregulation remains largely unknown, and dopaminergic neurons affected in PD are more susceptible to the OS-related neurotoxicity, identifying a precise target would be far more beneficial.

This chapter intends to elucidate a time course for some of the inflammatory factors being released by the N9 mouse microglial cell line activated by LPS *in vitro* to determine when they are at their highest concentrations. Activated N9 cells were then analysed for release of hepcidin into cell culture supernatant. Once the optimum time and LPS concentration were determined, the N27 dopaminergic rat cell line was then exposed to these inflammatory factors for various time points by supernatant transference of the microglial conditioned medium.

Neuronal exposure to inflammation may affect changes in iron metabolism and lead to subsequent cell death, so gene expression of iron regulatory proteins was monitored, as were changes in overall iron levels.

Table 3.1 Iron Regulatory Proteins Studied
This table depicts the iron regulatory proteins monitored throughout this study, their main functions, cellular location, and factors that cause either upregulation or downregulation (Simovich, 2002).
Abbreviations: IRE/IRP= Iron Regulatory Element/Iron Regulatory Protein System

Iron Regulatory Protein	Abbreviation	Principal Function	Location	Upregulation	Downregulation
Hepcidin	HAMP	Main iron regulatory hormone, binds FPN	Intracellular	LPS, IL6, TfR2, Increased Fe	Hypoxia, Fe deficiency
Ferroportin	FPN	Iron export	Transmembrane	High Fe IRE/IRP	Low Fe IRE/IRP, HAMP
Ferritin Heavy Chain	FtH1	Iron storage	Intracellular	High Fe IRE/IRP	Low Fe IRE/IRP
Transferrin Receptor	TfR	Iron import	Transmembrane	Low Fe IRE/IRP	High Fe IRE/IRP
Divalent Metal Ion Transporter	DMT1	Iron import	Transmembrane	Low Fe IRE/IRP	High Fe IRE/IRP
Aconitase	Aco1	Cellular regulation	Intracellular	Fe	Increased Fe
Iron Responsive Element Binding Protein	IREb2	Cellular regulation	Intracellular	Fe	Increased Fe

3.2 Chapter Objectives

This chapter aims to complete the following objectives:

1. Investigate the time course of inflammatory factors released by LPS-activated N9 microglial cells.
    a. Corroborate the N9 microglial cell line suitability as an *in vitro* model of inflammation caused by microglial activation via confirmation of N9 expression of macrophage-specific proteins.
    b. Assess the release of inflammatory factors after N9 treatment with LPS.
    c. Assess the effects of the microglial inflammatory response on gene expression of iron regulatory proteins in microglia.
    d. Assess intracellular iron expression in microglia after treatment with LPS.
    e. Assess the microglial release of hepcidin after LPS activation.
    f. Define the optimum LPS concentration and incubation time point to elicit a sufficient inflammatory response without affecting cell viability to utilise for neuronal exposure to inflammatory factors.

2. Investigate the effects of microglial inflammatory factors on iron regulatory proteins in the N27 dopaminergic neuronal cell line.
    a. Corroborate the N27 dopaminergic neuron cell line suitability as an *in vitro* model of Parkinson's disease substantia nigra neurons via verification of their neuronal markers and their lack of response to LPS exposure.
    b. Determine the ideal time point of neuronal exposure to inflammatory factors in microglial conditioned media at which to observe the greatest effects on iron metabolism for use in subsequent study.
    c. Validate key experimental results using primary neurons.

3.3 Experimental Methods

3.3.1 Investigating the Time Course of Inflammatory Factors Released by LPS-Activated N9 Microglial Cells

To complete the first directive investigating the time course of inflammatory factors released by activated microglial cells, various LPS concentrations and incubation periods were tested and optimised. First, the *in vitro* N9 cell line (Section 2.1.3) was examined for suitability at modelling Parkinsonian inflammation, after which they were activated by LPS treatment at varying concentrations in order to monitor several released inflammatory factors. This data was used to determine the optimum LPS concentration and incubation time point to elicit a sufficient inflammatory response to utilise for subsequent study with neuronal exposure to inflammatory factors. The experimental design is now described in further detail, with a representative model shown in Figure 3.1.

In order to determine the suitability of the N9 microglial cell line as an *in vitro* model of inflammation, N9 expression of macrophage-specific protein Iba1 was confirmed via Western Blot (Section 2.5.2). N9 cells were plated with cumulative densities from 0.5 to 3 million cells per well in a 6 well plate. After a 24h resting period to allow cellular recovery, cells were lysed with RIPA buffer and a protease inhibitor (PI), whereupon Western Blots were run to confirm Iba1 lysate expression (Figure 3.1A). To serve as negative controls without any Iba1 presence, N27 lysates and a blank well without any cells were run in parallel.

To assess the time-course of the microglial inflammatory factor release in N9 cells and to determine the optimum LPS incubation period, N9 cells were plated in 6 well plates at a density of 35 x 10^4 cells per well (Section 2.3.1.1). After a 24h rest period, cells were exposed to varying LPS concentrations (0-1µg/ml) for various incubation periods (1-24h). Upon completion of incubation, the supernatant was collected for analysis of microglial activation levels resulting from LPS treatment via ELISA (IL1ß, IL6, TNF) (Section 2.4.3), Griess assay (to determine nitric oxide production from nitrite levels) (Section 2.4.2), or mass spectrometry (to assess hepcidin presence) (Section 2.7) (Figure 3.1B). Cells were also lysed after the appropriate incubation periods in order to assess the cellular gene expression of iron regulatory proteins through RT-PCR (Section 2.6), protein expression via Western Blots, or iron uptake via the ferrocene assay (Section 2.4.4) (Figure 3.1C). Results were used to establish an optimal incubation time with sufficient inflammatory mediator expression for which to harvest LPS-activated microglial conditioned media for subsequent neuronal exposure.

After N9 cell treatment with LPS and analysis of the inflammatory factor release, a sub-maximal dose was chosen utilising the minimum amount of LPS to avoid microglial

overstimulation or inciting cytotoxicity, while still eliciting a sufficient stimulation of the inflammatory response. To ensure the treatment dosages did not stimulate cytotoxicity in the N9 cells, 3 viability assays were performed: NR, MTS and Bradford (Section 2.4.1). N9 cells were seeded in a 96 well plate at a density of 10 x 10^3 cells per well and left 24h to rest, after which they were treated with increasing doses of LPS (0-1µg/ml) for the optimised incubation period of 24 hours (Figure 3.1D). Cell viability was then determined via the 3 assays. Utilising the inflammatory mediator and viability results, a sub-maximal LPS dosage was then selected to elicit a sufficient inflammatory response without affecting cell viability in longer incubation periods. This dosage was applied to all subsequent experiments for microglial activation, unless otherwise indicated, and the N9 supernatant treated with the optimally determined LPS concentration after 24h incubation is hereafter referred to as microglial conditioned medium (MCM).

Utilising the optimally determined time points and LPS dosage, N9 cells were activated and supernatant collected (24h) for analysis by mass spectrometry to determine if microglia were synthesising and releasing hepcidin upon activation. Sample concentrations were calculated using peak area ratios versus a calibration standard curve.

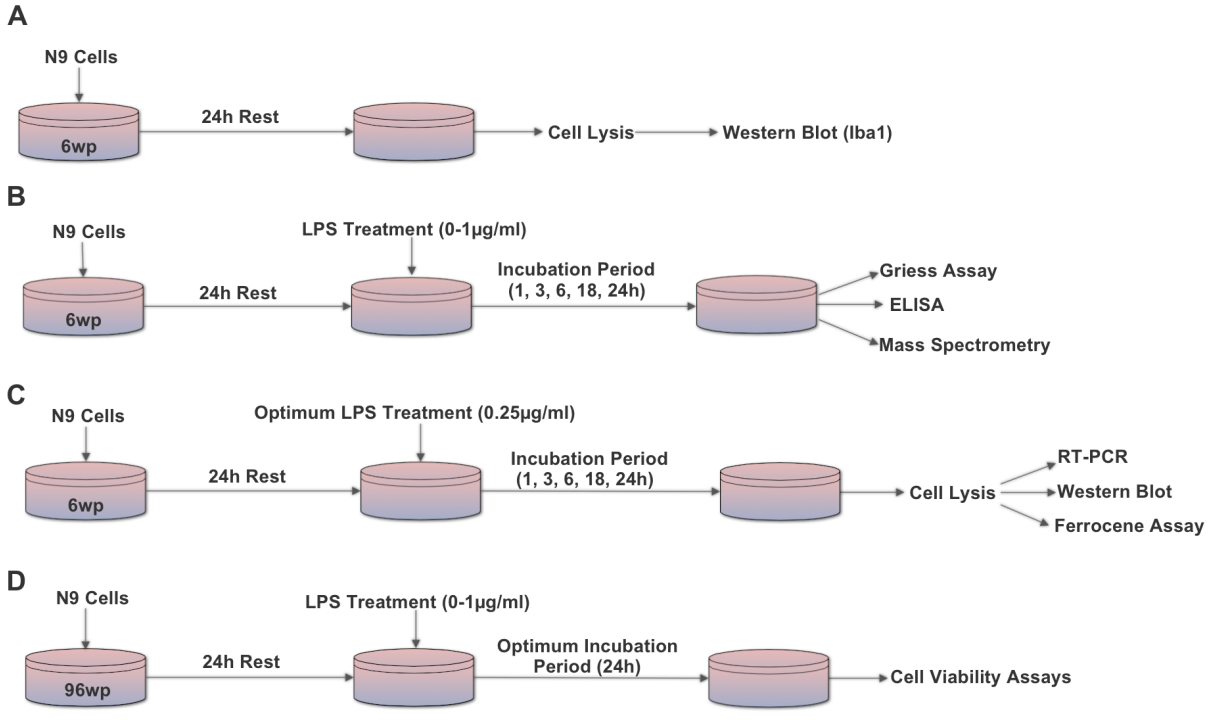

Figure 3.1 Experimental Designs for N9 Cell Treatment
Experimental design for investigation into inflammatory factors released by N9 cells at varying LPS concentrations and incubation times (B), optimising LPS incubation periods to induce inflammation (C), and optimisation of LPS treatment to avoid overstimulation or loss of cell viability whilst maintaining microglial activation (D). Western blots helped determine N9 suitability as a microglial inflammatory model (A).
Abbreviations: 6wp= 6 well plate, 96wp= 96 well plate, h=hours, LPS= lipopolysaccharide.

3.3.2 Investigating the Effects of Microglial Inflammatory Factors on Iron Regulatory Proteins in the N27 Dopaminergic Neuronal Cell Line

The second directive was to use the optimised microglial activation in order to investigate their effects on iron regulation in neurons using the N27 dopaminergic cell line (Section 2.1.4). Firstly, the N27 neuronal cell line suitability as a Parkinsonian model of dopaminergic neurons was assessed, followed by N27 treatment with MCM. Neuronal viability was evaluated after MCM exposure to establish an optimum incubation period, and finally neurons were examined for any changes to iron regulatory proteins. The experimental design is represented in Figure 3.2.

Firstly, N27 cells were tested for expression of neuronal markers NeuN and TH via Western Blot to confirm their suitability for use as a cell culture model of PD. Cells were plated with increasing densities from 0.5 to 4 million cells per well in a 6 well plate. After 24h rest, cells were lysed with RIPA buffer and PI, and cell lysates were run through Western Blot gels to measure NeuN and TH expression (Figure 3.2A). N9 cell lysates and a blank well were run concurrently to serve as negative controls.

N27 cells were monitored for any changes in viability at different levels of microglial activation. N9 cells were plated in 6 well plates (35 x 10^4 cells per well), left to rest 24h, then treated with a range of LPS doses (0-1µg/ml) for the optimum incubation period of 24h. The supernatant was collected and used to treat N27 cells (seeded 10 x 10^3 cells per well in 96wp) (Figure 3.2B). After 24h, three viability assays were performed (MTS, NR, and Bradford) to determine whether or not the microglial-released inflammatory factors used to treat N27s incurred a loss of neuronal cell viability at the before-determined optimal dosage. Next, N27s were seeded at a concentration of 30 x 10^4 cells per well in 6 well plates, rested for 24h, then exposed to the optimal microglial conditioned medium for a variety of time points (1-48h). After each incubation period, cells were lysed and collected for evaluation of iron regulatory protein gene expression via RT-PCR, protein expression via Western Blots, or iron uptake via ferrocene assay (Figure 3.2C). Experimental results helped ascertain the effects of inflammation on neuronal iron metabolism.

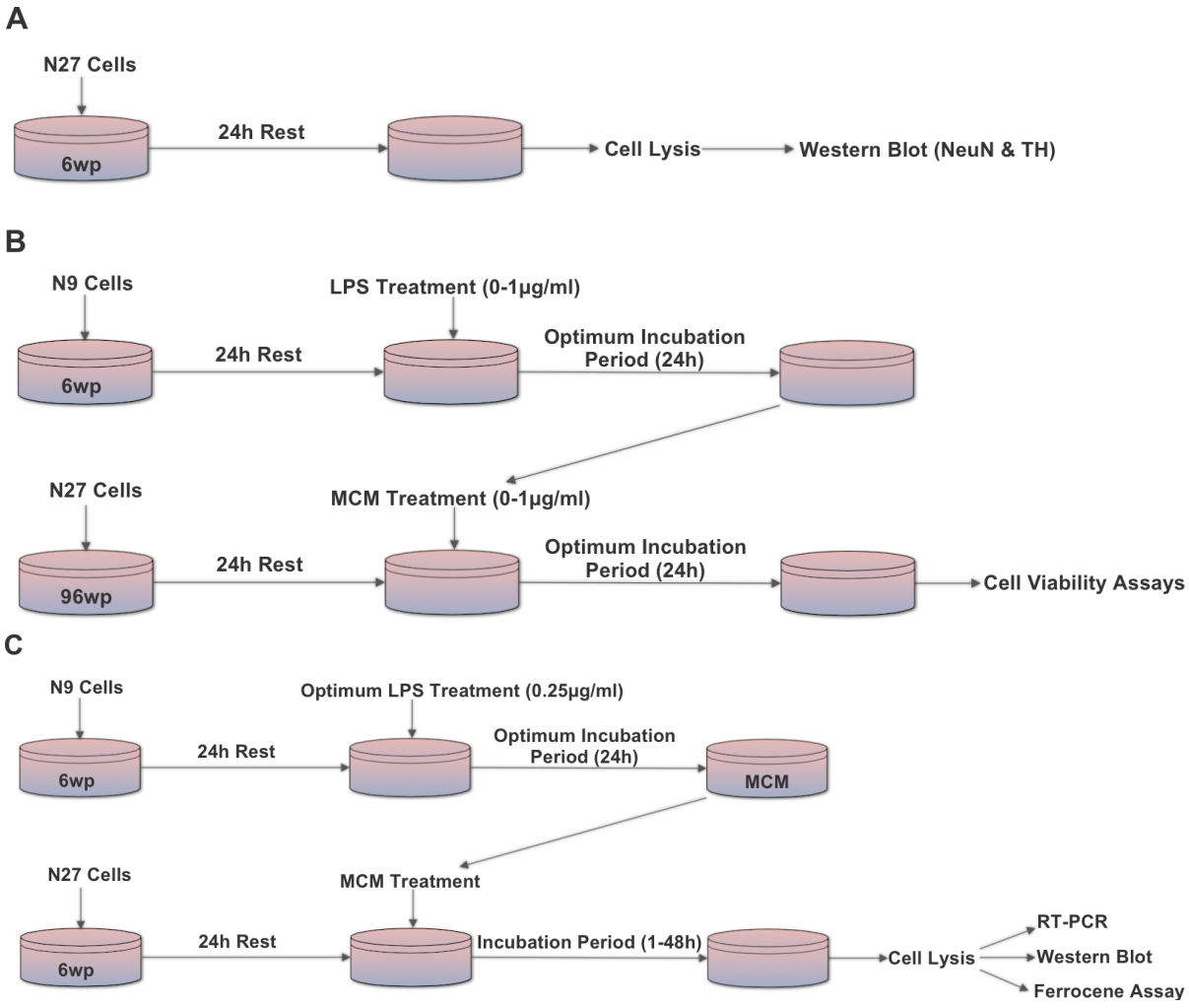

Figure 3.2 Experimental Designs for N27 Cell Treatment
Experimental design for investigation into the effects of inflammatory factors released by N9 cells on iron regulation in N27 dopaminergic neurons. Suitability of the N27 cell line for use as a Parkinsonian disease model via Western Blot analysis of neuronal proteins (A), optimisation of MCM inflammatory factors to monitor exposure effects on neuronal cell viability (B), optimising MCM incubation periods to observe consequences of inflammation on neuronal gene and protein expression, and iron uptake (C).
Abbreviations: 6wp= 6 well plate, 96wp= 96 well plate, h=hours, LPS= lipopolysaccharide, MCM=microglial conditioned medium.

3.3.3 Investigating the Effects on Iron Regulatory Proteins in Primary Neurons

Upon cell extraction from E18 rat pups, primary hippocampal neurons (Section 2.1.6) were seeded (600,000c/w) into pre-coated (poly-L-ornithine 2h, 3 PBS washes, 4µg/ml laminin coating ON) 6 well plates, and left to rest 24 hours to allow cultures to recover from any stress. Several attempts at treatment with MCM (24h) led to death of the neuronal cultures, which is most likely due to the shock of a different growth medium containing serum. As a result, primary cultures were only treated with direct LPS (0.25µg/ml 24h), and then collected for analysis via qRT-PCR or ferrocene assay.

3.3.4 Statistical Analysis

Experiments run in 6wp were performed three times independently with one single well per run, while those in 96wp were performed three independent times with triplicate wells per run. Results were then pooled to calculate the mean result for each test, with all conveyed data representing mean ± standard error mean (SEM). Western Blot data for confirmation of cellular markers to determine correlation with increasing cellular density, and data from mass spectrometry hepcidin quantification in N9 supernatant were analysed using linear regression. Data for determination of the microglial inflammatory response for dosage and incubation optimisation, including that from the Griess and ELISA assays, was analysed via 1-way ANOVA including Dunnett's Multiple Comparison post-hoc test. RT-PCR and ferrocene assay results for both N29 and N27 treatments were compared by 1-way ANOVA. RT-PCR utilised Dunnett's Multiple Comparison post-hoc test to compare all data to the control column, while ferrocene assay analysis employed Bonferroni's Multiple Comparison test in order to compare all data groups to their own specific control column. Cell viability data for both N9 and N27 cells were evaluated with 1-way ANOVA and Dunnett's Multiple Comparison post-hoc test. All statistical analyses were run on the Prism 5 for MAC OS X program (Version 5.0a, GraphPad Software Inc).

3.4 Results

3.4.1 Confirming Iba1 Expression in N9 Cells

Western Blot results from microglial cells plated at cumulating cell densities, along with two negative controls (blank well and N27 cells), evaluate the protein concentrations of the microglial marker Iba1 in N9 cells. If N9 cells do indeed represent a microglial phenotype, then they should express microglial markers. The greater the number of N9 cells, should therefore reflect in a greater amount of detected protein expression. Hence, it was predicted that Iba1 protein should have a positive correlation to increasing cell densities, and that neither negative control should demonstrate any Iba1 expression. Results affirm these predictions with a significant linearly increasing trend (R^2= 0.9597) (Figure 3.3). Iba1 protein expression data is determined by densitometry analysis and presented in the graphs below.

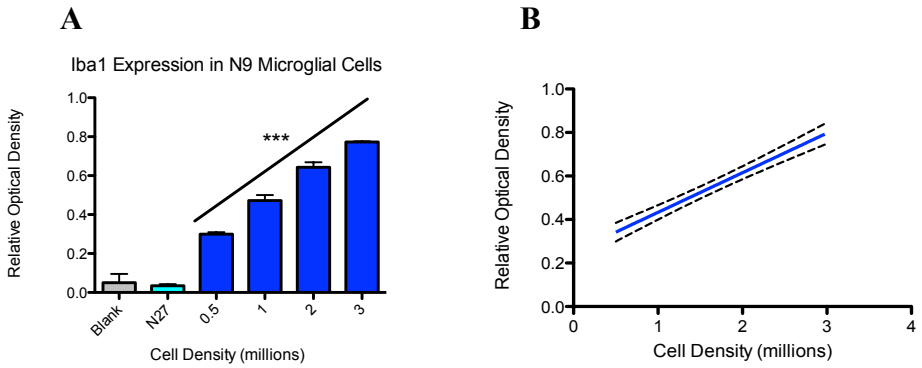

Figure 3.3 Confirmation of Iba1 Protein Expression in N9 Microglial Cells and N27 Dopaminergic Neurons as Measured by Western Blot Analysis. Increasing densities of N9 cells were lysed and their Iba1 microglial marker protein expression was determined via Western Blot in order to confirm a corresponding increase in expression. One blank well devoid of any cells, and another seeded with N27 cells (2 x 10^6 cells/well) were run in parallel acting as negative controls that should not express any Iba1. All wells were run with an equal volume of lysate preparation. Densitometry analysis presenting mean ± SEM for all measured samples verifies a linearly increasing Iba1 expression with cell density (A). Dotted lines represent the linear regression ± 95% confidence band lines of best fit (B).

3.4.2 Optimising LPS Concentration and Exposure Times with N9 Cells for Use in All Successive Experiments

N9 cells were treated with a range of LPS concentrations or vehicle control for 1-24h, after which various assays monitored for levels of microglial activation and their release of inflammatory factors. ELISA assays quantified levels of pro-inflammatory cytokines (IL1ß, IL6, TNF), while the Griess assay detected nitrite ion concentration to calculate the amount of nitric oxide present (Figure 2.8 A-D). NR, MTS and Bradford assays were then performed to ascertain whether higher doses of LPS had a cytotoxic effect on cells. Results from the three assays, showed no significant loss of cell viability up to a concentration of 1µg/ml LPS at 24h (Figure 2.9 A-C). Extrapolating from this data, a concentration of 0.25µg/ml was selected for use in all ensuing experimentation as the optimal sub-maximal LPS concentration.

3.4.2.1 Relative Gene Expression of Iron Regulatory Proteins in N9 Cells via PCR

Next, this optimum LPS concentration was utilised to activate N9 microglia and measure their relative gene expression of iron regulatory proteins of interest using qRT-PCR (Figure 3.4). mRNA was extracted from N9 cells after treatment with the optimized 0.25µg/ml concentration for a range of incubation periods (1-24h). Lysates were collected, and cDNA was extracted to measure gene expression levels via PCR. Significantly increased fold change from control were observed with hepcidin (3h=3.389 ± 0.52, $p<0.001$), ferroportin (18h=1.825 ± 0.17, $p<0.01$), ferritin (18h=2.419 ± 0.57, $p<0.05$), transferrin receptors (18h=1.601 ± 0.12, $p<0.01$), and DMT1 (18h=3.38 ± 0.2, $p<0.001$) expression.

Analysis of all assays after N9 cell treatments with LPS led to determination that the optimum concentration sufficient to induce an inflammatory response and release of pro-inflammatory cytokines and reactive nitrogen species was 0.25µg/ml. Evaluation of cell viability and relative gene expression data from qRT-PCR proved that 24h exposure to LPS was sufficient to elicit a strong inflammatory response. Thus, the optimised concentration and incubation period were applied in all future experiments to generate microglial conditioned medium.

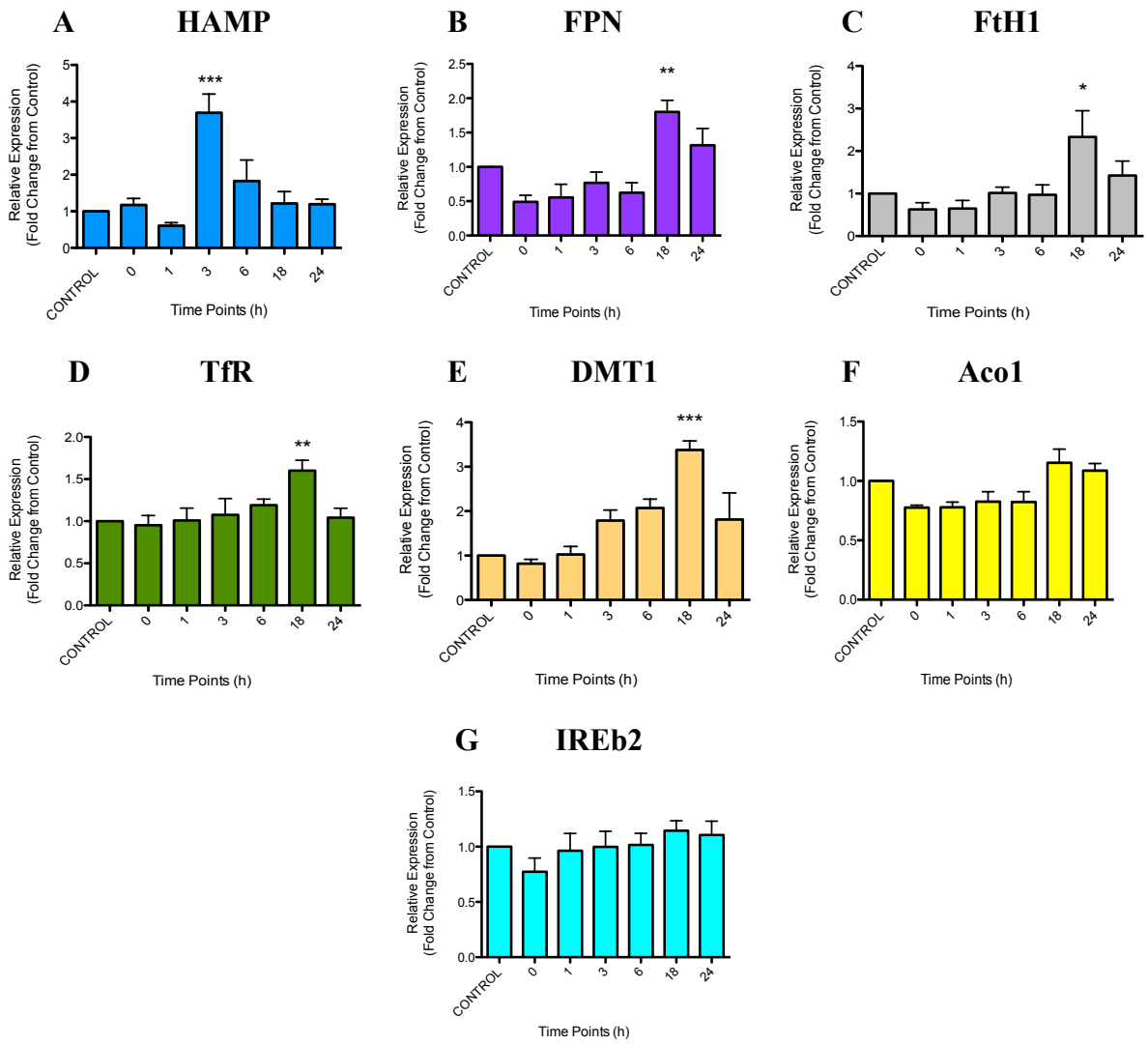

Figure 3.4 Changes in Relative Gene Expression of Iron Regulatory Proteins in LPS-Treated N9 Microglia
N9 cells were seeded (350,000c/w in 6wp) and rested 24h before being treated with LPS to induce their inflammatory response. LPS was added directly to wells, whereby cells were incubated for a range of time points in order to deduce optimum LPS exposure periods for which to elicit the greatest changes to relative gene expression of iron regulatory proteins. Cell lysates were collected and processed to extract mRNA and synthesise cDNA. Relative gene expression was then measured via qRT-PCR. Data is analysed by ΔΔCt method, presenting results as a fold change from the ß-actin control housekeeping gene. Results from the iron regulatory proteins hepcidin (HAMP A), ferroportin (FPN B), ferritin (FtH1 C), transferrin receptors (TfR D), DMT1 (E), Aconitase 1 (Aco1 F), iron responsive element b2 (IREb2 G) show several significant changes. Hepcidin is upregulated at 3h, with a sharp decrease thereafter. Ferroportin, ferritin, TfR and DMT1 were all upregulated at 18h, with a quick reduction afterwards as the cells are rebalanced via homeostatic mechanisms. Aco1 and IREb2 show no significant upregulation. These results suggest that the inflammatory response in activated microglia exerts noticeable alterations to the homeostasis of certain key iron regulatory proteins. *n=3.*

3.4.2.2 Iron Expression in N9 Microglia After LPS Treatment

N9 cells were treated with optimised LPS for a range of time points (1-24h), whereupon the ferrocene assay was performed in order to observe for any changes in microglial intracellular iron expression following instigation of the inflammatory response (Figure 3.5). Significant increases were determined at the 24h incubation period compared to control (LPS= 0.489 ± 0.02, $p<0.001$; Control= 0.373 ± 0.02). This confirms that the microglial inflammatory response is sufficient to elicit iron dyshomeostasis at the optimised LPS treatment concentration after 24h incubation.

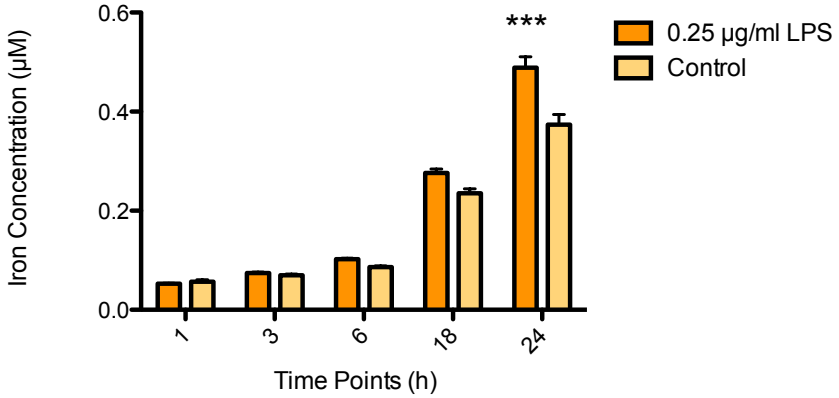

Figure 3.5 Increased N9 Iron Levels after LPS Treatment as Assessed by Ferrocene Assay
N9 cells were seeded (350,000c/w) and treated with LPS (0.25µg/ml) or a vehicle control for a range of incubation periods (1-24h). Analysis reveals elevated intracellular iron concentrations at the 24h time point. Data represents mean ± SEM for all replicates. *Asterisks indicate statistical significance compared to control: ***p<0.001. n=3.*

3.4.3 Determination of Hepcidin Release by Activated Microglia

Supernatants from N9 microglial cells activated by LPS (0.25µg/ml) at the optimally determined key time-point (24h) were collected (n=3) and measured by mass spectrometry at King's College London for hepcidin presence. It was predicted that microglia may be a source of hepcidin during inflammation. Results, however, indicate no hepcidin presence within supernatant samples (Figure 3.6).

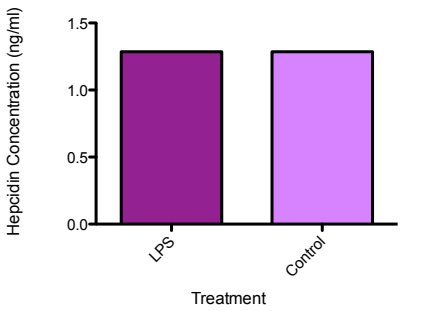

Figure 3.6 Hepcidin Quantification by Mass Spectrometry
Supernatant samples were collected from N9 cultures that had been treated with an optimised LPS concentration (0.25µg/ml) or control (dH2O) for a key time point (24h) (n=3). Hepcidin concentrations were measured and determined via mass spectrometry at another lab in King's College London. Results established no significant differences between hepcidin levels in activated microglial supernatant as compared to the control.

3.4.4 Confirming NeuN and TH Expression in N27

Neuronal cells seeded at increasing cell densities (6wp, 24h) were plated with two negative controls to determine the protein expression of neuronal markers (NeuN and TH). If N27 cells did indeed represent the phenotype of dopaminergic neurons, then they should express neuronal markers. The increasing number of N27 cells should thus provide a positive linear expression to TH and NeuN markers. It was predicted that neuronal marker proteins should positively correlate with cell density, and the negative controls of a blank well and N9 cells should not demonstrate any neuronal marker expression. Results confirm these predictions with a significant linearly increasing trend shown in TH as well as both splice variants of NeuN (46kDa & 48kDa) ($R^2 > 0.90$ in all 3 linear regressions) (Figure 3.7). This neuronal marker immunoreactivity as detected by immunoblot densitometry thus confirms that N27 cells can be labelled as dopaminergic neurons.

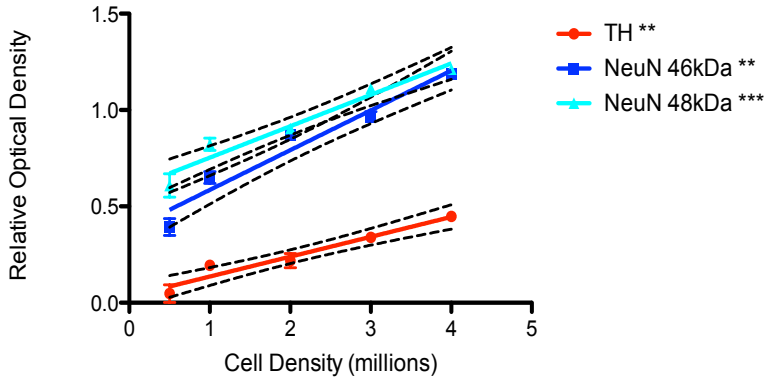

Figure 3.7 Confirming Neuronal Marker TH and NeuN Protein Expression in N27 Dopaminergic Neurons and N9 Microglia as Measured by Western Blot Analysis. Increasing densities of N27 cells were lysed and their neuronal marker protein expression was determined via Western Blot in order to confirm a corresponding increase in expression. One well devoid of any cells, and another seeded with N9 cells (2×10^6 cells/well) were run in parallel as negative controls that should not express any neuronal markers. Densitometry analysis verifies a linearly increasing neuronal marker expression along with cell density. Dotted lines represent the linear regression 95% confidence bands lines of best fit.

3.4.5 LPS Does Not Directly Induce Changes in N27 IRP Gene Expression

Once N27 cells had been verified as containing neuronal markers, they could be used as the cell line on which to expose microglial inflammatory factors in order to observe effects of inflammation on iron metabolism. However, transference of microglial conditioned medium to neuronal cells could expose neurons to trace amounts of LPS within the culture medium. In order to accurately draw conclusions that all observed effects were as a result of the microglial inflammatory factors within the media, and not as a consequence of direct LPS exposure, N27 cells were seeded (500,000c/w) in a 6wp, rested 24h, then exposed to 0.25µg/ml LPS (24h). This was the amount used to treat microglial cells, so any neuronal exposure from the conditioned media would be at levels less than 0.25µg/ml. PCR results demonstrate no significant changes in any of the iron regulatory proteins after 24h LPS exposure (Figure 3.8).

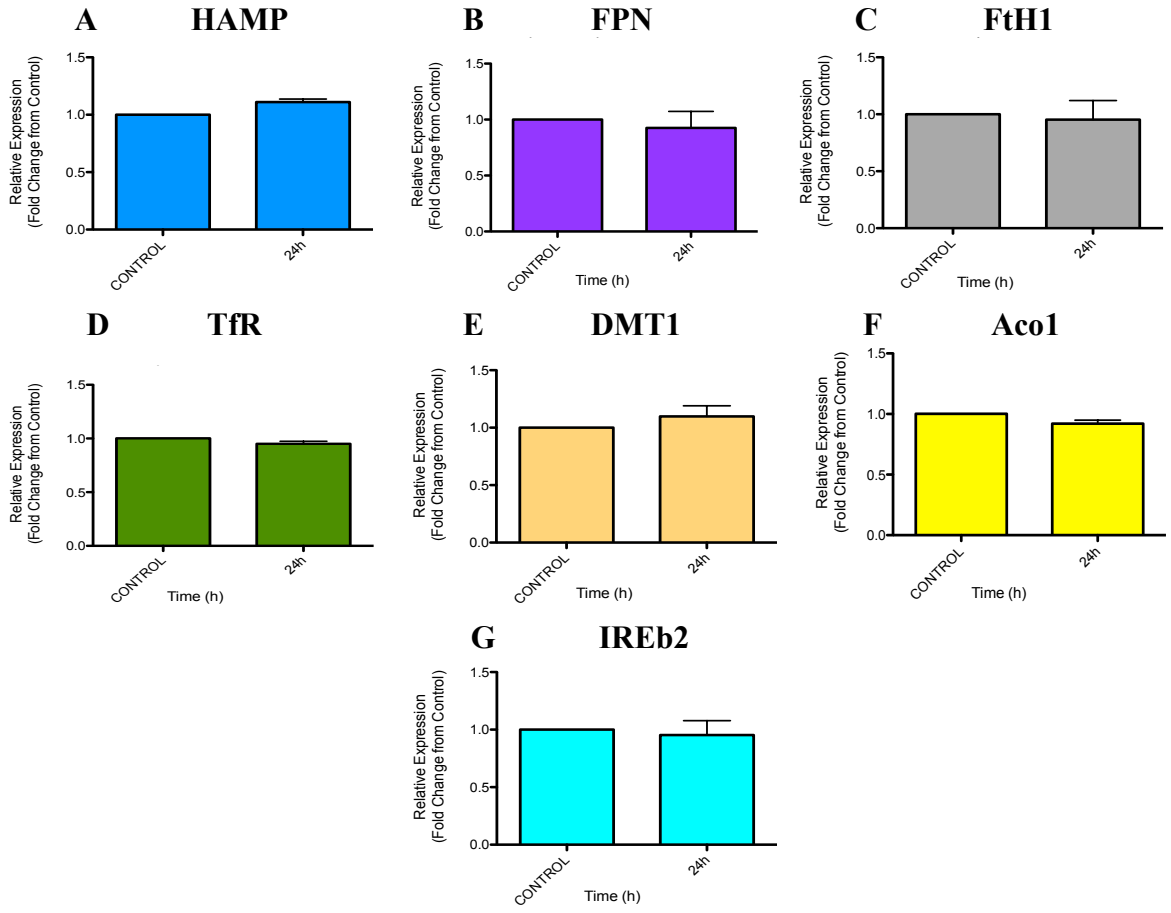

Figure 3.8 LPS Does Not Directly Induce Changes in N27 IRP Gene Expression
N27 cells (500,000c/w) were treated directly with 0.25µg/ml LPS for 24h, then lysates collected for mRNA extraction and cDNA synthesis for analysis of relative gene expression using qRT-PCR. Data is analysed by ΔΔCt method, presenting results as a fold change from the ß-actin control housekeeping gene, and presented as mean ± SEM for all replicates. Results from the iron regulatory proteins (HAMP (A), FPN (B), Ferritin (C), TfR (D), DMT1 (E), Aconitase 1 (F), IREb2 (G)) do not show any significant changes in N27 relative gene expression. This verifies that N27 cells are not affected by LPS, and thus any observed effects result from microglial inflammatory factors within applied microglial conditioned media. *n=3.*

3.4.6 Effects of Microglial Conditioned Medium on Iron Expression in N27 Dopaminergic Neurons

To establish the optimal exposure point of neurons to inflammatory factors for utilisation in subsequent experimentation, the effects on iron metabolism were observed after various incubation periods. Results from both iron regulatory protein gene expression via PCR, and iron levels via ferrocene assay were analysed.

3.4.6.1. Relative Gene Expression of Iron Regulatory Proteins in N27 Cells via PCR

Gene expression of iron regulatory proteins of interest in treated N27 cells were determined via qRT-PCR (Figure 3.9). mRNA was extracted from N27 cells after varied exposure (1-48h) to microglial conditioned medium (MCM) (N9 24h incubation with 0.25μg/ml LPS), then expression levels were measured via qRT-PCR. Significant increases were observed with hepcidin (3h=1.771 ± 0.11), transferrin receptors (24h=2.019 ± 0.28), and DMT1 (18h= 1.768 ±0.12, 24h=2.618 ± 0.28) expression compared to control ($p<0.001$ for all three). Hepcidin levels increased sharply at 3h, then dropped a statistically significant amount below control. DMT1 and TfR increased from 18h and 24h, respectively, and both remained significantly elevated above control for hours afterwards.

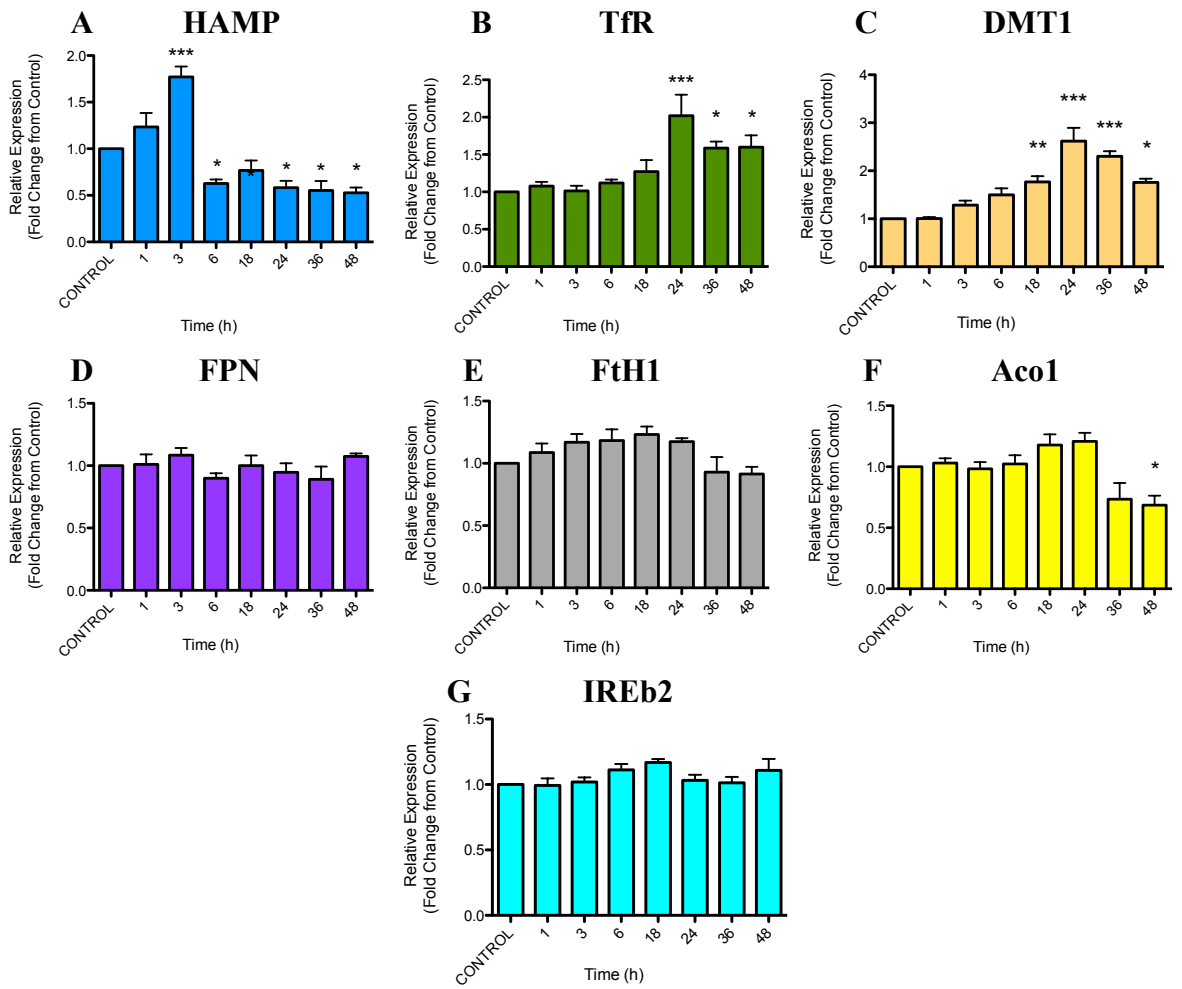

Figure 3.9 Changes in Iron Regulatory Protein Gene Expression in MCM-Treated N27 Dopaminergic Neurons. N27 dopaminergic neurons were seeded (500,000c/w), rested 24h, and treated with MCM for a range of time points (1-48h) to analyse changes to IRP gene expression via qRT-PCR. Data is analysed by ΔΔCt method, presenting results as a fold change from the ß-actin control housekeeping gene. Neuronal culture results demonstrate upregulation of 3 key iron regulatory proteins, including HAMP (A), TfR (B) and DMT1 (C). Hepcidin increases would induce intracellular iron sequestration, while TfR and DMT1 would instigate elevations to iron influx. Thus, results infer alterations to iron regulatory protein homeostasis in dopaminergic neurons exposed to microglial inflammation. Data is represented as mean ± SEM of all replicates. *Asterisks indicate statistical significance compared to control: *p<0.05, **p<0.01, ***p<0.001. n=3.*

3.4.6.2. Iron Uptake in N27 Cells via Ferrocene Assay

Gene expression has demonstrated altered levels of certain iron regulatory proteins, which could lead to variations in iron concentration. In order to determine the effects of inflammatory factors on neuronal iron, the ferrocene assay was used on N27 cells to quantify overall intracellular iron (Figure 3.10). N27 cells exposed to MCM failed to exhibit any changes in neuronal iron content compared to control in the first 6 hours. By 18h, both control and MCM treated conditions demonstrated a marked increase. However, at 24h the control treated neurons rebalanced their intracellular iron, while MCM-treated neurons did not. These neurons exhibited a statistically substantial increase in iron levels at 24h (0.436 ± 0.01, $p<0.001$) compared to control (0.3401 ± 0.01). Comparison with gene expression points to hepcidin and DMT1 upregulation as possible sources for this elevated intracellular iron at 24h. This data confirms that the microglial inflammatory response is capable of inducing changes to neuronal iron regulation culminating in raised intracellular iron.

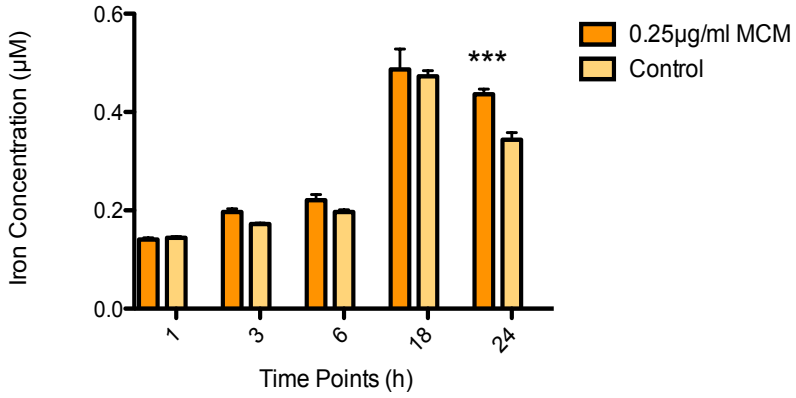

Figure 3.10 Increased N27 Iron Levels after MCM Treatment as Assessed by the Ferrocene Assay
N27 cells were seeded (500,000c/w) and treated with microglial conditioned medium or a vehicle control for a range of incubating exposure times (1-24h). Results reveal amplified intracellular iron concentrations at the 24h incubation period. Data represents mean ± SEM for all replicates. *Asterisks indicate statistical significance compared to control: ***p<0.001. n=3.*

3.4.6.3. N27 Cell Viability After MCM Exposure

Since the optimum MCM LPS dosage and incubation period had been previously established for all succeeding studies involving MCM treatment to N27s, it must be determined whether or not neuronal exposure to such inflammatory factors for 24h resulted in a loss of cell viability. Thus, microglia were exposed to a range of LPS doses (0.0625-1µg/ml) for 24h, whereupon these various conditioned media were applied to N27 cells (24h) to monitor for any differences in three viability assays (Figure 3.11 A-C). Results indicate that none of the microglial conditioned media prepared using a variety of LPS concentrations for 24h incubation instigated significant neurotoxicity to N27 neurons compared to control. This confirms that the optimal LPS dosage (0.25µg/ml) and incubation (24h) for MCM is suitable for use to treat N27 cells without affecting cell viability, and can be utilised for all subsequent work.

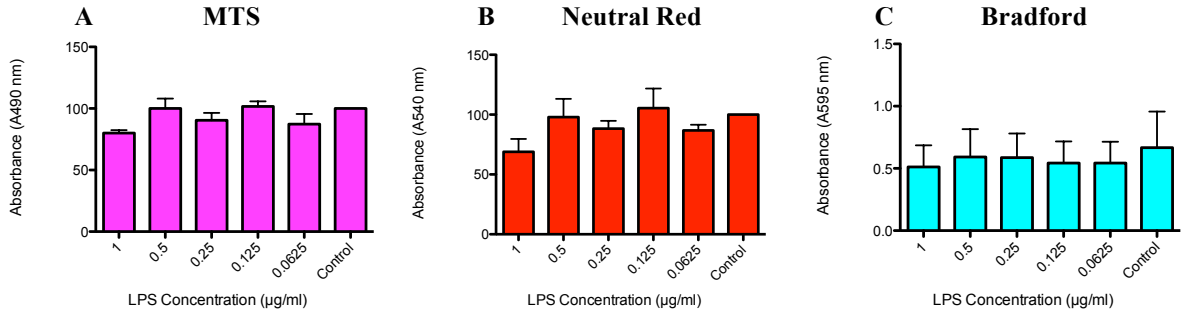

Figure 3.11 Optimising MCM Exposure in N27 Cells for Successive Treatments
N27 cells were seeded (500,000c/w) and treated (24h) with conditioned medium from microglia prepared via 24h exposure to a range of LPS concentrations (0.0625g/m-1µg/ml) or a vehicle control. N27 cells were collected for analysis of cell viability by three viability assays: MTS, Neutral Red and Bradford (A, B, and C, respectively). The dose responses showed no statistically significant loss of cell viability at any of the LPS concentrations. This indicates that an MCM with 0.25µg/ml, as was defined as the optimal LPS concentration for subsequent experimental use, has no significant cytotoxic effect during exposure to N27 neurons. Data is presented as mean ± SEM. *n=3.*

3.4.7 Verification Using Primary Neurons

Once experiments had been run on N27 cells, key results were validated using primary hippocampal cells. Embryonic day 18 rat pup cells were seeded onto pre-coated plates (24h) to ensure cells were completely relaxed and established on the plates. Primary neurons were unable to survive upon treatment with MCM (24h as with N27), as confirmed under a microscope, so instead were treated directly with LPS (0.25µg/ml 24h), after which cells were used for either qRT-PCR (Figure 3.12A) or ferrocene (Figure 3.12B) assays. As with N27 cells, PCR results revealed no significant changes in the iron regulatory proteins, except a slight increase observed in DMT1 ($p<0.05$). About 2-3% of primary neuron culture populations consist of glia, to which the observed DMT1 increase is possibly attributed from microglial activation by LPS. DMT1 also presented with the largest increase in N27 neurons at 24h (2.618 ± 0.28), compared to increases seen in TfR (2.019 ± 0.28), so perhaps this helps account for why only DMT1 presented with a slight increase in primary neuron populations.

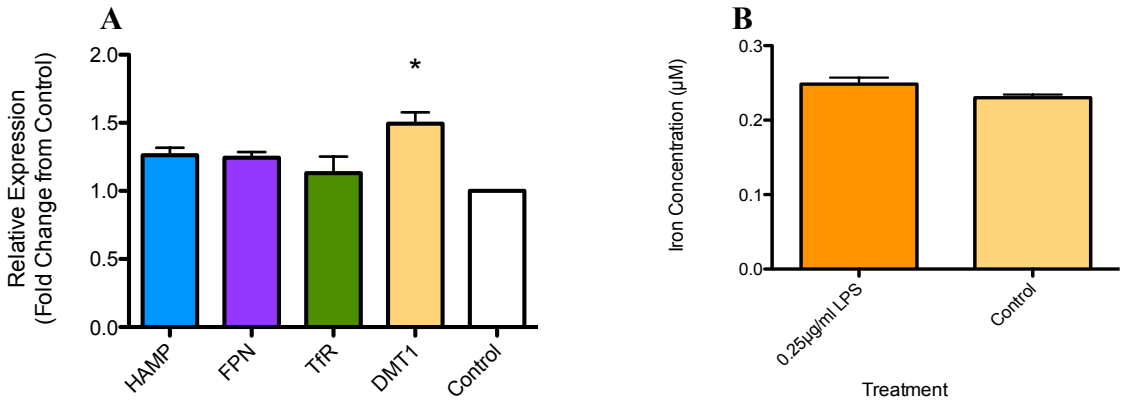

Figure 3.12 Primary Neuron Results After Direct LPS Treatment
Primary hippocampal E18 rat cells were seeded on pre-coated plates (poly-L-ornithine and 4µg/ml laminin), rested for 24 hours, after which cells were treated with 0.25µg/ml LPS (24h). Cells were then lysed for mRNA determination of gene expression via RT-PCR (A) or for iron quantification via ferrocene assay (B). Results determined a slightly significant upregulation in DMT1 expression. As it was previously substantiated that neurons did not express TLR4 receptors and thus no response from direct LPS treatment, this may account for the lack of similarity to previous N27 + MCM experiments. The significant DMT1 change may be due to the slight presence of microglia within primary cultures. *Asterisks indicate statistical significance compared to control: *p<0.05. n=3.*

3.5 Discussion

This chapter has demonstrated that microglia can be activated sufficiently by LPS to produce an inflammatory response triggering the release of pro-inflammatory cytokines and NO into the cell culture supernatant. These inflammatory mediators were abundant enough to induce a change in neuronal iron metabolism, even after short-term incubation periods, indicating that inflammation has a key role in affecting the cellular regulation of iron. If such significant changes are stimulated to occur in the short-term, which are shown to revert back to normal by lack of reduced cell viability, it still may be deduced that longer-term inflammation and the resulting iron overload may lead to a chronic feedback mechanism affecting downstream neurodegeneration observed in PD pathogenesis. Key results in this chapter were employed to define a suitable LPS concentration and incubation period for microglial activation *in vitro*, as well as for succeeding neuronal application.

Microglial activation was accomplished by direct treatment of N9 cells with LPS, which is known to elicit a robust inflammatory response. Microglial toll like receptors are activated by LPS treatment, resulting in the production of pro-oxidant enzymes and pro-inflammatory cytokines including NO, IL1, IL6, and TNF, both *in vivo* (Qin, 2007; Tanaka, 2013) and *in vitro* (Sawada, 1992; Possel, 2000). This can be confirmed here by the ELISA and Griess assay results. To fully comprehend the mechanism of microglial activation, a time course of released inflammatory factors was determined to select the ideal conditions for subsequent treatment to neuronal cells (Section 2.3.1.5). Results were evaluated to deduce which time point had the greatest significance overall. It was deemed that 24h had the greatest increase for all 4 measures of pro-inflammatory mediators, and thus was the time point selected for all future incubation periods of microglial cells with LPS. The 24h LPS exposure has successfully been used previously in this lab as well as other studies (Dean, 2010; Correa, 2011) to activate microglia for removal and application of MCM to other cell types.

LPS concentration was determined by analysis of both cell viability assays and release of pro-inflammatory mediators. As there was no significant loss of viability at any of the applied concentrations (0.0625-1µg/ml), the final decision was assigned after evaluation of the robustness of microglial activation. Taking results from activated microglia release of pro-inflammatory cytokines (Section 2.3.1.4) into consideration, it was deemed that 0.25µg/ml was sufficient to elicit an immune response. This sub-maximal dosage was preferable to using the higher 1µg/ml dosage, and was thereafter applied as the optimal LPS concentration for all subsequent microglial activations. Thus, a submaximal LPS concentration would be exposed

to cells, to successfully activate microglia whilst also ensuring protection against overstimulation and cytotoxicity.

The optimal LPS concentration was employed to treat microglia for a range of time points for detection of any alterations in cellular iron handling. Significant changes were identified in several key regulatory proteins, which could signify an important link between instigation of the microglial inflammatory response as seen in PD with dysregulation of iron metabolism. No changes to gene expression were observed in either Aco1 or IREb2. However, it was observed here that hepcidin peaked at 3h, after which it declined towards control levels. Similarly, ferroportin, ferritin, transferrin receptors, and DMT1 levels all increased significantly at 18h, followed by full dampening by 24h. This quick inhibition in all cases suggests that microglia are adept at quickly regulating changes to their iron regulation. Increased levels of hepcidin, as occurs with inflammation and IL6 (Ganz, 2003; Ilyin, 2003), would result in downregulation of ferroportin and subsequent intracellular iron sequestration. Ferroportin exhibits a significant increase at 18h, perhaps as a cellular attempt to rebalance levels. This homeostatic increase is not observed in neurons, which would produce enduring neuronal iron sequestration. Next, ferritin exhibited significant upregulation at 18h. This is a protective mechanism to augment levels of iron storage in order to reduce labile iron pools and prevent iron-mediated toxicity. Again, this protection was not shared in neuronal behaviour, making neurons more vulnerable to iron toxicity, and leading to the postulation that neurons exhibit dysregulations of iron during inflammation. Microglial cells also displayed increased gene expression for both TfR and DMT1, which would both facilitate iron influx. Since microglia appear better able to cope with excess iron, this influx may represent a neuroprotective mechanism in attempt to sequester iron away from neighbouring neurons. In total, these results demonstrate substantial changes to microglial iron expression upon their activation and induction of the inflammatory response. These changes could point to a noteworthy role of microglial inflammation and subsequent dyshomeostasis of intracellular iron in perpetuating neuronal degeneration in the PD brain.

Applying the determined optimal values for LPS dosage and treatment exposure time points, activated N9 microglial supernatant samples were collected and measured for hepcidin presence by mass spectrometry. It was postulated that since microglia were responsible for releasing various pro-inflammatory cytokines and ROS/RNS upon activation, that it was possible they could also release the master iron regulator hepcidin. Hepcidin is known to be upregulated during inflammatory conditions in the periphery (Nemeth, 2003) and in the brain cortex and SN (Wang, 2008), and can cause iron dysregulation in neurons by impeding intracellular iron efflux at a time when iron levels are already increased. The iron overload

could then lead to cellular toxicity and death. It was demonstrated here that hepcidin gene expression within microglial cells was upregulated at 3h, while iron levels within microglia increased at 24h after LPS-activation. However, mass spectrometry results revealed no significant differences between activated samples compared with control. This leads to the conclusion that while microglial cells upregulate the HAMP gene upon activation, the hepcidin is not being released. Another possible explanation could be that hepcidin gene expression was upregulated at 3h, while the mass spectrometry hepcidin measurements were taken at 24h. If gene expression was upregulated at 3h, and most likely increased protein expression shortly thereafter, it is conceivable that any released hepcidin was rebalanced via homeostatic mechanisms and was no longer detectable at 24h. This is confirmed from the HAMP relative gene expression results, as it appears that microglial rebalancing of changes to IRP levels occurs quite quickly, with all changes observed dampened by the next measured incubation point at 6h. Future studies could determine hepcidin protein expression, to establish a time line if and when the increased gene expression translated to increased protein expression. Then hepcidin levels in microglial supernatant could be re-quantified by mass spectrometry at the approximate time following hepcidin synthesis, possibly around 4h.

While an immune response is crucial for a healthy pathogenic defense, overexposure to these inflammatory factors can lead to detrimental effects on neurons. Inflammation accompanied by OS results in damage and ensuing degeneration of nigral dopaminergic neurons, which is the hallmark of PD. Previous studies have found that neuronal behavior under such conditions can be studied by exposure to inflammatory factors via LPS activation of microglia (Liu, 2000; Gao, 2002). Since iron levels within the Parkinson's brain are present in higher concentrations within the basal ganglia (Hill, 1984; Dexter, 1989), which also contains higher levels of microglia (McGeer, 1988) that can release pro-oxidant inflammatory mediators, this particular neuronal population is at greater risk of OS and its consequential cellular damage. It is postulated here that chronic inflammation can produce downstream effects in neuronal iron regulation, leading to augmented iron levels, which feeds the Fenton reaction and furthers OS to advance free radical formation and greater cellular damage.

This study observed the effects of neuronal exposure to inflammatory factors released from activated microglia. Results here indicate that inflammatory exposure leads to an increase of mRNA in several key iron regulatory proteins: hepcidin (3h), DMT1 (from 18h), TfR (24h), as well as increased intracellular iron levels (24h) in both dopaminergic neurons and microglia. Cell viability assays confirmed that any observed neuronal changes were due to the effects of microglial factors, and not from cell loss. Any effects of residual LPS within the MCM was

ruled out by results evidencing that neuronal gene expression is not directly activated by LPS as they do not possess the necessary TLR4 receptors. When primary hippocampal cells were directly treated with LPS, they confirmed no changes in gene expression, with the exception of DMT1 ($p<0.05$). This could be due to the fact that primary cultures contain about 2-3% glial cells. Since DMT1 in N27 cells demonstrated the greatest increases in gene expression, beginning earlier on (18h), it is possible that this pronounced response influenced glial cells present within the primary neuronal cultures, resulting in the slight effect observed only in DMT1. Another study found similar results, where even with a higher LPS concentration (1µg/ml), DMT1 but neither FPN nor hepcidin exhibited a slight mRNA increase in hippocampal neurons (Urrutia, 2013). This effect was not sufficient enough to translate to higher iron levels as quantified by the ferrocene assay.

Analysis of the observed IRP changes after neuronal treatment with microglial inflammatory factors first sees an increase of hepcidin at 3h returning below control thereafter, which is consistent with previous studies (Marques, 2009). An increase in hepcidin results in ferroportin internalisation, and decreased cellular iron export (Nemeth, 2004). So if the observed upregulation in hepcidin gene expression translates to elevated protein expression, then it could be hypothesised that intracellular iron should increase with loss of export. The Marques paper posits that IL6 directly contributes to the increase in hepcidin gene expression, seen after primary rat epithelial cells were incubated with IL6 for 6h. Contrarily, Urrutia (2013) found that direct IL6 treatment significantly induce hepcidin expression in astrocytes and microglia, but demonstrated no change in hippocampal neuron hepcidin mRNA whatsoever. It was also determined that hepcidin mRNA was undetectable in hippocampal neurons (Urrutia, 2013), however, dopaminergic neurons in this project exhibited quantifiable hepcidin mRNA stimulated by MCM treatment. A potential explanation for this discrepancy could be the difference in cell type. Since MCM contains peak concentrations of all three pro-inflammatory cytokines at the moment of transfer to neurons, the detected 3h HAMP increase may be attributed to any of them. However, data analysis shows that IL1ß levels are quite low in comparison to IL6 or TNF, thus effects are more likely to be caused by the latter two. The increase may have been affected by either TNF, which was present and known to activate the NFκB pathway (Zhang 2001), although Urrutia demonstrated no hepcidin mRNA changes with direct TNF application, or by another inflammatory mediator present within the MCM. IL6 is shown to likewise induce hepcidin (Kemna, 2005) in *in vitro* and *in vivo* studies of murine and human hepatocytes (Nemeth, 2004; Wrighting, 2006; Pietrangelo, 2007; Mayeur, 2014), and

plasma (Hohaus, 2010; Banzet, 2012). Furthermore, IL6, but neither IL1ß nor TNF, was demonstrated to upregulate hepcidin expression in dopaminergic and cortical neurons (Qian, 2014). Nitric oxide is also shown to have no effect on hepcidin induction, as nitric oxide synthase inhibitors failed to dampen hepcidin production (Lee, 2005). Thus, it can be deduced from this data that from IL1ß, IL6 or TNF, IL6 is most likely the instigating factor.

Next, DMT1 began to increase from 18h, consistent with previous findings (Urrutia, 2013). These changes may result from hepcidin (at 3h) or more likely from continuous TNF exposure, which have both proven to increase DMT1 levels (Wang, 2005). Finally, TfR increased at 24h. This could potentially be associated with the inflammation-triggered increases in iNOS, and its consequential NO production, which was at peak concentrations upon neuronal treatment. NO in combination with activated microglia-released superoxide (Colton, 1996) results in formation of peroxynitrite, while hydroxyl formation results from the reaction between ferrous iron and H_2O_2 (Noronha-Dutra, 1993; Pacher, 2007).

An increase in iron, as observed later on at 24h, along with the microglial inflammatory factors would result in free radical formation, which can damage mitochondrial DNA and further impede respiration and energy production (Cadenas, 2000). NO also instigates neuronal hypoxia as it competes against oxygen for cytochrome oxidase binding in mitochondrial respiration (Brown, 2003), leading the cascade from neuronal ATP starvation towards cell death. Hypoxia has proven to upregulate both TfR and DMT1 leading to increased total iron (Lis, 2005; Li, 2007; Wang, 2010). The effects observed in TfR require a longer exposure time, with a previous study demonstrating a 16h hypoxic exposure was necessary to induce changes to TfR (Lok, 1999). Thus, it is possible that the mRNA changes observed with TfR were due to increasing levels of hypoxia. Additionally, earlier upregulation of hepcidin at 3h would begin to augment intracellular iron sequestration, which could aid in perpetuating the inflammatory response, and trigger mechanisms resulting in TfR and DMT1 induction. Such mechanisms could include hypoxia or iron-mediated dysregulation of the IRP/IRE system leading to IRP binding and upregulated TfR and DMT1. Perhaps if hepcidin is responsible, this could explain the difference in time points from 3h hepcidin upregulation to 24h TfR and DMT1 upregulation, to account for the time to induce such changes. Future work could carry out the same experiment with an extension of the time course, in order to determine how long the elevations to neuronal iron observed at 24h remain before dampening back to control.

Increased levels of all these IRPs would result in augmented cellular iron, so this could explain why only 24h demonstrated greater overall neuronal intracellular iron levels. With the exception of hepcidin, which peaked at 3h, the greatest increases in neuronal IRP mRNA

expression were observed at 24h. It remains unknown from the experiments conducted here whether or not increases in IRP gene expression were translated to increases in protein expression. Previous findings have demonstrated that this is indeed the case (Mann, 1994; Urrutia, 2013). This supports deeper investigation using a suitable and reliable protein quantification of these key IRPs in future studies. Considering the time to induce protein expression in order to create the greatest effects on iron metabolism, along with the information gathered above detailing the possible pathways causing these observed changes that may require longer incubation periods, the time point of 24h was selected as the ideal point for which to expose N27 cells to MCM inflammatory factors. Thus, all subsequent study employed this incubation period.

Comparing the overall findings between N9 results and those of N27 cells, it was observed that hepcidin, TfR and DMT1 increased in both microglia and dopaminergic neurons, around similar time points. However, microglia also exhibited increases in ferroportin and ferritin expression (18h), which was not witnessed at all in neurons. While both demonstrated increased intracellular iron levels (24h) as quantified via ferrocene assay, likely as a result of increased iron import due to the inflammatory reaction, it appears that only the microglia had a protective mechanism capable of sequestering the excess iron into ferritin storage or exporting it via FPN. Microglia then demonstrated that any observed IRP changes reverted to control levels by 24h, however, neurons continued to express altered levels up until 48h. This may be explained by the observed fact that microglia could limit the inflammatory reaction by sequestering or exporting any free, reactive iron, leading to a reduction in OS, thus allowing cells to return to a physiological equilibrium after the inflammatory insult had dissipated. Neurons, on the other hand, were unable to handle the iron influx, lacking the protective mechanism witnessed in microglia. This headed a self-perpetuating cycle of iron overload and OS that left neurons struggling to minimise the effects of the inflammatory exposure, as IRP levels only began to revert back to control from 36h in TfR and not until 48h with DMT1. Results shown here would concur with previous findings that dopaminergic neurons are particularly vulnerable to disruptions such as with iron accretion and OS (Hunot, 1996; Surmeier, 2011). It can be inferred that the outcome of a more chronic, continuous exposure to such inflammation, as seen in PD, could be a diminished capacity to overcome the amplified iron levels and resultant OS, leading to a loss of nigral neurons.

3.6 Conclusions

In conclusion, it has been established here that microglial cell cultures treated with LPS release pro-inflammatory mediators that can be harnessed for treatment of neuronal cultures in order to determine their effects on neuronal iron metabolism. An optimal treatment concentration and incubation period was determined to instigate the inflammatory response significant enough to produce inflammatory factors, but below the threshold that would negatively affect cellular viability. These factors were subsequently applied to dopaminergic neuronal cultures, resulting in fluctuations of key iron regulatory proteins which may explain the observed augmented intracellular iron levels.

CHAPTER 4:

Evaluation of whether pro-inflammatory cytokines released in high concentrations from activated microglia initiate changes in the iron metabolism of N27 dopaminergic neurons

4. Evaluation of whether pro-inflammatory cytokines released in high concentrations from activated microglia initiate changes in the iron metabolism of N27 dopaminergic neurons

A time-dose-response for the microglial inflammatory response to LPS treatment, and the effects of this inflammation on iron regulation was discussed in the previous chapter. Using the optimally deduced LPS concentration and exposure times to create MCM for neuronal application led to certain significant changes in their iron metabolism, including altered hepcidin, TfR and DMT1 gene expression and elevations to total intracellular iron concentrations. This chapter outlines the methods used to deduce whether commonly released microglial pro-inflammatory cytokine factors triggered these observed iron metabolism changes in neurons. N27 dopaminergic neurons and primary neuron cultures were treated with individual cytokines, IL1ß, IL6 and TNF, to observe if they induced the same previously observed effects. In addition to application of exogenous cytokines, this hypothesis was also tested by using antibody neutralisation of cytokines in MCM. Thus, N27 cells were treated with MCM as before, however, only after the MCM was first incubated with cytokine-neutralising antibodies. It was hypothesised that if these cytokines were responsible for the previously observed effects from MCM treatment, then their removal from MCM should diminish any changes.

4.1 Introduction

Pro-inflammatory cytokines are inflammatory mediators that can cause downstream effects on iron regulation. It was hypothesised at the end of Chapter 3 that some factor released from activated microglia is responsible for triggering N27 iron metabolism changes, however it remains to be determined which. This chapter will determine if commonly released pro-inflammatory factors may be responsible. IL6 is known to induce hepcidin mRNA expression (Nemeth, 2004), both IL6 and TNF treatment can increase DMT1 and decrease FPN expression in neurons (Urrutia, 2013), TNF can also directly facilitate apoptotic cell death (Smith, 2012), while microglial superoxide can release iron from ferritin stores (Yoshida, 1995), and changes in cellular iron activate the IRP1/IREb2-IRE pathway which retain a posttranscriptional regulation of TfR, DMT1 and ferritin expression (Kato, 2007).

It has been previously determined that upon activation, microglia are capable of releasing a multitude of pro-inflammatory factors. Prolonged inflammation and continuous release of factors, such as IL1ß and IL6, can promote necroptotic cell death; such neuroinflammatory mediators may be implicated in disease progression. Evidence from past experiments has reported elevated cytokine levels within the PD SN (Mogi, 1996; Nagatsu, 2000; Nagatsu, 2005) that have neurotoxic effects (Sawada, 2006). Studies carried out in section 3 have determined LPS-activated microglial release of NO, IL1ß, IL6 and TNF. Treatment with the activated microglial conditioned medium, shown to contain these pro-inflammatory cytokines, demonstrated an effect on neuronal iron metabolism. However, it remains to be defined which specific factor is causing the observed effects.

To better comprehend which specific element in MCM was responsible for triggering neuronal iron metabolism changes, the rat dopaminergic N27 cell line was cultured *in vitro* with direct treatment of accumulative physiological concentrations of several key pro-inflammatory cytokines (IL1ß, IL6, TNF). Cells were monitored for any changes to intracellular iron levels and IRP gene expression, in order to determine whether the previously observed changes could be attributed to one particular cytokine. Results were replicated using *in vitro* primary hippocampal rat neurons. Cell viability following direct cytokine exposure was also measured to ensure any observed results were not from loss of cell survival.

4.2 Chapter Objectives

This chapter aims to complete the following objectives:

1. Assess whether individual microglial-released pro-inflammatory mediators in high concentrations are responsible for triggering neuronal iron metabolism changes.

Upon treatment of N27 cells with increasing levels of key cytokines at optimal exposure times as determined in Chapter 3:

   a. Measure cell viability after direct cytokine treatments to determine which concentration is acceptable for future neuronal exposures to key cytokines.
   b. Assess IRP mRNA expression after direct cytokine treatments.
   c. Assess iron levels after direct cytokine treatments.

2. Confirm results using primary hippocampal neurons treated with the optimised cytokine concentrations.
   a. Assess IRP mRNA expression after direct cytokine treatments.
   b. Assess iron levels after direct cytokine treatments.
   c. Compare results to those of N27 cells.

3. Determine whether previously achieved results from direct MCM treatment were a caused from either IL6 or TNF by MCM antibody neutralisation prior to N27 application.
   a. Prepare original MCM and then treat with antibody neutralisation for IL6 and TNF.
   b. Assess IRP mRNA expression after treatment with neutralised MCM.
   c. Assess iron concentrations after treatment with neutralised MCM.

4.3 Experimental Methods

4.3.1 Observing Effects of Physiological Concentrations of Inflammatory Cytokines on Dopaminergic Neurons

Previous ELISA experiments determined that certain pro-inflammatory cytokines (IL1ß, IL6, TNF) with known influences on iron regulatory proteins were present in significant levels within the MCM. ELISAs, as measured here in this project, determined the cytokine concentrations within MCM (which ranged from 0.4-6.3ng/ml depending on individual cytokines), so these were used to replicate equal or higher concentrations (0-200ng/ml) using individual cytokines on N27s and primary neurons. It was hypothesised that one of these mediators may be responsible for affecting the observed changes. As it remained unclear which specific inflammatory mediator was involved, each one was individually used to treat N27 cells. Results were compared to those observed in the previous chapter, to draw conclusions as to which cytokine may be attributed to the changes.

Using the optimised time course previously determined, N27 cells were seeded (500,000c/w in 6wp), left to rest overnight, and then each plate was individually treated with only one specific cytokine at a range of recombinant cytokine concentrations (0-200ng/ml) (IL1ß= ThermoFisher, PRC0814; IL6= Peprotech, 400-06; TNF= Peprotech, 400-14) (Section 2.3.2). A control well was run in parallel, treated with an equal volume of water. After incubation (3h or 24h), cells were lysed for assessment by either PCR (Section 2.6) or ferrocene assay (Section 2.4.4). Cell viability was also measured to ensure direct cytokine treatment did not prove too neurotoxic (Section 2.4.1), whereby three assays were run on N27 cells (10,000c/w in 96wp) treated with the same range of cytokine concentrations for 24h.

Upon completion of the N27 treatments with cytokines, primary neuronal cultures (Section 2.1.6) were seeded on poly-L-ornithine and laminin pre-coated plates for either PCR (600,000c/w, 6wp) or ferrocene assay (495,000c/w, 12wp), left to rest overnight, and then treated with 10ng/ml using the same recombinant cytokines as above (24h). A negative control well treated with only vehicle control was run in parallel.

4.3.2 Eliminating IL6 and TNF as Effectors of Observed MCM Changes

Since both IL6 and TNF treatment of N27s resulted in slightly significant increases in hepcidin gene expression, these two pro-inflammatory cytokines were selected for neutralisation. Since either cytokine alone did not replicate observed MCM effects, and if original effects remain even after IL6 and TNF antibody neutralisation within MCM, then this could prove that neither was responsible for effecting changes on neuronal iron metabolism. MCM was prepared as per protocol using LPS-activated microglial N9 cells (24h). Upon

completion of the incubation period, supernatants were removed into a blank 6wp without any cells. Each well was treated with both IL6 and TNF antibodies at pre-determined concentrations deemed sufficient to neutralise cytokines according to the revised literature. IL6 (Abcam, ab9730) was reconstituted and added at a concentration of 0.36µg/ml, while TNF (Abcam, ab34674) had a recommended neutralising dose of 5µg/ml. The antibody-treated supernatant was incubated under cellular conditions in covered 6 well plates for 1h in an incubator. A parallel plate was run as a control with MCM supernatant incubating 1h without the addition of the cytokine antibodies. After 1h incubation to allow sufficient antibody binding for neutralisation of any IL6 and TNF present within the microglial conditioned media (1hMCM-IL6-TNF), the supernatant was removed and 1.5ml added to aspirated wells containing seeded (500,000c/w, 6wp; 300,000c/w, 12wp) and rested (24h) N27 cells, along with 0.5ml fresh complete RPMI. The control plate was run using the same protocol, so N27 cells were treated with 1h-incubated MCM (1hMCM) only. After a 24h incubation period as before, cells were lysed for analysis by either PCR or ferrocene assay.

4.3.3 Statistical Analysis

All experiments run in 6wp were performed three independent times, with one single well per run. Tests using 96wp were performed three independent times, but with three wells per run. Mean outcomes were calculated for each test, with data representing mean ± SEM. qRT-PCR, cellular viability and ferrocene analyses were individually compared by 1-way ANOVA with, respectively, Dunnett's, Dunnett's and Bonferroni's Multiple Comparison post-hoc tests to compare data groups to the control. All statistical analyses were performed on the Prism 5 for MAC OS X software.

4.4 Results

4.4.1 Determination of Cytokine Concentration for Exposure Upon Analysis of Cell Viability

Previous experiments observed the effects of neuronal treatment with MCM on iron metabolism. This study also wished to look at effects of specific cytokines after direct treatment onto dopaminergic N27 cultures. To ensure that treatment conditions had no effect on cellular viability, three assays were performed, including MTS, Neutral Red and Bradford assays. Results determined no statistically significant neurotoxicity with any direct IL1ß, IL6 or TNF treatments at concentrations less than 50ng/ml (Figure 4.1). 100 and 200ng/ml did demonstrate some significance compared to control, signifying a slight loss in cellular viability at the higher cytokine doses. From this data, it was thus determined that a concentration of ≤ 50ng/ml would be suitable for direct cytokine treatments. Comparing this with other works successfully exposing neuronal cells to direct cytokine treatments (Liu, 1994; Romero, 1996; Urrutia, 2013), as well as previously mentioned results of LPS-activated microglia-released cytokine quantification via ELISA to determine physiological levels, it was thus determined that a concentration of either 10 or 50ng/ml would be utilised for all future cytokine treatments. This was deemed sufficient to elicit an inflammatory response, without passing the threshold affecting neuronal viability.

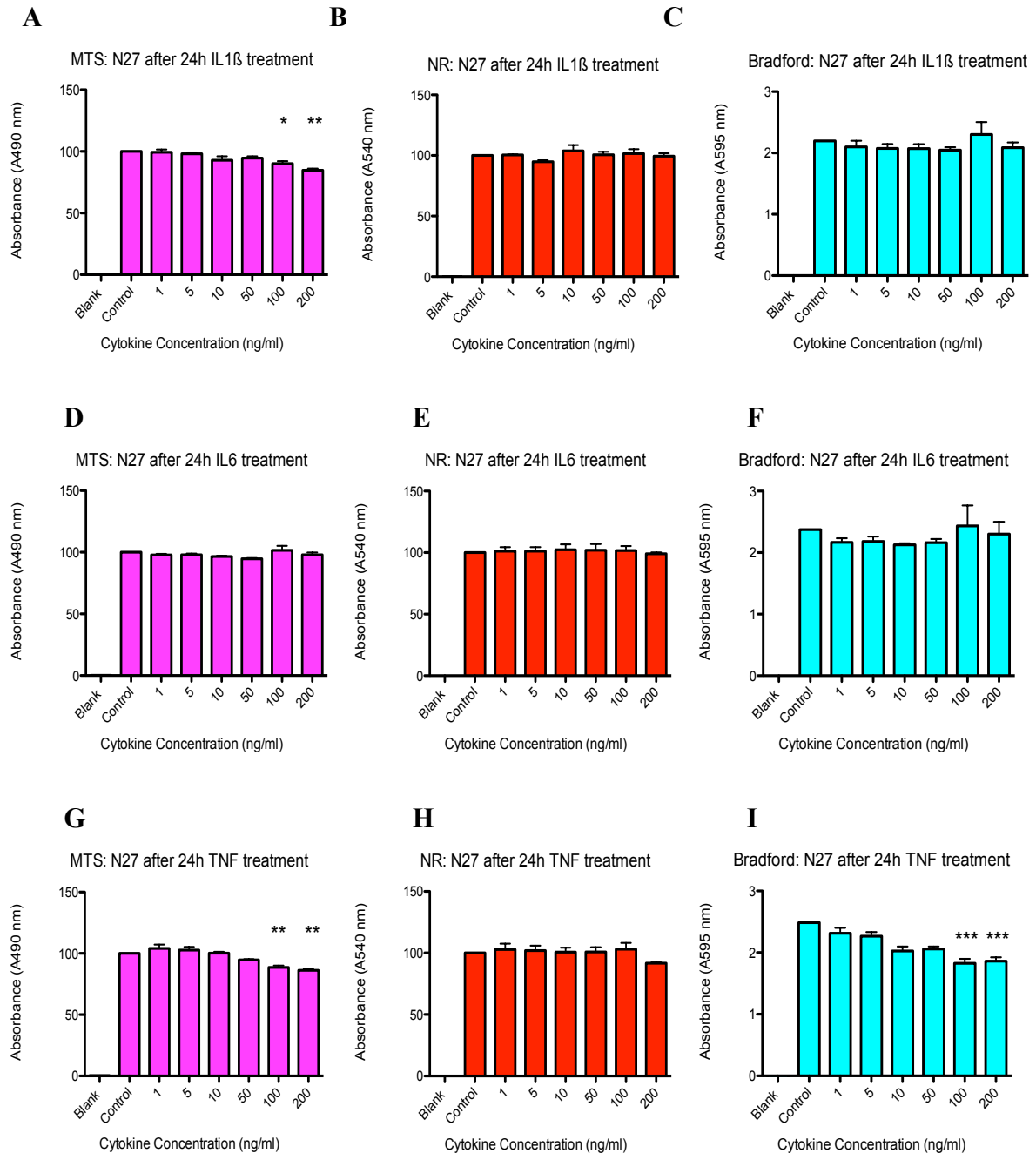

Figure 4.1 Cell Viability in N27 Cells After Direct Cytokine Treatment
Dopaminergic N27 cells were seeded (500,000c/w), and individually treated *in vitro* (24h) with direct concentrations of 3 distinct cytokines: IL1ß (A-C), IL6 (D-F) and TNF (G-I) or vehicle control in order to discern which one was responsible for previously detected changes in neuronal iron metabolism. Treatment concentrations ranged from 0-200ng/ml. Upon performing 3 cellular viability assays (MTS=pink, NR=red, Bradford=turquoise), analyses determined no statistically significant decreases in cellular viability with any treatment at concentrations equal to or below 50ng/ml. This means that N27 cultures could be treated to observe the effects of direct cytokines on iron metabolism at concentrations ≤50ng/ml, without any cytotoxic effects. Data is presented as mean ± SEM from 3 individual experiments. *Statistical significance as compared to control is indicated by asterisks*: *$p<0.05$, **$p<0.01$, ***$p<0.001$. $n=3$.

4.4.2 Analysis of Cytokine Treatment Effects on Neuronal Iron Regulation

Upon determining which cytokine concentration would be suitable for use, the higher 200ng/ml concentration was eliminated due to its toxic effects on cell viability. N27 cells (500,000c/w in 6wp) were then exposed to each individual cytokine at a range of concentrations (0-100ng/ml) for 24h. After this time, gene expression for the iron regulatory proteins was examined. Subsequently, the two optimised concentrations of 10 and 50ng/ml were used to treat N27 cells (500,000c/w in 6wp) for 3h and 24h for ferrocene assay analysis of intracellular iron concentrations. The 3h time point was selected since this was when hepcidin presented with an increase in gene expression upon MCM treatment. Previous results demonstrated significant changes to IRP gene expression following N27 treatment with MCM. This chapter aims to elucidate which of the three possible pro-inflammatory cytokines may be responsible for these changes.

4.4.2.1 IL1ß

First, IL1ß was examined, and N27 cells were directly treated with a range of IL1ß concentrations for 24h. Cells were processed and analysed via qRT-PCR (Figure 4.2). Results do not indicate any increased IRP expression. In fact, several IRP proteins (FPN, FtH1, TfR) show a significant decrease in expression from IL1ß exposure when compared to control (Figure 4.2 B-D). FPN results demonstrate reduced expression: 1 and 5ng/ml display $p<0.05$, while concentrations from 10-100ng/ml have $p<0.01$. TfR are more significantly reduced, with $p<0.001$ for all concentrations 1-100ng/ml. Analysis by ferrocene assay demonstrated a slight increase in iron levels at 24h ($p<0.05$) with the 10ng/ml treatment as compared to control. The higher concentration did not present with any significant changes in iron expression (Figure 4.3).

4.4.2.2 IL6

Next, IL6 was used to test N27 cells for 24h, following the same protocol and range of treatment concentrations. Upon completion of qRT-PCR analysis, results revealed slight increases in HAMP gene expression (Figure 4.4A) as a result of direct IL6 treatment in the lower concentrations of 1ng/ml and 5ng/ml (respectively, 1.735 ± 0.14, 1.818 ± 0.34; $p<0.05$). There was also a slight decrease in TfR (Figure 4.4D) at the highest treatment dosage of 100ng/ml when compared to control (0.6587 ± 0.09, $p<0.05$). Analysis of iron levels revealed a slight increase of intracellular iron (Figure 4.5) at the 50ng/ml dosage compared to control (respectively, 0.272 ± 0.03 vs 0.208 ± 0.01; $p<0.05$).

4.4.2.3 TNF

The third pro-inflammatory cytokine analysed was TNF. After N27 incubation with the range of TNF concentrations 24h, PCR results determined a slight increase in HAMP gene expression (Figure 4.6A) at the lowest dosage of 1ng/ml (1.946 ± 0.34, $p<0.05$). As with IL1ß & IL6 treatment, TfR results (Figure 4.6D) established a decreasing trend beginning with 10ng/ml down to 100ng/ml as compared to control results (0.675 ± 0.08 to 0.614 ± 0.06; $p<0.05$ and $p<0.01$ respectively). However, there was no translation to any changes in iron levels, as determined by the ferrocene assay (Figure 4.7).

4.4.2.4 Cytokine Treatment Effects on Primary Neuronal Cultures

Upon completion of cytokine optimisation and treatments on N27 cells, primary neuronal cultures were extracted and treated with individual cytokines at the optimised 10ng/ml concentration for 24h. 10ng/ml was chosen since it did not demonstrate any loss of cell viability, remained within physiological concentrations and yet was still sufficient enough to elicit a response. PCR results did not detect any changes in levels of HAMP, FPN, TfR, or DMT1 gene expression as compared to control following direct cytokine treatment (Figure 4.8). 1-way ANOVA also failed to discover any increased levels of intracellular iron following the ferrocene assay analysis (Figure 4.9). Results concur with those of the N27 cells, with the exception that even less of a response was established in primary cultures in regards to gene expression upregulation from cytokine treatment. It may be inferred from the lack of iron metabolism changes after primary neuronal cultures were exposed to pro-inflammatory cytokines IL1ß, IL6 and TNF, that none of these are directly responsible for triggering the original changes from MCM treatment.

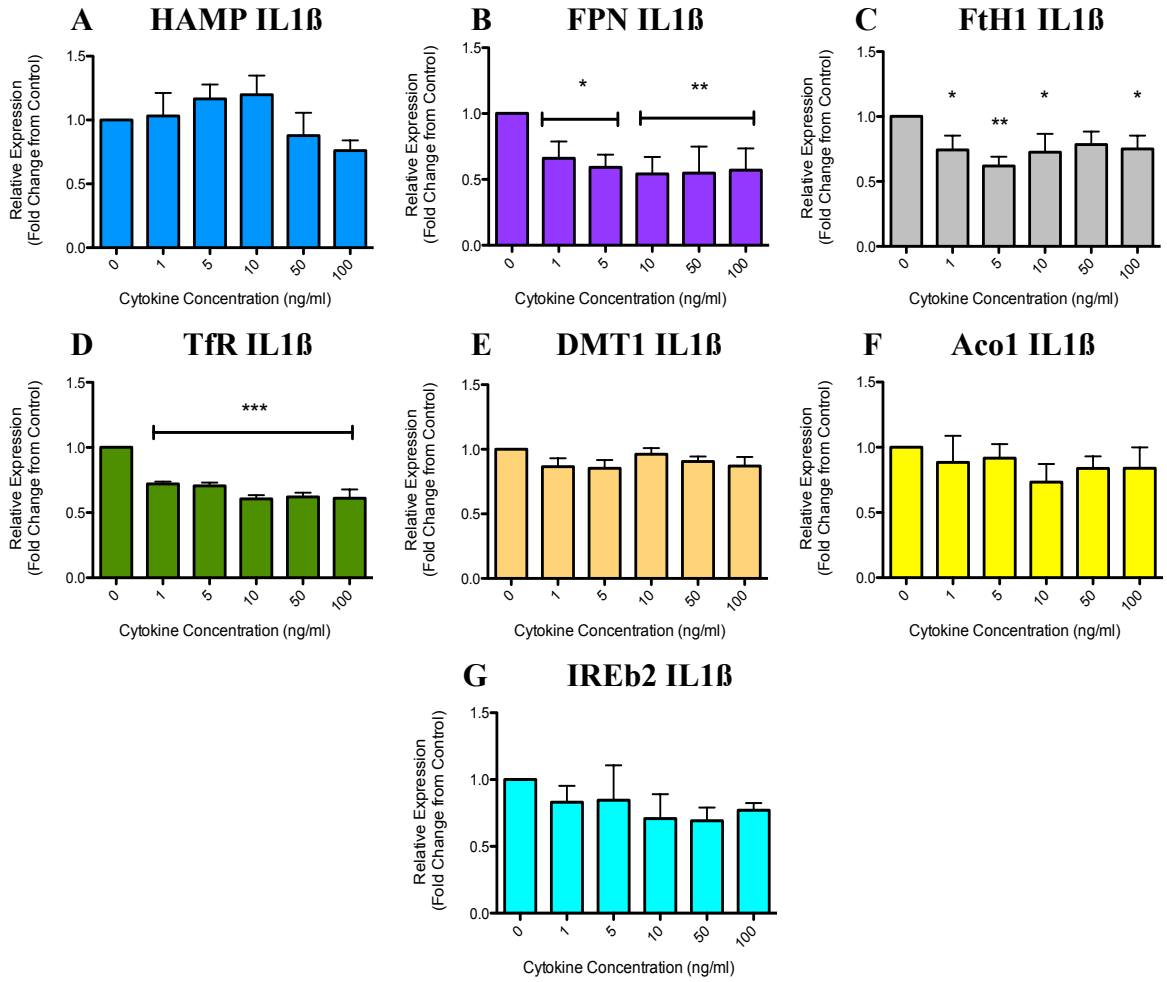

Figure 4.2 Relative Gene Expression in N27 Neurons After Direct IL1ß Treatment
N27 cells directly treated with a range of IL1ß concentrations (0-100ng/ml) or vehicle control for 24h were analysed by qRT-PCR for changes to iron regulatory proteins (HAMP, FPN, FtH1, TfR, DMT1, Aco1, and IREb2), normalised by ßactin housekeeping gene. Results here demonstrate no increased expression of any of the seven examined iron regulatory proteins as seen with N27 treatment from MCM. There were, however, some significant decreases observed in FPN (B), FtH1 (C), and TfR (D). This infers that IL1ß was not responsible for triggering iron dysregulation. Data represents mean ± SEM of 3 individual experiments. *Statistical significance as compared to control is indicated by asterisks*: *$p<0.05$, **$p<0.01$, ***$p<0.001$. *n=3.*

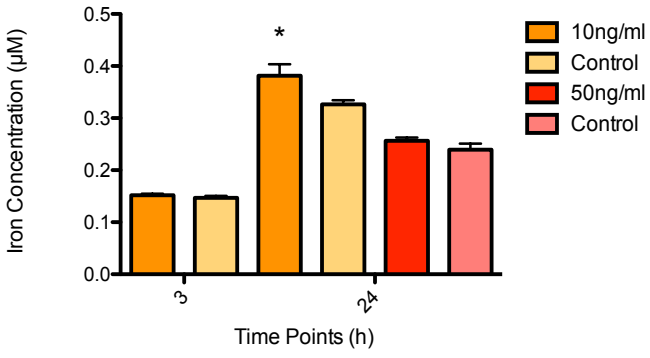

Figure 4.3 Iron Expression in N27 Neurons After Direct IL1ß Treatment
Upon N27 culture treatment for either 3h or 24h with 10ng/ml or 50ng/ml IL1ß or vehicle control, cells were collected and lysed for intracellular iron expression analysis by the ferrocene assay. Dose response data indicates a significant increase in iron from control at the 24h time point with 10ng/ml treatment. Data represent mean ± SEM of individual experiments. *Statistical significance as compared to control is indicated by asterisks*: *$p<0.05$. *n=3.*

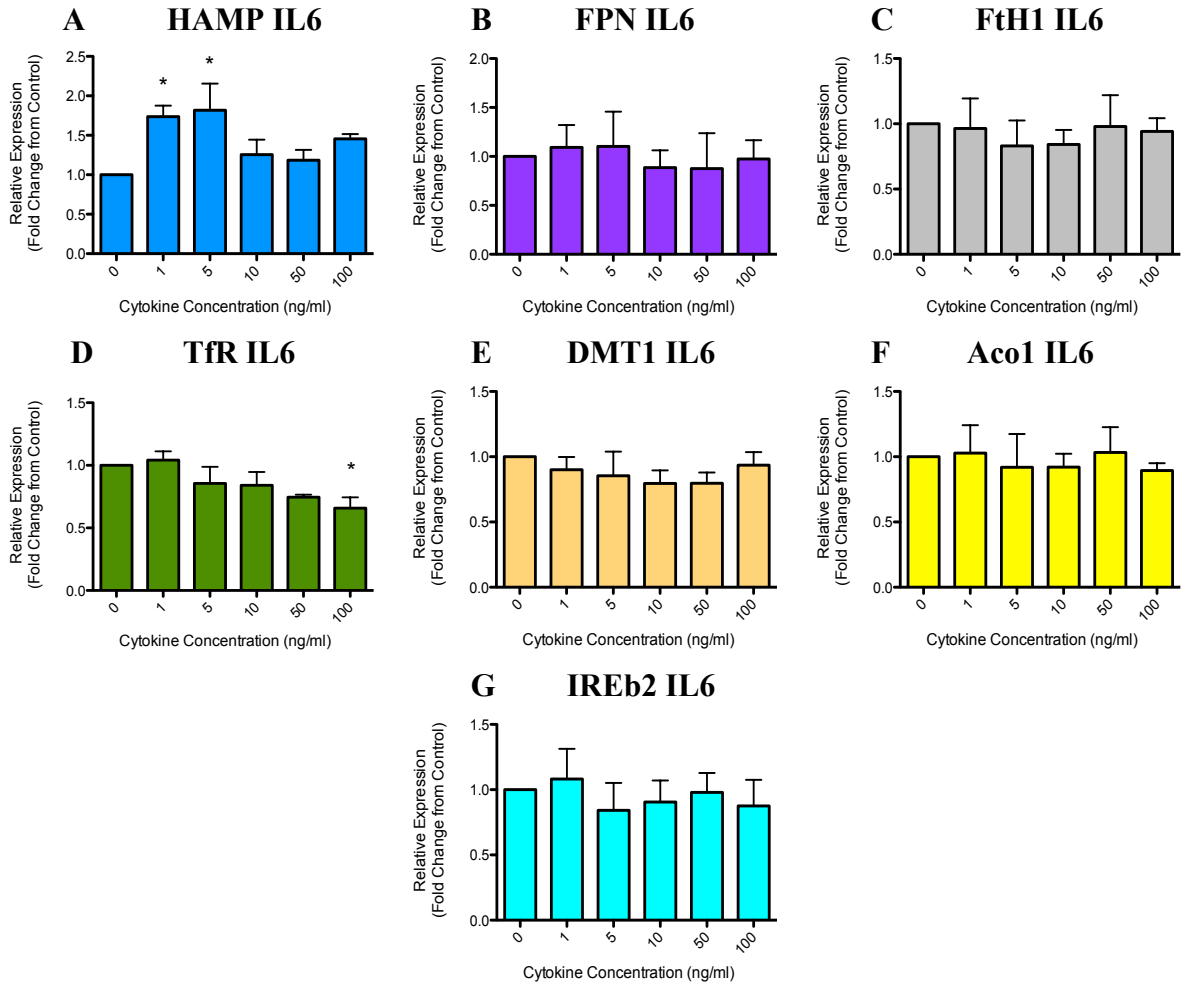

Figure 4.4 Relative Gene Expression in N27 Neurons After Direct IL6 Treatment
N27 cells directly treated with a range of IL6 concentrations (0-100ng/ml) or vehicle control for 24h were analysed by qRT-PCR for iron regulatory proteins (HAMP, FPN, FtH1, TfR, DMT1, Aco1, IREb2), normalised by ßactin housekeeping control gene. Results here demonstrate a slight increase in expression of HAMP (A) at 1 and 5ng/ml treatment concentrations only. Higher concentrations did not reveal any other deviations in expression from control. None of the other six examined IRPs demonstrated any increased expression. TfR (D) also displayed a slight decrease in expression at the highest concentration of 100ng/ml only. Data represent mean ± SEM of individual experiments. *Statistical significance as compared to control is indicated by asterisks*: *$p<0.05$. *n=3.*

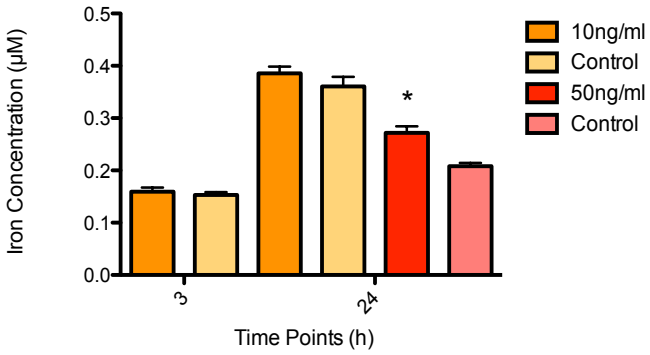

Figure 4.5 Iron Expression in N27 Neurons After Direct IL6 Treatment
Upon N27 treatment for 3h or 24h with either 10ng/ml or 50ng/ml IL6 or vehicle control, cells were collected and processed for ferrocene assay analysis of intracellular iron. Dose response data indicates a slightly significant increase in iron from control at 24h after treatment with only 50ng/ml IL6. Data represents mean ± SEM for individual experiments. *Statistical significance as compared to control is indicated by asterisks*: *$p<0.05$. *n=3.*

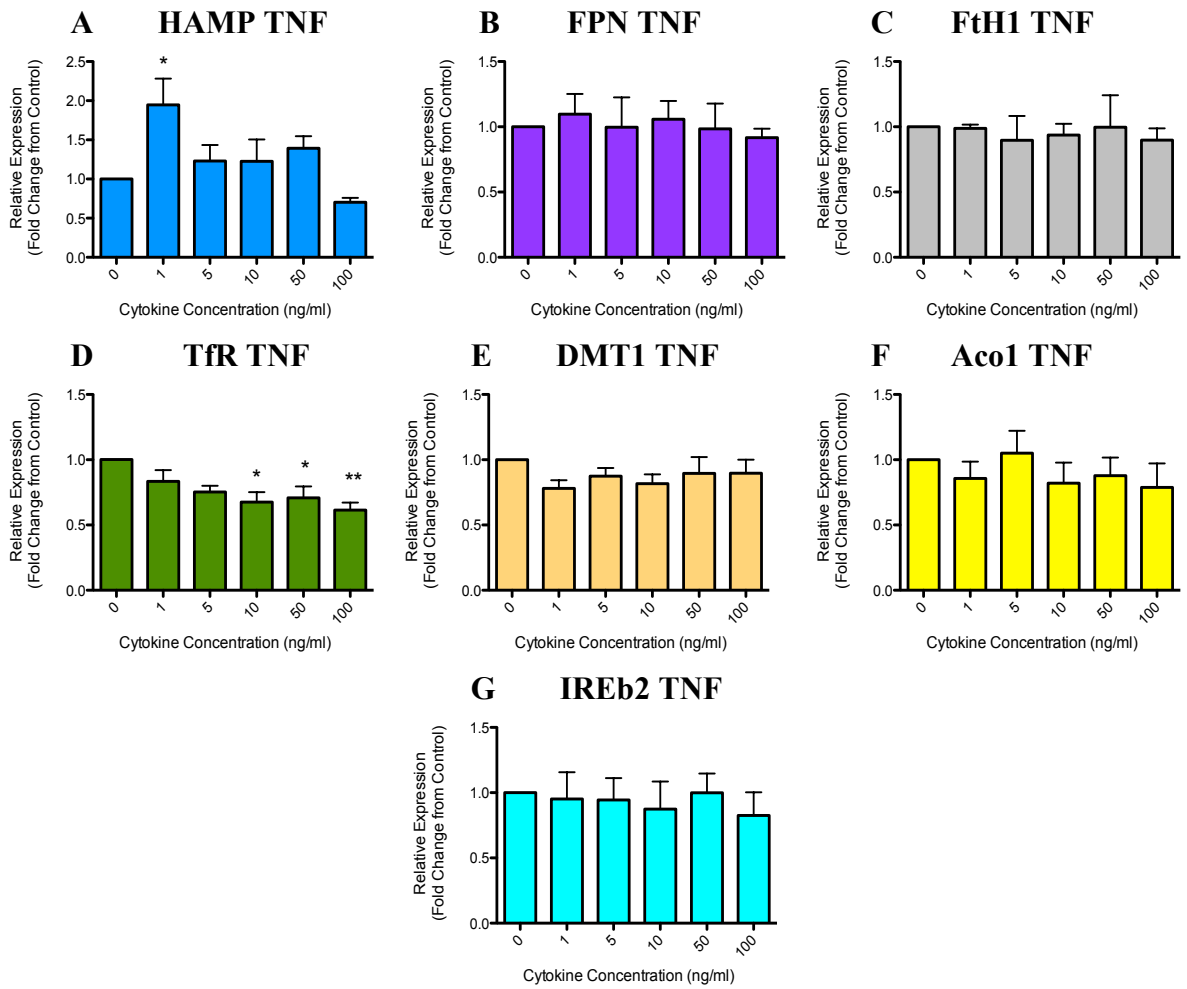

Figure 4.6 Relative Gene Expression in N27 Neurons After Direct TNF Treatment
N27 cells directly treated with a range of TNF concentrations (0-100ng/ml) or vehicle control for 24h were analysed for changes to relative gene expression of iron regulatory proteins by qRT-PCR, with normalisation to the ßactin housekeeping control gene. Results here demonstrate a slight increase in expression of HAMP (A) at 1 and 5ng/ml treatment concentrations only. Higher concentrations did not reveal any other deviations in expression from control. None of the other six examined iron regulatory proteins demonstrated any increased expression. TfR (D) also displayed a slight decrease in expression at the highest concentration of 100ng/ml only. Data represents mean ± SEM of individual experiments. *Statistical significance as compared to control is indicated by asterisks*: *$p<0.05$. $n=3$.

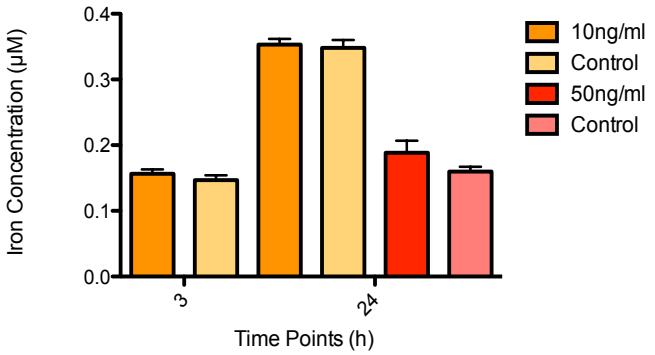

Figure 4.7 Iron Expression in N27 Neurons After Direct TNF Treatment
Upon N27 treatment for 3h or 24h with 10ng/ml or 50ng/ml TNF or vehicle control, cells were collected and lysed for ferrocene assay analysis of intracellular iron expression. Dose response data does not establish any significant changes in iron compared to control with TNF treatment. This suggests TNF is not responsible for inducing the observed intracellular iron increases following MCM treatment. Data represents mean ± SEM. $n=3$.

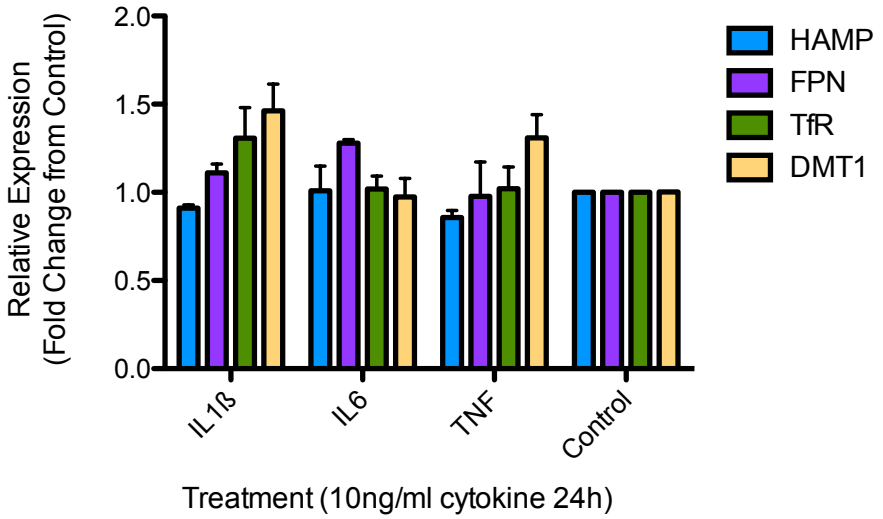

Figure 4.8 Relative Gene Expression in Primary Neurons After Direct Treatment with Pro-Inflammatory Cytokines. Primary hippocampal neuron cultures were seeded on poly-L-ornithine and laminin pre-coated plates for PCR (600,000c/w, 6wp), left to rest overnight, and then treated for 24h with either vehicle control or 10ng/ml pro-inflammatory cytokines IL1ß, IL6 or TNF. After incubation, cells were collected and lysed for quantitation of gene expression via qRT-PCR, with normalisation to the ßactin housekeeping control gene. Genes examined here included HAMP, FPN, TfR, and DMT1. Results determined no significant changes to iron regulatory protein gene expression in these neurons following treatment with pro-inflammatory cytokines. It may be deduced from this data that another microglial-released factor is mediating the previously observed changes in iron metabolism. Data represents mean ± SEM of individual experiments. *n=3.*

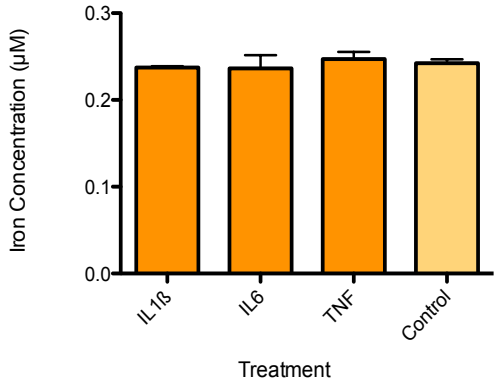

Figure 4.9 Iron Expression in Primary Neurons After Direct Treatment with Pro-Inflammatory Cytokines Primary hippocampal neurons were seeded on poly-L-ornithine and laminin pre-coated plates for ferrocene assay (495,000c/w, 12wp), left to rest overnight, and then directly treated for 24h with either vehicle control or 10ng/ml of pro-inflammatory cytokines: IL1ß, IL6 or TNF. Following incubation, cells were collected and lysed for ferrocene assay analysis of intracellular iron expression. No statistically significant changes in iron levels were determined, thus it may be surmised that none of these three pro-inflammatory cytokines were able to induce the before-seen elevations to neuronal iron expression. It remains to be determined which microglial-released mediator is responsible for changes to neuronal iron metabolism. Data represents mean ± SEM. *n=3.*

4.4.3 Confirm MCM Iron Changes did not result from IL6 or TNF Exposure

N27 cells were treated with either MCM incubated in anti-IL6 and anti-TNF antibodies for 1h (1hMCM-IL6-TNF), or original MCM also incubated 1h (1hMCM), for a 24h incubation period as before. Results demonstrated a moderate increase in TfR and DMT1 gene expression (respectively, 1.398 ± 0.08 and 1.35 ± 0.08, with control at 1) (Figure 4.10), with an increasing iron trend that was not statistically significant (0.211 ± 0.01 vs control 0.196 ± 0.01) (Figure 4.11). Surprisingly, the 1hMCM treatment also showed a linearly increasing trend in iron after 24h but without any statistical significance from control (0.208 ± 0.02 vs control 0.151 ± 0.02) (Figure 4.11). This is unexpected since previous MCM treatment demonstrated highly significant elevations in iron expression at the same time point (0.437 ± 0.01 vs control 0.34 ± 0.01).

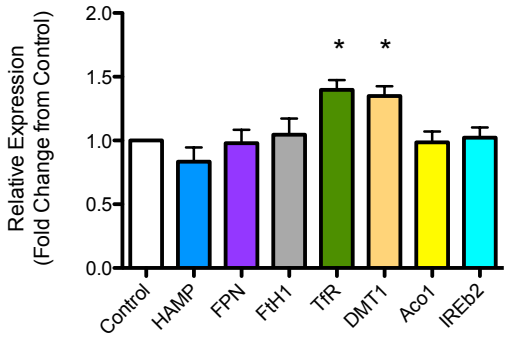

Figure 4.10 Relative Gene Expression of IRPs in N27 Neurons After Cytokine Neutralisation
N27 cells were seeded (500,000c/w) and treated with a neutralised MCM. This was first prepared as usual by treatment of microglia with LPS (0.25µg/ml) for 24h. Next, this fresh MCM was incubated 1h in blank wells, with the addition of anti-IL6 (0.36µg/ml) and anti-TNF (5µg/ml) antibodies, or vehicle control, to neutralise the microglial-released IL6 or TNF within the supernatant prior to neuronal treatment. Upon completion of the 24h incubation period, cells were collected. mRNA was extracted, and cDNA synthesised to determine relative gene expression via qRT-PCR, with normalisation by the ßactin housekeeping gene. Data analysis by the $\Delta\Delta C_t$ method demonstrates moderate upregulation in TfR and DMT1 gene expression relative to control. This antibody neutralisation presents a muted increase in both TfR and DMT1 levels when compared with results from regular MCM treatment. This suggests that the factors driving IRP changes are still active in the medium. Data represent mean ± SEM. *Statistical significance as compared to control is indicated by asterisks*: *$p<0.05$. *n=3.*

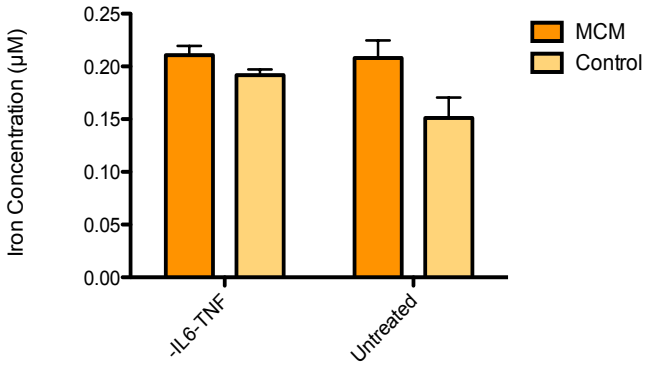

Figure 4.11 Intracellular Iron Levels in N27 Neurons After Cytokine Neutralisation
Microglial conditioned medium was prepared as usual from 24h LPS-activated microglial supernatant. This was pipetted into blank cell-free wells, and left to neutralise under cellular conditions in an incubator for 1h with IL6 (0.36µg/ml) and TNF (5µg/ml) antibodies (-IL6-TNF), or vehicle control. A parallel control plate was run with untreated MCM. N27 cells were then treated with either 1hMCM-IL6-TNF or untreated 1hMCM, and left to incubate 24h. Cells were then collected and lysed for determination of intracellular iron levels by the ferrocene assay. Analysis demonstrates no significant increases in iron levels after either treatment. The lack of increased iron levels within the untreated samples was unexpected, since N27 MCM treatment previously demonstrated a significant increase in iron expression at 24h. This led to the determination that the inflammatory factor within MCM responsible for initiating changes to neuronal iron regulation was quenched by the 1h incubation period prior to neuronal treatment. Data represents mean ± SEM for 3 individual experiments. *n=3*.

4.5 Discussion

The aim of this chapter was to discover whether pro-inflammatory cytokines released in high concentrations by activated microglia during an inflammatory response may be accountable for the significant changes to IRP gene expression and elevated cellular iron witnessed upon original N27 treatment with MCM. Evidence demonstrated here shows that direct cytokine treatment had several slight effects on IRP gene expression and iron levels in N27 dopaminergic rat cells *in vitro*, however, they do not appear to be significant enough to have cause the aforementioned changes.

While IL1ß failed to demonstrate any increased levels of gene expression, there were several decreased levels in FPN, FtH1, and TfR compared to control. If these changes in relative gene expression translate to changes in protein, then reductions in these regulatory proteins would result in an increase of intracellular iron, which may account for the slight elevation in iron levels observed at 24h. Reductions in FPN and TfR would, respectively, impede iron export and import, while lowered FtH1 production may affect iron storage capacities during conditions of severe iron overload. If no iron is entering or exiting the cell, but total intracellular iron levels as measured by the ferrocene assay have increased, it can be deduced that either the labile iron pool is increasing from an oxidative release of iron from proteins, or iron levels are being maintained in intracellular stores. However, reduced ferritin expression would impede the ability to store excess iron. The lack of significant escalations in any gene expression indicate that IL1ß cannot be held accountable for causing the previously witnessed increases in IRP expression, and thus it must be eliminated as instigator for any observed changes viewed with MCM treatment. The trigger must be due to another inflammatory factor present within the supernatant from LPS-activated microglia.

Next, IL6 was examined, which did stimulate a slight increase in HAMP gene expression at the 1 and 5ng/ml doses. IL6 is known to regulate HAMP gene expression (Wrighting, 2006) and induce hepcidin mRNA (Nicolas, 2002; Nemeth, 2004), so this may explain the observed increases. So perhaps IL6 in MCM mediates an increase in hepcidin reflected in HAMP upregulation 3h later. Analysing iron levels exposed a slight increase at the higher IL6 dosage of 50ng/ml after a 24h incubation period. It may be thought to be attributed to the marginal increase in hepcidin, which would sequester iron within cells, however TNF exposure presented with similar increases in hepcidin without any resultant iron increases. Additionally, elevated iron was observed with 50ng/ml treatment, which did not present with any elevated hepcidin expression. Thus, the elevated iron levels may result directly from exposure to high

levels of IL6. Although significant, the observed effects were not sufficient enough to be the sole cause of the experimental results obtained from N27 cells after incubation with MCM. So while direct IL6 treatment was able to induce an inflammatory response in N27 cells, and somewhat increase hepcidin and intracellular iron levels, it can be reasoned that the main source triggering the observed effects in N27s remains to be elucidated.

Lastly, it was thought that TNF may exert an effect on neuronal iron regulation after direct exposure. TNF is a prominent neuroinflammatory mediator capable of inciting free radical mediated stress, showing an increased presence in the Parkinson's brain (Boka, 1994; Mogi, 1994). In these experiments, neuronal treatment with TNF resulted in increased HAMP gene expression at the lowest dosage (1ng/ml) only, which is less than the effect observed succeeding IL6 exposure. This was followed by diminishing levels of TfR gene expression from 10ng/ml down to 100ng/ml. While the significant decrease observed at 100ng/ml may be accredited to cellular toxicity at the high dosage, this does not justify the decreased levels at 10 and 50ng/ml. Instead, this may be due to the post-transcriptional control of the IRP/IRE system. In situations of high iron, IRP binding activity is lost leading to degradation of mRNAs, which may also be used to explain the decrease in TfR observed with IL6 treatment. Additionally, other studies confirm a decreased expression of TfR and TfR-mediated iron uptake following TNF treatment (Fahmy, 1993), potentially serving as a neuroprotective mechanism. Furthermore, nitric oxide can be induced by TNF (Romero, 1996), and has been shown to significantly reduce IRP2 binding to diminish TfR expression (Oliveira, 1999; Kim & Ponka, 2000). Extrapolating from these results, it may be deduced that TNF is not capable of altering expression of iron regulatory proteins resulting in elevated intracellular iron concentrations.

While, as predicted, IL1ß did not show any increase in HAMP expression, it is curious that TNF did, since other works have shown that both IL1ß and TNF are actually capable of inhibiting hepcidin synthesis, not stimulating it (Nemeth, 2003). This result was not replicated in primary neuronal cultures, where neither IL1ß, IL6 nor TNF were able to trigger any significant iron metabolism changes in any IRP gene expression or intracellular iron concentrations. This may indicate that perhaps another mechanism is entirely responsible.

Neuroinflammation has been insinuated as a crucial element associated with PD neurodegeneration, and the Parkinsonian brain has been shown to have increased TNF levels and receptors within the SN (Boka, 1994; Mogi, 2000; McGuire, 2001), leaving SN dopaminergic neurons vulnerable to pro-inflammatory TNF signalling. The fastest hepcidin stimulatory response is a result of inflammatory and iron overload pathways (Nemeth, 2004), leaving the hypoxic pathway as a possible cause of the later hepcidin upregulation seen at 24h

with direct cytokine treatment, and not after 24h in MCM. On the other hand, it could be that while inflammation had a slight affect, these specific cytokines applied alone just did not have as significant of an influence on inflicting changes to IRP gene expression compared to what was previously observed. This was confirmed by lack of any significant IRP expression changes nor any increased iron expression following cytokine treatment in primary neuronal cultures.

Data from N27 cells treated with either 1hMCM-IL6-TNF (MCM incubated for 1h with IL6 and TNF antibodies) or 1hMCM (original MCM incubated for 1h) were very interesting. It was believed that neither IL6 nor TNF cytokines were responsible for observed elevated iron levels and increased gene expression observed from N27 treatment with MCM. Thus, 24h neutralisation of IL6 and TNF cytokines from within MCM supernatant should result in the same effect as previously witnessed after 24h of original MCM, with increased TfR and increased DMT1 gene expression, as well as significantly increased iron levels. Instead, no change in iron was observed, while only a slight increase in TfR and DMT1 gene expression was perceived. If IL6 and TNF were proven to have no effect, it was left to question what could be effecting this change in observations. The only difference in protocols was that antibody neutralisation required a one-hour incubation period, allowing time for antibodies to neutralise cytokines released into MCM supernatant. However, it is also possible that another active inflammatory mediator within the MCM affecting the previously observed changes, was being degraded during this 1h incubation period, thus diminishing its ability to exert its effects on N27 cells. This is confirmed when the 1hMCM also showed no increased iron expression. 1hMCM supposedly contained the same components as MCM, with the sole difference being the 1h incubation. Thus, this information implies the presence of an activated microglia-released inflammatory mediator, that is neither IL6 nor TNF, but that is rapidly degraded under cellular incubation conditions. One could deduce from this that it is a short-term free radical, capable of exerting significant effects to instigate downstream consequences that would continue to be seen even after radical action had been inhibited.

In conclusion, it can be inferred from this data that while certain significant variations from control were observed in either gene expression or iron levels after individual N27 treatment with either IL1ß, IL6, or TNF, these changes were not as extensive as those detected following MCM treatment. This is confirmed by a lack of any changes from primary neuronal culture treatment with these cytokines. A conclusion may be drawn that pro-inflammatory cytokines were able to affect a slight inflammatory response on hepcidin at low concentrations in N27 cells, however, another inflammatory mediator released by activated microglia must be held

accountable for a more potent inflammatory response. Results from cytokine neutralisation studies coincide with this theory, while also implying that this inflammatory mediator has a short half-life since a 1h cytokine neutralisation period was able to simultaneously diminish its effects. Further experimentation and research into the literature would be required in order to properly identify this inflammatory mediator.

4.6 Conclusions

It is unlikely that any of the three cytokines, IL1ß, IL6 or TNF, were solely responsible for initiating the iron regulation changes previously observed in N27 dopaminergic neurons after treatment with microglial conditioned medium. While there were some slight changes in gene expression and iron levels observed with direct cytokine treatment, they were not significant enough to represent what was previously detected. Thus, it must be concluded that another inflammatory factor present within the MCM must be affecting these changes. Further investigation is necessary to identify which specific factor could be instigating these results.

CHAPTER 5:

Investigation of hydrogen peroxide released by activated microglia as a contributing factor to initiate changes observed in the iron metabolism of N27 dopaminergic neurons

5. Investigation of hydrogen peroxide released by activated microglia as a contributing factor to initiate changes observed in the iron metabolism of N27 dopaminergic neurons

It was previously determined that a short-lived microglial inflammatory factor may be instigating changes to neuronal iron metabolism, and was thus hypothesised that hydrogen peroxide (H_2O_2) could be responsible. This chapter outlines methods applied to test this hypothesis. First, it was confirmed that microglia do in fact release substantial quantities of H_2O_2 into the supernatant following LPS treatment. Next, N27 cells were directly treated with H_2O_2 to examine the effects on iron regulatory proteins and intracellular iron levels. Results were then confirmed using primary neuronal cultures. It was revealed that H_2O_2 had a very strong effect on neuronal iron metabolism. H_2O_2 dissipation was then used to explain the previously observed muted changes in neuronal iron metabolism after treatment with MCM that had been incubated 1h before application to neurons as a control with cytokine antibodies treatment. Finally, to further confirm that H_2O_2 is the inflammatory mediator responsible for instigating neuronal dysregulation of iron, cells were treated with catalase to neutralise any effects of H_2O_2. The significant reduction in increased iron regulatory protein gene expression confirmed the effects of H_2O_2.

5.1 Introduction

PD has been proven to present with increased iron levels within the SN (Dexter, 1992), which can exacerbate production of reactive oxidative species and lead to neurodegeneration of vulnerable dopaminergic populations. It has been theorised that an inflammatory mediator released by activated microglia is affecting homeostasis of iron regulatory proteins within neurons. This altered iron handling would cause a dysregulation of intracellular iron. While iron is crucial for proper cellular functioning, excess labile iron has proven neurotoxic (Youdim, 2004; Kaur, 2009) and capable of propagating neuronal injury. Thus, proper regulation is critical, especially during times of inflammation. Chronic inflammation can in turn lead to downstream events contributing to neurodegeneration observed in PD (Chen, 2003). It was first believed here that the responsible mediator was one of three pro-inflammatory cytokines (IL1ß, IL6, TNF), shown to be present in significantly elevated levels within microglial conditioned media. While direct treatment of individual cytokines on neuronal cultures proved to have minor effects on hepcidin mRNA upregulation with IL6 and TNF, they did not result in the same increased observations of TfR and DMT1 upregulation or elevated intracellular iron levels as with MCM treatment. Thus, it remained to be determined which mediator was responsible for these changes.

Extensive research into literature involving microglial-released inflammatory mediators (Twig, 2001; Garden, 2006; Block, 2007; Block, 2007), combined with the knowledge that an increased ferrous iron-containing labile iron pool would lead to iron oxidation via Fenton chemistry in the presence of H_2O_2 to produce hydroxyl radicals contributing to cellular OS (Lemire, 2013), led to a new potential target. Further investigation into mechanisms behind iron-induced OS led to the deduction that H_2O_2 may serve as another prospective candidate for affecting the observed changes in iron regulatory proteins. Since OS in microglia generates NADPH oxidase capable of oxidising cellular NADPH to oxygen for a concomitant production of superoxide (Twig, 2001), and the superoxide dismutase reaction with superoxide creates H_2O_2, then one could infer that OS would be accompanied by a rise in H_2O_2 levels. It has already been discovered that iron is dysregulated, leading to raised levels. Perhaps the elevated H_2O_2 along with the presence of increased ferrous iron continuously feeds the Fenton reaction, which in turn uses the ferric iron product to run Haber-Weiss chemistry, initiating a positive feedback loop of OS dependent cell death that may have an important role in PD dopaminergic neuron degeneration. Since dopamine synthesis, oxidation and catabolism can all contribute to H_2O_2 production (Maker, 1981; Gluck, 2002), and PD SN has demonstrated decreased levels

of peroxidase and catalase to detoxify the H_2O_2 surfeit (Ambani, 1975; Kish, 1985; Sofic, 1992), then perhaps dopaminergic neurons in Parkinson's grow more susceptible to negative consequences associated with excess H_2O_2 that can then potentiate OS-mediated neurodegeneration. This theory is supported with evidence that reductions in both ferrous iron and H_2O_2 proved neuroprotective in N27 dopaminergic neurons (Cantu, 2011).

Thus, this chapter aims to fully classify the consequences of H_2O_2 treatment on neuronal iron metabolism *in vitro* to potentially identify the MCM mediator capable of instigating significant changes to dopaminergic neuronal iron handling. This would act as a model of PD OS that may eventually lead to dopaminergic neurodegeneration. First, significant H_2O_2 presence within microglial conditioned media was confirmed. Effects of direct H_2O_2 treatment were then assessed *in vitro* using the N27 rat dopaminergic cell line, followed by result confirmation using E18 primary hippocampal neuronal cultures. Cells were treated with stabilised H_2O_2 concentrations, and then processed for any changes in iron metabolism for comparison with results from N27 and primary cell treatment with MCM, in order to determine if H_2O_2 was able to induce the foreseen variations. It was hypothesised that the attenuating effects observed after 1h MCM incubation with cytokine antibodies (in Chapter 4) were as a result of decomposition of the microglial inflammatory mediator during the 1h incubation period before cell treatment. So this chapter aims to explain those results by incubating H_2O_2–conditioned medium for 1h under similar conditions to determine any diminution in result effects. Finally, to prove that any observed effects were a direct result of H_2O_2 treatment with neuronal cultures, cells were treated with catalase-neutralised H_2O_2 to determine if this was able to fully attenuate the inflammatory stimuli.

5.2 Chapter Objectives

This chapter aims to complete the following objectives:

1. Confirm the presence of hydrogen peroxide in microglial conditioned medium.
    a. Create MCM by treating microglia with optimised LPS and exposure time.
    b. Quantify hydrogen peroxide in the MCM supernatant using an assay kit.

2. Assess whether H_2O_2 is a potential candidate as the microglial-released inflammatory mediator responsible for affecting previously observed changes in neuronal iron metabolism.
    a. N27 cells will be treated with various concentrations of H_2O_2 to assess for:
        i. IRP mRNA expression following direct H_2O_2 treatment.
        ii. Intracellular iron levels following direct H_2O_2 treatment.
    b. N27 results will be confirmed using primary neuronal cultures to assess for:
        i. IRP mRNA expression following direct H_2O_2 treatment.
        ii. Intracellular iron levels following direct H_2O_2 treatment.

3. Assess and explain effects observed after 1h MCM incubation with cytokine antibodies by incubating hydrogen peroxide for 1h to confirm it as a sufficient period for H_2O_2 decomposition to attenuate previously observed changes in neuronal iron metabolism.
    a. Assess IRP mRNA expression after treating N27 with 1h dissipated H_2O_2.
    b. Assess intracellular iron levels after treating N27 with 1h dissipated H_2O_2.

4. Confirm H_2O_2 as the microglial inflammatory mediator causing iron metabolism changes by instigating a loss of observed effects after H_2O_2 neutralisation by catalase.
    a. Determine IRP mRNA expression after treating N27 with catalase.
    b. Assess intracellular iron levels after treating N27 with catalase.

5.3 Experimental Methods

5.3.1 Confirming expression of hydrogen peroxide in microglial conditioned media

The first step in determining the suitability of H_2O_2 as the culpable inflammatory mediator was to prove that microglia were actually capable of releasing significant quantities of H_2O_2. N9 cells were seeded (350,000c/w, 6wp), left to rest ON, and then treated with either vehicle control (dH2O) or 0.25µg/ml LPS as normal for MCM production (Section 2.3.1.3). After discarding centrifuged supernatant pellets, a hydrogen peroxide assay kit (Abcam, ab102500) was used as per the manufacturer's instructions to quantify H_2O_2 concentrations within the microglial supernatant (Section 2.4.5). Each 6wp contained n=3 for each treatment condition, and a total of 3 plates were run individually for a total n=3. Results were deduced from a standard curve line of best fit determined from a fresh set of standards with known H_2O_2 concentrations ranging from 0-5nM.

5.3.2 Testing the effects of direct hydrogen peroxide treatment on N27 and primary neurons

To establish whether H_2O_2 was able to exert a significant effect on neuronal iron metabolism, N27 cells were seeded (500,000c/w, 6wp) and treated to a range of H_2O_2 concentrations (0-200µM) for 3 and 24h (Section 2.3.3). The concentration range was determined by taking the physiological H_2O_2 levels determined above (Section 5.3.1.), and then applying a range including concentrations below and above these levels. Cells were then processed for analysis by the ferrocene assay (Section 2.4.4), to determine significance with any particular H_2O_2 concentration. Using those results, several significant concentrations were applied to N27 cells for analysis of gene expression by qRT-PCR (Section 2.6). These results were confirmed by direct H_2O_2 treatment in primary neuronal cultures.

5.3.3 Explaining effects observed in N27 treatment with key cytokines using decomposed H_2O_2

In order to explain the effects observed with MCM treatment where key cytokines were neutralised by a 1h incubation with antibodies, and to link the effects to loss of H_2O_2, 100µM H_2O_2 in complete RPMI was pipetted into blank 6 well plates (Section 2.3.3.1). Plates were then incubated for 1h under cellular incubation conditions, whereupon previously seeded N27 cells (500,000c/w, 6wp) were washed and aspirated. Wells were then treated with the decomposed H_2O_2 media for 24h, and analysed for gene and iron expression for comparison to previous data.

5.3.4 Confirming the effects of hydrogen peroxide treatment on N27 neurons using catalase treatment

If separate neuronal treatment with MCM or direct H_2O_2 revealed changes to iron regulation, and MCM is proven to contain significant levels of H_2O_2, then it can be postulated that the H_2O_2 is behind the observed effects. To confirm this, quenching of H_2O_2 by catalase should also quench the changes to iron regulation (Section 2.3.3.2). Established cultures of N27s (500,000c/w, 6wp) were treated with either 100μM H_2O_2, 100μM H_2O_2 + 100U/ml catalase, or 100U/ml catalase. The same conditions were then repeated using 200μM H_2O_2. In a parallel plate, N27 cells were treated with MCM or MCM + 100U/ml catalase. All conditions were incubated for the optimised 24h incubation period. Cells were then lysed for collections and analysis by PCR or ferrocene assays.

5.3.5 Statistical Analysis

All experiments were run three independent times. Mean values were calculated for all experiments, and data expressed as mean ± SEM. For detection and quantification of H_2O_2 in conditioned media, sample concentrations were interpolated from a standard curve line of best fit using linear regression. Results between the 2 groups were compared using the unpaired t test. A 1-way ANOVA with Dunnett's post-hoc multiple comparisons test with comparison to each control dataset was utilised for both gene expression and ferrocene assay statistical analysis. Bonferroni's multiple comparison post-hoc test was employed to measure differences between treatment states with 1 hour decomposed H_2O_2 treatments. All statistical analyses were calculated using GraphPad Prism software.

5.4 Results

5.4.1 Confirming expression of hydrogen peroxide in microglial conditioned media

N9 cells were seeded in 6wp and treated with 0.25µg/ml LPS or control (dH2O) for 24h to make MCM. Following incubation, MCM supernatant was collected and processed using a H_2O_2 assay kit to quantify the levels of H_2O_2 released into the supernatant by activated microglial cells. As hypothesised, LPS-treated microglia were capable of releasing significant levels of H_2O_2 into the supernatant used as MCM when compared to the control (respectively, 11.21 ± 0.30 vs 8.09 ± 0.26 µM, $p<0.0001$) (Figure 5.1). This confirms that MCM used to treat neuronal cells contained significant levels of H_2O_2 potentially capable of exerting a lasting effect on iron regulation.

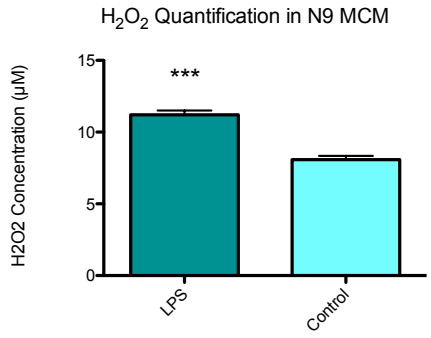

Figure 5.1 Quantifying H_2O_2 Expression in MCM supernatant using an H_2O_2 assay
Microglial N9 cells were seeded (350,000c/w), rested 24h, and then activated with 0.25µg/ml LPS for 24h, as per the previously optimised protocol to produce MCM. Control wells were run in parallel, where N9 cells were treated with a vehicle control. Upon completion of incubation, supernatant was collected and immediately processed following the manufacturer instructions for the hydrogen peroxide assay kit (Abcam) to quantify total supernatant H_2O_2. Results exhibited a highly significant increase in hydrogen peroxide ($p<0.001$), indicating that the LPS-induced inflammatory response does indeed provoke microglial production and release of H_2O_2 into the supernatant. This suggests that H_2O_2 is a possible candidate for the microglial-released inflammatory factor inflicting changes to neuronal iron metabolism. Each experiment was run with three wells for each condition, on three independent occasions. Data represents mean ± SEM for all nine values. *Statistical significance compared to control is represented by asterisks: ***$p<0.001$. $n=3$.*

5.4.2 *Measuring the Effects of H_2O_2 Treatment on Iron Regulation in N27 Neurons*

It was postulated that H_2O_2 was responsible for the effects observed with MCM treatment to neurons. In order to prove this, N27 cells were treated directly with various concentrations of H_2O_2 (0-200µM) for both 3h and 24h, and analysed by the ferrocene assay (Figure 5.2) to determine if H_2O_2 exacted any effect on iron expression. Control cells were treated with an equal volume of vehicle control (dH_2O). The 3h time point was chosen since previous gene expression measured HAMP changes only at 3h, while 24h was the previously determined optimum incubation period. Concentrations of H_2O_2 ≥100µM obtained significantly increased levels of iron uptake in N27 cells at 24h (200µM=0.219 ± 0.02, $p<0.001$; 100µM= 0.204 ± 0.01, $p<0.05$; Control= 0.151 ± 0.003).

Next, the two H_2O_2 concentrations demonstrating significant differences compared to control (200 and 100µM) were chosen for treatment (24h only) to monitor gene expression of the iron regulatory proteins in N27 cells. As speculated, results verified that H_2O_2 had profound effects on iron regulation in neurons. The 200µM concentration affected all iron regulatory proteins with great significance, barring DMT1, which only exhibited a significant increase at the lower concentration of 100µM (2.336 ± 0.24, $p<0.01$) (Figure 5.3). 100µM also saw an increase in TfR (2.477 ± 0.23, $p<0.01$). The 200µM treatment resulted in the following increases in iron regulatory protein gene expression, compared to a control at 1: HAMP=11.38 ± 1.50, FPN=6.759 ± 0.54, FtH1=7.632 ± 0.84, TfR=3.936 ± 0.04, IREb2=20.51 ± 2.59, all $p<0.001$. Additionally, there was a significant decrease in Aco1 with 200µM (0.310 ± 0.03), which may result from H_2O_2 degradation of the Aco1 iron-sulphur cluster leading to increased IRP1 binding activity.

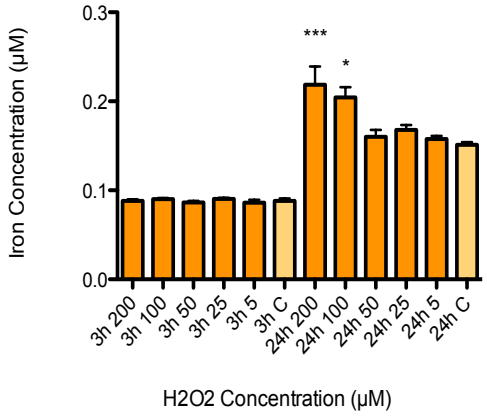

Figure 5.2 Increased Iron Levels in N27 Neurons after H_2O_2 Treatment as Assessed by the Ferrocene Assay
N27 cells were seeded (500,000c/w), rested (24), and then treated with a range of H_2O_2 concentrations or vehicle control for 3h and 24h. Cells were lysed and processed to quantify intracellular iron levels via the ferrocene assay. Analysis presented with no changes in intracellular iron levels at 3h, however, 24h demonstrated a significantly increased iron uptake at the highest 2 concentrations used (200µM & 100µM). This signifies that H_2O_2 maintains the ability to increase intracellular iron in dopaminergic neurons. Data represents mean ± SEM. *Statistical significance is denoted by asterisks: *p<0.05, ***p<0.001. n=3.*

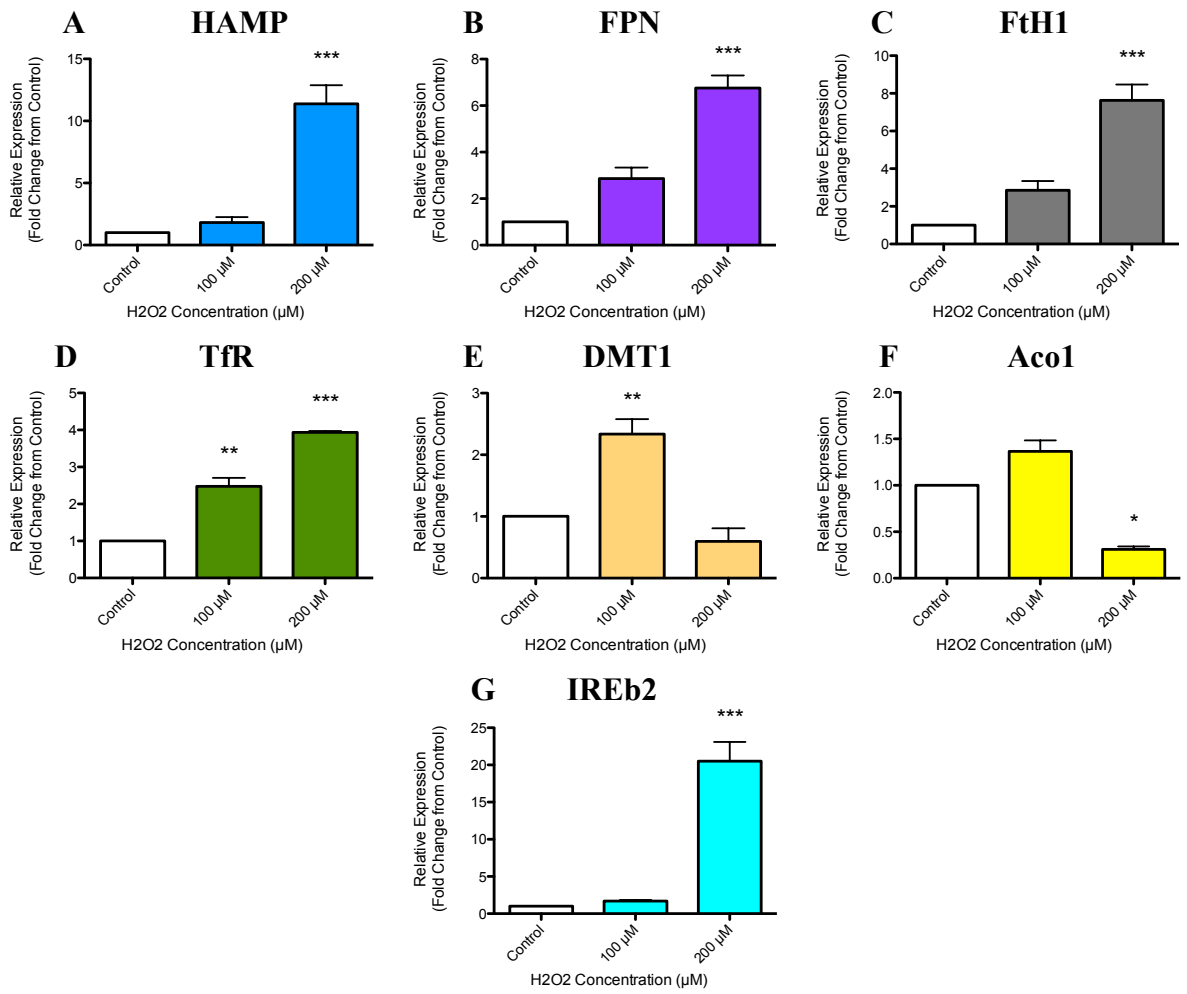

Figure 5.3 Relative Gene Expression of IRPs in N27 Neurons after H_2O_2 Treatment
N27 cells were seeded (500,000c/w), rested (24h), and then treated with either 200µM or 100µM H_2O_2, or vehicle control (24h). were analysed for changes in IRP gene expression, including HAMP (A), FPN (B), FtH1 (C), TfR (D), DMT1 (E), Aco1 (F), IREb2 (G). Results displayed greatly significant changes with 200µM in all IRPs, except in DMT1, which only revealed increased expression after 100µM treatment. This substantiates the assumption that H_2O_2 is capable of instigating significant changes to neuronal iron homeostasis via dysregulation of their iron regulatory proteins. Graphs represent mean ± SEM for all results, normalised to the ßactin housekeeping gene. *Statistical significance is denoted by asterisks: *p<0.05, **p<0.01, ***p<0.001. n=3.*

Next, these results needed to be confirmed using primary neurons. Applying the same protocol, cells were directly treated with 100µM H_2O_2. Results indicate a significant increase in iron levels after neuron treatment with H_2O_2 (0.256 ± 0.01 vs control 0.230 ± 0.004, $p<0.05$) (Figure 5.4). To assess gene expression, primary neurons were extracted and treated with 100µM H_2O_2 (24h). Results (Figure 5.5) illustrate statistically significant increases in HAMP (9.658 ± 1.47), FPN (8.869 ± 1.56) and DMT1 (2.431 ± 0.14). All data corresponds to that from N27 cells, in that both neuronal cell types exhibited changes in behavior subsequent to direct H_2O_2 treatment, which led to dysregulated iron metabolism as witnessed from increased iron expression as well as significant changes to IRP gene expression.

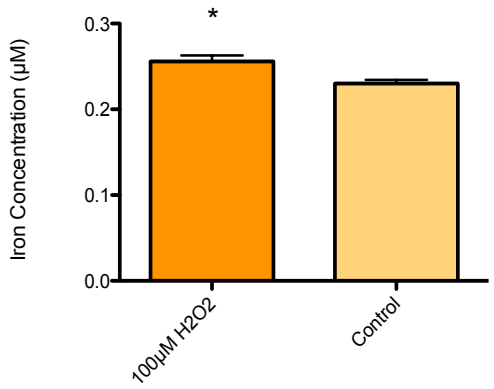

Figure 5.4 Increased Iron Expression in Primary Neurons after H_2O_2 Treatment as Assessed by Ferrocene Assay. Primary neuronal cells were treated with 100µM H_2O_2 or vehicle control for 24h, and intracellular iron was determined via the ferrocene assay. Analysis demonstrated a significantly increased iron expression as compared to the control, which validates previous studies in N27 cultures. Graphs represent mean ± SEM. *Statistical significance is denoted by asterisks: *p<0.05. n=3.*

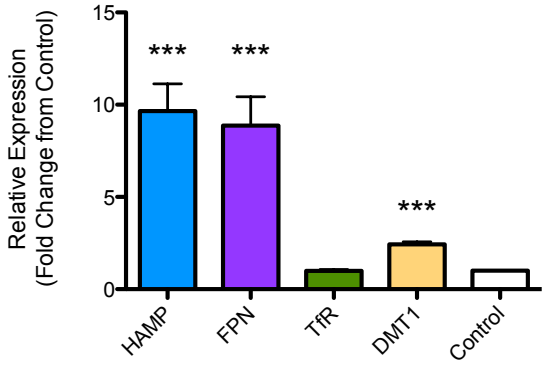

Figure 5.5 Relative Gene Expression of IRPs in Primary Neurons after H_2O_2 Treatment
Primary neuronal cells treated with 100µM of H_2O_2 or vehicle control for 24h were analysed by qRT-PCR for changes in iron regulatory protein gene expression, testing for those which previously demonstrated significant changes, including HAMP, FPN, TfR, DMT1. Data was normalised with fold change from control using ßactin housekeeping gene. As with N27 cells, primary cultures exhibit very significant increases in gene expression for all measured genes, except TfR. Graphs represent mean ± SEM for all results, normalised to a housekeeping gene. *Statistical significance is denoted by asterisks: ***p<0.001. n=3.*

5.4.3 Decomposed H_2O_2

A significant decrease was found between iron expression in N27 following direct H_2O_2 treatment, and treatment following a 1h incubation period to allow for H_2O_2 decomposition (respectively, 0.455 ± 0.03 and 0.349 ± 0.01, $p<0.001$) (Figure 5.6). While the decomposed treatment still maintained a significant increase in iron expression as compared to control (0.089 ± 0.002), the decreased signal infers a significant H_2O_2 decomposition in the one hour incubation time frame. Since 100µM is closer to physiological levels of H_2O_2, only the genes expressing significant changes from direct treatment with 100µM H_2O_2 (TfR and DMT1) were measured with decomposed H_2O_2. As expected, analysis of these IRP gene expression results presented with a significantly reduced signal following the 1h incubation period (Figure 5.7). The 24h treatment following 1h H_2O_2 incubation managed to completely quench any significant increases in both genes when compared to direct H_2O_2 treatment results. For TfR, H_2O_2 treatment had much higher expression (2.477 ± 0.23) than the decomposed treatment (1.815 ± 0.13). This was similar in DMT1 gene expression, with direct H_2O_2 (2.336 ± 0.24) higher than decomposed H_2O_2 (1.118 ± 0.08).

Figure 5.6 Changes in Iron Uptake after N27 treatment with Decomposed H_2O_2
N27 cells were seeded (500,000c/w), rested (24), and then treated for 24h with either 100µM H_2O_2 directly, or 100µM H2O2 after a 1h decomposition period under cellular incubation conditions, as was performed during the cytokine 1h incubation period prior to N27 treatment to ensure IL6 and TNF antibody binding. Both conditions had a control run in parallel, where cells were treated with an equal volume of vehicle control. Following incubation, cells were lysed for analysis of intracellular iron levels via the ferrocene assay. As before, direct H_2O_2 treatment resulted in a profound increase in iron expression after 24h ($p<0.001$). Similarly, the decomposed H_2O_2 treatment revealed a significant iron increase compared to control, but also disclosed a significant decrease ($p<0.001$) compared to the direct H_2O_2 treatment expression. This implies that the 1h incubation period was sufficient to elicit a statistically significant weakening in H_2O_2 signal within conditioned medium. Bars represent mean ± SEM. *Statistical significance is indicated by asterisks: ***p<0.001. n=3.*

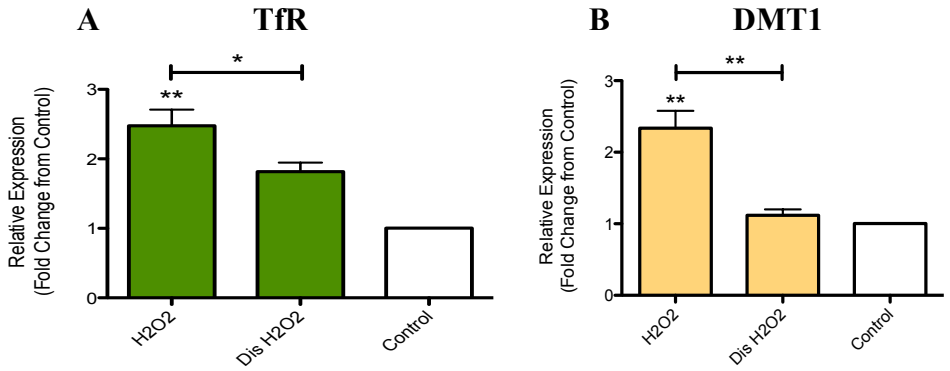

Figure 5.7 Relative Gene Expression after N27 treatment with Decomposed H_2O_2
N27 cells were seeded (500,000c/w), rested (24h), and then treated with direct 100µM H_2O_2 or 100µM H2O2 after a 1h decomposition period, or a vehicle control, for 24h. After incubation, cells were collected and processed for analysis by qRT-PCR. As before, direct H_2O_2 treatment resulted in significantly increased gene expression after 24h. However, the decomposed H_2O_2 treatment failed to establish any increases in gene expression for either TfR or DMT1 when compared to control. Interestingly, there was also a significant decrease in expression between direct H_2O_2 treatment and the decomposed treatment in both genes, with a complete dampening of upregulation. This implies that the 1h incubation period was sufficient to elicit a statistically significant diminution in H_2O_2 signal within the conditioned medium, which could explain the muted expression observed in the anti-IL6-TNF cytokine treatment control. Bars represent mean ± SEM. *Statistical significance is indicated by asterisks: *p<0.05, **p<0.01. n=3.*

5.4.4 Loss of observed effects after H_2O_2 neutralisation with catalase

N27 cells were treated with either 100µM H_2O_2, 100µM H_2O_2 + 100U/ml catalase, or 100U/ml catalase. The same conditions were then repeated using 200µM H_2O_2 (Figure 5.8 A-D). As observed in previous results, N27 treatment with either 100 or 200µM H_2O_2 resulted in significant increases in IRP gene expression. Subsequent treatment with catalase was able to substantially quench the increased expression at the 100µM concentration (HAMP=2.438 ± 0.46 to 1.142 ± 0.07; FPN=2.875 ± 0.09 to 0.597 ± 0.06; TfR= 3.431 ± 0.35 to 1.921 ± 0.15, $p<0.01$), but not at the 200µM. The exception here is with DMT1, which showed a quenching signal with both concentrations, and where the 100µM treatment elicited a greater increase in gene expression compared to 200µM (100µM treatment vs catalase=2.91 ± 0.06 vs 2.080 ± 0.07, $p<0.001$; and 200µM= 2.442 ± 0.28 vs 1.636 ± 0.19, $p<0.01$). This is consistent with past results. N27 treatment with catalase alone showed no significant change from control in gene expression for any of the measured IRPs.

In order to determine whether the previously observed changes to iron metabolism seen with neuronal treatment with MCM could be quenched with catalase, N27 cells were also treated with either MCM or MCM + 100U/ml catalase and gene expression measured (Figure 5.8 E-F). Neither HAMP nor FPN presented with any significant decreases in gene expression (data not shown), although FPN had a decreasing trend. This may be due to the fact that neither HAMP nor FPN presented with significant increased expression followsing 24h MCM

exposure, so there was no signal for catalase to quench. However, increased expression for both TfR and DMT1 were completely terminated by simultaneous catalase treatment (MCM vs MCM + catalase: TfR= 2.982 ± 0.07 vs 1.076 ± 0.08; DMT1= 3.345 ± 0.27 vs 0.814 ± 0.07).

Next, N27 cells treated with the same conditions as above were measured for iron expression. In accordance with previous data, both 200μM and 100μM H_2O_2 elicited a significant increase in iron levels compared to control (200μM=0.134 ± 0.01; 100μM= 0.119 ± 0.01; Control= 0.081 ± 0.003, $p<0.001$) (Figure 5.9A). Catalase alone had no effect on cellular iron levels, however, catalase in addition to both 200μM and 100μM H_2O_2 resulted in complete termination of the observed increases in iron (200μM + Catalase= 0.086 ± 0.002; 100μM + Catalase= 0.091 ± 0.002). The decrease from 200μM H_2O_2 treatment to 200μM + Catalase treatment had a p value of <0.001, while the 100μM to 100μM + Catalase had a p value <0.01.

Consistent with previously determined data, N27 treatment with MCM here caused a significant increase in intracellular iron levels compared to control (respectively, 0.194 ± 0.02 vs 0.095 ± 0.01, $p<0.001$). Consistent with H_2O_2 treatments above, supplementing MCM supernatant with 100U/ml of catalase likewise resulted in complete quenching of the increased iron expression when compared to levels from MCM treatment (MCM + Catalase= 0.120 ± 0.01, $p<0.01$) (Figure 5.9B). Catalase treatment alone had no change in expression compared to control.

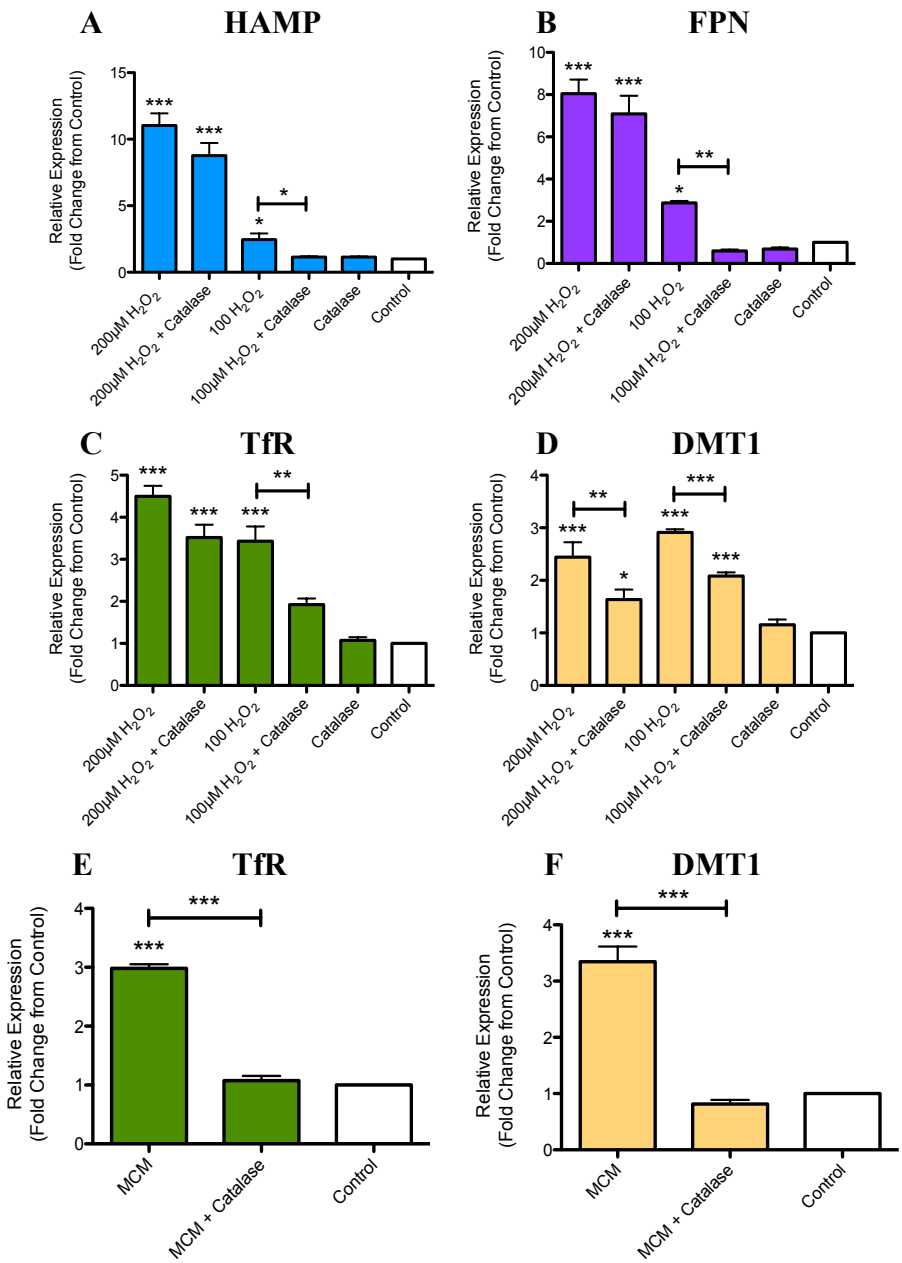

Figure 5.8 Relative IRP Gene Expression in N27 Neurons Treated with Catalase
N27 cells were treated with either 200μM H_2O_2, 200μM H_2O_2 + 100U/ml catalase, 100μM H_2O_2, 100μM H_2O_2 + 100U/ml catalase, 100U/ml catalase alone or vehicle control for 24h. Cells were collected, and after mRNA extraction and cDNA synthesis, gene expression for key IRPs (HAMP, FPN, TfR, DMT1) were measured via qRT-PCR. Results show that the 200μM H_2O_2 elicited a substantial increase in gene expression for all IRPs tested (A-D), with non-significant reductions occurring from catalase treatment (except DMT1, which demonstrated a significant quenching effect from catalase $p<0.01$). 100μM treatment also presented with increased gene expression in all IRPs, however, the catalase treatment was able to significantly extinguish these signals near or below control levels (again with the exception of DMT1, which demonstrated significant quenching with catalase $p<0.001$, however it was still significantly above control). Catalase treatment alone had no significant changes compared to control. For comparison between previous results after N27 MCM treatment, cells were then treated with either MCM, MCM + 100U/ml catalase, or a vehicle control (E-F). As with previous MCM treatment, neither HAMP nor FPN showed any upregulation after 24h, and the catalase likewise had no dampening effects so that both treatment conditions were statistically no different from control (data not shown). Also as before, MCM caused a significant increase in both TfR (E) and DMT1 (F) gene expression. Addition of catalase was able to completely terminate these detected increases. This infers that previously observed gene upregulation from MCM treatment may be attributed to activated microglial release of hydrogen peroxide. Bars represent mean ± SEM. *Statistical significance is denoted by asterisks: *p<0.05, **p<0.01, ***p<0.001. n=3.*

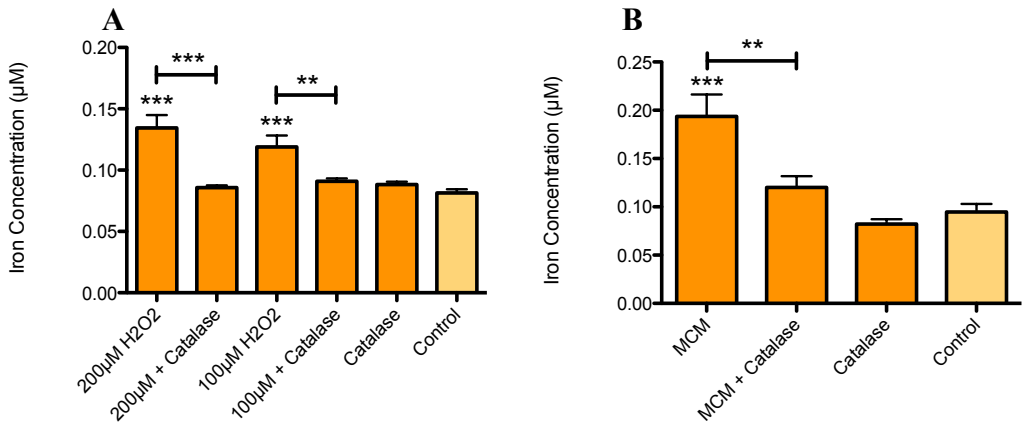

Figure 5.9 Changes in Iron Uptake in N27 Cells Treated with Catalase as Assessed by Ferrocene Assay
Since previous MCM treatment elicited increases in iron, and the instigating factor remained unknown, it was postulated that H_2O_2 may be responsible. To confirm this theory, MCM was treated with catalase, which catalyses disproportionation of hydrogen peroxide. N27 cells were seeded (500,000c/w), rested (24h), then treated (24h) with either 200µM H_2O_2, 200µM H_2O_2 + 100U/ml catalase, 100µM H_2O_2, 100µM H_2O_2 + 100U/ml catalase, 100U/ml catalase alone or vehicle control (A). To compare with initial results obtained from 24h MCM treatment to N27 cells, N27 cells here were also treated with MCM, MCM + 100U/ml catalase, 100U/ml catalase or vehicle control (B). All samples were collected and measured for intracellular iron levels via the ferrocene assay. Results confirm previous data, showing that both 200µM and 100µM H_2O_2 treatment elicited a substantial increase in iron levels compared to control, as did MCM treatment. Addition of catalase was able to completely terminate any increased iron expression for all three treatment conditions. Graphs represent mean ± SEM. *Statistical significance is denoted by asterisks: **p<0.01, ***p<0.001. n=3.*

5.5 Discussion

Experiments from the previous chapter with direct cytokine treatment on neurons demonstrated little changes to iron metabolism. Since hepcidin expression peaked at 3h following neuron treatment with MCM, and cytokine treatment did show significant increases in HAMP gene expression, it can be hypothesised that IL6 and TNF exposure were able to affect HAMP expression. However, there is no evidence that they cause the previously observed changes to iron regulatory proteins and intracellular iron levels at 24h. Thus, it must be concluded that another inflammatory mediator released by microglia must be responsible. Extensive literature research into such mediators identified one such possible oxidant as H_2O_2.

H_2O_2 is a reactive oxygen species released by activated microglia. Other sources include superoxide dismutation during mitochondrial respiration, dopamine deamination by monoamine oxidase (MAO), and NADPH oxidase (Nox) activity (Maker, 1981; Gao, 2003; Infanger, 2006). Under physiological conditions, H_2O_2 acts as a crucial signalling intermediate involved in redox regulation. Detoxification systems are in place to ensure levels are maintained in safe concentrations, with enzymes such as catalase or glutathione peroxidase able to decompose H_2O_2 into water and oxygen (Dringen, 1997; Dringen, 2005). However, in uncontrolled concentrations, H_2O_2 can oxidise nearby cellular compartments causing OS. Accompanied by excess iron found in the Parkinsonian SN (Dexter, 1989), H_2O_2 could feed the Fenton reaction to result in production of hydroxyl radicals, which along with increased ROS and RNS can lead to neuronal damage. This further activates microglia, which can initiate a feedback loop potentiating neurodegeneration. Since evidence indicates that the PD brain presents with increased SOD activity (Marttila, 1988) to dismutate superoxide into H_2O_2, as well as significantly increased MAO activity in the SN (Riederer, 1986) to catalyse dopamine oxidation with H_2O_2 by-products, as well as microglia-released Nox enhancing neurotoxicity by producing H_2O_2 (Gao, 2003), and diminished concentrations of H_2O_2 scavenger GSH in the PD SNpc (Perry, 1982; Kish, 1985; Riederer, 1989), this all points to simultaneous enhanced production and decreased clearance of H_2O_2 that could cause an amplified vulnerability specific to dopaminergic neurons. Additionally, familial PD pathogenesis can occur from mutation to DJ-1, which is an H_2O_2 scavenger present in the SN (Yasuda, 2017). DJ-1 knockout mice are found to be more sensitive to the toxic effects of OS, leading to dopaminergic cell loss as seen in PD (Di Nottia, 2017). H_2O_2 could thus play an important neurodegenerative role in PD pathophysiology.

Microglia and macrophages have been proven to release H_2O_2 upon activation (Coraci, 2002; Kraft, 2004; Mander, 2006). This was confirmed, as it was revealed here that LPS-activated microglia were able to release significant amounts of H_2O_2 into the supernatant (Figure 5.1), proving that neurons treated with MCM were exposed to the peroxide. If the previously observed neuronal changes were to be attributed to H_2O_2 then direct treatment with H_2O_2 should present with similar changes. This was confirmed as it was determined that high concentrations of H_2O_2 were able to elicit a very strong response from all 7 iron regulatory proteins. This was not observed in past results with MCM treatment, which only demonstrated changes to HAMP, TfR and DMT1. This discrepancy is likely due to the excessive dosage of 200μM used here, which is higher than physiological levels. However, the fact remains that H_2O_2 was able to elicit substantial upregulation in all measured iron regulatory proteins. The lower H_2O_2 concentration of 100μM was still able to generate a significant increase in both TfR and DMT1 expression at 24h, which happen to be the two genes expressing changes with MCM treatment at 24h. The elevations are consistent with previous MCM treatment results, with similar increases in gene expression produced under both conditions. At 24h, N27 treated with MCM presented increased TfR gene expression of 2.019 ± 0.28, while 100μM H_2O_2 treatment caused a similar increase of 2.477 ± 0.23. Regarding DMT1 in N27, 24h MCM treatment resulted in an increase of 2.618 ± 0.28, while 100μM H_2O_2 elicited an elevation of 2.336 ± 0.24. DMT1 in primary neurons was also very similar, with 24h exposure to 100μM H_2O_2 causing an increase of 2.431 ± 0.14. Since MCM and H_2O_2 treatments both elicit similar escalations in IRP gene expression, this points to a very significant correlation relating H_2O_2 as an instigating factor to changes in neuronal iron metabolism during inflammation. These increases in IRP gene expression also coincide with a simultaneous increase in intracellular iron at 24h following H_2O_2 treatment. It can be inferred that since H_2O_2 is a mediator present within the MCM, while also able to directly affect TfR and DMT1 gene expression here as well as in previously published data (Cairo, 1996; Pantopoulos, 1997; Mueller, 2001; Andriopoulos, 2007; Jiang, 2010), it is possible that H_2O_2 triggered the aforementioned changes to neuronal iron metabolism.

So far, my results have demonstrated that H_2O_2 treatment is capable of inducing significant changes to neuronal IRP gene expression and overall iron levels. In order to prove that the results observed could be fully attributed to the effects of H_2O_2 exposure, it could be assumed that H_2O_2 decomposition by the antioxidant catalase should sufficiently neutralise any observed effects. Catalase is an enzyme capable of catalysing the decomposition of H_2O_2 into

water and oxygen (Dringen, 1997). If the observed IRP and iron changes are due to H_2O_2 exposure, then addition of catalase should quench any effects. This hypothesis was confirmed when the outcomes from neuronal treatment with H_2O_2 combined with catalase, managed to entirely suppress any upregulated gene expression (Figure 5.8). The catalase managed to significantly decrease gene expression at the 200μM dosage, but was not sufficient enough to completely quench the upregulation. This is likely due to the excessively high concentration administered as one large bolus, overriding the detoxification capabilities of the catalase. The 200μM dosage was also much higher than physiological levels, so mainly served to present the effects that H_2O_2-mediated OS were able to induce on neuronal iron metabolism. However, the 100μM dosage presented complete dampening to control levels in HAMP, FPN, and TfR relative gene expression, with DMT1 showing a significant decrease, although without full stifling. Intracellular iron levels from both H_2O_2 treatment dosages were also completely dampened to control levels by addition of catalase. This data indicates that catalase is sufficient to reduce effects of H_2O_2 on gene expression in N27 neurons.

Results thus far indicate that H_2O_2 has a very significant role in the inflammation induced changes to neuronal iron metabolism. To further confirm that the peroxide was responsible for previously determined changes with conditioned medium, cells were incubated with freshly prepared MCM or MCM combined with catalase. Data corresponds to that of direct H_2O_2 treatment, in that the addition of catalase was able to completely prevent upregulation of both TfR and DMT1 gene expression in N27 treated with MCM (Figure 5.8 E-F). Intracellular iron levels were also reduced to control levels following catalase treatment of N27 cells incubated with MCM (Figure 5.9B). Thus, it may be concluded with sufficient evidence that observed increases in intracellular iron levels, as well as upregulation of iron regulatory proteins TfR and DMT1 may be attributed to the presence of H_2O_2 within the microglial conditioned media. This is an essential finding, in that it proves activated microglia release significant levels of H_2O_2 capable of inducing changes to neuronal iron metabolism that may lead to iron-mediated neurotoxicity. The majority of this microglial H_2O_2 is most likely generated as a result of phagocytic activation of NAPDH oxidase (Babior, 2000), which is then able to propagate further microglial activation (Zhang, 2005; Mander, 2006). Since Nox is upregulated in the PD SN (Wu, 2003), this excess H_2O_2 can have a deleterious effect on nigral dopaminergic neurons.

Referring to the effects observed following neuronal treatment with 1hMCM-IL6-TNF from the previous chapter, it was originally found that MCM alone resulted in a significant increase in TfR and DMT1. It was also determined in Chapter 4 that direct treatment with, separately, IL1ß, IL6 and TNF failed to induce upregulation in those two genes. It was

theorised that a 1h incubation of MCM (1hMCM) with antibodies against IL6 and TNF (1hMCM-IL6-TNF) prior to exposing neurons should produce no changes to the original MCM on N27 results since IL6 and TNF were deemed not responsible for the changes. Both 1hMCM-IL6-TNF and 1hMCM were run in parallel. While PCR relative gene expression data presented the expected upregulation of both TfR and DMT1 (Figure 4.10), they were somehow significantly lower than the original increases (Figure 3.9) (dropping significance from $p<0.001$ to $p<0.05$). Results from iron expression with 1hMCM-IL6-TNF demonstrated no increased iron levels, as expected, but neither did the 1hMCM treatment (which previously presented substantial elevations in iron). This data was puzzling at first. Something must have changed during the 1h incubation, diminishing the effects on neuronal iron regulation. This led to the concept that the inflammatory mediator affecting changes within the MCM had a short half-life causing it to be sufficiently decomposed within the 1h incubation, thereby weakening its effects. These results finally led to the hypothesis that H_2O_2 may be responsible instead.

This theory was tested with neuronal exposure to either H_2O_2 or H_2O_2 applied to blank wells and incubated for 1h prior to treatment ($1hH_2O_2$), as with the 1hMCM. Increased iron levels from H_2O_2 treatment were significantly attenuated following $1hH_2O_2$ treatment, although not sufficiently to completely remove expression. Levels of both H_2O_2 and $1hH_2O_2$ here seem to be higher than those previously detected. A possible explanation for this disparity is the use of younger neurons at a lower passage number here. Such deviations were accounted for, as both conditions were run in parallel using the same neuronal cultures and seeding conditions, so comparisons may be drawn within experiments but not across previous data. H_2O_2 activity and rate of decomposition can also be affected by divergences in pH levels and antioxidant presence (Tachiev, 2000; Hug, 2003), which may help account for the deviations in iron expression levels. Nonetheless, gene expression of TfR and DMT1 demonstrated fully mitigated levels equal to control (Figure 5.7). Thus, 1h incubation of H_2O_2 prior to neuronal exposure effectually diminishes its effects. This effectively clarifies the reason behind the variance in expression following 1hMCM and 1hMCM-IL6-TNF treatment, and also provides further evidence of H_2O_2 involvement in the propagation of an inflammatory response causing dysregulated iron homeostasis in neurons.

Data analysed here from *in vitro* neuronal treatment identify H_2O_2 as an essential inflammatory mediator with a potentially critical role in the dysregulation of neuronal iron metabolism in PD. Such a discovery would be an exciting subject for further study. Future work may involve more accurate monitoring of H_2O_2 expression in microglia and neurons under control and inflammatory conditions. H_2O_2 levels were measured here in microglial

MCM, however, readings were taken 30 minutes after removal of supernatant from activated microglia due to the hydrogen peroxide assay kit processing time. It has been demonstrated here that a 1h incubation period is sufficient to diminish H_2O_2 levels, thus it can be inferred that 30m may also have a significant effect. Therefore, the H_2O_2 levels determined here may be diminished during the assay protocol, and not be a truly accurate representative of the levels within cultures. HyPer is a genetically encoded H_2O_2 biosensor that has been established as very accurate for such investigation (Malinouski, 2011), which may prove useful in future studies. Alternatively, intracellular H_2O_2 levels may be accurately quantified in living cells using carbon nanoelectrodes with the addition of the Prussian Blue catalyst for H_2O_2 reduction and subsequent nanosensor current response detection (Fernandez, 2016), or magnetic resonance imaging detection of H_2O_2 production of benzoic acid in living cells (Lippert, 2011). Results found here also warrant more in depth investigation into H_2O_2 effects in future *in vivo* experiments.

5.6 Conclusions

It was postulated that the inflammatory mediator within microglial conditioned medium responsible for causing previously viewed effects may be H_2O_2. Results from this chapter conclude that direct treatment of neurons with H_2O_2 results in greatly significant changes to iron levels and iron regulatory protein gene expression. All effects were quenched after treatment with the H_2O_2 antioxidant catalase. Similarly, catalase muted effects previously observed after neuronal treatment with microglial conditioned medium. Thus, it can be concluded from this data that H_2O_2 may be identified as the microglia-released inflammatory mediator that is directly responsible for causing the observed changes to iron metabolism in neurons. Such changes could eventually alter long term cellular iron metabolism, which has been shown to have a role in PD neuronal degeneration, thus helping to develop understanding of various factors contributing to parkinsonian cellular loss.

CHAPTER 6:

Assessment of the effects of continued exposure to activated microglial inflammatory factors on neuronal iron metabolism in co-culture conditions

6. Assessment of the effects of continued exposure to activated microglial inflammatory factors on neuronal iron metabolism in co-culture conditions

This chapter aims to create a more representative model of continuous exposure to microglial factors by introducing Transwell co-culture systems, where microglia and neurons are grown together. Microglial activation was then able to provide neurons with a continued exposure to inflammatory factors, in order to prevent loss of any short lived factors during MCM transfer. The effects of long-term exposure to inflammatory factors were then measured by observing changes to neuronal iron metabolism. It was determined that microglial presence appeared to have neuroprotective effects, with neurons demonstrating increases to IRP gene expression from earlier time points, and lower peak expression overall. This implies a greater spread, allowing for improved neuronal equilibration, which was confirmed by a lack of increased neuronal iron. Microglia also begin to take up excess iron from earlier time points, protecting neighbouring neurons from iron mediated toxicity.

6.1 Introduction

It has been determined thus far that LPS activates the microglial inflammatory response, and the microglial conditioned medium can be employed to trigger changes in neuronal iron metabolism. The exact mechanism of action behind such changes remains elusive, however, it has also been determined that direct treatment with certain key inflammatory mediators, IL6, TNF and H_2O_2, may have a defining role in initiating iron accumulation. It is postulated that such mediators may work in a synergistic fashion, with the pro-inflammatory cytokines affecting the increases in 3h hepcidin expression, while the H_2O_2 affects 24h changes. There may be other untested mediators present that add to the collaborative effort of inducing iron dysmetabolism perceived in Parkinsonian nigral neurons. It has already been established here that 1h incubation of MCM prior to neuronal treatment abates the detected reactions seen with immediate treatment. This predicates grounds for the presence of certain short lived factors within the microglial conditioned medium. It can similarly be implied that collection of conditioned media into Eppendorfs, followed by a 5 minute centrifugation and then neuronal treatment, may be sufficient time to diminish effects of any present short lived free radicals. In this way, other mediators may lose their effects, making it difficult to accurately measure the outcomes of neuronal treatment after an inflammatory response.

Moreover, the mechanism of treatment here involves activating microglia, followed by removal of the inflammatory mediator-containing conditioned media for separate treatment to neuronal cells. This type of solitary exposure may be useful for experimental replication and isolation of cells for analysis, however, it is not truly representative of the Parkinson's brain environment. PD neurons would be continually exposed to glial released factors. To more efficiently model the PD milieu in order to comprehend the effects leading to improper neuronal iron regulation, this chapter intends to elucidate the changes to iron metabolism following incubation with both microglia and neurons together. A Transwell co-culture system was developed where both neurons and microglia were cultured on opposing sides of a permeable membrane. This system has been utilised successfully in previous analyses into microglial and neuronal interactions (Hemmer, 2001; Gibbons, 2006; Kim, 2009; Liu, 2009). Addition of LPS would instigate an inflammatory reaction in the microglia, and as disclosed here in Section 3.4.5 (Figure 3.8), the LPS would have no direct effect on N27 cells. Inflammatory mediators released by microglia would then be able to persistently pass through the permeable membrane to exert their effects directly onto neurons in a more realistic model of disease.

The mechanism of inflammatory action on iron metabolism may involve numerous targets, which may only be accurately calculated experimentally under more physiological conditions. Along with the inflammatory action, it is also known that glia may have neuroprotective properties and lend assistance to support neuronal recovery (Streit, 1998; Streit, 2000; Polazzi, 2001; Streit, 2002; Neumann, 2008; Lambertsen, 2009). So it remains unclear whether co-culture with glia will result in neuroprotective or neurotoxic consequences. Microglial-neuronal co-culture, and the subsequent persistent exposure to any released factors following LPS treatment, may reveal disparate results upon comparison to those from a singular exposure to inflammatory conditioned medium. Thus, an enhanced understanding of the mechanisms of action during continuous co-culture exposure between microglia and neurons would be an essential factor to the study of inflammatory effects on iron metabolism.

6.2 Chapter Objectives

This chapter aims to complete the following objectives:

1. Establish N9 microglia and N27 neurons on opposite sides of a permeable membrane in a Transwell co-culture system.

2. Activate N9 cells with LPS and observe the effects of long-term exposure to inflammatory factors in neurons for comparison with previous data.
    a. Assess IRP gene expression in N27 cells following co-culture treatments.
    b. Assess iron levels following co-culture treatments in both cell types.

6.3 Experimental Methods

6.3.1 Neuronal and Microglial Co-Culture Transwell Systems

To accurately model a more physiological environment where all microglial mediators were able to exert their effects from continuous exposure onto neurons, a Transwell co-culture system was established as described in Section 2.2.5.1 (Figure 6.1). For this, N27 cells were seeded into the bottom of a cell plate (300,000c/w, 6wp) in complete RPMI. Upon confirmation of cell adherence, a Transwell insert containing 0.4µm semi-permeable membranes was placed on top of established cultures. N9 cells were then seeded (250,000c/w) into these inserts. After a 24h rest period, with both cultures fully established on opposing sides of the permeable membranes, LPS (0.25µg/ml) or vehicle control were added directly to microglial cells for 24h incubation. Lysates were then analysed via qRT-PCR (Section 2.6) or ferrocene assay (Section 2.4.4).

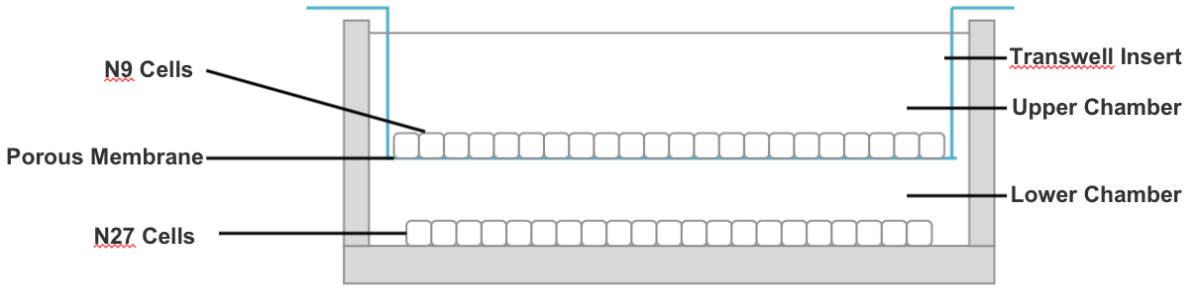

Figure 6.1 2-Transwell Co-Culture System
A schematic representation of the 2-Transwell co-culture system. N9 cells were seeded (250,000c/w) into the upper chamber of the Transwell insert, after N27 cells had been seeded (300,000c/w) in the lower chamber. After resting (24h), N9 cells were treated with LPS (0.25µg/ml 24h).

6.3.2 Statistical Analysis

Conditions were independently repeated in triplicate. All data expressed represent the mean ± SEM. Statistical comparisons between groups were analysed by 1-way ANOVA followed by Dunnett's post-hoc test comparing all groups to the control. A probability with p value $p<0.05$ was considered statistically significant. All statistical analyses were executed utilising GraphPad Prism software.

6.4 Results

N27 cells seeded at the bottom of Transwell wells were analysed for changes to gene expression subsequent to microglial activation by LPS for a range of time points. Any microglial factors released upon their inflammatory response activation were able to cross freely through a porous membrane to act upon neuronal cultures. As expected, there were significant increases in expression of HAMP, TfR and DMT1 mRNAs, but not in any of the other iron regulatory proteins measured (FPN, FtH1, Aco1, IREb2) (Figure 6.2). HAMP increased significantly at 3h (1.332 ± 0.04, $p<0.01$), TfR increased at both 18 and 24h (respectively, 1.676 ± 0.09, $p<0.01$; 2.002 ± 0.16, $p<0.001$), and DMT1 increased from 6 to 24h (respectively, 1.301 ± 0.03; 1.327 ± 0.01; 1.515 ± 0.03, all $p<0.001$). Similarly, there was an increase in microglial intracellular iron levels compared to control (0.485 ± 0.02 vs control 0.366 ± 0.02, $p<0.001$) (Figure 6.3B) as was also viewed with previous microglial activation at 24h.

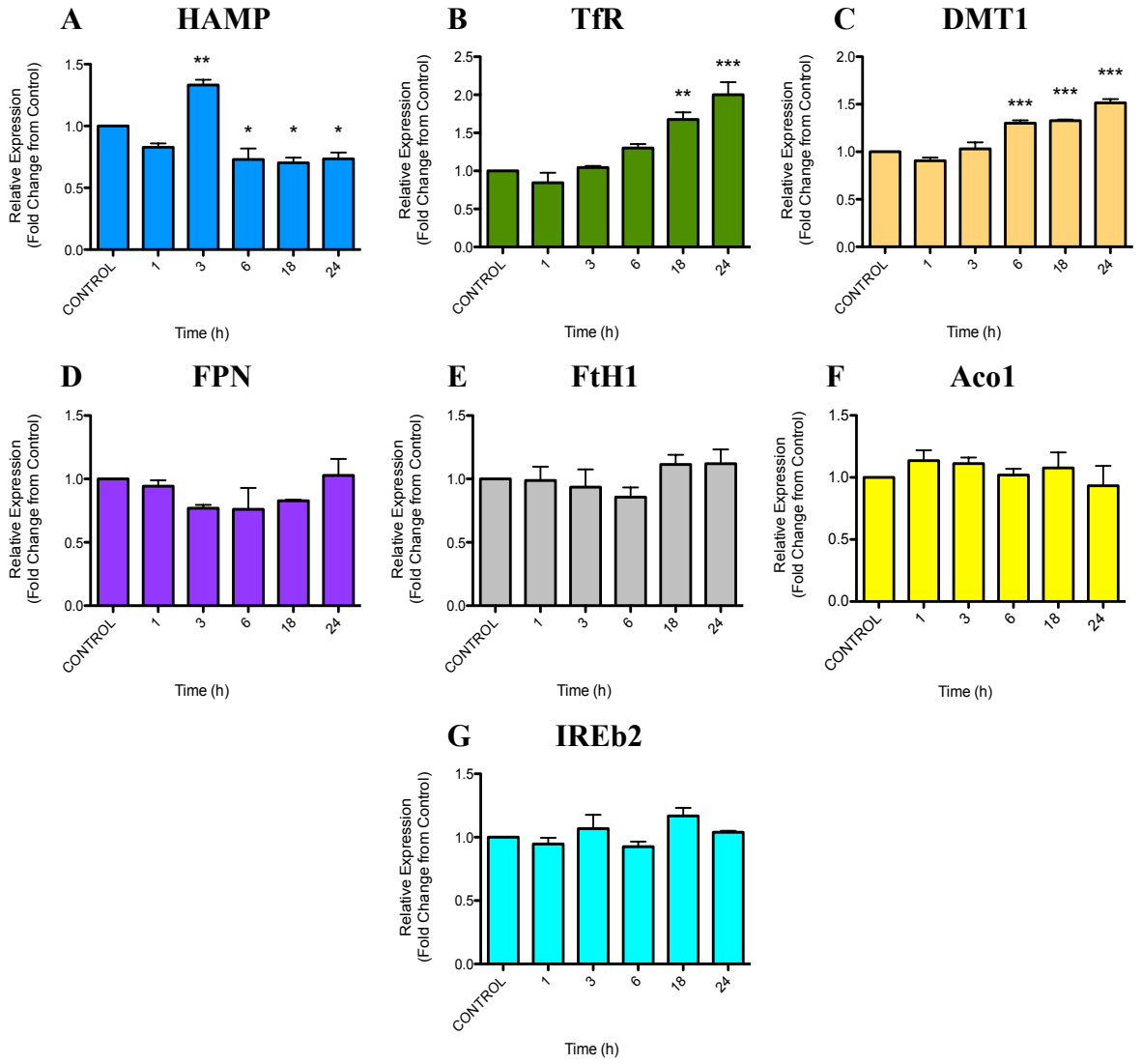

Figure 6.2 Relative Gene Expression in N27 Neurons after Co-Culture Transwell Incubation with Microglia
A Transwell co-culture system was established with N9 microglia (250,000c/w) at the top of Transwell inserts, and N27 (300,000c/w) seeded at the bottom of cell plate wells, on the opposite side of the semi-permeable porous membrane. Microglia were activated using the optimised LPS concentration (0.25µg/ml) for a range of time points (1-24h), after which N27 cell lysates were collected for analysis of relative gene expression via qRT-PCR. Changes to IRP gene expression were measured to determine the effects of long-term exposure to microglial released factors on dopaminergic neurons. Data was normalised using data measured from the ßactin housekeeping gene. Results showed similar increases of gene expression compared to those in mono-culture in HAMP (A), TfR (B), and DMT1 (C), with no changes in any of the other iron regulatory proteins measured (FPN (D), FtH1 (E), Aco1 (F), IREb2 (G)). Graphs represent mean ± SEM. *Statistical significance from control is indicated by asterisks: *p<0.05, **p<0.01, ***p<0.001. n=3.*

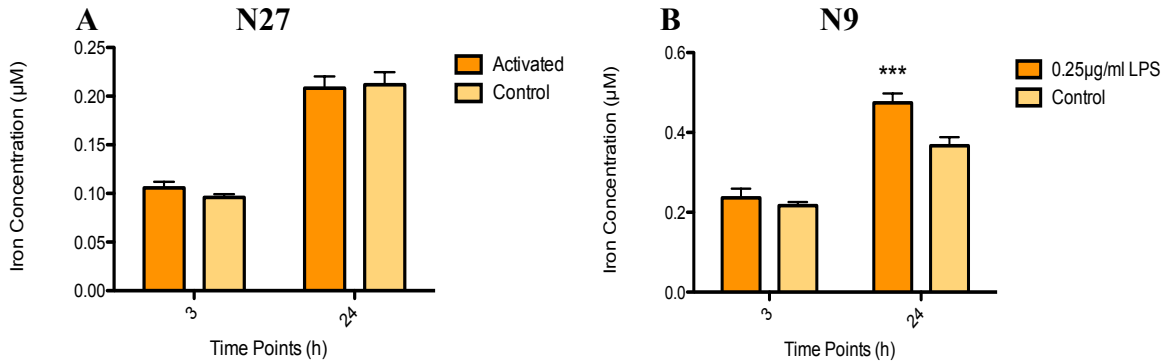

Figure 6.3 Intracellular Iron Levels in N27 Neurons and N9 Microglia as Assessed by Ferrocene Assay after Co-Culture Transwell Incubation. Neuronal N27 cells (300,000c/w at bottom of well) and microglial N9 cells (250,000c/w in top insert) were co-cultured on opposite sides of a semi-permeable Transwell insert. After being established for 24h, microglia were activated with the optimised protocol of LPS (0.25µg/ml) for 24h. Control plates were run in parallel using the same experimental conditions, but instead applying a vehicle control to microglia. Cell lysates for both N27 (A) and N9 (B) were collected separately and assessed for changes in iron uptake and intracellular expression via the ferrocene assay. N27 cells failed to exhibit any of the previously determined increases in iron levels, whereas N9 data displayed a statistically significant increase in iron expression following LPS-induced inflammatory response in microglia co-cultured with neurons. This may represent a microglial-mediated neuroprotection. Graphs represent mean ± SEM. *Statistical significance from control is indicated by asterisks: ***p<0.001. n=3.*

6.5 Discussion

Results from this chapter have determined that co-culture incubation of activated microglia and neurons, with persistent exposure to inflammatory mediators, presented with similar changes in iron regulatory genes as previously observed with mono-cultures. However, there were a few deviations. Beginning with relative gene expression in N27 dopaminergic neurons, it appears that co-incubation with microglia seems to reduce the experimentally observed increases, while also showing significance at an earlier time point. Hepcidin originally showed a significant yet transient increase in mRNA expression at 3h after MCM exposure (1.771 ± 0.11, $p<0.001$). This was similarly observed in the Transwell cultures, yet exhibiting less of an increase (1.332 ± 0.042, $p<0.01$). Transferrin receptors originally demonstrated a significant increase in mono-culture with MCM treatment only at 24h (2.019 ± 0.28, $p<0.001$), this same increase was observed in Transwell co-cultures (2.002 ± 0.16, $p<0.001$), however, a significant increase compared to control also emerged at 18h in Transwell co-cultures (1.676 ± 0.09, $p<0.01$). Similarly, DMT1 exhibited increasing levels of mRNA expression from 18h (1.768 ± 0.12) to 24h (2.618 ± 0.28) following MCM treatment, however, co-culture DMT1 already presented a significantly increased expression by 6h (1.301 ± 0.03, $p<0.001$), then increasing at 18h (1.327 ± 0.01) and 24h (1.515 ± 0.04). In comparison to mono-culture results, there appeared to be significantly increased levels reached sooner in co-culture cells in both neuronal TfR (appearing at 18h), and DMT1 (appearing at 6h). Levels of peak points were also lower than previously observed. It may be postulated that the presence of microglia evens out peak expression. Neurons begin to show changes to iron regulatory gene expression earlier on, however the changes at later times are reduced as cells may be able to better equilibrate the iron load. If microglia are also assisting neurons by iron uptake into cells, this may signify a neuroprotective effect. Looking at iron levels, both N9 in mono and co-cultures had significant increases in iron expression after 24h activation ($p<0.001$). On the other hand, while N27 mono-culture displayed a significant increase after 24h exposure to MCM (0.4365 ± 0.01, $p<0.001$), N27 cells in co-culture revealed no such increases in intracellular iron expression at the same time point (0.2082 ± 0.01) compared to control (0.212 ± 0.01). Microglia were previously shown to upregulate ferritin gene expression (Section 3.4.2.1, Figure 3.4), thus this elevated microglial iron may represent their iron sequestration away from neurons.

Alternatively, there may be neuronal feedback acting on the microglia in co-cultures, leading to a dampening of the inflammatory effects. Neurons uphold an inhibitory signalling with microglia to regulate their immune response and avoid cytotoxicity (Barclay, 2002).

CD200 produced by neurons can react with microglial CD200 receptors (CD200R), helping to preserve the microglial resting state, thereby reducing their release of inflammatory factors (Wright, 2003). If neurons are co-cultured with microglia, addition of LPS would serve to activate the immune response, however, healthy neuronal presence could potentially attenuate the microglial response. Whilst the co-culture setup here prevents direct interaction between neuronal CD200 and microglial CD200R, soluble neuronal factors have demonstrated the ability to upregulate CD200R expression (Luo, 2010).This could also help account for the dampening of effects observed on changes to neuronal iron regulatory protein gene expression, and the loss of elevated intracellular iron concentrations. It may be of use for future studies to analyse for any changes to pro-inflammatory cytokines within the co-culture medium as compared to MCM, in order to determine if neuronal interaction with microglia is able to influence microglial activation as evidenced by a reduction in microglial release of inflammatory factors. Overall, the amplified levels of neuronal gene expression were not as high upon co-culture incubation, and increased significance commenced at earlier time points, pointing to improved iron distribution and homeostasis. Additionally, N27 cells in co-culture were also spared from increases in intracellular iron. These results infer a protective role of microglia, or microglia-neuron interactions, in regulating iron levels.

It would appear that the presence of microglia somehow spreads out the effects on neuronal IRP mRNA gene expression, causing an earlier observance of significant increases. This must reduce the sudden overload on neuronal cells, allowing them to maintain a more equilibrated environment, which is supported by the fact that neuronal iron levels no longer increase at the 24h time point. If iron regulatory proteins are activated earlier on, perhaps this allows neurons more time to equalise the surplus iron, maintaining cellular iron homeostasis and preventing iron-related toxicity, rather than having to balance a sudden excessive iron influx. Microglia also uptake iron, which is supported by the elevated intracellular iron increases at 24h. If microglia are able to take on excess iron, this would further support neuronal cells, preventing them from acquiring iron from the extracellular space, and thus reducing the sudden onset of iron overload on regulation systems. Evidence from these results support this theory. While N9 cells only show statistically significant increases in intracellular iron at the 24h time point, which are at nearly equal levels for both treatment conditions (mono=0.489 ± 0.02; co=0.485 ± 0.02), results shows that co-culture microglia take up a great deal more iron by the 3h time point, with significantly high levels (0.236 ± 0.02). Thus, it may be inferred that the microglial neuroprotective features become activated under situations of inflammation and high iron. The

cells then begin to take up excess iron to protect neighbouring neurons from iron mediated toxicity. Future work may look at iron levels over more time points to determine whether this increase is consistent up to 24h under co-culture treatment conditions in comparison to the levels within mono-culture cells. Further investigation may also illuminate what initiated the earlier microglial iron uptake only when cells were exposed to neurons.

It has been found that the PD brain presents with excess total SN iron (Dexter, 1991) and many iron-loaded glial cells possibly acting as iron sources (Jellinger, 1990), with studies showing up to a 30% increased microglial iron content during inflammation (Urrutia, 2013). Studies also established suppression of macrophage iron efflux upon conditions of iron loading due to cytokine activation of IRP systems leading to FPN downregulation (Wang, 2013), implying that glial cells are adept at retaining excess free iron. Comparisons between different brain cell types similarly discovered that microglia maintained a superior proficiency at iron accumulation, followed by astrocytes and then neurons (Bishop, 2011). This is supported by the increased capacity for iron uptake observed within these results. Microglial cells were able to take in greater levels of iron from ferric ammonium citrate than neurons, presenting with more than double the amount of intracellular iron at 24h in co-culture (N9= 0.485 ± 0.02; N27= 0.208 ± 0.01). So if glia are acquiring and retaining excess iron in attempts at neuroprotection, this may lead to downstream iron toxicity that may then be released upon microglial cell death to exert effects on neighbouring neurons. Results warrant further knowledge into the mechanisms behind microglial iron uptake in PD models, and its effects on iron metabolism in neurons.

6.6 Conclusions

Results from this chapter infer a neuroprotective role from the presence of microglia in co-culture. Microglia were able to uptake greater concentrations of iron, potentially shielding neurons from the pressure of excess iron overloading. This effect was able to spread out and reduce increases to hepcidin, transferrin receptor and DMT1 mRNA, as well as completely extinguish the previously observed increased intracellular iron within neurons. These outcomes highlight the need for additional investigation into the neuroprotective verses neurotoxic effects of microglia on neurons in times of surplus iron, including the beneficial effects of functioning neuronal-microglial signalling in dampening microglial inflammatory activation, and what goes wrong in PD to inhibit this beneficial effect.

CHAPTER 7:

Inflammatory mediator effects on astrocytes, and astrocytic effects on iron metabolism in dopaminergic neurons after exposure to microglial inflammatory factors

7. Inflammatory mediator effects on astrocytes, and astrocytic effects on iron metabolism in dopaminergic neurons after exposure to microglial inflammatory factors

This chapter first aims to elucidate the effects of microglial inflammatory factors on iron regulation in astrocytes. It was determined that astrocytes, like microglia, appear to have an iron buffering mechanism during inflammation. While astrocytic gene expression of hepcidin, transferrin receptors and DMT1 were upregulated following MCM treatment, unlike neurons, astrocytes also upregulated ferritin storage. Next, the addition of astrocytes to the Transwell co-culture system was performed, in order to create a more realistic model of the intact brain, and to assess whether astrocytes affect previously observed changes to neuronal iron metabolism. Results provided insight into a potentially neuroprotective effect of astrocytes on neuronal iron homeostasis.

7.1 Introduction

Astrocytes are glial cells ubiquitously expressed within the central nervous system. They are involved in both pro-inflammatory and anti-inflammatory activities. While astrocytes may provoke inflammatory responses and neuronal death with actions such as release of cytotoxins or radicals to increase ROS (Liddelow, 2017), they also provide neuronal support (Faulkner, 2004) with a protective framework to contain inflammation via scar formation (Myer, 2006; Renault-Mihara, 2008), regulation of ion and metabolite homeostasis (Simard, 2004), and neuronal provision of neurotrophic factors and antioxidants (Chen, 2001; White, 2008) that can help reduce neuronal oxidative stress (Genis, 2014). Several studies provide evidence for a more neuroprotective capacity, with astrocytes perpetuating neuronal survival, and a disturbance of astroglial functioning resulting in greater neuronal vulnerability to toxicity (Giulian, 1993; Liu, 1999; Suárez-Fernández, 1999). OS is an event associated with the neurodegenerative cascade witnessed in PD, with glial cells acting as significant contributors (Jenner, 1998). Astrocytes become increasingly activated within the PD SN, upregulating neuroprotective activity such as levels of glutathione peroxidase to protect against dopaminergic cell death (Ishida, 2006). H_2O_2 has also been shown to play a substantial role in increasing OS. Results from previous chapters concur with this theory, demonstrating significant effects on iron handling in both neurons and microglia. If H_2O_2 was able to affect changes in other cell types, perhaps it may have an effect on astrocytes as well. Since astrocytes are able to upregulate their antioxidant defence in response to oxidative stress (Röhrdanz, 2001), and significantly detoxify H_2O_2 levels (Dringen, 1998), it has been proposed that astrocytes mediate neuroprotective effects against H_2O_2-stimulated oxidative stress in dopaminergic neurons (Langeveld, 1995). This was investigated here to further the understanding of inflammatory mediator effects on astrocyte iron homeostasis, and the efficacy of astrocytic protection to dopaminergic neurons *in vitro*.

This chapter aims to examine the consequences of the innate microglial immune response and released inflammatory factors on iron handling in astrocytes. First, the astrocyte phenotype was confirmed when cells were tested for expression of glial fibrillary acidic protein (GFAP), a cytoskeletal filament protein utilised in astrocyte identification. Next, the astrocytic response to microglial-released inflammatory factors was assessed *in vitro* by C6 astrocyte cell line exposure to previously optimised microglial conditioned medium. There is already ample evidence of astrocytic reactivity due to inflammatory exposure, including alterations in gene expression (Eddleston, 1993; Urrutia, 2013). This was examined further by enumerating any

changes to astrocytic iron metabolism following microglial inflammatory mediator exposure. Once completed, the consequences of astrocytic incubation with both activated microglia and dopaminergic neurons using an *in vitro* tri-culture model of the Parkinson's milieu was investigated in order to ascertain whether astrocyte presence mitigates deleterious deviations in neuronal iron metabolism due to inflammatory mediators. Since astrocytes express TLR4 receptors and are thus directly susceptible to activation via LPS (Chow, 1999; Bowman, 2003; Blanco, 2005; Gorina, 2011), the design for Transwell cultures was modified accordingly, and microglia were pulse activated with lipopolysaccharide separately, before incubation with astrocytes and dopaminergic neurons.

If glia provide a neuroprotective effect, any changes in astrocyte functioning, coupled with increases in iron and OS can lead to oxidative damage and eventually neuronal death. As astrocyte function has proven to be both neuroprotective and anti-inflammatory, as well as neurotoxic, comprehensive study into their precise mechanism of action under different circumstances remains of crucial importance. Since the specific means of SN neuronal degeneration in Parkinson's remains elusive, the effects of astrocytes cultured with dopaminergic neurons under inflammatory conditions may prove interesting.

7.2 Chapter Objectives

This chapter aims to complete the following objectives:

1. Investigate the effects of microglial inflammatory factors on iron regulatory proteins in the C6 astrocytic cell line.
    a. Corroborate the suitability of the C6 astrocytic cell line.
    b. Determine whether astrocyte exposure to microglial conditioned medium affects cell viability.
    c. Define the effects of astrocyte exposure to inflammatory factors to determine whether microglial inflammatory mediators affect astrocytic iron metabolism, and compare with changes observed in neurons and microglial cells.
        i. Assess IRP mRNA changes after C6 treatment with MCM.
        ii. Assess intracellular iron concentrations after C6 treatment with MCM.

2. Assess the effects of astrocyte presence on neurons.
    a. Confirm microglial activation following a strong 2-hour LPS pulse exposure by assessment of pro-inflammatory cytokines and nitric oxide release.
    b. Evaluate changes to neuronal iron metabolism by establishing a tri-culture system with neurons and astrocytes seeded on inserts. Microglia would be pulse-stimulated, and then the other cell lines added for exposure to inflammatory factors.
        i. Assess IRP mRNA expression in N27 after Transwell co-culture.
        ii. Assess N27 intracellular iron levels after Transwell co-culture.

7.3 Experimental Methods

7.3.1 Determining the Effects of Microglial Conditioned Media on C6 Astrocytic Cell Line

The first directive of this chapter was to investigate the effects of microglial inflammatory factors on astrocytes using the C6 cell line (Section 2.1.5). The initial line of examination was to confirm the C6 cell line suitability for *in vitro* examination into astrocytes. Next, cells were activated by previously determined and optimised MCM (Section 3.4.2) for a range of incubation periods.

In order to confirm the suitability of the C6 cell line as an *in vitro* model to study astrocyte behaviour during a microglial inflammatory reaction, cellular expression of GFAP was confirmed using Western Blot protein determination (Section 2.5.2). C6 cells were seeded in increasing densities from 0.5 to 4 million cells per well in a 6 well plate. Following a 24h rest period, cells were lysed and protein quantified via Western Blots using an anti-GFAP antibody. Both N27 cell lysates and a blank well void of any cells were run in parallel to serve as negative controls devoid of any GFAP protein.

To assess the astrocytic time-course of changes to iron regulatory proteins following microglial activation, cells were seeded (350,000c/w, 6wp) and rested 24h. They were then treated with collected and centrifuged MCM for exposure to microglial inflammatory factors for a range of time points (1-24h). The experimental model below represents cellular treatment conditions (Figure 7.1). After incubation, C6 cells were lysed according to protocols for analysis of IRP gene expression via RT-PCR (Section 2.6) or cellular iron uptake via ferrocene assay (Section 2.4.4). Cell viability assays (Section 2.4.1) Neutral Red, MTS and Bradford were also performed in 96wp (10 x 10^3 c/w) following treatment to ensure that the optimised MCM exposure for the longest time point of 24h did not elicit cytotoxicity within astrocytes.

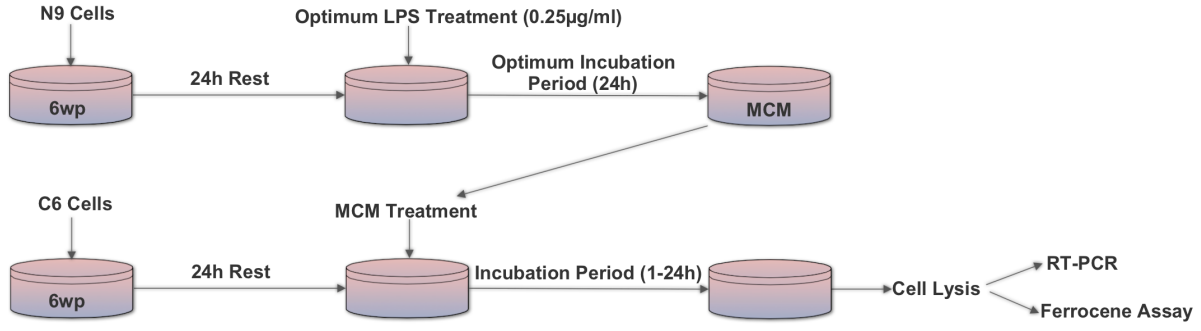

Figure 7.1 Schematic Model Representing C6 Cell Treatment with MCM
Experimental design to investigate the effects of microglial inflammatory factors on astrocyte iron metabolism. N9 cells were plated (350,000c/w) and activated by treatment with the previously determined optimal LPS concentration (0.25µg/ml) for 24h. Following N9 LPS-activation, the MCM supernatant was collected and transferred to established cultures of C6 astrocytes for a range of exposure times (1-24). A vehicle control was also used to treat C6 cells in parallel. Cells were then lysed for analysis via RT-PCR or ferrocene assay. *Abbreviations: 6wp= 6 well plate, h=hours, LPS= lipopolysaccharide, MCM= microglial conditioned medium.*

7.3.2 Examining whether an Astrocytic Presence Modifies the Effects of Inflammatory Factors from Activated Microglia on Neuronal Iron Metabolism

Next, the addition of astrocytes to neuronal and microglial co-cultures was performed to determine if they affect any alterations in neuronal iron metabolism. Since astrocytes are directly susceptible to LPS activation, the design for Transwell cultures was modified accordingly. First, N9 cells were seeded (300,000c/w, 6wp) and rested overnight. Meanwhile, Transwell inserts were turned upside down to cautiously seed C6 cells (125,000c/w) onto the underside of the insert's permeable membrane. After a 3h period of cell adhesion, inserts were gently flipped upright into a 6 well plate with complete RPMI. N27 cells were then seeded into the top of the insert (200,000c/w) for adherence to the opposite side of the permeable membrane. After 24h rest, N9 microglia were pulse activated using a higher dosage of LPS (0.5µg/ml) for a 2-hour exposure period. Cells were washed gently to remove any residual LPS in order to ensure C6 were not LPS-activated. Next, Transwell inserts containing rested and established N27 and C6 cultures on opposing sides of the semi-permeable membrane, were transferred into wells containing the pulse-activated N9 cells for a range of incubation times (Figure 7.2). N27 cells were then collected and measured for changes to IRP gene expression. Results were then compared to those previously collected.

Since previous data determined that the optimum time point for microglial activation after incubation with LPS was for a period of 24 hours, it must also be confirmed that a 2h pulse activation was sufficient to induce an inflammatory response. To measure microglial activation, N9 cells were seeded in 6wp, rested 24h, and then treated for two hours with a higher concentration of LPS (0.5µg/ml). Following incubation, supernatant was collected and analysed for release of pro-inflammatory factors via the Griess assay (NO) or via ELISA (IL1ß, IL6 and TNF).

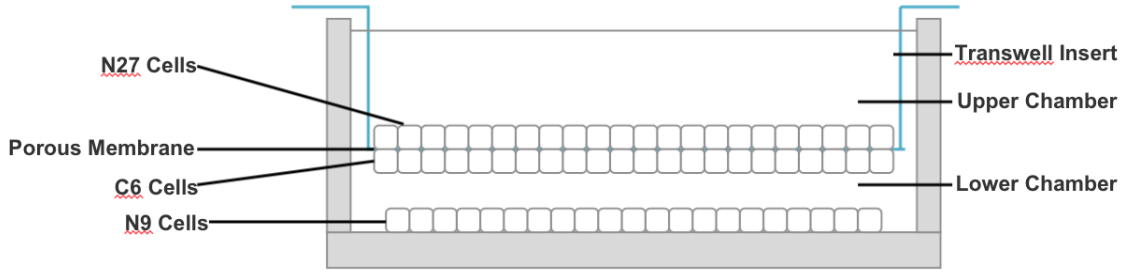

Figure 7.2 Experimental Schematic Representing Tri-Culture Transwell Conditions
N9 cells were established in separate wells (300,000c/w). Meanwhile, C6 cells (125,000c/w) were seeded on upside-down Transwell inserts, to grow on the underside of the permeable membrane. After a 3h cell adherence period, inserts were turned right-side up into new 6wp containing complete RPMI. N27 cells (200,000c/w) were then cultured into the insert's upper chamber. After a 24h resting period, microglia were pulse activated with 0.5µg/ml LPS for 2 hours. Cells were gently washed in warmed complete medium to remove LPS traces, and then Transwell inserts containing N27 and C6 were gently transferred on top of activated N9 cultures for a range of incubation periods.

7.3.3 Statistical Analysis

Experiments run in 6wp were executed three separate times, whereby means were calculated. All data represents mean ± standard error mean. Data for determination of the effects of inflammation on astrocytes, including RT-PCR and ferrocene assays, was analysed by 1-way analysis of variance, utilising, respectively, either Dunnett's or Bonferroni's Multiple Comparison post-hoc test to equate each dataset to the control. Cellular viability analyses were also completed utilising 1-way ANOVA with Dunnett's post-hoc test. ELISA results were first examined using regression analysis on a polynomial line of best fit to calculate sample protein concentrations. All statistical analyses were performed on the Prism 5 MAC OS X GraphPad Software, and a p value <0.05 was considered as statistically significant.

7.4 Results

7.4.1 Confirming GFAP Protein Expression in C6 Astrocytic Cells

Firstly, since GFAP is an astrocytic protein, expression levels are used as an indicator of astrocytic presence. To confirm the astrocytic phenotype of the C6 cell culture line, GFAP levels were measured in increasing densities of C6 cells using Western Blot immunoblotting. If C6 represent the astrocytic phenotype, they should thus express the GFAP astrocytic marker. Extrapolating from this, the more C6 cells, then the more GFAP protein. Hence, it was postulated that increasing quantities of astrocytic cells should also increase measured levels of GFAP. This was confirmed by Western Blot results, demonstrating no GFAP immunoreactivity in negative controls (blank and N27 cells), but a significant linearly increasing trend with C6 cells (R^2= 0.867, p<0.0001) (Figure 7.3).

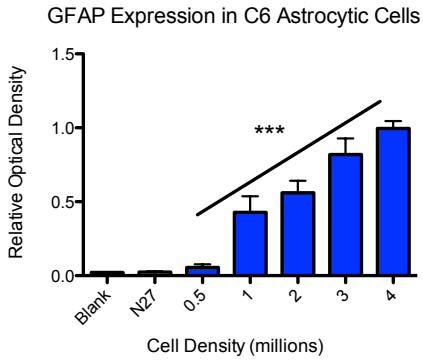

Figure 7.3 Confirmation of GFAP Protein Expression in C6 Astrocytes and N27 Dopaminergic Neurons as Determined by Western Blot Analysis. Increasing cell densities of C6 astrocytic cells and N27 dopaminergic neurons (2 x 10^6 c/w) were plated, and measured for GFAP protein expression via Western Blot analysis in order to confirm a corresponding elevated protein expression along with cell density. A blank well was run in parallel. Results demonstrated a significantly increasing trend of GFAP protein directly proportional to increasing levels of C6 cell densities, as measured via Western Blot. As expected, no immunoreactivity was observed within either two negative controls, including a blank well or N27 neuronal cells. Results imply that since GFAP is an astrocytic-associated protein, then increasing GFAP expression with increasing C6 cell density signifies that the cells are indeed astrocytic. Bars represent mean ± SEM from densitometry analysis of individual experiments. *Statistical significance is denoted by asterisks: ***p<0.001. n=3.*

7.4.2 Effects of Microglial Conditioned Medium on Astrocytic Cells

7.4.2.1 C6 Astrocytic Cell Viability after MCM exposure

Three viability tests, MTS, NR and Bradford assays, were employed to determine whether C6 astrocyte incubation with the optimised MCM dosage, containing inflammatory factors released by activated microglia, affected cellular viability. Results failed to ascertain any significant cellular toxicity as a consequence of MCM treatment in any of the three assays (Figure 7.4). Thus, study with C6 exposure was continued, utilising the optimally deduced MCM dosage.

7.4.2.2 Alterations to Astrocytic Iron Regulation following C6 Cell Treatment with MCM

Upon determining that the applied dosage of MCM for 24h did not result in any loss of C6 cellular viability, cells were then treated for a range of time periods (1-24h), and lysates were collected for analysis of gene expression (Figure 7.5). Analysis detected significant increases as compared to control in four of the seven tested iron regulatory proteins. Hepcidin increased at 18h (1.716 ± 0.2), while transferrin receptors displayed increased levels at both 18h (1.603 ± 0.09) and 24h (1.893 ± 0.16). DMT1 demonstrated even more substantial increases at 18h (2.362 ± 0.2) and 24h (3.631 ± 0.2). Unlike neurons, C6 cells also presented with sizably amplified ferritin expression at 18h (1.887 ± 0.16). The remaining three iron regulatory proteins (FPN, Aconitase1, IREb2) demonstrated no significant change from control at any of the measured time points (data not shown). Iron uptake was then determined via the ferrocene assay (Figure 7.6). Results demonstrate an increasing trend as compared to control beginning at 6h. Statistical significance was reached only at the 24h time point (0.409 ± 0.01, compared to control 0.248 ± 0.01, $p<0.001$).

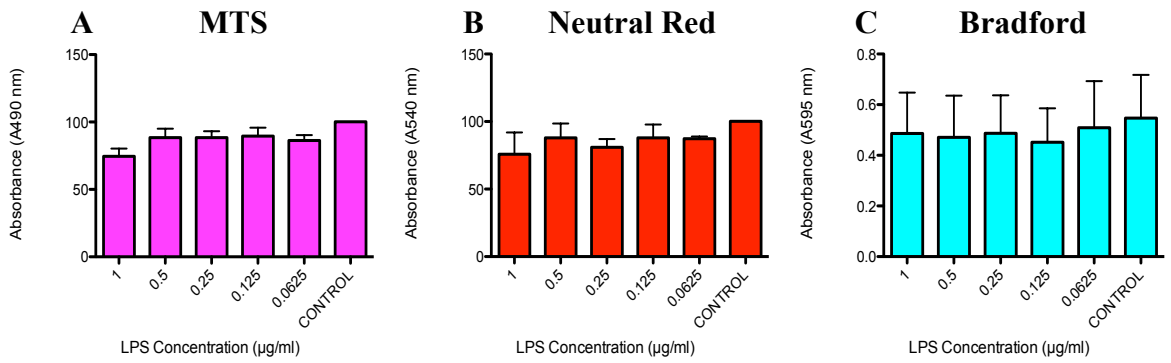

Figure 7.4 Astrocytic Cell Viability following MCM Treatment
C6 cells were seeded (350,000c/w), rested (24h), and then treated (24h) with microglial conditioned medium prepared via 24h exposure to a range of LPS concentrations (0.0625-1µg/ml) or vehicle control. C6 cells were then analysed for any detectable changes to cellular viability using three assays: MTS (A), Neutral Red (B) and Bradford (C). The dose responses demonstrated no statistically significant toxicity to astrocytes following MCM treatment. This indicates that an MCM in the middle range of 0.25µg/ml, as is the defined optimal LPS concentration, has no significant cytotoxic effect on astrocytic C6 cells. Thus, it may be applied for all subsequent experiments with C6 cells. Graphs represent mean ± SEM. *n=3.*

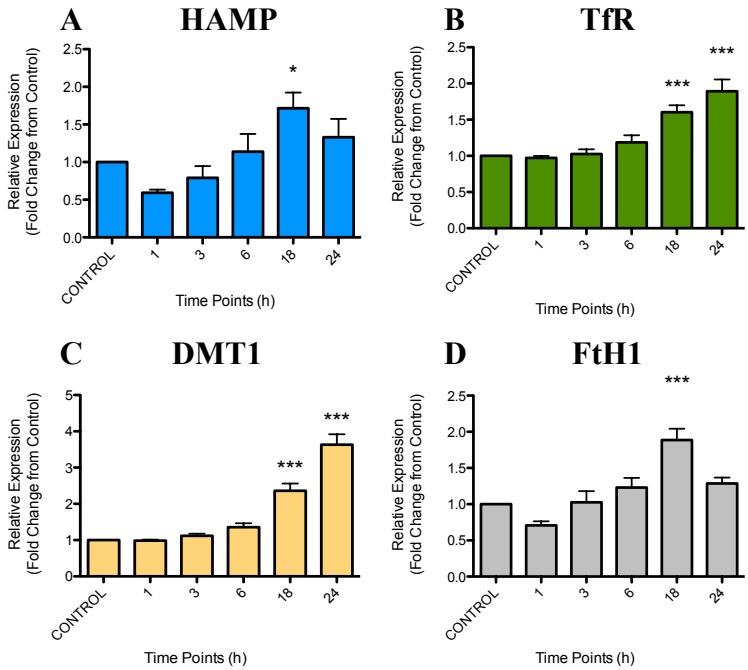

Figure 7.5 Changes in Relative Gene Expression of IRPs in C6 Astrocytic Cells following MCM Treatment
C6 cells were seeded (350,000c/w), rested (24h), and then treated with optimised microglial conditioned medium (prepared by N9 microglial treatment with 0.25µg/ml LPS or vehicle control for 24h) for a range of time periods (1-24h). Lysates were then collected and processed for analysis of relative gene expression via qRT-PCR for several key iron regulatory proteins: HAMP (A), TfR (B), DMT1 (C), FtH1 (D) (data for FPN, Aco1, IREb2 not shown). Data was normalised using a ßactin housekeeping gene. Only the proteins demonstrating a significant change in gene expression when compared to control are displayed here. Significant increases in expression were observed from 18h in HAMP, TfR, DMT1 and FtH1, when compared to control. This infers that activated microglial-released factors are able to induce changes to astrocytic iron regulation. It also appears that astrocytes, like microglia, have a cytoprotective mechanism of ferritin iron storage upregulation to protect against iron-mediated toxicity, which dopaminergic neurons do not appear to have. Graphs represent mean ± SEM. *Statistical significance is denoted by asterisks: *p<0.05, **p<0.01, ***p<0.001. n=3.*

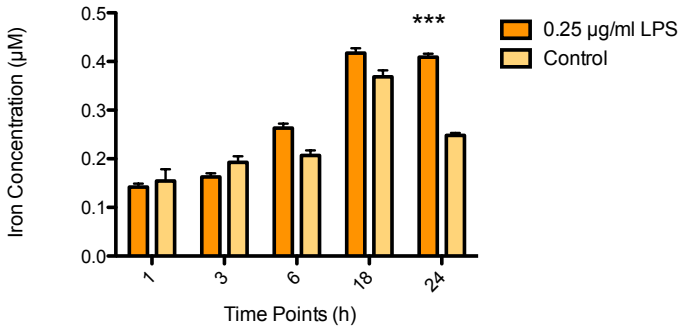

Figure 7.6 Intracellular Iron Expression as Assessed by the Ferrocene Assay in C6 Astrocytic Cells following MCM Treatment. C6 astrocytic cells were seeded (350,000c/w), rested (24h), and then treated with MCM (prepared by microglial activation by 0.25µg/ml LPS or vehicle control for 24h) for various time points (1-24h). Following incubation, cells were lysed and iron expression determined via the ferrocene assay. Results demonstrate an increasing trend beginning at 6h, however, statistical significance compared to control was only determined at 24h. This signifies the effects of microglial inflammatory factors on inducing significant changes to iron homeostatic mechanisms in astrocytes. Graphs represent mean ± SEM. *Statistical significance is denoted by asterisks: ***p<0.001. n=3.*

7.4.3 Effects of Astrocytic Presence on Neurons Exposed to MCM

7.4.3.1 Validation of Microglial Activation after 2h Pulse LPS Activation

To ensure the 2h pulse exposure to 0.5µg/ml LPS was sufficient to activate microglia for Transwell tri-culture, the release of pro-inflammatory mediators into culture supernatant was investigated (Figure 7.7 A-D). Analysis of ELISA results determined a significant increase verses control in IL1ß (0.266 ± 0.04 vs 0.081 ± 0.01), IL6 (6.254 ± 0.61 vs 3.323 ± 0.38) and TNF (0.961 ± 0.02 vs 0.307 ± 0.05) at 24h. While measurements from the Griess assay also displayed increased levels of nitric oxide at 24h (11.25 ± 0.19 vs control 6.178 ± 0.002). Thus, it can be deduced that a stronger LPS dosage (0.5µg/ml) for a 2h pulse exposure was sufficient to elicit an inflammatory response in microglial cells.

7.4.3.2 Transwell Tri-Culture System

A Transwell Tri-Culture experimental system was setup using neurons, astrocytes and microglia cultured within the same wells. This model was designed in order to establish any fluctuations in observed effects on neuronal iron metabolism when co-cultured with different glial cells. Results concluded that neurons failed to exhibit any increased expression compared to control in any of the IRPs measured, including in those that had previously demonstrated increased expression (Figure 7.8). Where previous N27 hepcidin expression after MCM treatment reached levels up to 1.771 at 3h, here it was 0.834 ± 0.07. TfR at 24h was similar to control (0.986 ± 0.07), while DMT1 was slightly increased from control (1.31 ± 0.17) but was not attributed any significance. FPN, however, demonstrated a marginally significant decrease

at 24h (0.479 ± 0.06) (Figure 7.8B). This was also a significant decrease from previous expression, which maintained levels near control in both N27 treated with MCM and N27 with N9 in co-culture (respectively, 0.947 and 1.03).

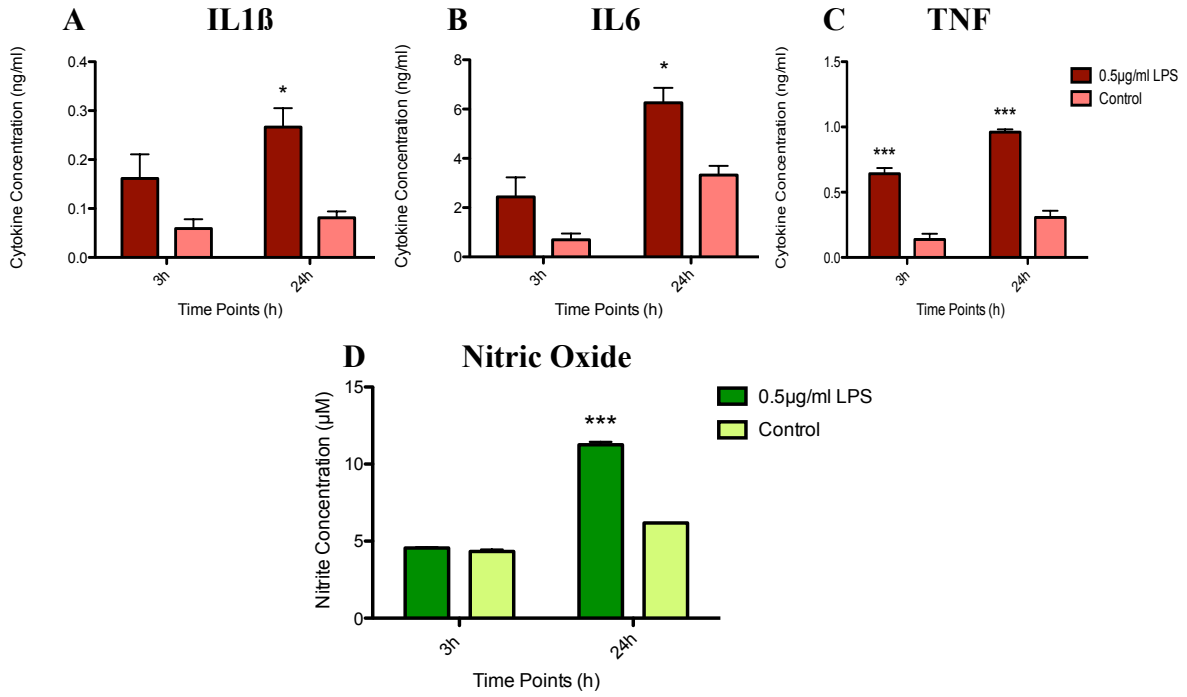

Figure 7.7 Confirmation of Sufficient Microglial Activation with a 2-hour LPS Pulse as Measured by ELISA and Griess Assays. Microglial N9 cells were seeded (350,000c/w), rested (24h), and then treated with the higher LPS dosage of 0.5µg/ml or vehicle control for a 2-hour period in order to determine if the pulse activation was sufficient to elicit an inflammatory response and microglial release of inflammatory mediators, for use in the tri-culture Transwell system. After the 2h incubation, cells were gently washed twice in warmed complete medium to remove all traces of LPS, and fresh complete medium added. Cells were left for either 3h or 24h, whereupon supernatant was collected and analysed via ELISA (IL1ß, IL6, TNF) or Griess assay (NO). Results for IL1ß (A), IL6 (B), TNF (C), and nitric oxide (D) provide sufficient evidence that the 2h pulse was adequate enough to stimulate microglia into emitting significant levels of pro-inflammatory mediators into the supernatant at the 24h time point for all measured conditions, and for both 3h and 24h in TNF. This confirms that a 2h pulse was sufficient for utilisation in the tri-culture experimental design. Bars represent mean ± SEM. *Statistical significance is denoted by asterisks: *p<0.05, ***p<0.001. n=3, each run in triplicate. Abbreviations: NO=nitric oxide.*

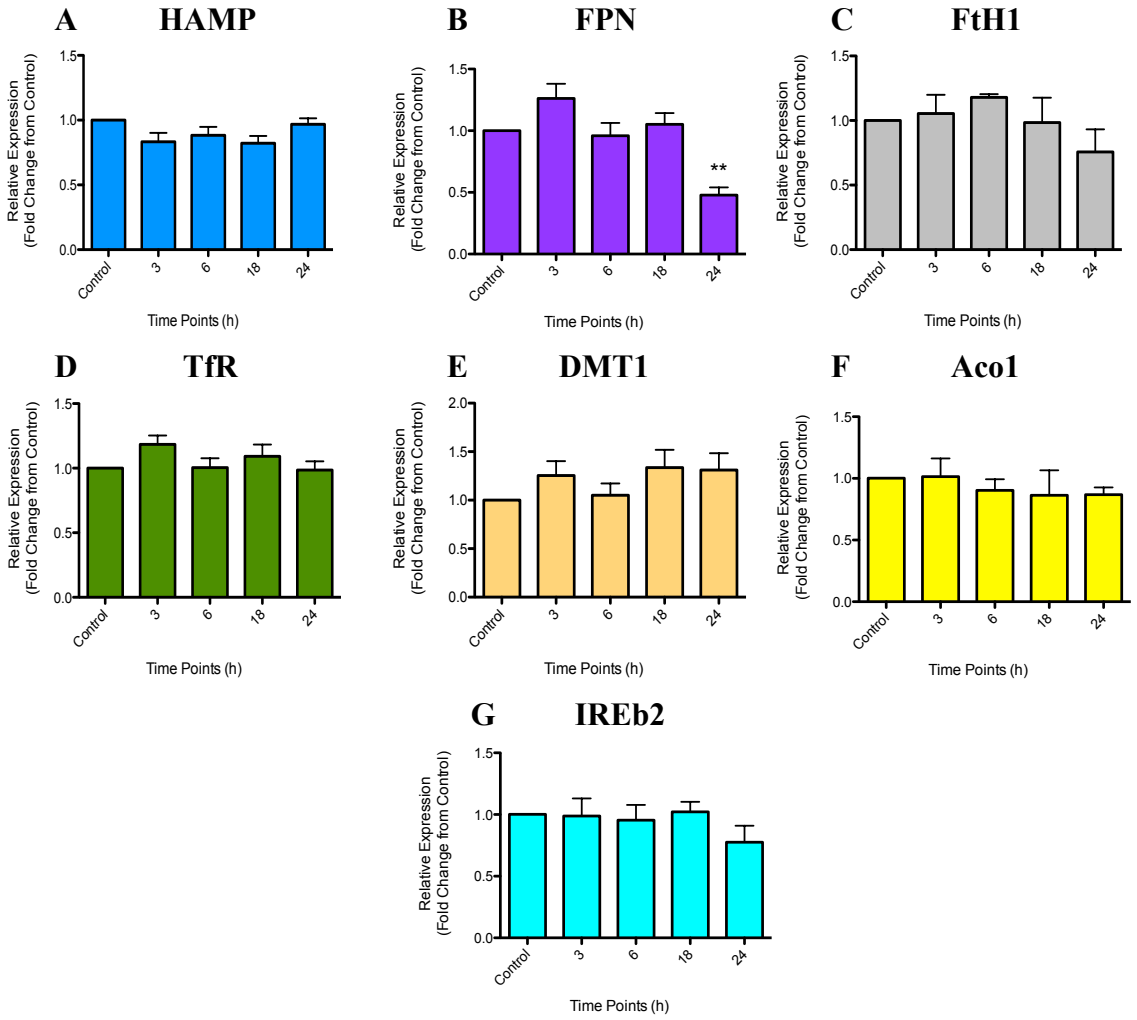

Figure 7.8 Relative Gene Expression in N27 Dopaminergic Neurons after Tri-Culture Transwell Incubation with Astrocytes and Microglia. A tri-culture system was designed to develop the previous co-culture system of microglia and dopaminergic neurons, in order to determine the effects of added astrocyte presence on neuronal iron metabolism. N27 neurons (200,000c/w) and C6 astrocytes (125,000c/w) were seeded onto opposing sides of a semi-permeable membrane. N9 microglial cells (300,000c/w) seeded at the bottom of plate wells were separately pulse-activated with 0.5µg/ml LPS or vehicle control for 2h. After this incubation period, wells were carefully washed twice with warmed complete medium to remove any residual traces of LPS. Immediately afterwards, Transwell inserts containing the established N27 and C6 cells were carefully inserted into the microglial wells for a range of time points. N27 cells were then collected, processed and analysed to detect any changes to gene expression via qRT-PCR for all of the previously measured iron regulatory proteins (HAMP=A, FPN=B, FtH1=C, TfR=D, DMT1= E, Aco1=F, IREb2=G). Results failed to detect any of the previously viewed increases in IRP expression. Unlike previous examinations, FPN demonstrated diminished expression at 24h in tri-culture. These results suggests that addition of astrocytes to Transwell cultures has provided a neuroprotective effect, preventing dysregulation of neuronal iron regulatory proteins as previously observed. Graphs represent mean ± SEM. *n=3.*

7.5 Discussion

This chapter has provided insight into both the effects of microglial inflammatory factors on astrocytes, as well as the effects of astrocytes on neuronal iron metabolism. It has been previously determined here that microglial-induced inflammation stimulates changes to iron regulatory proteins in dopaminergic neurons. It was then discovered that iron metabolism in astrocytes was also affected by inflammatory factors, and that astrocyte presence appears to mitigate these changes in neurons. It can thus be deduced that astrocytes provide a neuroprotective effect, which could help alleviate the burden of iron overload observed during Parkinsonian pathogenesis.

Inflammatory mediators released from activated microglia were able to elicit changes to astrocytic iron homeostasis. Once cell viability was proved to not be affected by MCM treatment, astrocytes were measured for any changes to cellular iron after exposure to microglial pro-inflammatory factors. Results display substantial changes similar to what was previously viewed in both neurons and microglia. There were significant increases in TfR and DMT1 at both 18h and 24h. In comparison, N9s displayed increases only at 18h, and N27 only at 24h. The astrocyte expression of TfR at 18h was almost exactly that seen in N9 cells (respectively, 1.603 ± 0.097 and 1.601 ± 0.12), while expression in N27s was only slightly greater (2.019 ± 0.28). This ascertains that inflammatory exposure causes a similar increase of transferrin receptor gene expression for all three cell types. TfR can be post-transcriptionally regulated by the IRP/IRE system, which stabilises mRNA during situations of low intracellular iron. Since greater TfR expression occurs at times when iron levels are beginning to rise or already are at significantly higher levels, it implies a secondary source. IRP activity may also be modulated by hypoxia (Lok, 1999; Tacchini 1999) and H_2O_2 (Pantopoulos, 1995), while TfR can also be transcriptionally regulated by cytokines (Fahmy, 1993; Seiser, 1993). Microglia have already proven to secrete significant levels of H_2O_2 which directly affect neuronal iron metabolism, and there is a correlation between increased hypoxia, oxidative stress, and inflammation (Snyder, 2017). So it is possible that increased TfR expression may be a result of inflammatory secretion of H_2O_2, consistent with previously determined results, which leads to amplified oxidative stress. Next, prior investigation into hepcidin expression determined a significant increase in both microglia and neurons after 3 hours. While N9s demonstrated the greatest HAMP increases, almost double that of neurons, astrocytes presented with similar increases to neurons, but at 18h instead. Astrocytic hepcidin induction may be triggered by increased iron levels, which occurs at the later time points, as opposed to from oxidative stress.

Considering DMT1, both microglia and astrocytes displayed greater increases than N27s. This implies that both cell types seem to increase expression of DMT1 at a faster rate than neurons, and beginning at earlier time points. This may be seen as a neuroprotective effect, in an attempt to sequester any excess iron to prevent neuronal overload with its toxic consequences. It has been previously determined that DMT1 expression is amplified in the PD SN, as well as in PD animal models (Salazar, 2008; He, 2011), which may lead to intracellular iron accumulation, and in turn, increased OS resulting in dopaminergic neuronal death. If DMT1 expression is increased mostly in glial cells, then excess extracellular iron may be sequestered away from neurons as much as possible, thus providing neuronal protection. Glial DMT1 can uptake both Tf iron, as well as non-transferrin bound iron (NTBI) (Garrick, 1999), while neuronal DMT1 has been specifically implicated in the demise of PD dopaminergic neurons (Salazar, 2008). If inflammatory mediators increase DMT1 expression levels in all three cell types, but more so in glia, it may represent a defence mechanism that is eventually outweighed by other factors such as excess iron, inflammation, and OS, with decreased antioxidant abilities and changes to iron handling.

Another neuroprotective mechanism in astrocytes may result from their generation of ferritin mRNA following MCM incubation for 18h. This trait was similarly witnessed in stimulated microglia at 18h, however failed to transpire in neuronal cells. Since ferritin is an iron storage molecule, its induction would help sequester astrocytic labile iron to minimise its toxic actions. It would appear that both glial cells have superior defence mechanisms in place compared to neurons. These may have implications for neuroprotection if astrocytes and microglia are sequestering excess extracellular iron in an attempt to maintain their own viability, or perhaps aid in protecting neuronal viability.

This conjecture was supported by results from Transwell tri-culturing of all three cell types. When in mono or co-culture and exposed to microglial inflammatory factors, neurons exhibited variations to relative gene expression of their iron regulatory proteins HAMP, TfR, and DMT1. Such variations would lead to escalations of intracellular iron, since hepcidin prevents iron egress, while both transferrin receptors and DMT1 would transport more iron into cells. This was confirmed by increases in intracellular iron expression following a 24h incubation period. However, the tri-culture results demonstrated no such changes. There were no increased levels of neuronal expression in any of the 7 measured iron regulatory proteins. A conclusion may be drawn from these results, insinuating a significant neuroprotective role of astrocytes on neuronal iron regulation, as astrocytes are capable of utilising a protective mechanism to diffuse excess iron and help clear the extracellular environment. Studies have determined that

astrocytes do indeed have a neuroprotective effect, with increased astrocytic resistance to iron toxicity (Kress, 2002), and a role in detoxifying the cellular environment from excess iron by buffering via DMT1 NTBI uptake (Pelizzoni, 2013). Since astrocytes proved to have significant increases in DMT1, with higher and longer expression than microglial cells, this may be attributed to their role in taking up excess iron as a protective mechanism shielding neighbouring neurons from iron-mediated oxidative stress. Studies concur with this, showing neuron and astrocyte co-cultures resulted in amplified antioxidant activity (Oide, 2006), with co-culture neurons more resistant to the effects of H_2O_2 (Desagher, 1996; Iwata-Ichikawa, 1999). This may be due to an upregulated antioxidant defence along with glial provision of glutathione to neurons which supports neuronal H_2O_2 detoxification (Sagara, 1993; Langeveld, 1995). Astrocyte co-cultures have proven to aid in diffusing the neurotoxicity of H_2O_2 on neurons via antioxidant actions of both glutathione peroxidase and catalase (Desagher, 1996), which correlates to neuroprotective results obtained in this thesis. Future work may include measurement of H_2O_2 concentrations within tri-culture media, for comparison with MCM levels to determine whether astrocytes do indeed exert beneficial antioxidant effects on neurons. Additionally, astrocytes provide neighbouring neurons with enough cysteine and glutathione precursors to instigate amplified neuronal glutathione levels (Dringen, 1999).

Only one variation was observed here that was not present in either N27 + MCM, or N27 co-culture data. This was the reduction of neuronal ferroportin gene expression at 24h. Ferroportin is an iron exporter, regulated by hepcidin or ceruloplasmin. Ferroportin is internalised and degraded with increased hepcidin (Rouault, 2006), or loss of ceruloplasmin ferroxidase activity increases extracellular ferrous iron, which then prevents ferroportin iron release and its degradation (Jeong, 2003). As hepcidin gene expression was not altered here, it does not support the assumption that elevations in hepcidin would degrade and reduce ferroportin levels. While the addition of astrocytes may help regulate neuronal iron homeostasis, it is possible that they are inducing a decrease in ceruloplasmin functioning. Significant ceruloplasmin diminutions, with corresponding reduction to their ferroxidase activity, have been observed in the PD SN (Tórsdóttie, 1999; Bharucha, 2008; Jin, 2011; Ayton, 2013). A potential cause for this observed difference may be the activated microglial generation of H_2O_2, which has proven to directly cause loss of ceruloplasmin ferroxidase activity (Olivieri, 2011). So an explanatory scenario could perhaps begin with activated microglia. They release iron following LPS activation as a result of their upregulated ferroportin gene expression at 18h (Figure 3.4), causing elevations to extracellular ferrous iron. This excess iron is possibly taken up by neuroprotective astrocytes, which exhibit increased

iron sequestration from upregulated HAMP, TfR and DMT1 expression (Figure 7.5), along with a protective buffering increase in storage molecule H-chain ferritin gene expression. Additionally, microglial production of H_2O_2 could impede neuronal ceruloplasmin ferroxidase activity (Olivieri, 2011), while there may be an additional factor released by astrocytes to prevent the extracellular ferrous iron from being oxidised in order to prevent ferric iron from binding to transferrin for neuronal entry. This increase in extracellular ferrous iron would then induce the observed reduction in neuronal ferroportin. In conjunction with glial scavenging of excess iron and free radicals, results presented here provide further evidence of the neuroprotective effects of astrocytes on neuronal iron metabolism.

The use of astrocytes therefore signifies a noteworthy prospect for further exploration of their protective mechanisms in iron and H_2O_2-induced OS *in vitro* and *in vivo*. Future investigations may also comprise determination of astrocytic iron expression following co-culture and tri-culture in order to ascertain whether their iron levels increase at a faster rate than in mono-culture as a result of neuronal protection. It may also be of interest to discover any possible attenuation of disrupted neuronal iron handling due to direct H_2O_2 exposure in an astrocyte co-culture system.

7.6 Conclusions

Results from this chapter ascertained a significant effect from culturing astrocytes with neurons on neuronal iron metabolism. Astrocytes also demonstrated an iron buffering mechanism by upregulating ferritin storage during exposure to inflammatory microglial mediators. Such a mechanism was similarly observed in microglia, but not in neurons, inferring that glial cells potentially have greater proficiency at iron handling compared to neurons. Conversely, neurons appear to lack such protective mechanisms, leaving them more susceptible to iron-mediated toxicity. If astroglial activity can be regulated with medication, to help maintain their neuroprotective properties, this insinuates a potential target for further investigation into protective therapies against Parkinson's neurodegeneration.

CHAPTER 8:

Discerning Downstream Consequences of Iron Metabolism Changes in Dopaminergic Neurons

8. Discerning downstream consequences of iron metabolism changes in dopaminergic neurons

This chapter examines the downstream effects of altered neuronal iron regulation by exposing dopaminergic neurons to inflammatory factors in microglial conditioned medium, and then analysing fluctuations in oxidative stress, mitochondrial membrane potential and cellular apoptosis and necrosis. Results displayed increased oxidative stress and both early and late apoptosis, as well as a significant loss of mitochondrial membrane potential. This indicates that dysregulated neuronal iron can instigate detrimental effects on the viability of dopaminergic neurons, potentially leading to neurodegeneration.

8.1 Introduction

Dopaminergic neurons have demonstrated alterations in iron handling as a result of exposure to inflammatory mediators. While PD presents with elevated levels of nigral iron, and various cellular vicissitudes leading to neurodegeneration of dopaminergic neurons in the SN, it remains to be determined whether the augmented iron directly effects cellular pathways leading to altered downstream cellular viability. In order to determine the consequences of raised cellular iron in eliciting neurodegenerative pathways, three factors were considered: oxidative stress, mitochondrial membrane potential, and apoptosis or necrosis.

The PD SN has presented with significantly increased levels of iron (Dexter, 1987; Dexter, 1989; Oakley, 2007), as well as being rich in dopamine, whose enzymatic and nonenzymatic formation results in H_2O_2 formation, with an increased PD dopamine turnover due to loss of dopaminergic neurons (Cohen, 1988; Fahn, 1992). While crucial for physiological cellular functioning, excess labile iron can prove neurotoxic. One such mechanism stems from Fenton chemistry, whereby labile iron reacts with oxidative species H_2O_2 to generate the reactive hydroxyl free radical. A greater pro-oxidant environment creates a feedback loop to further cultivate radical formation, so that enhanced ROS eventually leads to situations of oxidative stress (OS). OS can then disassemble the cytosolic aconitase iron-sulphur cluster via simultaneously elevated NO and H_2O_2, allowing for increased IRP1 binding activity (Pantopoulos, 1996; Pantopoulos, 1997; Caltagirone, 2001) thereby further promoting cellular iron increases. H_2O_2 exposure also diminishes ferritin synthesis and causes increases in TfR mRNA (Bresgen, 2015), which corresponds to results in previous chapters. Superoxide is also able to release iron from aconitase (Brand, 2004), potentiating IRP1 binding, and can mobilise iron from ferritin stores (Biemond, 1984; Yoshida, 1995), thereby increasing labile iron pools. Increasing levels and imbalanced iron homeostasis would result in further free radicals and ROS production. Coupled with the decreased antioxidant capacity of PD dopaminergic neurons (Riederer, 1989), this creates a perfectly synchronised pro-oxidant environment of cumulative iron, providing strong evidence for a link between changes in iron metabolism and OS.

Mitochondrial function is likewise disturbed in PD, potentially leading to neurodegeneration from excess ROS, debilitated energy production, and eventually mitochondria-activated apoptosis via cytochrome c translocation (Kluck, 1997). The respiratory electron transport chain is a major site of ROS production, with its first component Complex I (CI) identified as key in ATP synthesis and establishment of the mitochondrial membrane potential (MMP), as well as in free radical generation. Functional mitochondria

maintain a MMP gradient across their inner membrane from proton pumping respiratory chains, however, several factors including disruptions to ATP supply and oxidative insults can lead to a deteriorating MMP (Keller, 1998; Gottlieb, 2003). Persistent MMP decline will eventually result in apoptosis initiation via release of the cytochrome c component of the respiratory chain, subsequent to matrix condensation (Gottlieb, 2003). Additionally, CI has a role in regulating the mitochondrial permeability transition pore (PTP) (Greenamyre, 2001). Pathological cellular environments can result in opening of this pore, a potential indication of imminent apoptosis. Studies in Parkinson's patients have deduced an inhibited CI activity within nigral cells (Schapira, 1990), while parkinsonian symptoms emerge following exposure to the toxin 1-methyl-4-1,2,3,6-tetrahydropyridine (MPTP), whose metabolite enters dopaminergic neuron mitochondria and disrupts CI function (Nicklas, 1987). Such defects can negatively affect cellular functioning via diminished ATP production, mitochondrial depolarisation and excess ROS. The correlation of CI defects to parkinsonian symptoms implies a significant influence between diminished mitochondrial function and MMP, with its ensuing augmented ROS, on dopaminergic neuronal death. If the membrane potential is affected by dysregulated iron handling, which is exacerbated by ROS, this can have ruinous downstream consequences associated to PD neuronal death.

Since mitochondria represent a target during situations of excess iron, further insight into how changes in cellular iron homeostasis may affect their functioning is crucial. MMP may be altered via oxidative species, for example when superoxide generated from Complexes I and III can be dismutated in the presence of ferrous iron and superoxide dismutase (Fe^{2+}-SOD) to generate H_2O_2 (Martilla, 1988). Similarly, CI defects as seen in PD can result in electron leakage which would cause a significant escalation in H_2O_2 production (Hensley, 1998). Berman (1999) presented evidence that the H_2O_2 produced from monoamine oxidase-catalysed oxidation of dopamine inhibited active mitochondrial respiration, specifically in complexes I-III. This proves a circling effect of ROS and peroxide production on declining mitochondrial functioning. Since increased H_2O_2 can react with ferrous iron, dysregulated iron levels may cause further decline in mitochondrial health, leading to cellular apoptosis. An *in vitro* PD model treated cells with MPP+, known to inhibit mitochondrial CI activity, and found no direct effect of MPP+ on mitochondrial membrane potential (Zhang, 2009). However, treated cells also incubated in ferrous iron demonstrated a substantial MMP diminution, suggesting the explicit involvement of iron on mitochondrial function. MPP+ treatment also results in increased ROS production, which would follow CI dysfunction, however another study outcome presented augmented ferrous iron from a corresponding increased expression of

DMT1 (Zhang, 2009). Amplified presence of ferrous iron may also stem from mobilisation of ferritin stores by superoxide (Biemond, 1984). It was also found that H_2O_2 was able to increase iron signalling by TfR-mediated uptake (Dhanasekaran, 2004). Effective mitochondrial functioning is crucial for cellular viability, with the delicate balance tipped towards apoptotic death when the augmented presence of reactive iron coupled with inflammatory H_2O_2 and ROS production disrupt CI activity and maintenance of MMP or permeability transition.

Apoptosis and necrosis are two forms of cellular death, with the former being a precisely organised caspase-mediated dismantling of cells, while the latter results from inadvertently uncontrolled death from inflammation and distresses to the cellular environment (Fink, 2005). Dysregulated iron homeostasis and increased iron levels can potentiate toxicity during an already stressed cellular environment by facilitating creation of reactive oxidative species, OS and changes to the mitochondrial membrane potential and permeability transition as mentioned above. Persistent changes can potentially lead to either form of cell death. Both varieties are measurable by detection of certain cellular alterations. Phosphatidylserine (PS), a phospholipid cell membrane component, is maintained on the inner cytoplasmic surface during physiological conditions. PS externalisation to the outer surface along with maintained membrane integrity marks an early apoptotic occurrence, whereby it can thus be detected for determination of early apoptosis (van Engeland, 1998). In order to differentiate between apoptotic and necrotic cells, the membrane-impermeant dye propidium iodide (PI) can also be applied for double-labelled analysis by flow cytometry. Since apoptotic cells maintain an intact membrane, PI can only permeate necrotic cells, thus permitting the distinctive quantification between the various types of cell death (Fink, 2005).

To promote comprehension of the properties of altered iron handling on cellular changes that may trigger neuronal death, this chapter aims to examine downstream consequences of increased iron in an *in vitro* PD model investigation using N27 dopaminergic cells exposed to inflammatory factors from microglial conditioned medium. OS was measured in live cells, and mitochondrial membrane potential, apoptosis and necrosis were measured using fluorescent probes.

8.2 Chapter Objectives

This chapter aims to complete the following objectives:

1. Investigate the downstream effects of altered iron metabolism in dopaminergic neurons, using the N27 cell line treated with MCM.
    a. Determine whether there are any alterations in oxidative stress.
    b. Establish any changes to the mitochondrial membrane potential.
    c. Ascertain whether altered iron metabolism leads to increases in apoptosis or necrosis in dopaminergic neurons.

8.3 Experimental Methods

8.3.1 Investigating the Downstream Effects of Altered Iron Metabolism in N27 Dopaminergic Neurons

In order to determine if the microglial inflammatory factor mediated changes in iron handling resulted in long-term alterations of dopaminergic neuron cellular pathways, three different experiments were performed to analyse levels of oxidant stress, mitochondrial membrane potential and two forms of cell death. Experimental measures involved usage of fluorescent microscopy and flow cytometry to measure the downstream effects of increased iron after both 24 and 48 exposure periods.

8.3.1.1 Oxidative Stress

CellRox Deep Red Reagent, a fluorogenic probe, was utilised to analyse levels of oxidative species within fixed cells. N27 cells were seeded (350,000c/w, 6wp) and rested 24h, followed by treatment with microglial conditioned medium for a 24h and 48h exposure (Section 2.3.1.3). At which point ThermoFisher CellRox reagent was directly pipetted onto live cells at a concentration of 5µM for 30m under cellular incubation conditions, as per the manufacturer's protocols (Section 2.8.1). This allowed sufficient time for the probe to permeate cells, whereby the non-fluorescent reduced state reagent localised within the cytoplasm. Greater presence of oxidants leads to greater reagent oxidation, resulting in a fluorescent product. Thus the fluorescence is directly proportional to the amount of oxidants, reflecting a quantification of cellular oxidative stress. Following incubation, medium was fully aspirated, cells were washed three time with PBS, and fixed with 3.7% PFA for 15m. A positive control of oxidative stress was run in parallel, where cells were treated with 15µM 6-OHDA. Plates were then analysed using a Nikon TS fluorescent microscope, using MicroManager software.

8.3.1.2 Mitochondrial Membrane Potential

MitoTracker (MT) Red, a fluorogenic cell permeant probe, was employed to measure cellular MMP (Section 2.8.2). The non-fluorescent reduced probe diffuses through the plasma membrane, where oxidation results in a fluorescent reagent capable of accumulating specifically within viable mitochondria as a result of their active membrane potential. If there was a decline in MMP, the extent of mitochondrial reagent accumulation would diminish. Since greater mitochondrial fluorescence represents optimum MMP activity, and vice versa, this method provides a quantifiable representative of mitochondrial membrane potential within live cells.

N27 cells were seeded onto coverslips in 6wp, rested 24h, and then incubated with MCM for either 24 or 48h. 100nM of freshly prepared MitoTracker Red probe in DMSO and serum-free medium was warmed to 37ºC. Cells were fully aspirated, washed in warmed serum-free RPMI, and treated with the MT probe for 25m. The stain was then aspirated from wells and washed with warmed serum-free RPMI. This was aspirated and replaced by warmed 4% PFA for 15m fixation. Wells were then rinsed twice in PBS, and analysed using the fluorescence microscope (Nikon TS), with excitation/emission at 579/599. Image analyses was performed using ImageJ.

8.3.1.3 Apoptosis and Necrosis

The dead cell apoptosis Invitrogen kit including Annexin V Alexa Fluor 488 and PI was utilised according to the manufacturer's protocol (Section 2.8.3). The Alexa Fluor dye is conjugated to Annexin V, which binds PS with high affinity. Since PS is translocated to the external membrane surface only during apoptosis, it thus provides access for fluorophore labelling of PS only in apoptotic cells, thus allowing for their effective quantification. The membrane-impermeant dye propidium iodide is only able to permeate dead cells, as apoptotic ones maintain their membrane potential. Once inside, PI binds nucleic acids to emit a red fluorescence, distinguishing between 4 different cellular populations: live cells, early apoptosis, late apoptosis, and necrosis. The first would present with low fluorescence, early apoptotic cells would show green fluorescence from Annexin V binding of PS, late apoptotic cells would demonstrate both membrane staining and PI nuclear staining, while necrotic cells should only present red nuclear staining.

N27 cells were seeded (350,000c/w, 6wp), rested 24h and treated with microglial conditioned medium as per usual. A negative control was run in parallel without MCM treatment, while an apoptotic positive control was treated with 1μM staurosporine. Cell media was fully aspirated, and washed twice with warmed PBS. Cells were scraped and collected using complete RPMI. Eppendorfs were centrifuged (200g, 5m), and the media carefully aspirated to isolate the cell pellet. Pellets were resuspended in prepared 1x annexin-binding buffer. Subsequently, cell density was calculated, and cells diluted to ~1 x 10^6 cells/ml. Staurosporine positive control samples were either unstained, or stained with Annexin V alone, PI alone, or Annexin V + PI. These samples were utilised to create the four gate settings on the flow cytometry software, representing each of the 4 cellular populations to be measured. Equally diluted sample cell suspensions were added to fresh eppendorfs, and double stained with Annexin V and 100μg/ml PI. All eppendorf tubes were incubated in the dark at room temperature for 15m, followed by

further dilution in annexin-binding buffer. Stained cells were placed on ice and immediately analysed via flow cytometry, with fluorescence emission at 530-575nm.

8.3.2 Statistical Analysis

Results obtained from the fluorescent microscope represent averaged data from 9 random fields per well taken for each run, with a minimum of 3 runs per sample condition. Results were normalised against the background. Results presented here represent the mean ± SEM of this data. One-way ANOVA with Bonferroni's multiple comparisons post-hoc test were utilised for analysis of all three experiments, to determine significance between MCM treated conditions verses control. All statistical analyses were accomplished employing GraphPad Prism 5 for Mac OS X software.

8.4 Results

8.4.1 Observing the Downstream Effects of Altered Iron Metabolism on Various Cellular Pathways

8.4.1.1 Examining Effects of Altered Iron Metabolism on Neuronal Oxidative Stress

Oxidative stress was measured in N27 dopaminergic neurons following exposure to inflammatory factors via treatment with microglial conditioned medium for the longer time periods of 24h and 48h (Figure 8.1). At the first time point, there was a statistically significant increase in fluorescence due to greater oxidative species when compared to control (0.173 ± 0.04 vs control 0.014 ± 0.003, $p<0.05$). 48h exposure resulted in an increased oxidative stress within control cells, however the treated cells demonstrated an even higher, statistically significant increase (0.273 ± 0.02 vs control 0.193 ± 0.01, $p<0.01$).

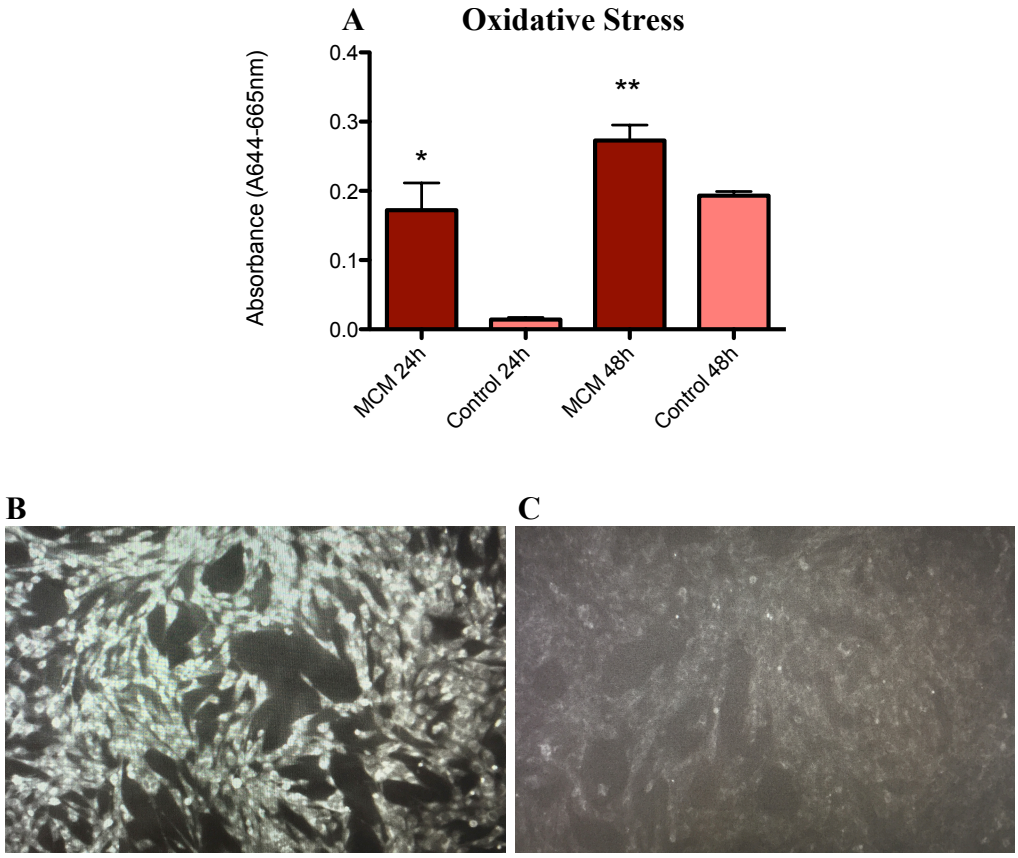

Figure 8.1 Oxidative Stress Observed in N27 Neurons after Exposure to Microglial Inflammatory Factors in MCM. N27 cells were seeded (350,000c/w), rested (24h), and treated with microglial conditioned medium or vehicle control for 24h and 48h, whereupon cells were treated with fluorescent probe CellRox Red (5µM) and incubated for 30m for cell permeation with the probe. A positive control for OS was run in parallel, where cells were treated with 15µM 6-OHDA. Cells were then fixed with 3.7% PFA for 15m. Wells were then analysed for changes to oxidative stress using a fluorescent microscope. The non-fluorescent reduced probe is oxidised into fluorescence according to the number of oxidants present within the cellular cytoplasm. Thus, the greater the number of oxidative species, with the enhanced cellular burden indicative of oxidative stress, then the greater the fluorescent signal. Results (A) demonstrate statistically significant increases of OS in MCM-treated dopaminergic neurons as compared to control. Bars represent mean ± SEM. Fluorescent microscope representative example images (10x magnification) display significantly greater fluorescence in 48h MCM-treated cells (B) as compared to control (C). *Statistical significance is denoted by asterisks: *p<0.05, **p<0.01. n=3, with mean taken from 9 random fields taken per well.*

8.4.1.2 Examining Downstream Changes of Altered Iron Metabolism on Neuronal Mitochondrial Membrane Potential

Altered iron handling effects on dopaminergic neuron mitochondrial health were measured by observing changes to membrane potential using the fluorescing MitoTracker Red probe (Figure 8.2). The reagent is only able to label healthy mitochondria, as passive diffusion into mitochondria depends on functionality of the membrane potential. The dye is retained even after loss of membrane potential during aldehyde fixation due to thiol-binding within mitochondria to produce a permanently-bound conjugate. Thus, a decrease of signal would signify a deficiency in mitochondrial potential. 24h demonstrated a statistically significant difference ($p<0.001$) between the MMP in MCM-treated cells (0.086 ± 0.001) compared to control (0.094 ± 0.002). 48h showed an increase in both treated (0.167 ± 0.0003) and untreated cells (0.174 ± 0.001), while the significant difference between the two conditions remained ($p<0.001$).

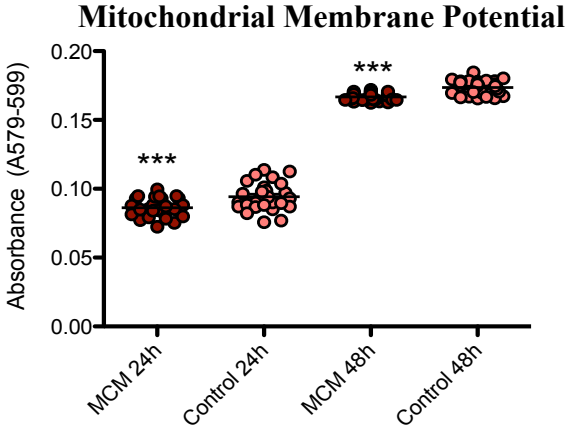

Figure 8.2 Changes to Mitochondrial Membrane Potential Detected after N27 Neuron Exposure to MCM N27 cells were seeded (350,000c/w), rested (24h), and treated with microglial conditioned medium or vehicle control for 24h and 48h, whereupon cells were treated with warmed 100nM fluorescent probe MitoTracker Red (25m) to measure changes to mitochondrial membrane potential. The non-fluorescent mitochondrion-selective probe enters the cell, where it passively diffuses into mitochondria, and is oxidised to fluorescence. The probe also binds to thiol groups within mitochondria to prevent a loss of signal from washing during aldehyde fixation. The probe fluoresces according to the degree of healthy membrane potential. Thus, the greater the fluorescence, the greater the MT accumulation within mitochondria, which implies a healthy functional mitochondrial membrane potential. A decrease in fluorescence would signify a corresponding decrease in reagent accumulation within mitochondria, and thus a loss of mitochondrial membrane potential. After incubation, the stain was then washed off with warmed medium, to remove any dye not held within mitochondria. Cells were then fixed with 4% PFA for 15m, and rinsed in PBS for analysis on a fluorescent microscope with excitation/emission at 579/599. Results demonstrate statistically significant fluorescent decreases in MCM-treated dopaminergic neurons as compared to control at both 24h and 48h. This implies a loss of mitochondrial membrane potential in treated cells, meaning MCM treatment inflicts changes to MMP. Points represent results of 9 random fields taken per well, normalised to the background. *Statistical significance is denoted by asterisks: ***p<0.001. n=3.*

8.4.1.3 Investigating Effects of Altered Iron Metabolism on Neuronal Apoptosis and Necrosis

The downstream effects of dysregulated iron leading to either regulated or uncontrolled cell death can be measured using the fluorescent Alexa Fluor Annexin V and propidium iodide flow cytometry protocol. Upon initiation of cellular apoptosis, phosphatidylserine translocates for exposure on the outer cellular surface, thus tagging the cell for apoptotic degradation. Annexin V has a strong affinity for PS, thus cellular treatment with Annexin V can label PS with a fluorophore to quantify the number of cells tagged for apoptosis. Higher Annexin V fluorescence represents a larger number of cells expressing PS, and thus more undergoing apoptosis. PI can only permeate dead cells, allowing for measurement of necrotic cells. Greater PI detection denotes higher levels of necrotic cells. Results indicate no significant changes between treated and control cell suspensions in apoptosis or necrosis at the 24h time point (Figure 8.3A), however, 48h (Figure 8.3B) presents with a statistically significant increase in late apoptosis (62.24 ± 1.01, $p<0.001$) compared to control (54.65 ± 1.02), as well as a decrease in early apoptosis (20.84 ± 0.96, $p<0.001$) compared to control (25.27 ± 0.75). It also appears that while live and necrotic cells were present at 24h, both had severe declines in expression by 48h. At 24h, treated cells presented slightly lower expression of live cells (35.88 ± 1.86) compared to control (37.19 ± 2.77), which was consistent at 48h albeit it at much lower expression (1.803 ± 0.22 vs control 3.289 ± 0.41).

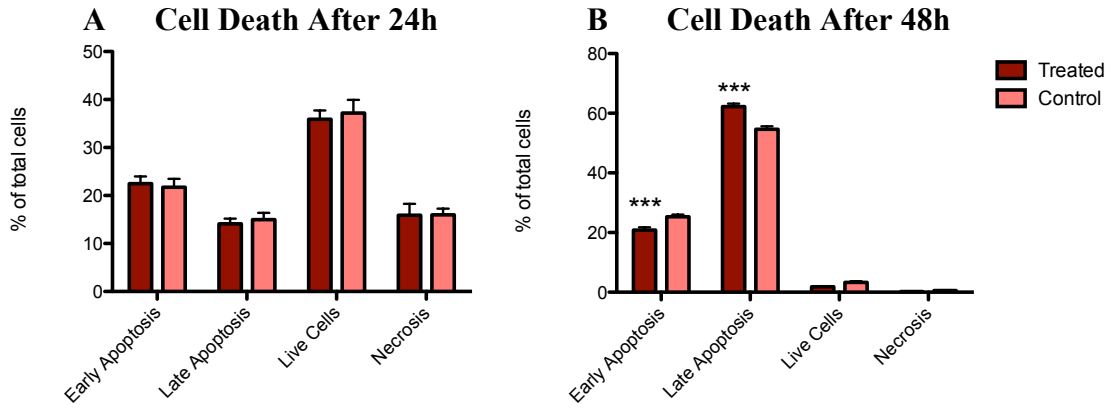

Figure 8.3 Alterations to Cell Death Mechanisms Detected in N27 Neurons after MCM Treatment
N27 cells were seeded (350,000c/w), rested (24h), and treated with microglial conditioned medium or vehicle control for 24h (A) and 48h (B), whereupon various stages of cell death were measured via flow cytometry using the fluorescent probes Alexa Fluor and PI. A negative control was run in parallel without MCM treatment, and a positive control for apoptosis was run with cells treated with 1µM staurosporine. Alexa Fluor is conjugated to Annexin V, which binds PS, thus greater Alexa Fluor fluorescence signifies more cells labelled for apoptosis with PS expression on their outer surface. PI is a membrane-impermeant dye only able to permeate dead cells without membrane potentials, whereupon they bind nucleic acids and emit fluorescence. Increased PI fluorescence thus implies a loss of membrane integrity indicative of necrotic cells. After incubation, cells were washed twice in PBS, scraped, collected in complete medium into eppendorfs, and pelleted by centrifugation (200g, 5m). Pellets were resuspended to appropriate dilutions and double stained with Annexin V and 100µg/ml PI. Cells were incubated in the dark 15m, and analysed via flow cytometry with fluorescence emission at 530-575nm. Live cells have low fluorescence, early apoptotic cells exhibit Annexin V binding, late apoptotic cells demonstrate both Annexin V membrane binding and PI nuclear staining, and necrotic cells only present PI staining. Results do not display any significant changes at the 24h MCM exposure period, however do exhibit a statistically significant increase in fluorescence for late apoptosis and reduced early apoptosis in MCM-treated dopaminergic neurons as compared to control at 48h. This signifies that MCM-mediated inflammation is causing an increase in dopaminergic neuron apoptosis. Graphs represent mean ± SEM. *Statistical significance is denoted by asterisks: ***p<0.001. n=3.*

8.5 Discussion

This chapter elucidates the effects of altered iron handling in dopaminergic neurons following exposure to microglial inflammatory factors on their downstream pathways leading to cell death. Previous chapters have provided results displaying cellular changes leading to variations in iron regulatory proteins, and eventually to increased levels of iron expression in N27 cells. Such consequences provide insight into potential causes for increased levels of iron observed within the PD SN. What remained to be determined was whether the perceived iron dysregulation led to initiation of further cellular pathways that could ultimately lead to degeneration of dopaminergic neurons. Analyses presented here provide substantiation that microglial inflammatory factors mediating altered neuronal iron homeostasis can indeed lead to augmented levels of oxidative stress, diminished mitochondrial membrane potential and eventual initiation of apoptosis. In depth interpretation and association of these outcomes with published data may aid comprehension of downstream neuronal pathways during a stressed internal environment resulting from altered iron regulation.

Beginning with oxidative stress, a 24h incubation presented with little change in control, but a slight increase in MCM treated cells. This is likely due to cells having sufficient space and nutrients to withstand the pressures of inflammatory factors. By the 48h incubation period, both control and treated cells saw increases in OS. MCM treated neurons presented significantly greater levels of OS compared to control, although the higher levels within control cells may be attributed to the overpopulation and reduced nutrient presence. It is possible that future experiments may aspirate and change growth medium after the 24h time point, however, the excess serum and nutrients may only serve to further overpopulate wells, adding excess strain to cells. Results may be confirmed using primary neuronal cultures to avoid such replication issues. The excess OS observed here within treated cells at both time points implies that altered iron metabolism within neurons ultimately leads to a strain on cellular antioxidant capacity.

Dopaminergic neurons are more vulnerable to the effects of excess ROS, especially in situations of dopaminergic cell death as in PD. While PD SN neurons have already proven to contain high levels of excess iron, these cells also present with greater production of H_2O_2 from both intracellular enzymatic oxidative dopamine degradation from dead neurons, and from a compensatory increase in dopamine production (Jenner, 1998). Evidence provided within this study, as well as others substantiates the direct H_2O_2 toxicity on neurons and neuronal iron metabolism (Mello Filho, 1984; Desagher, 1996). Intracellular levels of reactive labile iron

may be controlled by inactivated storage into ferritin (Harrison, 1996), however, not only has the PD brain shown to lack increased levels of ferritin (Faucheux, 2002), but superoxide and reducing radicals have been proven to maintain the capacity for iron mobilisation out of ferritin stores (Biemond, 1984; Monteiro, 1989), while H_2O_2 treatment has led to diminished ferritin expression (Dev, 2015). H_2O_2 and nitric oxide can even disassemble aconitase iron-sulphur clusters, leading to increased IRP1 binding activity, greater TfR regulation, and amplified iron influx (Pantopoulos, 1996; Pantopoulos, 1997; Caltagirone, 2001). The Dev (2015) study also proved downstream augmented levels of neuronal labile iron pool following direct H_2O_2 treatment due to changes in IRE-IRP binding activity. PD brains provide further evidence of OS damage from reduced glutathione peroxidase, catalase and GSH levels specifically within the SN, leaving it even more vulnerable to H_2O_2 toxicity (Ambani, 1975; Kish, 1985; Sofic, 1992). If PD systems are already deficient in antioxidant supply, coupled with excess reactive oxidant species and H_2O_2 production, and dysregulated iron metabolism leading to increased labile iron pools within the SN, it seems inevitable that they will eventually sustain significant oxidative damage.

Alterations to the mitochondrial membrane potential are indicative markers of impaired mitochondrial function, that may occur along with increased membrane permeability as a sign of early apoptosis (Zhang, 2009). Treatment of the dopaminergic cell line with microglial inflammatory factors shown to alter iron levels resulted in significantly decreased MMP at both measured time points as compared to control. Interestingly, it would be expected that by 48h the MMP would have decreased even further than at 24h. However, results here determined an almost doubled level of expression at 48h in both treated and control cells, which could be a consequence of cell growth. The 48h wells would have a significantly greater number of cells present, which would contribute to a higher fluorescent signal. This data draws an association between increased iron expression and changes to mitochondrial function. Mitochondria supply vital cellular energy, however are also the greatest source of oxidative species due to continued ROS production during aerobic metabolism. Impaired mitochondrial function could have ruinous consequences, with persistent decline leading to initiation of cellular apoptosis. CI of the electron transport chain helps establish the MMP and facilitate ATP synthesis, however, it is additionally an important site of free radical generation. Disrupted CI function, as seen in PD, with subsequent electron leakage contributes to H_2O_2 production (Hensley, 1998; Berman, 1999), H_2O_2 disruption of iron regulation via upregulated TfR and DMT1 (Dhanasekaran, 2004; Zhang, 2009), and superoxide-mediated iron reduction facilitating release from ferritin stores (Biemond, 1984). Thus, augmented iron expression and altered

levels of iron regulatory proteins could have an effect on mitochondrial activity, succeeded by unrestrained ROS production. Oxidative species such as H_2O_2 are capable of reacting with labile iron to self-perpetuate even greater ROS levels. Such high levels surpass cellular detoxification mechanisms, and if antioxidant function is already decreased, as seen in PD, this could cause mitochondrial activation of apoptotic processes leading to demise of dopaminergic neurons.

Finally, analysis of apoptotic and necrotic cell expression following inflammatory exposure offered further proof of the altered iron handling contribution to downstream neurodegeneration. Previous results demonstrated variations to OS and MMP at 24h, yet only the longer incubation time period of 48h exhibited statistically significant changes to cell death as compared to control. This may signify that 24h may not be a sufficient time frame to allow such changes to surpass cellular protective detoxification mechanisms. Analysing the data for apoptosis, it can be seen that 24h only demonstrates slight increases in late apoptosis for both treated and control conditions, however this expression significantly increases by 48h. Control maintained a higher number of early apoptotic cells, with lower levels of late apoptotic cells at 48h compared to treated cells, most likely due to maintenance of antioxidant protective mechanisms and less disruption to iron regulation. Conversely, treated cells demonstrated a decreased number of early apoptotic cells and a statistically significant increase in late apoptotic cells, indicating that the majority had transitioned to the later stage of cell death by this time point, while the control cells were slower in reaching the late apoptotic stage. Considering live cells, control conditions result in greater expression compared to treatment conditions at both time points, which is to be expected, although differences were not statistically significant. However, the numbers at 48h for both treatment conditions plummeted to very low levels, denoting a loss of viable cells. This may pertain to both the earlier presence of necrosis and apoptosis, as well as a total of 72h being a long time within 6 well plates. Once cell replication overpopulates the wells, nutrients become in short supply and excess cellular debris can affect viability. Perhaps future experimental replications can include study of primary neuronal cultures to avoid this issue. Initially, 24h results revealed the occurrence of necrotic cells, however, necrotic expression was almost entirely eliminated by 48h. This indicates that there may be a sudden initial cellular stress resulting in uncontrolled necrosis at 24h, although a longer incubation period allows the cells to reach a point of systemic stress and initiation of controlled cellular demise.

There is great debate as to defining mechanisms behind dopaminergic cell death in PD, with the specific cause as yet unknown. Narrowing the field to iron toxicity nonetheless

provides ample therapeutic potential. Reflecting on the literature of this topic, it can be observed that ROS, OS, and excess iron are all implicated in perpetuating neurodegeneration in Parkinson's (Hirsch, 2000; Liu, 2002), with neuronal death propagated directly by microglial-mediated H_2O_2 (Théry, 1991; Behl, 1994). Since the SN presents with higher iron concentrations than other brain areas (Sofic, 1988; Youdim, 1989; Sofic, 1991), these dopaminergic neurons are at greater risk of iron-induced OS and the resultant neuronal death. The PD SN also shows evidence of ferroptosis, which is typified by reduced GPX4 activity (Dixon, 2012). This hydroperoxidase helps scavenge H_2O_2 (Yang, 2016), so loss of function would add to cytotoxic H_2O_2 accumulation. Concomitant superoxide and H_2O_2 from surplus ROS generation may participate in Fenton chemistry under situations when excess labile iron is free to participate in redox reactions. This contributes to hydroxyl radical formation, and initiation of neurodegenerative cascades. If this remains true, then disruption of any part of this chain by controlling superfluous iron or oxidative species should result in curative features. Various iron chelator studies have established the neuroprotective potential of subduing excessive iron accretion, positively confirming that iron dysregulation may be culpable in nigrostriatal pathology occasioning dopaminergic neurodegeneration (Ben-Shachar, 1991; Ben-Shachar, 2004; Jian, 2006). Impaired systemic functioning from iron-overload was reversed with chelator treatment, supporting their neuroprotective potential. Antioxidant studies also provide evidence of neuroprotection and mitigating inflammatory cascades via inhibition of oxidant-induced degeneration (Bastianetto, 2000; Levites, 2002; Testa, 2005; Louboutin, 2010). Notably, most major PD models manipulate the oxidative environment via CI inhibitors (Rotenone, MPTP), disruption of mitochondrial respiration (6-OHDA) or microglial activation by inflammatory response initiators (LPS, 6-OHDA), to selectively devastate dopaminergic neuron populations, induce parkinsonian symptoms and mimic parkinsonian pathology (Sherer, 2002; Testa, 2005; Rodriguez-Pallares, 2007). This highlights a prominent role for maintenance of the cycle comprising oxidative species, mitochondrial performance, and iron regulation. More thorough understanding of such mechanisms can have great implications for facilitating control of unregulated processes leading to dopaminergic neurodegeneration as witnessed within the parkinsonian SN. This can, in turn, provide a therapeutic prospective to preserve iron regulation, thus preventing the onset of prolonged oxidative stress and consequential self-perpetuating neuronal loss.

8.6 Conclusions

Results from this study established significant downstream effects in dopaminergic neurons exposed to microglial inflammatory factors, in an *in vitro* PD model. The inflammatory factors were able to induce changes to iron regulation within neurons, instigating substantial increases in cellular iron. When these neurons were then measured for longer term effects on cellular mechanisms that may lead to cell death, it was observed that such changes led to increases in oxidative stress, defects in mitochondrial membrane potential, and amplified levels of late apoptotic cells. Such findings emphasise the importance of maintaining iron homeostasis to avoid instigating downstream pathways that ultimately lead to death of dopaminergic neurons.

CHAPTER 9:

General Discussion

9. General Discussion

9.1 Overview of Principal Findings

The Parkinson's brain is characterised by a significant dopamine depletion as a result of degeneration of dopaminergic nigrostriatal neurons. Present therapies aim to reverse dopamine loss by providing secondary access to the neurotransmitter in the form of the precursor levodopa. However, this serves merely as a symptomatic therapy, failing to address the cause or attenuate neurodegenerative mechanisms. Furthermore, levodopa administration has actually been proven to exacerbate neuronal oxidative stress via hydrogen peroxide production (Nutt, 1984), as well as causing significantly diminished Complex I activity, specifically observed within the striatum and substantia nigra following chronic levodopa administration to rats (Przedborski, 1993). Coupled with inevitable development of incapacitating levodopa-generated dyskinesias, there remains great necessity for development of more effective neuroprotective strategies.

This thesis examines the hypothesis that microglial inflammatory factors could produce alterations in cellular iron handling, which in turn, may alter downstream pathways instigating the cascade towards neuronal demise, as observed in PD. Several objectives were set at the project commencement, with the subsequent aim to pursue them as an addendum to existing knowledge on inflammation and changes in iron metabolism during parkinsonian pathogenesis. These objectives include:

1. Profile the time course of inflammatory factors released by activated microglia, and investigate these inflammatory factor effects on iron regulation in microglia, astrocytes, and dopaminergic neurons, with the intent of detecting if any differences between cell types may account for greater neuronal vulnerability in PD.
2. Evaluate which of these microglial inflammatory mediators may be responsible for initiating changes in iron regulation observed in dopaminergic neurons, with the aim of detecting and/or eliminating potential targets as effectors of iron dyshomeostasis.
3. Determine any disparities in neuronal iron metabolism following transient versus continued exposure to microglial inflammatory factors, with the aim of confirming previous *in vitro* results by conducting them under more realistic conditions.
4. Examine the effects of supplementary astrocyte presence on iron regulation in dopaminergic neurons following exposure to microglial inflammatory factors, with the intention of ascertaining whether astrocytes provide a neuroprotective effect.

5. Discern whether inflammation-induced changes to neuronal iron metabolism initiate cellular death pathways, with the intention of elucidating potential neurotoxic properties of iron overload to provide a more rational target for novel PD therapeutic agents.

Results from this investigation first showed that inflammatory factors from activated microglia caused alterations in iron regulation leading to augmented iron expression in all three examined cell types, microglia, astrocytes, and dopaminergic neurons. All three cell lines exhibited upregulation of gene expression in key iron regulatory proteins, including hepcidin, transferrin receptors and DMT1, subsequent to inflammatory exposure. Interestingly, glial cells also presented evidence of iron buffering mechanisms by upregulated levels of ferritin storage molecules, while microglia additionally expressed augmented iron exporter ferroportin levels. This disparity between neuronal and glial iron regulation highlights neuronal vulnerability to iron dysregulation with a potential glial neuroprotective effect.

Next, it was hypothesised that microglial-released pro-inflammatory cytokines may be responsible for instigating the observed changes in neuronal iron regulation. Results shown here determined that while some of these inflammatory cytokines managed to trigger slight upregulation of hepcidin mRNA and intracellular iron, direct cytokine treatment failed to generate the significant changes previously observed with microglial conditioned medium treatment. This realisation led to the discovery that hydrogen peroxide could reproduce the changes in iron metabolism.

Thirdly, co-culture experiments exposed dopaminergic neurons to a continuous supply of microglial inflammatory factors in order to mimic more realistic conditions and create a better model of the PD brain. This data displayed similar results to previous experiments with monoculture neuronal exposure to inflammatory factors, albeit with a few differences. Most notably, while still presenting a significant upregulation, the additional presence of microglial cells attenuated the previously observed neuronal hepcidin mRNA increases. Upregulation of TfR and DMT1 were also initiated at earlier time points than with neurons alone. This greater dispersal of altered iron regulation appears to have reduced neuronal stress allowing for improved regulatory capabilities.

Fourthly, addition of astrocytes to the co-culture milieu resulted in complete reversal of any previously observed changes in neuronal iron. This inhibition of iron upregulation suggests a significant neuroprotective effect of astrocytes by mitigating the inflammatory effects on neuronal iron regulation.

Lastly, it was determined that persistent neuronal exposure to microglial inflammatory factors initiated downstream cellular signalling leading to cell death. Neuronal inflammation precipitated an escalation of cellular oxidative stress, and diminished mitochondrial functioning via diminution of the mitochondrial membrane potential. A combination of altered iron regulation, increased iron expression, augmented cellular oxidative species surpassing cellular detoxification and disturbed energy production, ultimately resulted in instigation of apoptosis. There was no evidence of necrosis at the later stages, implying that neuronal death was initiated solely by apoptotic mechanisms.

Collectively, this data emphasises the significance of disruption to iron metabolism on cellular physiology. Recurrent exposure to toxic mediators and the resultant iron upregulation may be somewhat mitigated by neighbouring glia, specifically astrocytes. However, inflammatory conditions, such as in PD, may result in astrogliosis which could potentially result in loss of astrocytic neuroprotection and iron buffering capacity. Once neuroprotective mechanisms have been surpassed by the inflammatory feedback loop, perpetuating excessive intracellular labile iron with decreased mitochondrial functioning and formation of oxidative species, neurons are inevitably labelled for apoptotic degeneration. The information presented here emphasises the need to break this propagating terminal cycle, and identifies potential targets to enhance neuroprotection in PD.

9.2 Implications of Findings

Initial studies detected significant effects of inflammation on iron regulation in microglia, astrocytes and neurons, with substantial differences between cell types. It is known that populations of nigral dopaminergic neurons are exceedingly vulnerable to oxidative stress, with vulnerabilities exacerbated in the PD brain. Data presented here suggest a possible reason for this may be excessive exposure to a specific array of microglial-released factors that are cumulatively responsible for neuronal degeneration. The production and biodegradation of dopamine exclusively exposes these neuronal populations to high levels of hydrogen peroxide. When accompanied by defects in mitochondrial proton pumping complexes as seen in PD, the mitochondrial dysfunction leads to superoxide production, which is then dismutated to H_2O_2. This is normally removed by GSH, however, the PD substantia nigra demonstrates reduced GSH levels (Riederer, 1989), resulting in higher H_2O_2 presence specifically within dopaminergic neurons. Continuously produced H_2O_2 may exceed available antioxidant levels, resulting in dangerously high concentrations. It was demonstrated here that these peroxides are proficient at directly altering expression of neuronal iron regulatory proteins affecting the overall intracellular iron concentration. Iron overload has been shown in neurons within the PD SNpc, and excessive iron has proven neurotoxic by association with oxidative damage. Chelation therapies have supported this theory by demonstrating mildly protective effects in PD models and clinical trials (Youdim, 2004; Devos, 2014). Additionally, glial cells appear to express iron buffering mechanisms lacking in neurons. In situations of iron overload, neurons upregulate TfR and DMT1, both which would increase iron accumulation causing further aggravation. Microglia and astrocytes show similar upregulation, but are better able to cope with excess iron due to upregulated iron storage in ferritin. Microglia additionally increased expression of ferroportin, which would result in iron export and a concomitant reduction of intracellular iron. This could be protective to microglial mechanisms, but may also cause upsurges of extracellular iron. If neurons are upregulating proteins involved in iron uptake, excess extracellular iron may provoke supplementary neuronal damage. This data indicates an exceptional vulnerability of dopaminergic neurons to iron insult, with glia exclusively possessing buffering mechanisms that may support their individual functioning, and possibly exacerbate already stressed neuronal regulatory systems.

Previous research provides evidence for the effects of pro-inflammatory cytokines on neuronal iron regulation. It has been shown that both IL6 and TNF cause increased iron levels in hippocampal neurons (Urrutia, 2013), however results here demonstrated this increase only

with IL6 and failed to demonstrate any changes to iron levels following direct TNF treatment. This discrepancy is not necessarily attributed to the difference in cell type, since here dopaminergic neurons were used, while the Urrutia study employed primary hippocampal neurons. Yet the primary neuron studies carried out for this thesis also utilised hippocampal cells, but nonetheless failed to detect any increases in iron due to direct TNF treatment. In support of results obtained here, another study determined a more neuroprotective activity whereby TNF treatment of hippocampal neurons was able to attenuate neuronal toxicity to iron (Barger, 1995). Perhaps another difference in experimental protocol may be attributed to the discrepancies, where the Urrutia study applied higher LPS levels (1µg/ml), as well as non-physiological concentrations of inflammatory cytokines (50ng/ml). This study first determined the physiological concentrations of pro-inflammatory cytokines released by activated microglia via ELISA, and then applied a range of concentrations including the physiological levels. Such contradictory findings may also be accredited to differences in iron content analysis protocols. This study utilised ferrocene assay of total intracellular iron, whereas the Urrutia study employed atomic absorption spectroscopy for determination of total iron. Collectively, results here were able to completely eliminate IL1ß as being responsible for instigating iron regulatory protein changes. With the exception of hepcidin, IL6 and TNF were also eliminated from activating observed neuronal changes to TfR and DMT1 expression. Certain concentrations of direct IL6 and TNF treatment were able to increase neuronal hepcidin levels. Reference to MCM results demonstrate that since MCM treatment had peak cytokine levels upon transfer to N27 cultures, either IL6 or TNF may be responsible for neuronal hepcidin upregulation at 3h. Since the literature presents a greater consistency in proving IL6 instigation of hepcidin, it is possible that IL6 is responsible for the observed changes. It is also possible that more than one signalling pathway exists to stimulate changes to iron homeostasis. Pro-inflammatory cytokine exclusion from responsibility to neuronal IRP changes led to the analysis of all additional microglial released factors. Pro-inflammatory cytokines IL6 and TNF produced a slight effect on HAMP upregulation, while H_2O_2 treatment caused robust changes to TfR and DMT1 gene expression, as well as elevations to intracellular iron levels. Perhaps another microglial-released mediator also affected HAMP expression, so that a combination of inflammatory mediators working in conjunction produce the final effects leading to neuronal demise.

It was determined here that hydrogen peroxide was released in significant quantities from activated microglia, and that high concentrations initiated significant changes in gene expression of all iron regulatory proteins in both N27 dopaminergic neurons and primary

hippocampal neurons. H_2O_2 decomposition also explained the lack of expected results following MCM antibody treatment. Extensive evidence provides further proof of the toxicity associated with neuronal exposure to H_2O_2, which reacts with labile iron in Fenton reactions to generate formation of damaging hydroxyl radicals (Cohen, 1983; Behl, 1994; Medina, 2002). It has also been determined that H_2O_2 can directly affect neuronal iron regulation leading to increased intracellular levels (Martins, 1995; Pantopoulos, 1997; Kakhlon, 2002). Thus, the neurotoxic effects of H_2O_2, along with the known reductions in PD antioxidants and the stresses placed on regulatory systems during times of combined excesses in iron and oxidative species, make it an ideal target for future investigations into preventative measures and therapeutic strategies.

Transwell studies provided insight into neuronal behaviour under more realistic conditions of continuous exposure to microglial and astrocytic-released factors. It was determined that while co-culture with microglia somewhat attenuated IRP gene expression upregulations as previously observed, the addition of astrocytes had a greater significance. Astrocytes were able to provide a complete neuroprotective effect, entirely banishing the previously measured neuronal iron elevations. This is in accordance with the observed changes in astrocytic ferritin upregulation, without any export via ferroportin upregulation as witnessed in microglia, implying an important role in sequestering abundant levels of iron away from causing damage to neuronal cells. Astrocytic iron influx and retention remains of vital importance, due to the neuroprotective potential of accruing excess iron (Pelizzoni, 2013). Additionally, astrocytes have been shown to have greater capacity for hydrogen peroxide detoxification than neurons, with previous co-culture experiments similarly showing protective effects of astrocytes on neurons due to greater H_2O_2 clearance (Desagher, 1996). Furthermore, astrocytes are able to provide neurons with cysteine precursors and amino acids necessary for neuronal glutathione synthesis (Dringen, 1999). While astrocytes express higher GSH levels compared to neurons, and are able to provide neuronal protection by decomposing excess H_2O_2, neuronal provision of components necessary to express GSH would afford additional support. Astrocytes become activated with inflammation in the PD brain (Giulian, 1988; Teismann, 2004), which may affect their iron buffering abilities. However, studies have shown beneficial effects of activated astrocytes in PD models, protecting SN dopaminergic neurons from 6-OHDA-mediated injury (Saura, 2003), and assisting neuronal survival (Kohutnicka, 1998). Thus, this highlights the importance of functional neuronal and astrocytic interactions, as well as the role of astrocytes in providing efficient neuronal support against oxidative stress. These findings emphasise the

complexities of cellular coping mechanisms, and the necessity for identifying which components may be useful neuroprotective targets for PD therapeutic strategies.

Lastly, it was determined in this study that exposure to microglial inflammatory factors led to mishandling of neuronal iron metabolism, which in turn led to downstream initiation of oxidative stress, disruption to mitochondrial functioning and eventual induction of apoptosis. This is consistent with previous findings relating to the toxic consequences of interference with iron regulation, and its implication in PD pathogenesis via the inception of OS (Jenner, 2003; Henchcliffe, 2008; Nikolova, 2012; Yana, 2013). If nigral physiological conditions include elevated basal OS, which is significantly increased in PD in conjunction with diminished antioxidants, it is only logical to conclude from this evidence that iron and OS maintain a substantial role in the neurodegenerative cascade towards deterioration of dopaminergic neurons. Moreover, results from this study concur with others in that neuronal death, under these circumstances, appears to occur by apoptosis rather than necrosis (Mochizuki, 1996; Anglade, 1997; Tatton, 1998; Lev, 2003). It is interesting that initially, necrosis was present, however at the commencement of full cellular decline, apoptotic mechanisms gained control. If this model may draw inferences to PD pathology, it would imply the existence of a completely proapoptotic means of controlled degeneration. Further assessment and understanding of the types of cell death directly involved in PD neurodegeneration may contribute to discovery of neuroprotective solutions. Collectively, it may be of use to define a neuroprotective prospect utilising the knowledge described here, by harnessing the astrocytic abilities at iron sequestration, preventing uncontrolled iron dysregulation and the concomitant OS by providing safe decomposition of hydrogen peroxide, and by utilising antiapoptotic components to stabilise or protect mitochondria from termination.

9.3 Results Summary

Studies conducted here elucidate the neurodegenerative pathways initiated by microglial activation, which may be of use for advancement of PD therapeutic treatments. Activated microglia release hydrogen peroxide which elicits a robust reaction in dopaminergic neurons, resulting in alteration of iron regulatory protein expression. Such changes in expression lead to toxic elevations of intracellular iron, which result in eventual onset of neuronal apoptosis. While higher levels of H_2O_2 were applied here in comparison to physiologically determined concentrations, their successful elicitation of neuronal IRP changes in an *in vitro* PD model verify their ability to induce neurotoxic alterations in cellular iron homeostasis. Further investigations presented a glial neuroprotective effect, able to attenuate excess iron deposition, evidenced by their ability to upregulate expression of the iron storage protein ferritin. This buffering mechanism was not present within dopaminergic neurons, indicating either an excess neuronal vulnerability to changes in iron regulation or a neuroprotective role of glial cells intended to sequester excess iron from neighbouring neurons. It may be hypothesised that while astrocytes are able to buffer and eliminate mishandling of neuronal iron following 24h incubation, astrocytes in the PD brain may present the same neuroprotection, however, subsequent to many weeks of buffering accompanied by disruptions to astrocytic physiology, the astroglia are no longer able to maintain the same level of protection. Results presented here represent various findings that may be collectively applied towards the understanding of glial neuroprotection and dopaminergic demise following iron mishandling in PD. This work also supports the potential neuroprotective effects of anti-inflammatory agents, where treatment with anti-inflammatory drugs ibuprofen (Gao, 2011) or antidiabetic glitazone (Brauer, 2015) presented associations with reduced PD incidence. Accordance with previous works, as well as several disparities, incites a need for supplementary exploration into this topic.

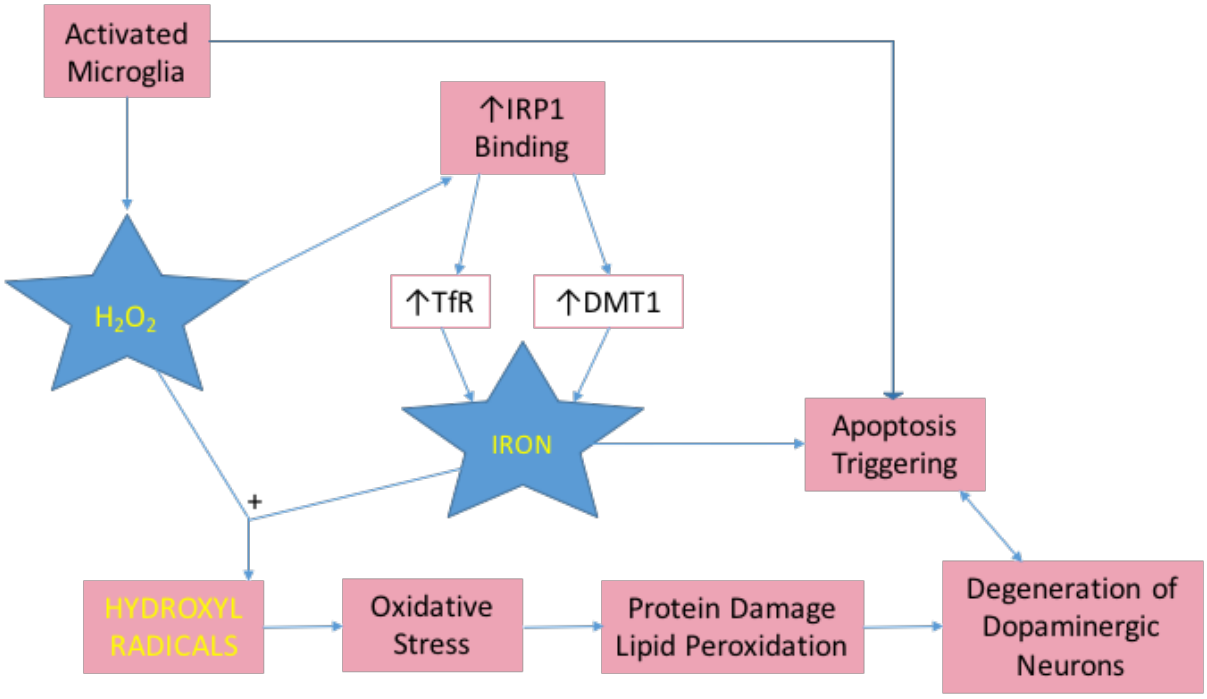

Figure 9.1 Summary of Principal Findings
This graphic demonstrates a summary of the principal findings in this thesis. Activated microglia release significant concentrations of hydrogen peroxide. H_2O_2 has demonstrated the capacity to affect changes to neuronal iron metabolism. It is capable of oxidising iron sulphur clusters from cytoplasmic aconitase, resulting in increased IRP1 binding to iron response elements. This, in turn, resulted in perceived elevations of TfR and DMT1 gene expression, as well as increased intracellular iron concentrations. The greater presence of ferrous iron in conjunction with H_2O_2 can feed the Fenton reaction into production of hydroxyl radicals. Surpassing the cellular antioxidant capacity can lead to oxidative stress as was measured here, along with changes to mitochondrial membrane potential and the eventual triggering of apoptosis. Thus, it was observed that activation of the innate microglial response has the potential to dysregulate neuronal iron metabolism, resulting in triggering of a pathway that may ultimately lead to degeneration of dopaminergic neurons. *Abbreviations: DMT1= Divalent Metal Transporter Ion 1, H_2O_2= Hydrogen Peroxide, IRP1= Iron Regulatory Protein 1, TfR= Transferrin Receptor.*

9.4 Restraints and Procedural Limitations

While the present study elucidated the effects of inflammation on neuronal iron metabolism in an *in vitro* PD model, several limitations remain. Most neuronal data were drawn from analysis of N27 dopaminergic cell line behaviour. This data was also confirmed in primary cultures of hippocampal cells. Although results were similar, and primary culture data were able to support N27 findings, there remained a few divergences. These may be attributed to differences in neuronal type or the presence of 2-3% glial cells within primary culture populations, making data interpretation less accurate. Additionally, N27 cell line immortalisation incorporates cancer cells to achieve continuous division without senescence, however cancer cells have been shown to have altered iron metabolism geared towards greater iron uptake and intracellular retention. This may include elevated TfR (Taetle, 1987) and DMT1 (Brookes, 2006) expression. While it may be useful to observe behaviour using dopaminergic primary culture neurons instead, this would take more time and create an added ordering expense, as extraction involves more precise work for a smaller number of cells. Depending on the method of isolation, dopaminergic cultures tend to have a much higher percentage of glia than hippocampal cultures. If dopaminergic cultures only contain about 20-30% of neurons, then results would be affected by significant glial presence and not reflect purely neuronal behaviour.

Next, the issue of cell culture use must be addressed. While cell lines are extremely useful for high throughput replication of identical cells, providing great reproducibility and high cell turnover to proceed quickly between experiments, they fail to fully represent physiological or pathological PD conditions. Individual N9, C6 or N27 cell lines provide a valuable means to isolate individual cellular behaviours in order to draw meaningful conclusions. For example, use of these cell lines in this study allowed for determination of a neuroprotective astrocyte function that would have been difficult to establish in mixed cellular populations. It also permitted for complete isolation and pursuant ability to fully attribute any observed characteristics to neuronal behaviour. Additionally, study of individual cells cannot fully replicate that of a PD brain, since the brain consists of a melange of various cell types working in harmonious conjunction. Isolation of one from another may incite alterations in normal behaviour, and eliminate both neurotoxic or neuroprotective effects. Moreover, nigral neurons within the human brain are under greater metabolic stress, which may add to these effects. Similarly, cell culture experimentation does not fully represent a Parkinson's brain, but instead allows for the breakdown of physiological processes occurring within Parkinson's for

individual observation. In this instance, this would include the study of the neuroinflammatory process to examine how it may impact neuronal iron metabolism. This influence was compensated for by consequent investigation using primary cells and co-cultures, which permitted for examination of several interacting components together to form a more complete understanding of what occurs in the brain.

Another point to consider is the immortalisation of cell culture. Immortalised cell lines retain distinctive properties such as lack of senescence, that do not reflect those of PD neurons. Immortalisation also alters the cellular genetic makeup so that cell lines may not fully reflect characteristics and behaviour of primary cells. This may, in turn, result in variations between iron requirements of immortalised cells compared to primary cells, which may influence the results of intracellular iron levels and gene expression of iron regulatory proteins. For example, it has been proven that the C6 cell line differentially expresses certain genes when compared with untransformed primary astrocyte cultures, including lower levels of FtH1 (Gunnersen, 2000). Lower ferritin levels may mean that cells express greater intracellular iron, or variations in other iron regulatory proteins. Taking this into consideration, cell lines were never passaged more than a certain number of times to avoid age-related morphological changes in phenotype. Furthermore, key results were replicated in primary cell cultures to account for any possible divergences between cell behaviour. Yet primary cell cultures also retain certain limitations, in that use of embryonic neurons are not truly representative of the behaviour of adult neurons in the Parkinson's brain, due to discrepancies in neuronal age-related pharmacology, mitochondrial function, electrophysiology and stressor susceptibility (Brewer, 2007). Considering the various investigatory options, use of cell lines in developing models of disease remains an extremely cost and time-effective means of consistent, reproducible, initial experimentation into topics of interest, while minimising animal experimentation. Once certain conclusions are drawn utilising cell culture investigations, greater indication of PD pathology may be achieved by *in vivo* experimentation.

Another study limitation is the application of LPS to activate the innate microglial inflammatory response. LPS is unlikely to be responsible for microglial activation within the Parkinson's brain, and is utilised here merely as a useful tool to provide a consistent, robust microglial inflammatory response. Since LPS induces activation via toll-like receptors (TLR), and TLR-induced stimulation of the microglial response has been shown to propagate cytotoxicity in neurodegenerative diseases (Lehnardt, 2010), then other possible treatments for similar activation of the innate immune response via the TLR- dependent pathway may closer resemble one that could occur in the human Parkinson's brain. This may include exposure to

various TLR agonists such as peptidoglycan (PGN), which stems from *Staphylococcus aureus* and stimulates microglial activation via TLR2 (Kielian, 2002; Kielian, 2005), or bacterial CpG DNA via TLR9 (Olson, 2004). Future experimentation may look into changes in iron metabolism via such an alternative form of microglial activation. This would also help to differentiate whether the observed changes in iron dyhomeostasis occur as a specific result of TLR4 signalling or if it merely ensues microglial inflammation. Additionally, the use of LPS as a model of Parkinson's disease neuroinflammation mainly addresses the microglial inflammatory response. While this study specifically aimed to determine the effects of microglial released compounds on the dysregulation of iron in dopaminergic neurons, it may be of use to determine whether other PD models result in the same observed behaviours. For example, the PD brain is known to exhibit a defect in mitochondrial CI activity. Since this relates to the generation of OS, it may be interesting to observe if treatment with CI inhibitors such as Rotenone or MPTP result in increases of hydrogen peroxide leading to variations in neuronal iron metabolism. This would place greater influence on neuronal cellular mechanisms rather than the influence directly from the microglial inflammatory response.

Lastly, it was concluded that neuronal iron metabolism was affected by exposure to microglial inflammatory factors. These conclusions were drawn based mainly on changes in gene expression and measurement of total intracellular iron via the ferrocene assay. These results may be attributed greater merit if protein levels were also measured. If increased gene expression of certain IRPs translated to increased protein levels, as observed in other studies (Urrutia, 2013), then it would confirm that toxic iron levels indeed resulted from inflammatory oxidative stress. Several procedural limitations were encountered in determination of protein levels. Since Western Blots serve more to confirm protein incidence rather than for accurate enumeration, the new MesoScale Discovery technique for precise protein quantification was attempted. While more common proteins, such as those of pro-inflammatory cytokines, are readily available in easy to use pre-made kits, the iron regulatory proteins in this study proved to be much more obscure. Building custom assays for this technique proved extremely time consuming as it required two different antibodies for each protein of interest. Ideally, antibodies should be raised in two different species, allowing for biotinylation of one and SULFO-Tagging of the second, but unfortunately, it was impossible to locate vendors providing each antibody of interest produced in two distinctive species, barring having them custom made. Instead, another protocol was applied, whereby both antibodies must contain external epitopes, and thus immunogen construction from synthetic peptides of a short linear sequence with transmembrane or intracellular epitopes were avoided to ensure external

epitopes were available for binding. Denaturing was attempted for potential avoidance of this issue, although to no avail. Both antibodies must also contain species reactivity to mouse and rat. The first antibody must be biotinylated, while the second must be ordered in sufficient quantities at a concentration of at least 1mg/ml to complete the SULFO-tagging process. The second antibody must also be supplied in PBS only buffer, free of any sodium azide or glycerol. Recombinant proteins should be used as a positive control, or else utilisation of a cell line under conditions known to express the protein of interest. Considering that these proteins of interest are difficult to find in the first place, this proved an extremely tiresome and gruelling process of almost one year in the making. Following several custom-orders of the secondary detection antibody, final completion of the protocol recipe with much appreciated help from the MesoScale representative, and abundant expense, to significant dismay, the assay nonetheless failed to work. The reason remains obscure, although it may pertain to the fact that primary antibodies with a complete immunogen could not be found. While direct communication with each manufacturer requested determination of each specific epitope to ensure they were available for external binding, not all companies were willing or able to share this information. Alternatively, it may be due to both antibodies having too similarly located epitopes, resulting in competitive binding at the same areas. Further investigation into this field should certainly include determination of how to accurately measure protein levels, perhaps by discovering where the MSD assay failed and employing corrective actions. Another alternative may include simultaneous protein and mRNA determination via flow cytometry using the Invitrogen PrimeFlow RNA Assay by applying customised probe sets.

9.5 Future Work

9.5.1 Further Development of in vitro Experimentation

To support current *in vitro* findings and for their further development, several additional investigations may be pursued. To begin with, results were carried out using a dopaminergic cell line and hippocampal primary cells. As previously discussed, it would be of use to confirm these findings in dopaminergic primary cells from foetal rat pups at embryonic day 13. These would provide the greatest similarity to physiological mechanisms within Parkinsonian dopaminergic neurons. It would also be of great value to complete protein determination, in order to assess whether altered mRNA expression translates to protein expression. Additionally, to improve cost efficiency, certain experiments were initially carried out at various time points, followed by a narrower focus depending on assessment of previous results. This resulted in 24h being the primary measured time point, as it provided the greatest variations. However, it was also determined that alterations in hepcidin expression occurred at the earlier 3h measurement. So, for example, it was postulated that although hydrogen peroxide affected gene expression at 24h, TNF may be responsible for the increases in hepcidin at 3h. Treatment of MCM without antibodies (-TNF) demonstrated that hepcidin did not increase at 24h, as previously observed with MCM treatment alone. However, it never increased at this time. Thus, it may be of more use to observe MCM-ab at 3h as well, to determine if this measurement also abolished the hepcidin increases. This would then prove that previously observed augmentation in HAMP expression at 3h was indeed caused by TNF or IL6 alone. Additionally, it may be of use to repeat the MCM-ab test as performed here, but with modification to the type of control used. Since antibodies were added to sample wells in order to neutralise cytokines within MCM, it may help to improve result significance by utilisation of a nonspecific immunoglobulin antibody instead of a vehicle control. It may also be of use to prove full antibody neutralisation via performing an IL6 and TNF ELISA following sample treatment with antibodies for 1h. Regarding the cytokine experiments, the investigation into effects of N27 treated with MCM with the addition of catalase were performed at 24h, with no observed changes in hepcidin, similarly confirming previous results. However, if TNF is causing alterations in hepcidin expression, and HAMP never presented an increase at 24h, then perhaps catalase had no effect on expression at 3h, so this could be investigated further.

As for the genes assessed, it may also be of use to measure any changes in frataxin and superoxide dismutase 1 (SOD1) genes. Frataxin (Fxn) is a mitochondrial protein directly involved in generation of iron sulphur clusters (ISC) (Stemmler, 2010). Reductions in Fxn would result in failure to construct necessary ISC, which would negatively affect cellular

functioning, as well as elevate mitochondrial iron levels due to its failure to be assembled into iron-sulphur clusters. Fluctuations in Ftx concentrations have proven to result in decreased MMP and neuronal degeneration via apoptosis (Palomo, 2011; Mincheva-Tasheva, 2014), both conditions observed in this study. It has also been shown that Fxn diminutions lead to significant mitochondrial iron accumulation resulting in oxidative damage (Karthikeyan, 2003). Thus, it would be of interest to detect whether such changes are also brought on by alterations in neuronal Fxn upon exposure to microglial inflammation. Fxn protein may also be easily quantified as per the protocol by Steinkellner (2010). Furthermore, astrocytes are known to protect neurons from oxidative stress, which was corroborated in this study from observation of neuroprotective functions. While neuronal degeneration may be an outcome of excessive vulnerability to certain factors such as hydrogen peroxide and other oxidative species, it may likewise be due to failure of support from neighbouring glia. A loss of astrocytic function may exacerbate toxic conditions. This has been proven in several studies where Fxn maintains a causative role, whereby a deficiency in astrocytic Fxn results in loss of neuroprotective support leading to neuronal degeneration (Navarro, 2010; Loria, 2015). Thus, greater investigation into astrocytic presentation of Fxn may be of importance in furthering understanding of iron regulation on neurodegeneration.

The SOD1 gene encodes for the superoxide dismutase enzymes responsible for superoxide degradation within both the cytosol and mitochondria. SOD catalyses superoxide disproportionation into oxygen and hydrogen peroxide to prevent superoxide-mediated cellular damage or its conversion to extremely cytotoxic peroxynitrite radicals in the presence of nitric oxide. However, excess SOD can likewise prove cytotoxic. Greater superoxide degradation should imply beneficial radical reductions; however, it occurs concomitantly with increased generation of hydrogen peroxide. H_2O_2 has already proven its neurotoxic effects here. Furthermore, during conditions of high NO and H_2O_2 as seen in PD, SOD has proven to act as an alternative source of peroxynitrite (McBride, 1999). Thus, changes to SOD1 resulting in elevated cellular SOD may prove disastrous to cells experiencing oxidative stress, and since dopaminergic neurons are in a constant state of OS, this mechanism may further strain cellular functioning during PD. This is evidenced by demonstrations that Parkinson's and Alzheimer's brains contain greater than 6-fold escalations of specific SOD1 isoforms, and 2.4-fold escalations of total SOD1 compared to matched controls (Choi, 2005). SOD1 overexpression in transgenic mice also exhibits substantial H_2O_2 elevations, accompanied by H_2O_2–mediated oxidative damage (Fullerton, 1998). Therefore, it may improve upon information presented in this project on the systemic effects of iron accumulation to determine whether either of these

two genes demonstrate upregulated expression following inflammation-induced iron dysregulation.

Subsequent to findings in astrocytic studies here, further consideration into the direct effects of hydrogen peroxide treatment on astrocyte function may prove of interest. It was observed that H_2O_2 affects neuronal iron regulation, thus it may be postulated that it may exert similar properties in astrocytes. Alternatively, astroglia have shown to contain buffering mechanisms that may support the strain of excessive oxidative species, thus an absence of major consequences following peroxide treatment is also possible. To rule out the postulation that astrocytes may also produce and release neurotoxic quantities of H_2O_2, its levels within astrocytic supernatant following MCM or LPS treatment could be quantified. Quantification methods here were not entirely accurate, since it has been proven that H_2O_2 levels may reduce with time, and the protocol requires 30m between supernatant collection and final analysis. Further studies in this field may utilise other H_2O_2 quantification methods such as *in vivo* microdialysis (Hyslop, 1995), or intraperitoneal injection with the catalase inhibitor aminotriazole (Fullerton, 1998). Likewise, astrocytic expression of catalase or glutathione peroxidase may be quantified in order to confirm whether they demonstrate a physiologically or pathologically greater expression than dopaminergic neurons, and therefore represent diminished vulnerability against its actions. Since full astrocytic physiology benefits neuronal function, broader understanding of mechanisms initiating injury would improve advancement in therapeutic strategies.

Considering the involvement of mitochondria in oxidative stress, and reductions in mitochondrial membrane potential leading to initiation of apoptosis, it may be of use to differentiate between whether elevated iron levels are increasing specifically within the mitochondria as well as in the cytosol. This may be performed by measurement of non-haem iron in the mitochondrial iron pool (Foury, 1997). Another method may include estimation of mitochondrial iron concentrations by isolating cellular mitochondria with measurement using inductively coupled plasma mass spectrometry (Karthikeyan, 2003). Iron measured in this thesis was performed via the ferrocene assay. Knowledge on mechanisms of iron accumulation would benefit from further enquiry. The labile iron pool in individual cell culture populations following inflammatory MCM treatment could also be measured via application of the fluorescent calcein aceotxymethyl ester chelator using a spectrofluorometer (Epsztejn, 1997; Kakhlon, 2002; Prus, 2007). This would substantiate evidence of increasing reactive labile iron during inflammation, as opposed to merely total intracellular iron, which may include unreactive iron stored within ferritin. Total iron distribution in specific cellular compartments

in *in vivo* PD model brain sections may also be measured via highly sensitive laser ablation inductively coupled plasma mass spectrometry. This could confirm this thesis' findings of increased cellular iron, which is in keeping with published PD murine model results exhibiting noteworthy elevations in nigral iron content when compared with controls utilising this technique (Hare, 2009).

9.5.2 Investigation to Determine if Findings may be Duplicated in vivo

Once a more comprehensive picture of *in vitro* mechanisms fuelling dopaminergic neuronal iron dysregulation towards cellular dysfunction is complete, the next logical step would be to apply the gained knowledge towards confirmation under more realistic PD model conditions via duplication *in vivo*. As cell culture involves microglial activation via treatment with lipopolysaccharide, this can be duplicated by intravenous LPS administration in rats. This would allow for investigation into confirming whether the inflammatory response in rats can produce similar variations in neuronal iron homeostasis. Since focal LPS injection to the brain can cause nigral cell loss (Tomás-Camardiel, 2004), LPS may be administrated by peripheral injection for a range of time exposures, substantia nigra tissue could be excised from brains, followed by processing via cryostat sectioning, and RT-PCR analysis of iron regulatory proteins within dopaminergic neurons identified by TH immunostaining. Furthermore, iron distribution may be analysed via electron microscopy, while differentiation between ferrous and ferric iron may be determined via spectrophotometric analysis of ferrous iron via ferrocene assay before addition of the reducing ascorbic acid (Sofic, 1988). Determination of the ferrous:ferric ratio in dopaminergic neurons exposed to pro-inflammatory microglial factors could help determine which iron oxidation state is directly affected by inflammation.

9.5.3 Supplementary Explorations

Results from *in vitro* cell culture models and *in vivo* rodent result validation provide invaluable evidence into the complexities of cellular pathophysiological mechanisms. This may include furthering current topic comprehension along with development of potential neuroprotective therapeutic targets for PD. Lack of definitive pathogenic instigators means they remain intriguing models of disease requiring superior substantiation into the causes of inflammatory neuronal iron dysregulation leading to toxic accumulation perceived within different neurodegenerative diseases. Combining the fields and narrowing research focus into discerning effects of hydrogen peroxide and oxidative species on IRP regulation and subsequent iron accrual, along with deviations to astrocytic neuronal support, may sustain

crucial advancements in disease understanding, leading to development of potential therapies able to actually inhibit or reverse PD pathogenesis.

Initial developmental work should include furthering *in vitro* comprehension of neuronal iron regulation. Most strikingly, the very promising neuronal reaction to hydrogen peroxide should be established further via both cell line and primary cell culture. This may be followed by *in vivo* physiological determination of hydrogen peroxide, as well as effects of treatment on neuronal iron metabolism. Isolating the source for prevention of iron dysregulation in human brains would help recommend targets for PD treatment, which would be the long term objective. Similar iron accumulation pathophysiology presents in other neurodegenerative conditions, including Alzheimer's Disease, Huntington's Disease and Multiple Sclerosis, and is associated with contribution to neuronal impairment. Such implications exemplify how prevention of such iron accrual would present an exciting focus for future neurodegenerative therapies. Thus, a refined comprehension of the instigating factors contributing to neurodegenerative iron accumulation in PD is necessary, with a focus on microglial inflammatory factors such as hydrogen peroxide, in order to advance to production of preventative or assuasive medical remedies.

9.6 Conclusions

In conclusion, this work delivers noteworthy indications that the cumulatively toxic effects of microglial inflammation can induce iron dysregulation in dopaminergic neurons that may ultimately lead to cellular demise via apoptosis. Investigations have disclosed significant neuroprotective effects of astrocytes, whose additional presence manages to attenuate the iron elevations and changes in regulatory proteins. It is also revealed here that pro-inflammatory cytokines are not entirely responsible for toxic changes to iron regulatory proteins, whereupon it was determined that hydrogen peroxide was in fact responsible for instigating said changes. Cumulatively, results determined in this study stipulate mechanisms responsible for maintenance or disruption to neuronal iron metabolism, and substantiates the iron and oxidative stress theory of neuronal degeneration. This evidence presents a model of cellular pathology occurring in the Parkinson's brain, whereupon further investigations may result in improved therapeutic strategies in PD.

REFERENCES

References

Adam-Vizi, V. (2005). Production of Reactive Oxygen Species in Brain Mitochondria: Contribution by Electron Transport Chain and Non–Electron Transport Chain Sources. *Antioxidants & Redox Signaling*, *7*(9–10), 1140–1149. http://doi.org/10.1089/ars.2005.7.1140

Adisetiyo, V., Jensen, J. H., Ramani, A., Tabesh, A., Di Martino, A., Fieremans, E., Helpern, J. A. (2012). In vivo assessment of age-related brain iron differences by magnetic field correlation imaging. *Journal of Magnetic Resonance Imaging*, *36*(2), 322–331. http://doi.org/10.1002/jmri.23631

Akaneya, Y., Takahashi, M., & Hatanaka, H. (1995). Interleukin-1 beta enhances survival and interleukin-6 protects against MPP+ neurotoxicity in cultures of fetal rat dopaminergic neurons. *Experimental Neurology*. http://doi.org/10.1006/exnr.1995.1082

Alberio, T., Lopiano, L., & Fasano, M. (2012). Cellular models to investigate biochemical pathways in Parkinson's disease. *FEBS Journal*. http://doi.org/10.1111/j.1742-4658.2012.08516.x

Alvarez, B., Denicola, A., & Radi, R. (1995). Reaction between Peroxynitrite and Hydrogen Peroxide: Formation of Oxygen and Slowing of Peroxynitrite Decomposition. *Chemical Research in Toxicology*, *8*(6), 859–864. http://doi.org/10.1021/tx00048a006

Ambani, L. M., Van, W., & Murphy, S. (1975). Brain Peroxidase and Catalase in Parkinson Disease. *Archives of Neurology*, *32*(2), 114–118.

Anderson, C., Checkoway, H., Franklin, G. M., Beresford, S., Smith-Weller, T., & Swanson, P. D. (1999). Dietary factors in Parkinson's disease: The role of food groups and specific foods. *Movement Disorders*, *14*(1), 21–27. http://doi.org/10.1002/1531-8257(199901)14:1<21::AID-MDS1006>3.0.CO;2-Y

Andrasi, E., Farkas, E., Scheibler, H., Reffy, A., & Bezur, L. (1995). Al, Zn, Cu, Mn and Fe levels in brain in Alzheimer's disease. *Archives of Gerontology and Geriatrics*, *21*(0167–4943), 89–97.

Andriopoulos, B., Hegedüsch, S., Mangin, J., Riedel, H. D., Hebling, U., Wang, J., Mueller, S. (2007). Sustained hydrogen peroxide induces iron uptake by transferrin receptor-1 independent of the iron regulatory protein/iron-responsive element network. *Journal of Biological Chemistry*, *282*(28), 20301–20308. http://doi.org/10.1074/jbc.M702463200

Anglade, P. (1997). Apoptosis and autophagy in nigral neurons of patients with Parkinson's disease. *Histology and Histopathology*, *12*(1), 25–31.

Antharam, V., Collingwood, J. F., Bullivant, J.-P., Davidson, M. R., Chandra, S., Mikhaylova, A., Dobson, J. (2012). High field magnetic resonance microscopy of the human hippocampus in Alzheimer's disease: Quantitative imaging and correlation with iron. *NeuroImage*, *59*(2), 1249–1260. http://doi.org/10.1016/j.neuroimage.2011.08.019

Antonini, A., & DeNotaris, R. (2004). PET and SPECT functional imaging in Parkinson's disease. *Sleep Medicine*, *5*(2), 201–206. http://doi.org/10.1016/j.sleep.2003.10.013

Aoki, S., Okada, Y., Nishimura, K., Barkovich, a J., Kjos, B. O., Brasch, R. C., & Norman, D. (1989). Normal deposition of brain iron in childhood and adolescence: MR imaging at 1.5 T. *Radiology*, *172*(2), 381–385. http://doi.org/10.1148/radiology.172.2.2748819

Arcuri, C., Mecca, C., Bianchi, R., Giambanco, I., & Donato, R. (2017). The Pathophysiological Role of Microglia in Dynamic Surveillance, Phagocytosis and Structural Remodeling of the Developing CNS. *Frontiers in Molecular Neuroscience*, *10*. http://doi.org/10.3389/fnmol.2017.00191

Armogida, M., Nisticò, R., & Mercuri, N. B. (2012). Therapeutic potential of targeting hydrogen peroxide metabolism in the treatment of brain ischaemia. *British Journal of Pharmacology*. http://doi.org/10.1111/j.1476-5381.2012.01912.x

Ayton, S., Lei, P., Duce, J. A., Wong, B. X. W., Sedjahtera, A., Adlard, P. A., Finkelstein, D. I. (2013). Ceruloplasmin dysfunction and therapeutic potential for Parkinson disease. *Annals of Neurology*, *73*(4), 554–559. http://doi.org/10.1002/ana.23817

Baba, M., Nakajo, S., Tu, P. H., Tomita, T., Nakaya, K., Lee, V. M., Iwatsubo, T. (1998). Aggregation of alpha-synuclein in Lewy bodies of sporadic Parkinson's disease and dementia with Lewy bodies. *The American Journal of Pathology*, *152*(4), 879–84. http://doi.org/10.1086/281267

Babior, B. M. (2000). Phagocytes and oxidative stress. *American Journal of Medicine*. http://doi.org/10.1016/S0002-9343(00)00481-2

Bal-Price, a, & Brown, G. C. (2001). Inflammatory neurodegeneration mediated by nitric oxide from activated glia-inhibiting neuronal respiration, causing glutamate release and excitotoxicity. *The Journal of Neuroscience: The Official Journal of the Society for Neuroscience*, *21*(17), 6480–6491. http://doi.org/21/17/6480 [pii]

Bandyopadhyay, S., Chandramouli, K., & Johnson, M. K. (2008). Iron-sulfur cluster biosynthesis. *Biochemical Society Transactions*, *36*(Pt 6), 1112–9. http://doi.org/10.1042/BST0361112

Banerjee, R., Becker, D. F., Dickman, M. B., Gladyshev, V. N., & Ragsdale, S. W. (2007). *Redox Biochemistry*. *Redox Biochemistry*. http://doi.org/10.1002/9780470177334

Banzet, S., Sanchez, H., Chapot, R., Bigard, X., Vaulont, S., & Koulmann, N. (2012). Interleukin-6 contributes to hepcidin mRNA increase in response to exercise. *Cytokine*, *58*(2), 158–161. http://doi.org/10.1016/j.cyto.2012.01.006

Barcia, C., Barreiro, A. F., Poza, M., & Herrero, M.-T. (2003). Parkinson's disease and inflammatory changes. *Neurotoxicity Research*, *5*(6), 411–417. http://doi.org/10.1007/BF03033170

Barcia, C., Sánchez Bahillo, A., Fernández-Villalba, E., Bautista, V., Poza Y Poza, M., Fernández-Barreiro, A., Herrero, M. T. (2004). Evidence of active microglia in substantia nigra pars compacta of parkinsonian monkeys 1 year after MPTP exposure. *GLIA*, *46*(4), 402–409. http://doi.org/10.1002/glia.20015

Barclay, A. N., Wright, G. J., Brooke, G., & Brown, M. H. (2002). CD200 and membrane protein interactions in the control of myeloid cells. *Trends in Immunology*, *23*(6), 285–290. http://doi.org/10.1016/S1471-4906(02)02223-8

Barger, S. W., Hörster, D., Furukawa, K., Goodman, Y., Krieglstein, J., & Mattson, M. P. (1995). Tumor necrosis factors alpha and beta protect neurons against amyloid beta-peptide toxicity: evidence for involvement of a kappa B-binding factor and attenuation of peroxide and Ca2+ accumulation. *Proceedings of the National Academy of Sciences*, *92*(20), 9328–32. http://doi.org/10.1073/pnas.92.20.9328

Bartzokis, G., Beckson, M., Hange, D. B., Marx, P., Foster, J. A., & Marder, S. R. (1997). MR evaluation of age-related increase of brain iron in young adult and older normal males. *Magnetic Resonance Imaging*, *15*(1), 29–35. http://doi.org/10.1016/S0730-725X(96)00234-2

Bartzokis, G., Cummings, J. L., Markham, C. H., Marmarelis, P. Z., Treciokas, L. J., Tishler, T. A., Mintz, J. (1999). MRI evaluation of brain iron in earlier- and later-onset Parkinson's disease and normal subjects. *Magnetic Resonance Imaging*, *17*(2), 213–222. http://doi.org/10.1016/S0730-725X(98)00155-6

Bartzokis, G., Cummings, J., Perlman, S., Hance, D. B., & Mintz, J. (1999). Increased Basal Ganglia Iron Levels in Huntington Disease. *Arch Neurol*, *56*, 569–574. http://doi.org/10.1001/archneur.56.5.569

Bastianetto, S., Ramassamy, C., Doré, S., Christen, Y., Poirier, J., & Quirion, R. (2000). The Ginkgo biloba extract (EGb 761) protects hippocampal neurons against cell death induced by beta-amyloid. *The European Journal of Neuroscience*, *12*(6), 1882–1890. http://doi.org/DOI 10.1046/j.1460-9568.2000.00069.x

Beard, J. (2003). Iron deficiency alters brain development and functioning. *The Journal of Nutrition*, *133*(5 Suppl 1), 1468S–72S.

Beard, J. L., Connor, J. R., & Jones, B. C. (1993). Iron in the Brain. *Nutrition Reviews*, *51*(6), 157–170.

Behl, C., Davis, J. B., Lesley, R., & Schubert, D. (1994). Hydrogen peroxide mediates amyloid ß protein toxicity. *Cell*, *77*(6), 817–827. http://doi.org/10.1016/0092-8674(94)90131-7

Belaidi, A. A., & Bush, A. I. (2016). Iron neurochemistry in Alzheimer's disease and Parkinson's disease: targets for therapeutics. *Journal of Neurochemistry*. http://doi.org/10.1111/jnc.13425

Ben-Shachar, D., Ashkenazi, R., & Youdim, M. B. H. (1986). Long-term consequence of early iron-deficiency on dopaminergic neurotransmission in rats. *International Journal of Developmental Neuroscience*, *4*(1), 81–88. http://doi.org/10.1016/0736-5748(86)90019-

Ben-Shachar, D., Eshel, G., Finberg, J. P. M., & Youdim, M. B. H. (1991). The Iron Chelator Desferrioxamine (Desferal) Retards 6-Hydroxydopamine-Induced Degeneration of Nigrostriatal Dopamine Neurons. *Journal of Neurochemistry*, *56*(4), 1441–1444. http://doi.org/10.1111/j.1471-4159.1991.tb11444.x

Ben-Shachar, D., Kahana, N., Kampel, V., Warshawsky, A., & Youdim, M. B. H. (2004). Neuroprotection by a novel brain permeable iron chelator, VK-28, against 6-hydroxydopamine lession in rats. *Neuropharmacology*, *46*(2), 254–263. http://doi.org/10.1016/j.neuropharm.2003.09.005

Benda, P., Lightbody, J., Sato, G., Levine, L., & Sweet, W. (1968). Differentiated rat glial cell strain in tissue culture. *Science (New York, N.Y.)*, *161*(3839), 370–1. http://doi.org/10.1126/science.161.3839.370

Bennett, J. P., & Piercey, M. F. (1999). Pramipexole--a new dopamine agonist for the treatment of Parkinson's disease. *Journal of the Neurological Sciences*, *163*(1), 25–31.

Berg, D., Grote, C., Rausch, W. D., Mäurer, M., Wesemann, W., Riederer, P., & Becker, G. (1999). Iron accumulation in the substantia nigra in rats visualized by ultrasound. *Ultrasound in Medicine and Biology*, *25*(6), 901–904. http://doi.org/10.1016/S0301-5629(99)00046-0

Berg, D., Gerlach, M., Youdim, M. B. H., Double, K. L., Zecca, L., Riederer, P., & Becker, G. (2001). Brain iron pathways and their relevance to Parkinson's disease. *Journal of Neurochemistry*. http://doi.org/10.1046/j.1471-4159.2001.00608.x

Berman, S. B., & Hastings, T. G. (1999). Dopamine oxidation alters mitochondrial respiration and induces permeability transition in brain mitochondria: Implications for Parkinson's disease. *Journal of Neurochemistry*, *73*(3), 1127–1137. http://doi.org/10.1046/j.1471-4159.1999.0731127.x

Beynon, S. B., & Walker, F. R. (2012). Microglial activation in the injured and healthy brain: What are we really talking about? Practical and theoretical issues associated with the measurement of changes in microglial morphology. *Neuroscience*. http://doi.org/10.1016/j.neuroscience.2012.07.029

Bharucha, K. J., Friedman, J. K., Vincent, A. S., & Ross, E. D. (2008). Lower serum ceruloplasmin levels correlate with younger age of onset in Parkinson's disease. *Journal of Neurology*, *255*(12), 1957–62. http://doi.org/10.1007/s00415-009-0063-7

Biemond, P., Van Eijk, H. G., Swaak, A. J. G., & Koster, J. F. (1984). Iron mobilization from ferritin by superoxide derived from stimulated polymorphonuclear leukocytes. Possible mechanism in inflammation diseases. *Journal of Clinical Investigation*, *73*(6), 1576–1579. http://doi.org/10.1172/JCI111364

Bisaglia, M., Soriano, M. E., Arduini, I., Mammi, S., & Bubacco, L. (2010). Molecular characterization of dopamine-derived quinones reactivity toward NADH and glutathione: Implications for mitochondrial dysfunction in Parkinson disease. *Biochimica et Biophysica Acta - Molecular Basis of Disease*, *1802*(9), 699–706. http://doi.org/10.1016/j.bbadis.2010.06.006

Bishop, G. M., Dang, T. N., Dringen, R., & Robinson, S. R. (2011). Accumulation of non-transferrin-bound iron by neurons, astrocytes, and microglia. *Neurotoxicity Research*, *19*(3), 443–451. http://doi.org/10.1007/s12640-010-9195-x

Blanco, A. M., Valles, S. L., Pascual, M., & Guerri, C. (2005). Involvement of TLR4/Type I IL-1 Receptor Signaling in the Induction of Inflammatory Mediators and Cell Death Induced by Ethanol in Cultured Astrocytes. *The Journal of Immunology*, *175*(10), 6893–6899. http://doi.org/10.4049/jimmunol.175.10.6893

Blaylock M.D., R. L. (2004). Chronic Microglial Activation and Excitotoxicity Secondary to Excessive Immune Stimulation: Possible Factors in Gulf War Syndrome and Autism. *Journal of American Physicians and Surgeons*, *9*(2), 46–51.

Block, M. L., & Hong, J. S. (2005). Microglia and inflammation-mediated neurodegeneration: Multiple triggers with a common mechanism. *Progress in Neurobiology*. http://doi.org/10.1016/j.pneurobio.2005.06.004

Block, M. L., & Hong, J.-S. (2007). Chronic microglial activation and progressive dopaminergic neurotoxicity. *Biochemical Society Transactions*, *35*(Pt 5), 1127–1132. http://doi.org/10.1042/BST0351127

Block, M. L., Zecca, L., & Hong, J.-S. (2007). Microglia-mediated neurotoxicity: uncovering the molecular mechanisms. *Nature Reviews Neuroscience*, *8*(1), 57–69. http://doi.org/10.1038/nrn2038

Boka, G., Anglade, P., Wallach, D., Javoy-Agid, F., Agid, Y., & Hirsch, E. C. (1994). Immunocytochemical analysis of tumor necrosis factor and its receptors in Parkinson's disease. *Neuroscience Letters*, *172*(1–2), 151–154. http://doi.org/10.1016/0304-3940(94)90684-X

Bonfoco, E., Krainc, D., Ankarcrona, M., Nicotera, P., & Lipton, S. A. (1995). Apoptosis and necrosis: two distinct events induced, respectively, by mild and intense insults with N-methyl-D-aspartate or nitric oxide/superoxide in cortical cell cultures. *Proceedings of the National Academy of Sciences*, *92*(16), 7162–7166. http://doi.org/10.1073/pnas.92.16.7162

Borenfreund, E., & Puerner, J. A. (1985). Toxicity determined in vitro by morphological alterations and neutral red absorption. *Toxicology Letters*, *24*(2–3), 119–124. http://doi.org/10.1016/0378-4274(85)90046-3

Bové, J., Zhou, C., Jackson-Lewis, V., Taylor, J., Chu, Y., Rideout, H. J., Przedborski, S. (2006). Proteasome inhibition and Parkinson's disease modeling. *Annals of Neurology*, *60*(2), 260–264. http://doi.org/10.1002/ana.20937

Bowman, C. C., Rasley, A., Tranguch, S. L., & Marriott, I. (2003). Cultured astrocytes express toll-like receptors for bacterial products. *GLIA*, *43*(3), 281–291. http://doi.org/10.1002/glia.10256

Braak, H., Del Tredici, K., Rüb, U., De Vos, R. A. I., Jansen Steur, E. N. H., & Braak, E. (2003). Staging of brain pathology related to sporadic Parkinson's disease. *Neurobiology of Aging*, *24*(2), 197–211. http://doi.org/10.1016/S0197-4580(02)00065-9

Bradford, M. M. (1976). A rapid and sensitive method for the quantitation of microgram quantities of protein utilizing the principle of protein-dye binding. *Analytical Biochemistry*, *72*(1–2), 248–254. http://doi.org/10.1016/0003-2697(76)90527-3

Brand, M. D., Buckingham, J. A., Esteves, T. C., Green, K., Lambert, A. J., Miwa, S., Echtay, K. S. (2004). Mitochondrial superoxide and aging: uncoupling-protein activity and superoxide production. *Biochem Soc Symp*, *71*(71), 203–213. http://doi.org/10.1042/bss0710203

Brand, M. D. (2016). Mitochondrial generation of superoxide and hydrogen peroxide as the source of mitochondrial redox signaling. *Free Radical Biology and Medicine*, *100*, 14–31. http://doi.org/10.1016/j.freeradbiomed.2016.04.001

Brauer, R., Bhaskaran, K., Chaturvedi, N., Dexter, D. T., Smeeth, L., & Douglas, I. (2015). Glitazone Treatment and Incidence of Parkinson's Disease among People with Diabetes: A Retrospective Cohort Study. *PLoS Medicine*, *12*(7). http://doi.org/10.1371/journal.pmed.1001854

Bresgen, N., & Eckl, P. M. (2015). Oxidative stress and the homeodynamics of iron metabolism. *Biomolecules*. http://doi.org/10.3390/biom5020808

Brewer, G. J., & Torricelli, J. R. (2007). Isolation and culture of adult neurons and neurospheres. *Nature Protocols*, *2*(6), 1490–1498. http://doi.org/10.1038/nprot.2007.207

Brissot, P., Bardou-Jacquet, E., Latournerie, M., Ropert-Bouchet, M., Island, M. L., Loréal, O., & Jouanolle, a-M. (2010). [Hereditary iron overload]. *Pathologie-Biologie*, *58*(5), 316–23. http://doi.org/10.1016/j.patbio.2009.10.011

Brookes, M. J., Hughes, S., Turner, F. E., Reynolds, G., Sharma, N., Ismail, T., Tselepis, C. (2006). Modulation of iron transport proteins in human colorectal carcinogenesis. *Gut*, *55*(10), 1449–1460. http://doi.org/10.1136/gut.2006.094060

Brooks, D. J. (2010). Imaging approaches to Parkinson disease. *Journal of Nuclear Medicine: Official Publication, Society of Nuclear Medicine*, *51*(4), 596–609. http://doi.org/10.2967/jnumed.108.059998

Brown, G. C., & Bal-Price, A. (2003). Inflammatory neurodegeneration mediated by nitric oxide, glutamate, and mitochondria. *Molecular Neurobiology*, *27*(3), 325–355. http://doi.org/10.1385/MN:27:3:325

Burdo, J. R., Menzies, S. L., Simpson, I. A., Garrick, L. M., Garrick, M. D., Dolan, K. G., … Connor, J. R. (2001). Distribution of Divalent Metal Transporter 1 and Metal Transport Protein 1 in the normal and Belgrade rat. *Journal of Neuroscience Research*, *66*(6), 1198–1207. http://doi.org/10.1002/jnr.1256

Buttke, T. M., McCubrey, J. A., & Owen, T. C. (1993). Use of an aqueous soluble tetrazolium/formazan assay to measure viability and proliferation of lymphokine-dependent cell lines. *Journal of Immunological Methods*, *157*(1–2), 233–240. http://doi.org/10.1016/0022-1759(93)90092-L

Cadenas, E., & Davies, K. J. (2000). Mitochondrial free radical generation, oxidative stress, and aging. *Free Radical Biology & Medicine*, *29*(3–4), 222–230. http://doi.org/10.1016/S0891-5849(00)00317-8

Cadet, J. L., & Brannock, C. (1998). Free radicals and the pathobiology of brain dopamine systems. *Neurochemistry International*, *32*(2), 117–31. Retrieved from http://www.ncbi.nlm.nih.gov/pubmed/9542724

Cairo, G., Castrusini, E., Minotti, G., & Bernelli-Zazzera, A. (1996). Superoxide and hydrogen peroxide-dependent inhibition of iron regulatory protein activity: a protective stratagem against oxidative injury. *FASEB Journal: Official Publication of the Federation of American Societies for Experimental Biology*, *10*(11), 1326–35. Retrieved from http://www.ncbi.nlm.nih.gov/pubmed/8836047

Calabrese, V. P., & Hadfield, M. G. (1991). Parkinsonism and extraocular motor abnormalities with unusual neuropathological findings. *Movement Disorders*, *6*(3), 257–260. http://doi.org/10.1002/mds.870060311

Calne, D., Dubini, A., & Stern, G. (1989). Did Leonardo describe Parkinson's disease? *New England Journal of Medicine*.

Caltagirone, A., Weiss, G., & Pantopoulos, K. (2001). Modulation of cellular iron metabolism by hydrogen peroxide. Effects of H2O2 on the expression and function of iron-responsive element-containing mRNAs in B6 fibroblasts. *Journal of Biological Chemistry*, *276*(23), 19738–19745. http://doi.org/10.1074/jbc.M100245200

Cantu, D., Fulton, R. E., Drechsel, D. A., & Patel, M. (2011). Mitochondrial aconitase knockdown attenuates paraquat-induced dopaminergic cell death via decreased cellular metabolism and release of iron and H 2O2. *Journal of Neurochemistry*, *118*(1), 79–92. http://doi.org/10.1111/j.1471-4159.2011.07290.x

Carvey, P. M., Chang, Q., Lipton, J. W., & Ling, Z. (2003). Prenatal exposure to the bacteriotoxin lipopolysaccharide leads to long-term losses of dopamine neurons in offspring: a potential, new model of Parkinson's disease. *Frontiers in Bioscience a Journal and Virtual Library*, *8*(10), s826–s837. http://doi.org/10.2741/1158

Castaño, a, Herrera, a J., Cano, J., & Machado, a. (1998). Lipopolysaccharide intranigral injection induces inflammatory reaction and damage in nigrostriatal dopaminergic system. *Journal of Neurochemistry*, *70*(4), 1584–1592. http://doi.org/10.1046/j.1471-4159.1998.70041584.x

Castellani, R. J., Siedlak, S. L., Perry, G., & Smith, M. a. (2000). Sequestration of iron by Lewy bodies in Parkinson's disease. *Acta Neuropathologica*, *100*(2), 111–114. http://doi.org/10.1007/s004010050001

Cereda, E., Cilia, R., Canesi, M., Tesei, S., Mariani, C. B., Zecchinelli, A. L., & Pezzoli, G. (2017). Efficacy of rasagiline and selegiline in Parkinson's disease: a head-to-head 3-year retrospective case–control study. *Journal of Neurology*, *264*(6), 1254–1263.

Chaudhuri, K. R., Healy, D. G., & Schapira, A. H. (2006). Non-motor symptoms of Parkinson's disease: diagnosis and management. *The Lancet Neurology*, *5*(3), 235–245. http://doi.org/10.1016/S1474-4422(06)70373-8

Chen, J. C., Hardy, P. A., Kucharczyk, W., Clauberg, M., Joshi, J. G., Vourlas, A., Henkelman, R. M. (1993). MR of human postmortem brain tissue: Correlative study between T2 and assays of iron and ferritin in Parkinson and Huntington disease. *American Journal of Neuroradiology*, *14*(2), 275–281.

Chen, Y., Vartiainen, N. E., Ying, W., Chan, P. H., Koistinaho, J., & Swanson, R. A. (2001). Astrocytes protect neurons from nitric oxide toxicity by a glutathione-dependent mechanism. *Journal of Neurochemistry*, *77*(6), 1601–1610. http://doi.org/10.1046/j.1471-4159.2001.00374.x

Chen, H., Zhang, S. M., Hernán, M. A., Schwarzschild, M. A., Willett, W. C., Colditz, G. A., Ascherio, A. (2003). Nonsteroidal Anti-inflammatory Drugs and the Risk of Parkinson Disease. *Archives of Neurology*, *60*(8), 1059. http://doi.org/10.1001/archneur.60.8.1059

Chen, X.-L., Zhang, Q., Zhao, R., & Medford, R. M. (2004). Superoxide, H2O2, and iron are required for TNF-alpha-induced MCP-1 gene expression in endothelial cells: role of Rac1 and NADPH oxidase. *American Journal of Physiology. Heart and Circulatory Physiology*, *286*(October 2003), H1001–H1007. http://doi.org/10.1152/ajpheart.00716.2003

Choi, J., Rees, H. D., Weintraub, S. T., Levey, A. I., Chin, L. S., & Li, L. (2005). Oxidative modifications and aggregation of Cu,Zn-superoxide dismutase associated with alzheimer and Parkinson diseases. *Journal of Biological Chemistry*, *280*(12), 11648–11655. http://doi.org/10.1074/jbc.M414327200

Chow, J. C., Young, D. W., Golenbock, D. T., Christ, W. J., & Gusovsky, F. (1999). Toll-like receptor-4 mediates lipopolysaccharide-induced signal transduction. *Journal of Biological Chemistry*, *274*(16), 10689–10692. http://doi.org/10.1074/jbc.274.16.10689

Cohen, G. (1983). The pathobiology of Parkinson's disease: biochemical aspects of dopamine neuron senescence. *Journal of Neural Transmission. Supplementum*, *19*, 89–103. Retrieved from http://www.ncbi.nlm.nih.gov/pubmed/6321651

Cohen, G., & Spina, M. B. (1988). Hydrogen Peroxide Production in Dopamine Neurons: Implications for Understanding Parkinson's Disease. *Progress in Parkinson Research*, 119–126. Retrieved from https://link.springer.com/chapter/10.1007/978-1-4613-0759-4_15

Colton, C., Wilt, S., Gilbert, D., Chernyshev, O., Snell, J., & Dubois-Dalcq, M. (1996). Species differences in the generation of reactive oxygen species by microglia. *Molecular and Chemical Neuropathology / Sponsored by the International Society for Neurochemistry and the World Federation of Neurology and Research Groups on Neurochemistry and Cerebrospinal Fluid*, *28*(1–3), 15–20. http://doi.org/10.1007/BF02815200

Conde, J. R., & Streit, W. J. (2006). Microglia in the aging brain. *Journal of Neuropathology and Experimental Neurology*, *65*(3), 199–203.

Connolly, B. S., & Lang, A. E. (2014). Pharmacological treatment of Parkinson disease: a review. *JAMA: The Journal of the American Medical Association*, *311*(16), 1670–83. http://doi.org/10.1001/jama.2014.3654

Connor, J. R., Phillips, T. M., Lakshman, M. R., Barron, K. D., Fine, R. E., & Csiza, C. K. (1987). Regional Variation in the Levels of Transferrin in the CNS of Normal and Myelin-Deficient Rats. *Journal of Neurochemistry*, *49*(5), 1523–1529.

Connor, J. R., Boeshore, K. L., Benkovic, S. A., & Menzies, S. L. (1994). Isoforms of ferritin have a specific cellular distribution in the brain. *Journal of Neuroscience Research*, *37*(4), 461–465. http://doi.org/10.1002/jnr.490370405

Connor, J. R., & Menzies, S. L. (1996). Relationship of iron to oligodendrocytes and myelination. *GLIA*, *17*(2), 83–93.

Contin, M., & Martinelli, P. (2010). Pharmacokinetics of levodopa. *Journal of Neurology*, 257. http://doi.org/10.1007/s00415-010-5728-8

Coraci, I. S., Husemann, J., Berman, J. W., Hulette, C., Dufour, J. H., Campanella, G. K., El Khoury, J. B. (2002). CD36, a Class B Scavenger Receptor, Is Expressed on Microglia in Alzheimer's Disease Brains and Can Mediate Production of Reactive Oxygen Species in Response to β-Amyloid Fibrils. *The American Journal of Pathology*, *160*(1), 101–112. http://doi.org/10.1016/S0002-9440(10)64354-4

Correa, F., Mallard, C., Nilsson, M., & Sandberg, M. (2011). Activated microglia decrease histone acetylation and Nrf2-inducible anti-oxidant defence in astrocytes: Restoring effects of inhibitors of HDACs, p38 MAPK and GSK3 *Neurobiology of Disease*, *44*(1), 142–151. http://doi.org/10.1016/j.nbd.2011.06.016

Coyle, D. E. (1995). Adaptation of C6 glioma cells to serum-free conditions leads to the expression of a mixed astrocyte-oligodendrocyte phenotype and increased production of neurite promoting activity. *Journal of Neuroscience Research*, *41*(3), 374–385. http://doi.org/10.1002/jnr.490410310

Crompton, D. E., Chinnery, P. F., Fey, C., Curtis, A. R. J., Morris, C. M., Kierstan, J., Burn, J. (2002). Neuroferritinopathy: A Window on the Role of Iron in Neurodegeneration. *Blood Cells, Molecules, and Diseases*, *29*(3), 522–531. http://doi.org/10.1006/bcmd.2002.0589

Cumings, J. N. (1948). The copper and iron content of brain and liver in the normal and in hepato-lenticular degeneration. *Journal of Trace Elements in Experimental Medicine*, *71*(4), 410–415. http://doi.org/10.1002/jtra.1025

Dallman, P. R., Siimes, M. A., & Manies, E. C. (1975). Brain Iron: Persistent Deficiency following Short-term Iron Deprivation in the Young Rat. *British Journal of Haematology*, *31*(2), 209–215. http://doi.org/10.1111/j.1365-2141.1975.tb00851.x

Das, A., Belagodu, A., Reiter, R. J., Ray, S. K., & Banik, N. L. (2008). Cytoprotective effects of melatonin on C6 astroglial cells exposed to glutamate excitotoxicity and oxidative stress. *Journal of Pineal Research*, *45*(2), 117–124. http://doi.org/10.1111/j.1600-079X.2008.00582.x

Daugherty, A., & Raz, N. (2013). Age-related differences in iron content of subcortical nuclei observed in vivo: A meta-analysis. *NeuroImage*, *70*, 113–121. http://doi.org/10.1016/j.neuroimage.2012.12.040

Dawson, T. M., Dawson, V. L., & Snyder, S. H. (1992). A novel neuronal messenger molecule in brain: the free radical, nitric oxide. *Annals of Neurology*, *32*(3), 297–311. http://doi.org/10.1002/ana.410320302

Dawson, T. M., Ko, H. S., & Dawson, V. L. (2010). Genetic Animal Models of Parkinson's Disease. *Neuron*. http://doi.org/10.1016/j.neuron.2010.04.034

Dayani, P. N., Bishop, M. C., Black, K., & Zeltzer, P. M. (2004). Desferoxamine (DFO)--mediated iron chelation: rationale for a novel approach to therapy for brain cancer. *Journal of Neuro-Oncology*, *67*, 367–377. http://doi.org/10.1023/B:NEON.0000024238.21349.37

De Domenico, I., Vaughn, M. B., Li, L., Bagley, D., Musci, G., Ward, D. M., & Kaplan, J. (2006). Ferroportin-mediated mobilization of ferritin iron precedes ferritin degradation by the proteasome. *The EMBO Journal*, *25*(22), 5396–5404. http://doi.org/10.1038/sj.emboj.7601409

De Domenico, I., Ward, D. M., di Patti, M. C. B., Jeong, S. Y., David, S., Musci, G., & Kaplan, J. (2007). Ferroxidase activity is required for the stability of cell surface ferroportin in cells expressing GPI-ceruloplasmin. *The EMBO Journal*, *26*(12), 2823–2831. http://doi.org/10.1038/sj.emboj.7601735

de Lau, L. M. L., Breteler, M. M. B., Greenamyre, J., Hastings, T., Litvan, I., Bhatia, K. (2006). Epidemiology of Parkinson's disease. *The Lancet. Neurology*, *5*(6), 525–35. http://doi.org/10.1016/S1474-4422(06)70471-9

de Rijk, M. C., Tzourio, C., Breteler, M. M., Dartigues, J. F., Amaducci, L., Lopez-Pousa, S., Rocca, W. A. (1997). Prevalence of parkinsonism and Parkinson's disease in Europe: the EUROPARKINSON Collaborative Study. European Community Concerted Action on the Epidemiology of Parkinson's disease. *Journal of Neurology, Neurosurgery, and Psychiatry*, *62*(1), 10–5. http://doi.org/10.1136/JNNP.62.1.10

Dean, J. M., Wang, X., Kaindl, A. M., Gressens, P., Fleiss, B., Hagberg, H., & Mallard, C. (2010). Microglial MyD88 signaling regulates acute neuronal toxicity of LPS-stimulated microglia in vitro. *Brain, Behavior, and Immunity*, *24*(5), 776–783. http://doi.org/10.1016/j.bbi.2009.10.018

Deas, E., Cremades, N., Angelova, P. R., Ludtmann, M. H. R., Yao, Z., Chen, S., Abramov, A. Y. (2016). Alpha-Synuclein Oligomers Interact with Metal Ions to Induce Oxidative Stress and Neuronal Death in Parkinson's Disease. *Antioxidants & Redox Signaling*, *24*(7), 376–391. http://doi.org/10.1089/ars.2015.6343

Demopoulos, H., Flamm, E., Seligman, M., Pietronigro, D., Tomasula, J., & DeCrescito, V. (1982). Further studies on free-radical pathology in the major central nervous system disorders: effect of very high doses of methylprednisolone on the functional outcome, morphology, and chemistry of experimental spinal cord impact injury. *Canadian Journal of Physiology and Pharmacology*, *60*, 1415–1424.

Desagher, S., Glowinski, J., & Premont, J. (1996). Astrocytes Protect Neurons from Hydrogen Peroxide Toxicity. *The Journal of Neuroscience*, *16*(8), 2553–2562.

Devasagayam, T. P. A., Tilak, J., Boloor, K. K., Sane, K. S., Ghaskadbi, S. S., & Lele, R. D. (2004). Free radicals and antioxidants in human health: current status and future prospects. *J Assoc Physicians India*, *52*(October), 794–804. http://doi.org/10.1016/S0300-483X(03)00149-5

Devos, D., Moreau, C., Devedjian, J. C., Kluza, J., Petrault, M., Laloux, C., Bordet, R. (2014). Targeting Chelatable Iron as a Therapeutic Modality in Parkinson's Disease. *Antioxidants & Redox Signaling*, *21*(2), 195–210. http://doi.org/10.1089/ars.2013.5593

Dexter, D. T., Wells, F. R., Agid, F., Agid, Y., Lees, A. J., Jenner, P., & Marsden, C. D. (1987). INCREASED NIGRAL IRON CONTENT IN POSTMORTEM PARKINSONIAN BRAIN. *The Lancet*. http://doi.org/10.1016/S0140-6736(87)91361-4

Dexter, D. T., Wells, F. R., Lee, A. J., Agid, F., Agid, Y., Jenner, P., & Marsden, C. D. (1989). Increased Nigral Iron Content and Alterations in Other Metal Ions Occurring in Brain in Parkinson's Disease. *Journal of Neurochemistry*, *52*(6), 1830–1836. http://doi.org/10.1111/j.1471-4159.1989.tb07264.x

Dexter, D. T., Carayon, A., Vidailhet, M., Ruberg, M., Agid, F., Agid, Y., Marsden, C. D. (1990). Decreased Ferritin Levels in Brain in Parkinson's Disease. *Journal of Neurochemistry*, *55*(1), 16–20. http://doi.org/10.1111/j.1471-4159.1990.tb08814.x

Dexter, D. T., Jenner, P., Schapira, A. H. V, & Marsden, C. D. (1992). Alterations in levels of iron, ferritin, and other trace metals in neurodegenerative diseases affecting the basal ganglia. *Annals of Neurology*, *32*(1 S), S94–S100. http://doi.org/10.1002/ana.410320716

Dexter, D. T., & Jenner, P. (2013). Parkinson disease: from pathology to molecular disease mechanisms. *Free Radical Biology and Medicine*, *62*, 132–144.

Dhanasekaran, A., Kotamraju, S., Kalivendi, S. V., Matsunaga, T., Shang, T., Keszler, A., Kalyanaraman, B. (2004). Supplementation of endothelial cells with mitochondria-targeted antioxidants inhibit peroxide-induced mitochondrial iron uptake, oxidative damage, and apoptosis. *Journal of Biological Chemistry*, *279*(36), 37575–37587.

Di Nottia, M., Masciullo, M., Verrigni, D., Petrillo, S., Modoni, A., Rizzo, V., Silvestri, G. (2017). DJ-1 modulates mitochondrial response to oxidative stress: clues from a novel diagnosis of PARK7. *Clinical Genetics*, *92*(1), 18–25. http://doi.org/10.1111/cge.12841

Dixon, S. J., Lemberg, K. M., Lamprecht, M. R., Skouta, R., Zaitsev, E. M., Gleason, C. E., Stockwell, B. R. (2012). Ferroptosis: An iron-dependent form of nonapoptotic cell death. *Cell*, *149*(5), 1060–1072. http://doi.org/10.1016/j.cell.2012.03.042

Do Van, B., Gouel, F., Jonneaux, A., Timmerman, K., Gelé, P., Pétrault, M., Devedjian, J. C. (2016). Ferroptosis, a newly characterized form of cell death in Parkinson's disease that is regulated by PKC. *Neurobiology of Disease*, *94*, 169–178. http://doi.org/10.1016/j.nbd.2016.05.011

Doder, M., Jahanshahi, M., Turjanski, N., Moseley, I. F., & Lees, A. J. (1999). Parkinson's syndrome after closed head injury: a single case report. *Journal of Neurology, Neurosurgery, and Psychiatry*, *66*(3), 380–385.

Dognin, J., & Crichton, R. R. (1975). Mobilisation of Iron from Ferritin Fractions of Defined Iron Content by Biological Reductants. *FEBS Letters*, *54*(2), 234–236.

Dorsey, E. R., Constantinescu, R., Thompson, J. P., Biglan, K. M., Holloway, R. G., Kieburtz, K., … Tanner, C. M. (2007). Projected number of people with Parkinson disease in the most populous nations, 2005 through 2030. *Neurology*. http://doi.org/10.1212/01.wnl.0000247740.47667.03

Dringen, R., & Hamprecht, B. (1997). Involvement of glutathione peroxidase and catalase in the disposal of exogenous hydrogen peroxide by cultured astroglial cells. *Brain Research*, *759*(1), 67–75. http://doi.org/10.1016/S0006-8993(97)00233-3

Dringen, R., Kussmaul, L., & Hamprecht, B. (1998). Detoxification of exogenous hydrogen peroxide and organic hydroperoxides by cultured astroglial cells assessed by microtiter plate assay. *Brain Research Protocols*, *2*(3), 223–228. http://doi.org/10.1016/S1385-299X(97)00047-0

Dringen, R., Kussmaul, L., Gutterer, J. M., Hirrlinger, J., & Hamprecht, B. (1999). The glutathione system of peroxide detoxification is less efficient in neurons than in astroglial cells. *Journal of Neurochemistry*, *72*(6), 2523–2530. http://doi.org/10.1046/j.1471-4159.1999.0722523.x

Dringen, R., Pfeiffer, B., & Hamprecht, B. (1999). Synthesis of the Antioxidant Glutathione in Neurons: Supply by Astrocytes of CysGly as Precursor for Neuronal Glutathione. *The Journal of Neuroscience*, *19*(2), 562–569.

Dringen, R., Gutterer, J. M., & Hirrlinger, J. (2000). Glutathione metabolism in brain. *European Journal of Biochemistry*, *267*(16), 4912–4916. http://doi.org/10.1046/j.1432-1327.2000.01597.x

Dringen, R., Pawlowski, P. G., & Hirrlinger, J. (2005). Peroxide detoxification by brain cells. In *Journal of Neuroscience Research* (Vol. 79, pp. 157–165). http://doi.org/10.1002/jnr.20280

Dringen, R., Bishop, G. M., Koeppe, M., Dang, T. N., & Robinson, S. R. (2007). The pivotal role of astrocytes in the metabolism of iron in the brain. *Neurochemical Research*, *32*(11), 1884–1890. http://doi.org/10.1007/s11064-007-9375-0

Dröge, W. (2002). Free Radicals in the Physiological Control of Cell Function. *Physiological Reviews*, *82*(1), 47–95. http://doi.org/10.1152/physrev.00018.2001

Du, F., Qian, Z. M., Luo, Q., Yung, W. H., & Ke, Y. (2015). Hepcidin Suppresses Brain Iron Accumulation by Downregulating Iron Transport Proteins in Iron-Overloaded Rats. *Molecular Neurobiology*, *52*(1), 101–114. http://doi.org/10.1007/s12035-014-8847-x

Eddleston, M., & Mucke, L. (1993). Molecular profile of reactive astrocytes- implications for their role in neurologic disease. *Neuroscience*, *54*(1), 15–36. http://doi.org/10.1016/0306-4522(93)90380-X

Elbaz, A., Carcaillon, L., Kab, S., & Moisan, F. (2016). Epidemiology of Parkinson's disease. *Revue Neurologique*. http://doi.org/10.1016/j.neurol.2015.09.012

Eng, L. F., Ghirnikar, R. S., & Lee, Y. L. (2000). Glial Fibrillary Acidic Protein : GFAP-Thirty-One Years (1969-2000). *Neurochemical Research*, *25*(9–10), 1439–1451. http://doi.org/10.1023/A:1007677003387

Epsztejn, S., Kakhlon, O., Glickstein, H., Breuer, W., & Ioav Cabantchik, Z. (1997). Fluorescence Analysis of the Labile Iron Pool of Mammalian Cells. *Analytical Biochemistry*, *248*(248), 31–40. http://doi.org/10.1006/abio.1997.2126

Fahmy, M., & Young, S. P. (1993). Modulation of iron metabolism in monocyte cell line U937 by inflammatory cytokines: changes in transferrin uptake, iron handling and ferritin mRNA. *The Biochemical Journal*, *296* (1), 175–181.

Fahn, S., & Cohen, G. (1992). The oxidant stress hypothesis in Parkinson's disease: evidence supporting it. *Ann Neurol*, *32*(6), 804–812. http://doi.org/10.1002/ana.410320616

Fahn, S., Oakes, D., Shoulson, I., Kieburtz, K., Rudolph, A., Lang, A., Parkinson Study Group. (2004). Levodopa and the Progression of Parkinson's Disease. *New England Journal of Medicine*, *351*(24), 2498–2508. http://doi.org/10.1056/NEJMoa033447

Fang, F., Chen, H., Feldman, A. L., Kamel, F., Ye, W., & Wirdefeldt, K. (2012). Head injury and Parkinson's disease: a population-based study. *Movement Disorders: Official Journal of the Movement Disorder Society*, *27*(13), 1632–5.

Faucheux, B. A., Hauw, J. J., Agid, Y., & Hirsch, E. C. (1997). The density of [125I]-transferrin binding sites on perikarya of melanized neurons of the substantia nigra is decreased in Parkinson's disease. *Brain Research*, *749*(1), 170–174. http://doi.org/10.1016/S0006-8993(96)01412-6

Faucheux, B. A., Martin, M. E., Beaumont, C., Hunot, S., Hauw, J. J., Agid, Y., & Hirsch, E. C. (2002). Lack of up-regulation of ferritin is associated with sustained iron regulatory protein-1 binding activity in the substantia nigra of patients with Parkinson's disease. *Journal of Neurochemistry*, *83*(2), 320–330.

Faulkner, J. R. (2004). Reactive Astrocytes Protect Tissue and Preserve Function after Spinal Cord Injury. *Journal of Neuroscience*, *24*(9), 2143–2155. http://doi.org/10.1523/JNEUROSCI.3547-03.2004

Fawcett, J. W., & Asher, R. A. (1999). The glial scar and central nervous system repair. *Brain Research Bulletin*. http://doi.org/10.1016/S0361-9230(99)00072-6

Fedorow, H., Tribl, F., Halliday, G., Gerlach, M., Riederer, P., & Double, K. L. (2005). Neuromelanin in human dopamine neurons: Comparison with peripheral melanins and relevance to Parkinson's disease. *Progress in Neurobiology*. http://doi.org/10.1016/j.pneurobio.2005.02.001

Feinstein, D. L., Galea, E., Roberts, S., Berquist, H., Wang, H., & Reis, D. J. (1994). Induction of nitric oxide synthase in rat C6 glioma cells. *Journal of Neurochemistry*, *62*(1), 315–321.

Fernandez, I., Mendes, C., Fabres, T., Troncoso, M., Andrade, M., Furuguen, A., Assumpcao, M. (2016). Concentration and time dependent predictive analysis of hydrogen peroxide as a pro-oxidant agent in boar sperm, and it intracellular and extracellular detection by luminescent and fluorescent probes. *Animal Reproduction Science*, *169*, 108–109.

Fields, R. D., & Stevens, B. (2000). ATP: An extracellular signaling molecule between neurons and glia. *Trends in Neurosciences*. http://doi.org/10.1016/S0166-2236(00)01674-X

Fink, S. L., & Cookson, B. T. (2005). Apoptosis, pyroptosis, and necrosis: Mechanistic description of dead and dying eukaryotic cells. *Infection and Immunity*. http://doi.org/10.1128/IAI.73.4.1907-1916.2005

Fish, W. W. (1988). Rapid Colorimetric Micromethod for the Quantitation of Complexed Iron in Biological Samples. *Methods in Enzymology*, 54:*158*(C), 357–364. http://doi.org/10.1016/0076-6879(88)58067-9

Flier, J., van Muiswinkel, F. L., Jongenelen, C. a. M., & Drukarch, B. (2002). The Neuroprotective Antioxidant α-lipoic Acid Induces Detoxication Enzymes in Cultured Astroglial Cells. *Free Radical Research*, *36*(6), 695–699. http://doi.org/10.1080/10715760290029155

Focht, S. J., Snyder, B. S., Beard, J. L., Van Gelder, W., Williams, L. R., & Connor, J. R. (1997). Regional distribution of iron, transferrin, ferritin, and oxidatively- modified proteins in young and aged Fischer 344 rat brains. *Neuroscience*, *79*(1), 255–261. http://doi.org/10.1016/S0306-4522(96)00607-0

Fong, K. L., McCay, P. B., Poyer, J. L., Keele, B. B., & Misra, H. (1973). Evidence that peroxidation of lysosomal membranes is initiated by hydroxyl free radicals produced during flavin enzyme activity. *Journal of Biological Chemistry*, *248*(22), 7792–7797.

Ford, P. C., Wink, D. A., & Stanbury, D. M. (1993). Autoxidation kinetics of aqueous nitric oxide. *FEBS Letters*. http://doi.org/10.1016/0014-5793(93)81748-O

Forni, G. L., Balocco, M., Cremonesi, L., Abbruzzese, G., Parodi, R. C., & Marchese, R. (2008). Regression of symptoms after selective iron chelation therapy in a case of neurodegeneration with brain iron accumulation. *Movement Disorders*, *23*(6), 905–908. http://doi.org/10.1002/mds.22002

Foury, F., & Cazzalini, O. (1997). Deletion of the yeast homologue of the human gene associated with Friedreich's ataxia elicits iron accumulation in mitochondria. *FEBS Letters*, *411*(2–3), 373–377. http://doi.org/10.1016/S0014-5793(97)00734-5

Frankola, K. A., Greig, N. H., Luo, W., & Tweedie, D. (2011). Targeting TNF-α to elucidate and ameliorate neuroinflammation in neurodegenerative diseases. *CNS & Neurological Disorders Drug Targets*, *10*(3), 391–403. http://doi.org/10.2174/187152711794653751

Fu, R., Shen, Q., Xu, P., Luo, J. J., & Tang, Y. (2014). Phagocytosis of microglia in the central nervous system diseases. *Molecular Neurobiology*, *49*(3), 1422–1434. http://doi.org/10.1007/s12035-013-8620-6

Fullerton, H. J., Ditelberg, J. S., Chen, S. F., Sarco, D. P., Chan, P. H., Epstein, C. J., & Ferriero, D. M. (1998). Copper/zinc superoxide dismutase transgenic brain accumulates hydrogen peroxide after perinatal hypoxia ischemia. *Annals of Neurology*, *44*(3), 357–364. http://doi.org/10.1002/ana.410440311

Funk, F., Lenders, J. P., Crichton, R. R., & Schneider, W. (1985). Reductive mobilisation of ferritin iron. *European Journal of Biochemistry*, *152*(1), 167–172. http://doi.org/10.1111/j.1432-1033.1985.tb09177.x

Gadient, R. A., & Otten, U. H. (1997). Interleukin-6 (IL-6)- A molecule with both beneficial and destructive potentials. *Progress in Neurobiology*. http://doi.org/10.1016/S0301-0082(97)00021-X

Gajjar, T. M., Anderson, L. I., & Dluzen, D. E. (2003). Acute effects of estrogen upon methamphetamine induced neurotoxicity of the nigrostriatal dopaminergic system. *Journal of Neural Transmission*, *110*(11), 1215–1224. http://doi.org/10.1007/s00702-003-0045-3

Galazka-Friedman, J., Friedman, A., & Bauminger, E. R. (2008). Iron in the brain. *Hyperfine Interactions*, *189*(1–3), 31–37. http://doi.org/10.1007/s10751-009-9926-7

Galea, E., Feinstein, D. L., & Reis, D. J. (1992). Induction of calcium-independent nitric oxide synthase activity in primary rat glial cultures. *Proc. Natl. Acad. Sci. U. S. A.*, *89*(22), 10945–10949. http://doi.org/10.1073/pnas.89.22.10945

Ganz, T. (2003). Hepcidin, a key regulator of iron metabolism and mediator of anemia of inflammation. *Blood*. http://doi.org/10.1182/blood-2003-03-0672

Ganz, T., & Nemeth, E. (2011). Hepcidin and Disorders of Iron Metabolism. *Annual Review of Medicine*, *62*(1), 347–360. http://doi.org/10.1146/annurev-med-050109-142444

Ganz, T., & Nemeth, E. (2012). Hepcidin and iron homeostasis. *Biochimica et Biophysica Acta - Molecular Cell Research*. http://doi.org/10.1016/j.bbamcr.2012.01.014

Gao, Z., Huang, K., Yang, X., & Xu, H. (1999). Free radical scavenging and antioxidant activities of flavonoids extracted from the radix of Scutellaria baicalensis Georgi. *Biochimica et Biophysica Acta - General Subjects*, *1472*(3), 643–650. http://doi.org/10.1016/S0304-4165(99)00152-X

Gao, H. M., Jiang, J., Wilson, B., Zhang, W., Hong, J. S., & Liu, B. (2002). Microglial activation-mediated delayed and progressive degeneration of rat nigral dopaminergic neurons: Relevance to Parkinson's disease. *Journal of Neurochemistry*, *81*(6), 1285–1297. http://doi.org/10.1046/j.1471-4159.2002.00928.x

Gao, H.-M., Liu, B., & Hong, J.-S. (2003). Critical role for microglial NADPH oxidase in rotenone-induced degeneration of dopaminergic neurons. *The Journal of Neuroscience: The Official Journal of the Society for Neuroscience*, *23*(15), 6181–6187. http://doi.org/23/15/6181

Gao, X., Chen, H., Schwarzschild, M. A., & Ascherio, A. (2011). Use of ibuprofen and risk of Parkinson disease. *Neurology*, *76*(10), 863–869.

Gao, J., Liu, R., Zhao, E., Huang, X., Nalls, M. A., Singleton, A. B., & Chen, H. (2015). Head injury, potential interaction with genes, and risk for Parkinson's disease. *Parkinsonism & Related Disorders*, *21*(3), 292–6. http://doi.org/10.1016/j.parkreldis.2014.12.033

Garden, G. A., & Möller, T. (2006). Microglia biology in health and disease. *Journal of Neuroimmune Pharmacology*. http://doi.org/10.1007/s11481-006-9015-5

Garrick, L. M., Dolan, K. G., Romano, M. A., & Garrick, M. D. (1999). Non-transferrin-bound iron uptake in Belgrade and normal rat erythroid cells. *Journal of Cellular Physiology*, *178*(3), 349–358. http://doi.org/10.1002/(SICI)1097-4652(199903)178:3<349::AID-JCP9>3.0.CO;2-R

Genis, L., Dávila, D., Fernandez, S., Pozo-Rodrigálvarez, A., Martínez-Murillo, R., & Torres-Aleman, I. (2014). Astrocytes require insulin-like growth factor I to protect neurons against oxidative injury. *F1000Research*. http://doi.org/10.12688/f1000research.3-28.v1

Gerhard, A., Pavese, N., Hotton, G., Turkheimer, F., Es, M., Hammers, A., Brooks, D. J. (2006). In vivo imaging of microglial activation with [11C](R)-PK11195 PET in idiopathic Parkinson's disease. *Neurobiology of Disease*, *21*(2), 404–412. http://doi.org/10.1016/j.nbd.2005.08.002

Gerlach, M., Ben-Shachar, D., Riederer, P., & Youdim, M. B. (1994). Altered brain metabolism of iron as a cause of neurodegenerative diseases? *Journal of Neurochemistry*, *63*(3), 793–807. http://doi.org/10.1046/j.1471-4159.1994.63030793.x

Gibbons, H. M., & Dragunow, M. (2006). Microglia induce neural cell death via a proximity-dependent mechanism involving nitric oxide. *Brain Research*, *1084*(1), 1–15. http://doi.org/10.1016/j.brainres.2006.02.032

Giulian, D., Woodward, J., Young, D. G., Krebs, J. F., & Lachman, L. B. (1988). Interleukin-1 injected into mammalian brain stimulates astrogliosis and neovascularization. *The Journal of Neuroscience: The Official Journal of the Society for Neuroscience*, *8*(7), 2485–2490.

Giulian, D., Vaca, K., & Corpuz, M. (1993). Brain glia release factors with opposing actions upon neuronal survival. *The Journal of Neuroscience: The Official Journal of the Society for Neuroscience*, *13*(1), 29–37. Retrieved from http://www.ncbi.nlm.nih.gov/pubmed/8423475

Glenn, J. A., Ward, S. A., Stone, C. R., Booth, P. L., & Thomas, W. E. (1992). Characterisation of ramified microglial cells: detailed morphology, morphological plasticity and proliferative capability. *J. Anat*, *180*, 109–118.

Glezer, I., Simard, A. R., & Rivest, S. (2007). Neuroprotective role of the innate immune system by microglia. *Neuroscience*. http://doi.org/10.1016/j.neuroscience.2007.02.055

Gluck, M., Ehrhart, J., Jayatilleke, E., & Zeevalk, G. D. (2002). Inhibition of brain mitochondrial respiration by dopamine: Involvement of H2O2 and hydroxyl radicals but not glutathione-protein-mixed disulfides. *Journal of Neurochemistry*, *82*(1), 66–74. http://doi.org/10.1046/j.1471-4159.2002.00938.x

Goedert, M. (2001). Alpha-synuclein and neurodegenerative diseases. *Nature Reviews. Neuroscience*, *2*(7), 492–501. http://doi.org/10.1038/35081564

Good, P. F., Hsu, A., Werner, P., Perl, D. P., & Olanow, C. W. (1998). Protein Nitration in Parkinson′s Disease. *Journal of Neuropathology and Experimental Neurology*, *57*(4), 338–342. http://doi.org/10.1097/00005072-199804000-00006

Goodwin, C.J., Holt, S.J., Downes, S., & Marshall, N.J. (1995). Microculture tetrazolium assays: a comparison between two new tetrazolium salts, XTT and MTS. *Journal of Immunological Methods*, *179*(1), 95–103. http://doi.org/10.1016/0022-1759(94)00277-4

Gordon, J., Amini, S., & White, M. K. (2013). General overview of neuronal cell culture. *Methods in Molecular Biology*. http://doi.org/10.1007/978-1-62703-640-5_1

Gorell, J., Ordidge, R., Brown, G., Deniau, J., Buderer, N., & Helpern, J. (1995). Increased iron-related MRI contrast in the substantia nigra in Parkinson's disease. *Neurology*, *45*(6), 1138–43. http://doi.org/10.1212/WNL.45.6.1138

Gorina, R., Font-Nieves, M., Márquez-Kisinousky, L., Santalucia, T., & Planas, A. M. (2011). Astrocyte TLR4 activation induces a proinflammatory environment through the interplay between MyD88-dependent NFκB signaling, MAPK, and Jak1/Stat1 pathways. *GLIA*, *59*(2), 242–255. http://doi.org/10.1002/glia.21094

Goswami, P., Gupta, S., Joshi, N., Sharma, S., & Singh, S. (2015). Astrocyte activation and neurotoxicity: A study in different rat brain regions and in rat C6 astroglial cells. *Environmental Toxicology and Pharmacology*, *40*(1), 122–139. http://doi.org/10.1016/j.etap.2015.06.001

Gottlieb, E., Armour, S., Harris, M., & Thompson, C. (2003). Mitochondrial membrane potential regulates matrix configuration and cytochrome c release during apoptosis. *Cell Death and Differentiation*, *10*, 709–717. http://doi.org/10.1038/

Granger, D. L., Taintor, R. R., Boockvar, K. S., & Hibbs, J. J. B. (1995). Determination of Nitrate and Nitrite in Biological Samples Using Bacterial Nitrate Reductase Coupled with the Griess Reaction. *Methods*, *7*(1), 78–83. http://doi.org/10.1006/meth.1995.1011

Greenamyre, J. T., Sherer, T. B., Betarbet, R., & Panov, A. V. (2001). Complex I and Parkinson's Disease. *IUBMB Life*, *52*, 135–141.

Grimbergen, Y. a M., Langston, J. W., Roos, R. a C., & Bloem, B. R. (2009). Postural instability in Parkinson's disease: the adrenergic hypothesis and the locus coeruleus. *Expert Review of Neurotherapeutics*, *9*(2), 279–290. http://doi.org/10.1586/14737175.9.2.279

Guevara, I., Iwanejko, J., Dembinska-Kiec, A., Pankiewicz, J., Wanat, A., Anna, P., Szczudlik, A. (1998). Determination of nitrite/nitrate in human biological material by the simple Griess reaction. *Clinica Chimica Acta*, *274*(2), 177–188. http://doi.org/10.1016/S0009-8981(98)00060-6

Gunnersen, J. M., Spirkoska, V., Smith, P. E., Danks, R., & Tan, S. S. (2000). Growth and migration markers of rat C6 glioma cells identified by serial analysis of gene expression. *Glia*, *32*(2), 146–54. http://doi.org/10.1002/1098-1136(200011)32:2<146::AID-GLIA40>3.0.CO;2-3 [pii]

Haacke, E. M., Makki, M., Ge, Y., Maheshwari, M., Sehgal, V., Hu, J., Grossman, R. I. (2009). Characterizing iron deposition in multiple sclerosis lesions using susceptibility weighted imaging. *Journal of Magnetic Resonance Imaging*, *29*(3), 537–544. http://doi.org/10.1002/jmri.21676

Haas, J., Storch-Hagenlocher, B., Biessmann, A., & Wildemann, B. (2002). Inducible nitric oxide synthase and argininosuccinate synthetase: co-induction in brain tissue of patients with Alzheimer's dementia and following stimulation with beta-amyloid 1-42 in vitro. *Neurosci Lett*, *322*(2), 121–125. http://doi.org/S0304394002000952 [pii]

Haavik, J., Almås, B., & Flatmark, T. (1997). Generation of reactive oxygen species by tyrosine hydroxylase: a possible contribution to the degeneration of dopaminergic neurons? *Journal of Neurochemistry*, *68*(1), 328–332. http://doi.org/10.1046/j.1471-4159.1997.68010328.x

Haaxma, C., Bloem, B. R., Borm, G. F., Oyen, W. J. G., Leenders, K. L., Eshuis, S., Shulman, L. M. (2007). Gender Differences in Parkinson's Disease. *Journal of Neurology, Neurosurgery, and Psychiatry*, *78*(8), 819–24. http://doi.org/10.1136/jnnp.2006.103788

Haehner, A., Hummel, T., Hummel, C., Sommer, U., Junghanns, S., & Reichmann, H. (2007). Olfactory loss may be a first sign of idiopathic Parkinson's disease. *Movement Disorders*, *22*(6), 839–842. http://doi.org/10.1002/mds.21413

Hallgren, B., & Sourander, P. (1958). The Effect of Age on the Non-Haemin Iron in the Human Brain. *Journal of Neurochemistry*, *3*(1), 41–51. http://doi.org/10.1111/j.1471-4159.1958.tb12607.x

Halliwell, B. (1987). Oxidants and human disease: Some new concepts. *FASEB Journal*, *1*(5), 358–364.

Han, J., Cheng, F. C., Yang, Z., & Dryhurst, G. (1999). Inhibitors of mitochondrial respiration, iron (II), and hydroxyl radical evoke release and extracellular hydrolysis of glutathione in rat striatum and substantia nigra: Potential implications to Parkinson's disease. *Journal of Neurochemistry*, *73*(4), 1683–1695. http://doi.org/10.1046/j.1471-4159.1999.731683.x

Hare, D., Reedy, B., Grimm, R., Wilkins, S., Volitakis, I., George, J. L., Doble, P. (2009). Quantitative elemental bio-imaging of Mn, Fe, Cu and Zn in 6-hydroxydopamine induced Parkinsonism mouse models. *Metallomics*, *1*(1), 53. http://doi.org/10.1039/b816188g

Hare, D., Ayton, S., Bush, A., & Lei, P. (2013). A delicate balance: Iron metabolism and diseases of the brain. *Frontiers in Aging Neuroscience*. http://doi.org/10.3389/fnagi.2013.00034

Harrison, P. M., & Arosio, P. (1996). The ferritins: Molecular properties, iron storage function and cellular regulation. *Biochimica et Biophysica Acta - Bioenergetics*. http://doi.org/10.1016/0005-2728(96)00022-9

Hashimoto, M., Hsu, L. J., Xia, Y., Takeda, a, Sisk, a, Sundsmo, M., & Masliah, E. (1999). Oxidative stress induces amyloid-like aggregate formation of NACP/alpha-synuclein in vitro. *Neuroreport*, *10*(4), 717–721. http://doi.org/10.1097/00001756-199903170-00011

He, Q., Du, T., Yu, X., Xie, A., Song, N., Kang, Q., … Jiang, H. (2011). DMT1 polymorphism and risk of Parkinson's disease. *Neuroscience Letters*, *501*(3), 128–131. http://doi.org/10.1016/j.neulet.2011.07.001

He, Q., Song, N., Xu, H., Wang, R., Xie, J., & Jiang, H. (2011). Alpha-synuclein aggregation is involved in the toxicity induced by ferric iron to SK-N-SH neuroblastoma cells. *Journal of Neural Transmission (Vienna, Austria: 1996)*, *118*(3), 397–406. http://doi.org/10.1007/s00702-010-0453-0

Hellemans, J., Mortier, G., De Paepe, A., Speleman, F., & Vandesompele, J. (2007). qBase relative quantification framework and software for management and automated analysis of real-time quantitative PCR data. *Genome Biology*, *8*(2), R19. http://doi.org/10.1186/gb-2007-8-2-r19

Hemmer, K., Fransen, L., Vanderstichele, H., Vanmechelen, E., & Heuschling, P. (2001). An in vitro model for the study of microglia-induced neurodegeneration: involvement of nitric oxide and tumor necrosis factor-alpha. *Neurochem Int*, *38*(7), 557–565.

Henchcliffe, C., & Beal, M. F. (2008). Mitochondrial biology and oxidative stress in Parkinson disease pathogenesis. *Nature Clinical Practice. Neurology*, *4*(11), 600–609. http://doi.org/10.1038/ncpneuro0924

Hensley, K., Pye, Q. N., Maidt, M. L., Stewart, C. a, Robinson, K. a, Jaffrey, F., & Floyd, R. a. (1998). Interaction of alpha-phenyl-N-tert-butyl nitrone and alternative electron acceptors with complex I indicates a substrate reduction site upstream from the rotenone binding site. *Journal of Neurochemistry*, *71*(6), 2549–2557. http://doi.org/10.1046/j.1471-4159.1998.71062549.x

Herlinger, E., Jamesonb, R. F., & Linerta, W. (1995). Spontaneous Auxoxidation of Dopamine. *Journal of the Chemical Society, Perkin Transactions 2*, (2), 259–263. Retrieved from http://pubs.rsc.org/en/content/articlepdf/1995/p2/p29950000259

Hermida-Ameijeiras, Á., Méndez-Álvarez, E., Sánchez-Iglesias, S., Sanmartín-Suárez, C., & Soto-Otero, R. (2004). Autoxidation and MAO-mediated metabolism of dopamine as a potential cause of oxidative stress: Role of ferrous and ferric ions. *Neurochemistry International*, *45*(1), 103–116. http://doi.org/10.1016/j.neuint.2003.11.018

Hill, J. M., & Switzer, R. C. (1984). The regional distribution and cellular localization of iron in the rat brain. *Neuroscience*, *11*(3), 595–603. http://doi.org/10.1016/0306-4522(84)90046-0

Hirsch, E. C., & Hunot, S. (2000). Nitric oxide, glial cells and neuronal degeneration in parkinsonism. *Trends in Pharmacological Sciences*. http://doi.org/10.1016/S0165-6147(00)01471-1

Höck, A., Demmel, U., Schicha, H., Kasperek, K., & Feinendegen, L. E. (1975). Trace element concentration in human brain: Activation analysis of cobalt, iron, rubidium, selenium, zinc, chromium, silver, cesium, antimony and scandium. *Brain*, *98*(1), 49–64. http://doi.org/10.1093/brain/98.1.49

Hohaus, S., Massini, G., Giachelia, M., Vannata, B., Bozzoli, V., Cuccaro, A., Leone, G. (2010). Anemia in Hodgkin's lymphoma: The role of interleukin-6 and hepcidin. *Journal of Clinical Oncology*, *28*(15), 2538–2543. http://doi.org/10.1200/JCO.2009.27.6873

Honarmand Ebrahimi, K., Bill, E., Hagedoorn, P.-L., & Hagen, W. R. (2012). The catalytic center of ferritin regulates iron storage via Fe(II)-Fe(III) displacement. *Nature Chemical Biology*, *8*(11), 941–948. http://doi.org/10.1038/nchembio.1071

Hopkin, K. A., Papazian, M. A., & Steinman, H. M. (1992). Functional Differences Between Manganese and Iron Superoxide Dismutases in Escherichia-Coli K-12. *Journal Of Biological Chemistry*, *267*(34), 24253–24258. Retrieved from isi:A1992KA26300020

Hortelano, S., Dallaporta, B., Zamzami, N., Hirsch, T., Susin, S. A., Marzo, I., Kroemer, G. (1997). Nitric oxide induces apoptosis via triggering mitochondrial permeability transition. *FEBS Lett*, *410*(2–3), 373–377. http://doi.org/S0014-5793(97)00623-6 [pii]

Hou, L., Zhou, X., Zhang, C., Wang, K., Liu, X., Che, Y., Hong, J. S. (2017). NADPH oxidase-derived H2O2 mediates the regulatory effects of microglia on astrogliosis in experimental models of Parkinson's disease. *Redox Biology*, *12*, 162–170. http://doi.org/10.1016/j.redox.2017.02.016

Hsu, L. J., Sagara, Y., Arroyo, A., Rockenstein, E., Sisk, A., Mallory, M., Masliah, E. (2000). α-synuclein promotes mitochondrial deficit and oxidative stress. *American Journal of Pathology*, *157*(2), 401–410. http://doi.org/10.1016/S0002-9440(10)64553-1

Hug, S. J., & Leupin, O. (2003). Iron-catalyzed oxidation of Arsenic(III) by oxygen and by hydrogen peroxide: pH-dependent formation of oxidants in the Fenton reaction. *Environmental Science and Technology*, *37*(12), 2734–2742. http://doi.org/10.1021/es026208x

Hughes, A. J., Daniel, S. E., Kilford, L., & Lees, A. J. (1992). Accuracy of clinical diagnosis of idiopathic Parkinson's disease: a clinico-pathological study of 100 cases. *Journal of Neurology, Neurosurgery, and Psychiatry*, *55*(3), 181–4. http://doi.org/10.1136/jnnp.55.3.181

Hunot, S., Boissière, F., Faucheux, B., Brugg, B., Mouatt-Prigent, A., Agid, Y., & Hirsch, E. C. (1996). Nitric oxide synthase and neuronal vulnerability in Parkinson's disease. *Neuroscience*, *72*(2), 355–363. http://doi.org/10.1016/0306-4522(95)00578-1

Huynh, M.-L. N., Fadok, V. A., & Henson, P. M. (2002). Phosphatidylserine-dependent ingestion of apoptotic cells promotes TGF-beta1 secretion and the resolution of inflammation. *The Journal of Clinical Investigation*, *109*(1), 41–50. http://doi.org/10.1172/JCI11638

Hyslop, P. A., Zhang, Z., Pearson, D. V., & Phebus, L. A. (1995). Measurement of striatal H2O2 by microdialysis following global forebrain ischemia and reperfusion in the rat: correlation with the cytotoxic potential of H2O2 in vitro. *Brain Research*, *671*(2), 181–186. http://doi.org/10.1016/0006-8993(94)01291-O

Iannilli, E., Stephan, L., Hummel, T., Reichmann, H., & Haehner, A. (2017). Olfactory impairment in Parkinson's disease is a consequence of central nervous system decline. *Journal of Neurology*, *264*(6), 1236–1246. http://doi.org/10.1007/s00415-017-8521-0

Ikeda, Y., & Long, D. M. (1990). The molecular basis of brain injury and brain edema: The role of oxygen free radicals. *Neurosurgery*. http://doi.org/10.1227/00006123-199007000-00001

Ilyin, G., Courselaud, B., Troadec, M. B., Pigeon, C., Alizadeh, M., Leroyer, P., Loréal, O. (2003). Comparative analysis of mouse hepcidin 1 and 2 genes: Evidence for different patterns of expression and co-inducibility during iron overload. *FEBS Letters*, *542*(1–3), 22–26. http://doi.org/10.1016/S0014-5793(03)00329-6

Infanger, D. W., Sharma, R. V., & Davisson, R. L. (2006). NADPH Oxidases of the Brain: Distribution, Regulation, and Function. *Antioxidants & Redox Signaling*, *8*(9–10), 1583–1596. http://doi.org/10.1089/ars.2006.8.1583

Ishida, Y., Nagai, A., Kobayashi, S., & Kim, S. U. (2006). Upregulation of protease-activated receptor-1 in astrocytes in Parkinson disease: astrocyte-mediated neuroprotection through increased levels of glutathione peroxidase. *Journal of Neuropathology and Experimental Neurology*, *65*(1), 66–77. http://doi.org/10.1097/01.jnen.0000195941.48033.eb

Ito, D., Imai, Y., Ohsawa, K., Nakajima, K., Fukuuchi, Y., & Kohsaka, S. (1998). Microglia-specific localisation of a novel calcium binding protein, Iba1. *Molecular Brain Research*, *57*(1), 1–9. http://doi.org/10.1016/S0169-328X(98)00040-0

Iwata-Ichikawa, E., Kondo, Y., Miyazaki, I., Asanuma, M., & Ogawa, N. (1999). Glial cells protect neurons against oxidative stress via transcriptional up-regulation of the glutathione synthesis. *Journal of Neurochemistry*, *72*(6), 2334–2344. http://doi.org/10.1046/j.1471-4159.1999.0722334.x

Jabs, T. (1999). Reactive oxygen intermediates as mediators of programmed cell death in plants and animals. *Biochemical Pharmacology*, *57*(3), 231–45. http://doi.org/10.1016/s0006-2952(98)00227-5

Jacobson, S. (1963). Sequence of myelinization in the brain of the albino rat. A. Cerebral cortex, thalamus and related structures. *Journal of Comparative Neurology*, *121*(1), 5–29. http://doi.org/10.1002/cne.901210103

Jafari, S., Etminan, M., Aminzadeh, F., & Samii, A. (2013). Head injury and risk of Parkinson disease: a systematic review and meta-analysis. *Movement Disorders : Official Journal of the Movement Disorder Society*, *28*(9), 1222–9. http://doi.org/10.1002/mds.25458

Jefferies, W. A., Brandon, M. R., Hunt, S. V., Williams, A. F., Gatter, K. C., & Mason, D. Y. (1984). Transferrin receptor on endothelium of brain capillaries. *Nature*, *312*(5990), 162–163. http://doi.org/10.1038/312162a0

Jellinger, K., Paulus, W., Grundke-Iqbal, I., Riederer, P., & Youdim, M. B. H. (1990). Brain iron and ferritin in Parkinson's and Alzheimer's diseases. *Journal of Neural Transmission- Parkinson's Disease and Dementia Section*, *2*(4), 327–340. http://doi.org/10.1007/BF02252926

Jenner, P., & Olanow, C. W. (1998). Understanding cell death in Parkinson's disease. *Annals of Neurology*, *44*(3 Suppl 1), S72–S84. http://doi.org/10.1002/ana.410440712

Jenner, P. (2003). Oxidative stress in Parkinson's disease. *Annals of Neurology*, *53 Suppl 3*, S26-36–8. http://doi.org/10.1002/ana.10483

Jeong, S. Y., & David, S. (2003). Glycosylphosphatidylinositol-anchored ceruloplasmin is required for iron efflux from cells in the central nervous system. *Journal of Biological Chemistry*, *278*(29), 27144–27148. http://doi.org/10.1074/jbc.M301988200

Jesberger, J., & Richardson, J. S. (1991). Oxygen free radicals and brain dysfunction. *The International Journal of Neuroscience*, *57*(1–2), 1–17. Retrieved from http://www.ncbi.nlm.nih.gov/pubmed/1938149

Jiang, H., Luan, Z., Wang, J., & Xie, J. (2006). Neuroprotective effects of iron chelator Desferal on dopaminergic neurons in the substantia nigra of rats with iron-overload. *Neurochemistry International*, *49*(6), 605–609.

Jiang, H., Song, N., Xu, H., Zhang, S., Wang, J., & Xie, J. (2010). Up-regulation of divalent metal transporter 1 in 6-hydroxydopamine intoxication is IRE/IRP dependent. *Cell Research*, *20*(3), 345–56. http://doi.org/10.1038/cr.2010.20

Jin, L., Wang, J., Zhao, L., Jin, H., Fei, G., Zhang, Y., Zhong, C. (2011). Decreased serum ceruloplasmin levels characteristically aggravate nigral iron deposition in Parkinson's disease. *Brain*, *134*(1), 50–58. http://doi.org/10.1093/brain/awq319

Johnson, L. V, Walsh, M. L., Bockus, B. J., & Chen, L. B. (1981). Monitoring of relative mitochondrial membrane potential in living cells by fluorescence microscopy. *The Journal of Cell Biology*, *88*(3), 526–35. http://doi.org/10.1083/jcb.88.3.526

Johnson, C. C., Gorell, J. M., Rybicki, B. a, Sanders, K., & Peterson, E. L. (1999). Adult nutrient intake as a risk factor for Parkinson's disease. *Int J Epidemiol*, *28*(6), 1102–1109. http://doi.org/10.1093/ije/28.6.1102

Jung, D. Y., Lee, H., Jung, B.-Y., Ock, J., Lee, M.-S., Lee, W. H., & Suk, K. (2005). TLR4, but not TLR2, signals autoregulatory apoptosis of cultured microglia: a critical role of IFN-beta as a decision maker. *Journal of Immunology (Baltimore, MD: 1950)*, *174*(10), 6467–6476. http://doi.org/10.4049/jimmunol.174.10.6467

Junn, E., & Mouradian, M. M. (2002). Human α-Synuclein over-expression increases intracellular reactive oxygen species levels and susceptibility to dopamine. *Neuroscience Letters*, *320*(3), 146–150. http://doi.org/10.1016/S0304-3940(02)00016-2

Jurgens, H. A., & Johnson, R. W. (2012). Dysregulated neuronal-microglial cross-talk during aging, stress and inflammation. *Experimental Neurology*. http://doi.org/10.1016/j.expneurol.2010.11.014

Kakhlon, O., Breuer, W., Munnich, A., & Cabantchik, Z. I. (2010). Iron redistribution as a therapeutic strategy for treating diseases of localized iron accumulation. *Canadian Journal of Physiology and Pharmacology*, *88*, 187–196. http://doi.org/10.1139/Y09-128

Kann, O., & Kovacs, R. (2006). Mitochondria and neuronal activity. *AJP: Cell Physiology*, *292*(2), C641–C657. http://doi.org/10.1152/ajpcell.00222.2006

Kanti Das, T., Wati, M. R., & Fatima-Shad, K. (2014). Oxidative Stress Gated by Fenton and Haber Weiss Reactions and Its Association With Alzheimer's Disease. *Archives of Neuroscience*, *2*(3). http://doi.org/10.5812/archneurosci.20078

Karthikeyan, G., Santos, J. H., Graziewicz, M. A., Copeland, W. C., Isaya, G., Van Houten, B., & Resnick, M. A. (2003). Reduction in frataxin causes progressive accumulation of mitochondrial damage. *Human Molecular Genetics*, *12*(24), 3331–3342. http://doi.org/10.1093/hmg/ddg349

Kato, J., Kobune, M., Ohkubo, S., Fujikawa, K., Tanaka, M., Takimoto, R., Niitsu, Y. (2007). Iron/IRP-1-dependent regulation of mRNA expression for transferrin receptor, DMT1 and ferritin during human erythroid differentiation. *Experimental Hematology*, *35*(6), 879–887. http://doi.org/10.1016/j.exphem.2007.03.005

Kaur, D., Yantiri, F., Rajagopalan, S., Kumar, J., Mo, J. Q., Boonplueang, R., Andersen, J. K. (2003). Genetic or pharmacological iron chelation prevents MPTP-induced neurotoxicity in vivo: A novel therapy for Parkinson's disease. *Neuron*, *37*(6), 899–909. http://doi.org/10.1016/S0896-6273(03)00126-0

Kaur, D., & Andersen, J. (2004). Does cellular iron dysregulation play a causative role in Parkinson's disease? *Ageing Research Reviews*. http://doi.org/10.1016/j.arr.2004.01.003

Kaur, D., Rajagopalan, S., & Andersen, J. K. (2009). Chronic expression of H-ferritin in dopaminergic midbrain neurons results in an age-related expansion of the labile iron pool and subsequent neurodegeneration: implications for Parkinson's disease. *Brain Research*, *1297*, 17–22. http://doi.org/10.1016/j.brainres.2009.08.043

Keller, J. N., Kindy, M. S., Holtsberg, F. W., St Clair, D. K., Yen, H. C., Germeyer, A., Mattson, M. P. (1998). Mitochondrial manganese superoxide dismutase prevents neural apoptosis and reduces ischemic brain injury: suppression of peroxynitrite production, lipid peroxidation, and mitochondrial dysfunction. *The Journal of Neuroscience: The Official Journal of the Society for Neuroscience*, *18*(2), 687–697.

Kemna, E., Pickkers, P., Nemeth, E., Van Der Hoeven, H., & Swinkels, D. (2005). Time-course analysis of hepcidin, serum iron, and plasma cytokine levels in humans injected with LPS. *Blood*, *106*(5), 1864–1866. http://doi.org/10.1182/blood-2005-03-1159

Kidane, T. Z., Sauble, E., & Linder, M. C. (2006). Release of iron from ferritin requires lysosomal activity. *American Journal of Physiology. Cell Physiology*, *291*(3), C445-55. http://doi.org/10.1152/ajpcell.00505.2005

Kielian, T., Mayes, P., & Kielian, M. (2002). Characterization of microglial responses to Staphylococcus aureus: Effects on cytokine, costimulatory molecule, and Toll-like receptor expression. *Journal of Neuroimmunology*, *130*(1–2), 86–99. http://doi.org/10.1016/S0165-5728(02)00216-3

Kielian, T., Esen, N., & Bearden, E. D. (2005). Toll-like receptor 2 (TLR2) is pivotal for recognition of S. aureus peptidoglycan but not intact bacteria by microglia. *GLIA*, *49*(4), 567–576. http://doi.org/10.1002/glia.20144

Kim, W. G., Mohney, R. P., Wilson, B., Jeohn, G. H., Liu, B., & Hong, J. S. (2000). Regional difference in susceptibility to lipopolysaccharide-induced neurotoxicity in the rat brain: role of microglia. *J Neurosci*, *20*(16), 6309–6316. http://doi.org/20/16/6309

Kim, S., Ponka, P. (2000). Effects of Interferon-γ and Lipopolysaccharide on Macrophage Iron Metabolism Are Mediated by Nitric Oxide-induced Degradation of Iron Regulatory Protein 2. *Journal of Biological Chemistry*, 275(9), 6220-6226. http://www.jbc.org/content/275/9/6220.full.pdf

Kim, Y. S. (2005). Matrix Metalloproteinase-3: A Novel Signaling Proteinase from Apoptotic Neuronal Cells That Activates Microglia. *Journal of Neuroscience*, *25*(14), 3701–3711. http://doi.org/10.1523/JNEUROSCI.4346-04.2005

Kim, Y. A., Lim, S.-Y., Rhee, S.-H., Park, K. Y., Kim, C.-H., Choi, B. T., Choi, Y. H. (2006). Resveratrol inhibits inducible nitric oxide synthase and cyclooxygenase-2 expression in beta-amyloid-treated C6 glioma cells. *International Journal of Molecular Medicine*, *17*(6), 1069–1075.

Kim, Y. A., Kim, G.-Y., Park, K.-Y., & Choi, Y. H. (2007). Resveratrol inhibits nitric oxide and prostaglandin E2 production by lipopolysaccharide-activated C6 microglia. *Journal of Medicinal Food*, *10*(2), 218–224. http://doi.org/10.1089/jmf.2006.143

Kim, Y.-J., Park, H.-J., Lee, G., Bang, O. Y., Ahn, Y. H., Joe, E., Lee, P. H. (2009). Neuroprotective effects of human mesenchymal stem cells on dopaminergic neurons through anti-inflammatory action. *Glia*, *57*(1), 13–23. http://doi.org/10.1002/glia.20731

Kish, S. J., Morito, C., & Hornykiewicz, O. (1985). Glutathione peroxidase activity in Parkinson's disease brain. *Neuroscience Letters*, *58*(3), 343–346. http://doi.org/10.1016/0304-3940(85)90078-3

Kluck, R. M., Bossy-Wetzel, E., Green, D. R., & Newmeyer, D. D. (1997). The release of cytochrome c from mitochondria: a primary site for Bcl-2 regulation of apoptosis. *Science*, *275*(5303), 1132–1136. http://doi.org/10.1126/science.275.5303.1132

Knutson, M. D. (2017). Iron Transport Proteins: Gateways of Cellular and Systemic Iron Homeostasis. *Iron Transporters and Iron Homeostasis*.

Kohgo, Y., Ikuta, K., Ohtake, T., Torimoto, Y., & Kato, J. (2008). Body iron metabolism and pathophysiology of iron overload. *International Journal of Hematology*. http://doi.org/10.1007/s12185-008-0120-5

Kohutnicka, M., Lewandowska, E., Kurkowska-Jastrzębska, I., Członkowski, A., & Członkowska, A. (1998). Microglial and astrocytic involvement in a murine model of Parkinson's disease induced by 1-methyl-4-phenyl-1,2,3,6-tetrahydropyridine (MPTP). *Immunopharmacology*, *39*(3), 167–180. http://doi.org/10.1016/S0162-3109(98)00022-8

Konradi, C., Riederer, P., & Youdim, M. B. (1986). Hydrogen peroxide enhances the activity of monoamine oxidase type-B but not of type-A: a pilot study. *Journal of Neural Transmission. Supplementum*, *22*, 61–73. Retrieved from http://www.ncbi.nlm.nih.gov/pubmed/3097261

Koppula, S., Kumar, H., Kim, I. S., & Choi, D. K. (2012). Reactive oxygen species and inhibitors of inflammatory enzymes, NADPH oxidase, and iNOS in experimental models of parkinsons disease. *Mediators of Inflammation*. http://doi.org/10.1155/2012/823902

Kotzbauer, P. T., Trojanowsk, J. Q., & Lee, V. M. (2001). Lewy body pathology in Alzheimer's disease. *Journal of Molecular Neuroscience: MN*, *17*(2), 225–232. http://doi.org/10.1385/JMN:17:2:225

Koutsilieri, E., Scheller, C., Tribl, F., & Riederer, P. (2002). Degeneration of neuronal cells due to oxidative stress—microglial contribution. *Parkinsonism & Related Disorders*, *8*(6), 401–406. http://doi.org/10.1016/S1353-8020(02)00021-4

Kraft, R., Grimm, C., Grosse, K., Hoffmann, A., Sauerbruch, S., Kettenmann, H., Harteneck, C. (2004). Hydrogen peroxide and ADP-ribose induce TRPM2-mediated calcium influx and cation currents in microglia. *Am J Physiol Cell Physiol*, *286*(1), C129-37. http://doi.org/10.1152/ajpcell.00331.2003

Kravitz, A. V., Freeze, B. S., Parker, P. R. L., Kay, K., Thwin, M. T., Deisseroth, K., & Kreitzer, A. C. (2010). Regulation of parkinsonian motor behaviours by optogenetic control of basal ganglia circuitry. *Nature*, *466*(7306), 622–6. http://doi.org/10.1038/nature09159

Kress, G. J., Dineley, K. E., & Reynolds, I. J. (2002). The relationship between intracellular free iron and cell injury in cultured neurons, astrocytes, and oligodendrocytes. *The Journal of Neuroscience : The Official Journal of the Society for Neuroscience*, *22*(14), 5848–5855. http://doi.org/20026601

Kroemer, G., Zamzami, N., & Susin, S. A. (1997). Mitochondrial control of apoptosis. *Immunology Today*. http://doi.org/10.1016/S0167-5699(97)80014-X

Lambertsen, K. L., Clausen, B. H., Babcock, A. A., Gregersen, R., Fenger, C., Nielsen, H. H., Finsen, B. (2009). Microglia Protect Neurons against Ischemia by Synthesis of Tumor Necrosis Factor. *Journal of Neuroscience*, *29*(5), 1319–1330. http://doi.org/10.1523/JNEUROSCI.5505-08.2009

Langeveld, C. H., Jongenelen, C. A. M., Schepens, E., Stoof, J. C., Bast, A., & Drukarch, B. (1995). Cultured rat striatal and cortical astrocytes protect mesencephalic dopaminergic neurons against hydrogen peroxide toxicity independent of their effect on neuronal development. *Neuroscience Letters*, *192*(1), 13–16. http://doi.org/10.1016/0304-3940(95)11596-O

Langston, J., Ballard, P., Tetrud, J., & Irwin, I. (1983). Chronic Parkinsonism in humans due to a product of meperidine-analog synthesis. *Science*, *219*(4587), 979–980. http://doi.org/10.1126/science.6823561

Lau, L. M. L. De, & Breteler, M. M. B. (2006). Epidemiology of Parkinson' s disease. *The Lancet. Neurology*, *5*(June), 525–535. http://doi.org/18(3) : 231 – 238

LaVaute, T., Smith, S., Cooperman, S., Iwai, K., Land, W., Meyron-Holtz, E., Rouault, T. a. (2001). Targeted deletion of the gene encoding iron regulatory protein-2 causes misregulation of iron metabolism and neurodegenerative disease in mice. *Nature Genetics*, *27*(2), 209–214. http://doi.org/10.1038/84859

Lawson, L. J., Perry, V. H., Dri, P., & Gordon, S. (1990). Heterogeneity in the distribution and morphology of microglia in the normal adult mouse brain. *Neuroscience*, *39*(1), 151–170. http://doi.org/10.1016/0306-4522(90)90229-W

Le, W., Rowe, D., Xie, W., Ortiz, I., He, Y., & Appel, S. H. (2001). Microglial activation and dopaminergic cell injury: an in vitro model relevant to Parkinson's disease. *The Journal of Neuroscience: The Official Journal of the Society for Neuroscience*, *21*(21), 8447–55. http://doi.org/21/21/8447 [pii]

Ledeboer, A., Brevé, J. J. P., Poole, S., Tilders, F. J. H., & Van Dam, A. M. (2000). Interleukin-10, interleukin-4, and transforming growth factor-β differentially regulate lipopolysaccharide-induced production of pro-inflammatory cytokines and nitric oxide in co-cultures of rat astroglial and microglial cells. *GLIA*, *30*(2), 134–142. http://doi.org/10.1002/(SICI)1098-1136(200004)30:2<134::AID-GLIA3>3.0.CO;2-3

Lee Mosley, R., Benner, E. J., Kadiu, I., Thomas, M., Boska, M. D., Hasan, K., Gendelman, H. E. (2006). Neuroinflammation, oxidative stress, and the pathogenesis of Parkinson's disease. *Clinical Neuroscience Research*, *6*(5), 261–281.

Lee, F. J., Liu, F., Pristupa, Z. B., & Niznik, H. B. (2001). Direct binding and functional coupling of alpha-synuclein to the dopamine transporters accelerate dopamine-induced apoptosis. *The FASEB Journal: Official Publication of the Federation of American Societies for Experimental Biology*, *15*(6), 916–26. http://doi.org/10.1096/fj.00-0334com

Lee, P., Peng, H., Gelbart, T., & Beutler, E. (2004). The IL-6- and lipopolysaccharide-induced transcription of hepcidin in HFE-, transferrin receptor 2-, and beta 2-microglobulin-deficient hepatocytes. *Proceedings of the National Academy of Sciences of the United States of America*, *101*(25), 9263–9265. http://doi.org/10.1073/pnas.0403108101

Lee, P., Peng, H., Gelbart, T., Wang, L., & Beutler, E. (2005). Regulation of hepcidin transcription by interleukin-1 and interleukin-6. *Proceedings of the National Academy of Sciences of the United States of America*, *102*(6), 1906–10. http://doi.org/10.1073/pnas.0409808102

Lees, A. J. (2007). Unresolved issues relating to the Shaking Palsy on the celebration of James Parkinson's 250th birthday. *Movement Disorders* (Vol. 22).

Lehnardt, S. (2010). Innate immunity and neuroinflammation in the CNS: The role of microglia in toll-like receptor-mediated neuronal injury. *GLIA*. http://doi.org/10.1002/glia.20928

Lemire, J. A., Harrison, J. J., & Turner, R. J. (2013). Antimicrobial activity of metals: mechanisms, molecular targets and applications. *Nature Reviews Microbiology*, *11*(6), 371–384. http://doi.org/10.1038/nrmicro3028

Leopold, N. A., & Kagel, M. C. (1996). Prepharyngeal dysphagia in Parkinson's disease. *Dysphagia*, *11*(1), 14–22. http://doi.org/10.1007/BF00385794

Lev, N., Melamed, E., & Offen, D. (2003). Apoptosis and Parkinson's disease. *Progress in Neuro-Psychopharmacology and Biological Psychiatry*. http://doi.org/10.1016/S0278-5846(03)00019-8

Lev, N., Ickowicz, D., Barhum, Y., Lev, S., Melamed, E., & Offen, D. (2009). DJ-1 protects against dopamine toxicity. *Journal of Neural Transmission*, *116*(2), 151–160. http://doi.org/10.1007/s00702-008-0134-4

Levine, A., Tenhaken, R., Dixon, R., & Lamb, C. (1994). H2O2 from the oxidative burst orchestrates the plant hypersensitive disease resistance response. *Cell*, *79*(4), 583–593. http://doi.org/10.1016/0092-8674(94)90544-4

Levine, S. M. (1997). Iron deposits in multiple sclerosis and Alzheimer's disease brains. *Brain Research*, *760*(1–2), 298–303. http://doi.org/10.1016/S0006-8993(97)00470-8

Levites, Y., Youdim, M. B. H., Maor, G., & Mandel, S. (2002). Attenuation of 6-hydroxydopamine (6-OHDA)-induced nuclear factor-kappaB (NF-kappaB) activation and cell death by tea extracts in neuronal cultures. *Biochemical Pharmacology*, *63*(1), 21–9. Retrieved from http://www.ncbi.nlm.nih.gov/pubmed/11754870

Li, J., Baud, O., Vartanian, T., Volpe, J. J., & Rosenberg, P. A. (2005). Peroxynitrite generated by inducible nitric oxide synthase and NADPH oxidase mediates microglial toxicity to oligodendrocytes. *Proceedings of the National Academy of Sciences of the United States of America*, *102*(28), 9936–9941. http://doi.org/10.1073/pnas.0502552102

Li, W.-W., Yang, R., Guo, J.-C., Ren, H.-M., Zha, X.-L., Cheng, J.-S., & Cai, D.-F. (2007). Localization of alpha-synuclein to mitochondria within midbrain of mice. *Neuroreport*, *18*(15), 1543–1546. http://doi.org/10.1097/WNR.0b013e3282f03db4

Li, Z., Lai, Z., Ya, K., Fang, D., Ho, Y. W., Lei, Y., & Ming, Q. Z. (2008). Correlation between the expression of divalent metal transporter 1 and the content of hypoxia-inducible factor-1 in hypoxic HepG2 cells. *Journal of Cellular and Molecular Medicine*, *12*(2), 569–579. http://doi.org/10.1111/j.1582-4934.2007.00145.x

Li, W. J., Jiang, H., Song, N., & Xie, J. X. (2010). Dose- and time-dependent α-synuclein aggregation induced by ferric iron in SK-N-SH cells. *Neuroscience Bulletin*, *26*(3), 205–210. http://doi.org/10.1007/s12264-010-1117-7

Li, W. J., Jiang, H., Song, N., & Xie, J. (2011). Oxidative stress partially contributes to iron-induced alpha-synuclein aggregation in SK-N-SH cells. *Neurotoxicity Research*, *19*(3), 435–442. http://doi.org/10.1007/s12640-010-9187-x

Liddell, J. R., Hoepken, H. H., Crack, P. J., Robinson, S. R., & Dringen, R. (2006). Glutathione peroxidase 1 and glutathione are required to protect mouse astrocytes from iron-mediated hydrogen peroxide toxicity. *Journal of Neuroscience Research*, *84*(3), 578–586. http://doi.org/10.1002/jnr.20957

Liddelow, S. A., Guttenplan, K. A., Clarke, L. E., Bennett, F. C., Bohlen, C. J., Schirmer, L., Barres, B. A. (2017). Neurotoxic reactive astrocytes are induced by activated microglia. *Nature*. http://doi.org/10.1038/nature21029

Lill, R., Hoffmann, B., Molik, S., Pierik, A. J., Rietzschel, N., Stehling, O., Mühlenhoff, U. (2012). The role of mitochondria in cellular iron-sulfur protein biogenesis and iron metabolism. *Biochimica et Biophysica Acta - Molecular Cell Research*. http://doi.org/10.1016/j.bbamcr.2012.05.009

Lin, K. T., Xue, J. Y., Sun, F. F., & Wong, P. Y. (1997). Reactive oxygen species participate in peroxynitrite-induced apoptosis in HL-60 cells. *Biochemical and Biophysical Research Communications*, *230*(1), 115–9. http://doi.org/10.1006/bbrc.1996.5897

Lin, M. T., & Beal, M. F. (2006). Mitochondrial dysfunction and oxidative stress in neurodegenerative diseases. *Nature*, *443*(7113), 787–795. http://doi.org/10.1038/nature05292

Linnartz-Gerlach, B., Neumann, H., Bodea, L., & Claude, J. (2014). Phagocytosis Pathways of Microglia Linked to Neurodegeneration. *Alzheimer's & Dementia*, *10*(4), 157.

Lippa, C. F., Fujiwara, H., Mann, D. M. A., Giasson, B., Baba, M., Schmidt, M. L., Trojanowski, J. Q. (1998). *Lewy Bodies Contain Altered α-Synuclein in Brains of Many Familial Alzheimer's Disease Patients with Mutations in Presenilin and Amyloid Precursor Protein Genes*. *The American Journal of Pathology* (Vol. 153). http://doi.org/10.1016/S0002-9440(10)65722-7

Lippert, A. R., Keshari, K. R., Kurhanewicz, J., & Chang, C. J. (2011). A hydrogen peroxide-responsive hyperpolarized 13C MRI contrast agent. *Journal of the American Chemical Society*, *133*(11), 3776–3779. http://doi.org/10.1021/ja111589a

Lis, A., Paradkar, P. N., Singleton, S., Kuo, H. C., Garrick, M. D., & Roth, J. A. (2005). Hypoxia induces changes in expression of isoforms of the divalent metal transporter (DMT1) in rat pheochromocytoma (PC12) cells. *Biochemical Pharmacology*, *69*(11), 1647–1655. http://doi.org/10.1016/j.bcp.2005.03.023

Liu, T., Clark, R. K., McDonnell, P. C., Young, P. R., White, R. F., Barone, F. C., & Feuerstein, G. Z. (1994). Tumor necrosis factor-alpha expression in ischemic neurons. *Stroke; a Journal of Cerebral Circulation*, *25*(7), 1481–1488.

Liu, D., Smith, C. L., Barone, F. C., Ellison, J. A., Lysko, P. G., Li, K., & Simpson, I. A. (1999). Astrocytic demise precedes delayed neuronal death in focal ischemic rat brain. *Brain Research. Molecular Brain Research*, *68*(1–2), 29–41.

Liu, B., Du, L., & Hong, J. S. (2000). Naloxone protects rat dopaminergic neurons against inflammatory damage through inhibition of microglia activation and superoxide generation. *The Journal of Pharmacology and Experimental Therapeutics*, *293*(2), 607–617.

Liu, B., Gao, H. M., & Hong, J. S. (2003). Parkinson's disease and exposure to infectious agents and pesticides and the occurrence of brain injuries: Role of neuroinflammation. *Environmental Health Perspectives*. http://doi.org/10.1289/ehp.6361

Liu, M., Cai, T., Zhao, F., Zheng, G., Wang, Q., Chen, Y., Chen, J. (2009). Effect of microglia activation on dopaminergic neuronal injury induced by manganese, and its possible mechanism. *Neurotoxicity Research*, *16*(1), 42–49. http://doi.org/10.1007/s12640-009-9045-x

Liu, Y., Sieprawska-Lupa, M., Whitman, W. B., & White, R. H. (2010). Cysteine is not the sulfur source for iron-sulfur cluster and methionine biosynthesis in the methanogenic archaeon Methanococcus maripaludis. *Journal of Biological Chemistry*, *285*(42), 31923–31929. http://doi.org/10.1074/jbc.M110.152447

Livak, K. J., & Schmittgen, T. D. (2001). Analysis of relative gene expression data using real-time quantitative PCR and. *Methods*, *25*, 402–408. http://doi.org/10.1006/meth.2001.1262

Lo Bianco, C., Ridet, J.-L., Schneider, B. L., Deglon, N., & Aebischer, P. (2002). alpha - Synucleinopathy and selective dopaminergic neuron loss in a rat lentiviral-based model of Parkinson's disease. *Proceedings of the National Academy of Sciences of the United States of America*, *99*(16), 10813–8. http://doi.org/10.1073/pnas.152339799

Loeffler, D. A., Connor, tJ R., Juneau, P. L., Snyder, tB S., Kanaley, L., DeMaggio, A. J., LeWitt, P. A. (1995). Transferrin and Iron in Normal, Alzheimer's Disease, and Parkinson's Disease Brain Regions. *Journal of Neurochemistry Lippincott-Raven Publishers Philadelphia J. Neurochem*, *65*, 710–716. http://doi.org/10.1046/j.1471-4159.1995.65020710.x

Logroscino, G., Marder, K., Graziano, J., Freyer, G., Slavkovich, V., LoIacono, N., Mayeux, R. (1997). Altered systemic iron metabolism in Parkinson's disease. *Neurology.*, *49*(3), 714–717.

Lok, C. N., & Ponka, P. (1999). Identification of a hypoxia response element in the transferrin receptor gene. *Journal of Biological Chemistry*, *274*(34), 24147–24152. http://doi.org/10.1074/jbc.274.34.24147

Loria, F., & Diaz-Nido, J. (2015). Frataxin knockdown in human astrocytes triggers cell death and the release of factors that cause neuronal toxicity. *Neurobiology of Disease*, *76*, 1–12. http://doi.org/10.1016/j.nbd.2014.12.017

Lotharius, J., & Brundin, P. (2002). Pathogenesis of Parkinson's disease: dopamine, vesicles and α-synuclein. *Nature Reviews Neuroscience*, *3*(12), 932–942. http://doi.org/10.1038/nrn983

Louboutin, J. P., Reyes, B. A. S., Agrawal, L., Van Bockstaele, E. J., & Strayer, D. S. (2010). HIV-1 gp120-induced neuroinflammation: Relationship to neuron loss and protection by rSV40-delivered antioxidant enzymes. *Experimental Neurology*, *221*(1), 231–245. http://doi.org/10.1016/j.expneurol.2009.11.004

Lull, M. E., & Block, M. L. (2010). Microglial Activation and Chronic Neurodegeneration. *Neurotherapeutics*, *7*(4), 354–365. http://doi.org/10.1016/j.nurt.2010.05.014

Lund, S., Christensen, K. V., Hedtjärn, M., Mortensen, A. L., Hagberg, H., Falsig, J., Leist, M. (2006). The dynamics of the LPS triggered inflammatory response of murine microglia under different culture and in vivo conditions. *Journal of Neuroimmunology*, *180*(1–2), 71–87. http://doi.org/10.1016/j.jneuroim.2006.07.007

Luo, X.-G., Zhang, J.-J., Zhang, C.-D., Liu, R., Zheng, L., Wang, X.-J., Chen, S.-D., & Ding, J.-Q. (2010). Altered Regulation of CD200 Receptor in Monocyte-Derived Macrophages from Individuals with Parkinson's Disease. *Neurochemical Research, 35*(4): 540-547. https://link.springer.com/article/10.1007/s11064-009-0094-6

Ma, D., Jin, S., Li, E., Doi, Y., Parajuli, B., Noda, M., Sonobe, Y., Mizuno, T., Suzumura, A. (2013). The neurotoxic effect of astrocytes activated with toll-like receptor ligands. *Journal of Neuroimmunology, 254* (1-2): 10-18. https://www.sciencedirect.com/science/article/pii/S0165572812002548?_rdoc=1

Machado, a., Herrera, a. J., Venero, J. L., Santiago, M., de Pablos, R. M., Villarán, R. F., Cano, J. (2011). Inflammatory Animal Model for Parkinson's Disease: The Intranigral Injection of LPS Induced the Inflammatory Process along with the Selective Degeneration of Nigrostriatal Dopaminergic Neurons. *ISRN Neurology*, *2011*, 1–16. http://doi.org/10.5402/2011/476158

Mahbub, S., Deburghgraeve, C. R., & Kovacs, E. J. (2012). Advanced Age Impairs Macrophage Polarization. *Journal of Interferon & Cytokine Research*, *32*(1), 18–26. http://doi.org/10.1089/jir.2011.0058

Maker, H. S., Weiss, C., Silides, D. J., & Cohen, G. (1981). Coupling of Dopamine Oxidation (Monoamine Oxidase Activity) to Glutathione Oxidation Via the Generation of Hydrogen Peroxide in Rat Brain Homogenates. *Journal of Neurochemistry*, *36*(2), 589–593. http://doi.org/10.1111/j.1471-4159.1981.tb01631.x

Malinouski, M., Zhou, Y., Belousov, V. V., Hatfield, D. L., & Gladyshev, V. N. (2011). Hydrogen peroxide probes directed to different cellular compartments. *PLoS ONE*, *6*(1). http://doi.org/10.1371/journal.pone.0014564

Mancuso, M., Davidzon, G., Kurlan, R. M., Tawil, R., Bonilla, E., Mauro, S. Di, & Powers, J. M. (2005). Hereditary Ferritinopathy: A Novel Mutation, Its Cellular Pathology, and Pathogenetic Insights. *J Neuropathol Exp Neurol*, *64*(4), 280–294. http://doi.org/10.1016/S0022-510X(02)00435-5

Mander, P. K., Jekabsone, A., & Brown, G. C. (2006). Microglia Proliferation Is Regulated by Hydrogen Peroxide from NADPH Oxidase. *The Journal of Immunology*, *176*(2), 1046–1052. http://doi.org/10.4049/jimmunol.176.2.1046

Mann, V. M., Cooper, J. M., Daniel, S. E., Srai, K., Jenner, P., Marsden, C. D., & Schapira, A. H. V. (1994). Complex I, Iron, and ferritin in Parkinson's disease substantia nigra. *Annals of Neurology*, *36*(6), 876–881. http://doi.org/10.1002/ana.410360612

Marder, K., Logroscino, G., Tang, M. X., Graziano, J., Cote, L., Louis, E., Mayeux, R. (1998). Systemic iron metabolism and mortality from Parkinson's disease. *Neurology*, *50*(4), 1138–40. Retrieved from http://www.ncbi.nlm.nih.gov/pubmed/9566409

Mark, R. J., Lovell, M. A., Markesbery, W. R., Uchida, K., & Mattson, M. P. (1997). A role for 4-hydroxynonenal, an aldehydic product of lipid peroxidation, in disruption of ion homeostasis and neuronal death induced by amyloid beta-peptide. *J Neurochem*, *68*(1), 255–264. http://doi.org/10.1046/j.1471-4159.1997.68010255.x

Marques, F., Falcao, A. M., Sousa, J. C., Coppola, G., Geschwind, D., Sousa, N., Palha, J. A. (2009). Altered iron metabolism is part of the choroid plexus response to peripheral inflammation. *Endocrinology*, *150*(6), 2822–2828. http://doi.org/10.1210/en.2008-1610

Martin, W., Wieler, M., & Gee, M. (2005). Quantitation of Regional Brain Iron Content with Magnetic Resonance Imaging. *Journal of the Neurological Sciences*, *238*, S260–S261.

Martinez-Ramirez, D., & Okun, M. S. (2016). Parkinson's Disease: Treatment. *Scientific American*, *May*. Retrieved from https://www.researchgate.net/profile/Daniel_Martinez-Ramirez/publication/303768315_Parkinson_Disease_Treatment/links/57618cf608ae244d0372ca5c/Parkinson-Disease-Treatment.pdf

Martins, E. A., Robalinho, R. L., & Meneghini, R. (1995). Oxidative stress induces activation of a cytosolic protein responsible for control of iron uptake. *Archives of Biochemistry and Biophysics*, *316*(1), 128–34. http://doi.org/10.1006/abbi.1995.1019

Marttila, R. J., Lorentz, H., & Rinne, U. K. (1988). Oxygen toxicity protecting enzymes in Parkinson's disease. Increase of superoxide dismutase-like activity in the substantia nigra and basal nucleus. *Journal of the Neurological Sciences*, *86*(2–3), 321–331. http://doi.org/10.1016/0022-510X(88)90108-6

Mayeur, C., Lohmeyer, L. K., Leyton, P., Kao, S. M., Pappas, A. E., Kolodziej, S. A., Steinbicker, A. U. (2014). The type I BMP receptor Alk3 is required for the induction of hepatic hepcidin gene expression by interleukin-6. *Blood*, *123*(14), 2261–2268. http://doi.org/10.1182/blood-2013-02-480095

McBride, A. G., Borutaité, V., & Brown, G. C. (1999). Superoxide dismutase and hydrogen peroxide cause rapid nitric oxide breakdown, peroxynitrite production and subsequent cell death. *Biochimica et Biophysica Acta - Molecular Basis of Disease*, *1454*(3), 275–288. http://doi.org/10.1016/S0925-4439(99)00046-0

McGeer, P. L., Itagaki, S., Boyes, B. E., & McGeer, E. G. (1988). Reactive microglia are positive for HLA-DR in the substantia nigra of Parkinson's and Alzheimer's disease brains. *Neurology*, *38*(8), 1285–1291. http://doi.org/10.1212/WNL.38.8.1285

McGeer, P. L., Schwab, C., Parent, A., & Doudet, D. (2003). Presence of Reactive Microglia in Monkey Substantia Nigra Years after 1-Methyl-4-Phenyl-1,2,3,6-Tetrahydropyridine Administration. *Annals of Neurology*, *54*(5), 599–604. http://doi.org/10.1002/ana.10728

McGuire, S. O., Ling, Z. D., Lipton, J. W., Sortwell, C. E., Collier, T. J., & Carvey, P. M. (2001). Tumor necrosis factor alpha is toxic to embryonic mesencephalic dopamine neurons. *Experimental Neurology*, *169*(2), 219–30. http://doi.org/10.1006/exnr.2001.7688

Medina, S., Martínez, M., & Hernanz, A. (2002). Antioxidants Inhibit the Human Cortical Neuron Apoptosis Induced by Hydrogen Peroxide, Tumor Necrosis Factor Alpha, Dopamine and Beta-amyloid Peptide 1-42. *Free Radical Research*, *36*(11), 1179–1184. http://doi.org/10.1080/10715760210006445

Mello Filho, A. C., Hoffmann, M. E., & Meneghini, R. (1984). Cell killing and DNA damage by hydrogen peroxide are mediated by intracellular iron. *The Biochemical Journal*, *218*(1), 273–5.

Mena, M. A., de Bernardo, S., Casarejos, M. J., Canals, S., & Rodríguez-Martín, E. (2002). The role of astroglia on the survival of dopamine neurons. *Molecular Neurobiology*, *25*(3), 245–263. http://doi.org/10.1385/MN:25:3:245

Meuth, S. G., Simon, O. J., Grimm, A., Melzer, N., Herrmann, A. M., Spitzer, P., Wiendl, H. (2008). CNS inflammation and neuronal degeneration is aggravated by impaired CD200-CD200R-mediated macrophage silencing. *Journal of Neuroimmunology*, *194*(1–2), 62–69. http://doi.org/10.1016/j.jneuroim.2007.11.013

Michel, P. P., Hirsch, E. C., & Hunot, S. (2016). Understanding Dopaminergic Cell Death Pathways in Parkinson Disease. *Neuron*. http://doi.org/10.1016/j.neuron.2016.03.038

Mikell, C. B., & McKhann, G. M. (2010). Regulation of Parkinsonian motor behaviors by optogenetic control of basal ganglia circuitry. *Neurosurgery*. http://doi.org/10.1227/01.neu.0000389744.90809.e8

Millonig, G., Ganzleben, I., Peccerella, T., Casanovas, G., Brodziak-Jarosz, L., Breitkopf-Heinlein, K., Mueller, S. (2012). Sustained submicromolar H2O2 levels induce hepcidin via signal transducer and activator of transcription 3 (STAT3). *Journal of Biological Chemistry*, *287*(44), 37472–37482. http://doi.org/10.1074/jbc.M112.358911

Min, S. K., Kim, C. R., Jung, S. M., & Shin, H. S. (2013). Astrocyte behavior and GFAP expression on Spirulina extract-incorporated PCL nanofiber. *Journal of Biomedical Materials Research - Part A*, *101*(12), 3467–3473. http://doi.org/10.1002/jbm.a.34654

Mincheva-Tasheva, S., Obis, E., Tamarit, J., & Ros, J. (2014). Apoptotic cell death and altered calcium homeostasis caused by frataxin depletion in dorsal root ganglia neurons can be prevented by BH4 domain of Bcl-xL protein. *Human Molecular Genetics*, *23*(7), 1829–1841. http://doi.org/10.1093/hmg/ddt576

Mishra, O. P., Delivoria-Papadopoulos, M., Cahillane, G., & Wagerle, L. C. (1990). Lipid Peroxidation as the Mechanism of Modification of Brain 5'Nucleotidase Activity In Vitro. *Neurochemical Research*, *15*(3), 237–242.

Mitsumoto, A., & Nakagawa, Y. (2001). DJ-1 is an indicator for endogenous reactive oxygen species elicited by endotoxin. *Free Radical Research*, *35*(6), 885–893. http://doi.org/10.1080/10715760100301381

Miyajima, H., Nishimura, Y., Mizoguchi, K., Sakamoto, M., Shimizu, T., & Honda, N. (1987). Familial apoceruloplasmin deficiency associated with blepharospasm and retinal degeneration. *Neurology*, *37*(5), 761–7. http://doi.org/10.1212/WNL.37.5.761

Miyazaki, E., Kato, J., Kobune, M., Okumura, K., Sasaki, K., Shintani, N., Niitsu, Y. (2002). Denatured H-ferritin subunit is a major constituent of haemosiderin in the liver of patients with iron overload. *Gut*, *50*(3), 413–9. http://doi.org/10.1136/gut.50.3.413

Mochizuki, H., Goto, K., Mori, H., & Mizuno, Y. (1996). Histochemical detection of apoptosis in Parkinson's disease. *Journal of the Neurological Sciences*, *137*(2), 120–123. http://doi.org/10.1016/0022-510X(95)00336-Z

Mogi, M., Harada, M., Riederer, P., Narabayashi, H., Fujita, K., & Nagatsu, T. (1994). Tumor necrosis factor-alpha (TNF-alpha) increases both in the brain and in the cerebrospinal fluid from parkinsonian patients. *Neuroscience Letters*, *165*(1–2), 208–210. http://doi.org/10.1016/0304-3940(94)90746-3

Mogi, M., Harada, M., Narabayashi, H., Inagaki, H., Minami, M., & Nagatsu, T. (1996). Interleukin (IL)-1ß, IL-2, IL-4, IL-6 and transforming growth factor levels are elevated in ventricular cerebrospinal fluid in juvenile parkinsonism and Parkinson's disease. *Neuroscience Letters*, *211*(1), 13–16. http://doi.org/10.1016/0304-3940(96)12706-3

Mogi, M., Togari, A., Kondo, T., Mizuno, Y., Komure, O., Kuno, S., Nagatsu, T. (2000). Caspase activities and tumor necrosis factor receptor R1 (p55) level are elevated in the substantia nigra from Parkinsonian brain. *Journal of Neural Transmission*, *107*(3), 335–341. http://doi.org/10.1007/s007020050028

Moncada, S., Palmer, R. M., & Higgs, E. A. (1991). Nitric oxide: physiology, pathophysiology, and pharmacology. *Pharmacological Reviews*, *43*(2), 109–42. http://doi.org/10.1017/CBO9781107415324.004

Monteiro, H. P., & Winterbourn, C. C. (1989). 6-Hydroxydopamine releases iron from ferritin and promotes ferritin-dependent lipid peroxidation. *Biochemical Pharmacology*, *38*(23), 4177–4182. http://doi.org/10.1016/0006-2952(89)90512-1

Moos, T., & Morgan, E. H. (2000). Transferrin and transferrin receptor function in brain barrier systems. *Cellular and Molecular Neurobiology*, *20*(1), 77–95. http://doi.org/10.1023/A:1006948027674

Mousavi, S. A., Malerød, L., Berg, T., & Kjeken, R. (2004). Clathrin-dependent endocytosis. *The Biochemical Journal*, *377*, 1–16. http://doi.org/10.1042/BJ20031000

Moussaoui, S., Obinu, M. C., Daniel, N., Reibaud, M., Blanchard, V., & Imperato, a. (2000). The antioxidant ebselen prevents neurotoxicity and clinical symptoms in a primate model of Parkinson's disease. *Experimental Neurology*, *166*(2), 235–245. http://doi.org/10.1006/exnr.2000.7516

Muckenthaler, M. U., Galy, B., & Hentze, M. W. (2008). Systemic iron homeostasis and the iron-responsive element/iron-regulatory protein (IRE/IRP) regulatory network. *Annual Review of Nutrition*, *28*, 197–213. http://doi.org/10.1146/annurev.nutr.28.061807.155521

Mueller, S., Pantopoulos, K., Hübner, C. a, Stremmel, W., & Hentze, M. W. (2001). IRP1 activation by extracellular oxidative stress in the perfused rat liver. *The Journal of Biological Chemistry*, *276*(25), 23192–6. http://doi.org/10.1074/jbc.M100654200

Mullen, R. J., Buck, C. R., & Smith, A. M. (1992). NeuN, a neuronal specific nuclear protein in vertebrates. *Development*, *116*, 201–211. http://doi.org/VL - 116

Mullin, S., & Schapira, A. (2013). α-Synuclein and Mitochondrial Dysfunction in Parkinson's Disease. *Molecular Neurobiology*, pp. 1–11. http://doi.org/10.1007/s12035-013-8394-x

Musci, G., Polticelli, F., & Patti, M.C.B. (2014). Ceruloplasmin-ferroportin system of iron traffic in vertebrates. *World Journal of Biological Chemistry*, 5(2): 204-215. https://www.ncbi.nlm.nih.gov/pmc/articles/PMC4050113/

Myer, D. J., Gurkoff, G. G., Lee, S. M., Hovda, D. A., & Sofroniew, M. V. (2006). Essential protective roles of reactive astrocytes in traumatic brain injury. *Brain*, *129*(10), 2761–2772. http://doi.org/10.1093/brain/awl165

Nagatsu, T., Mogi, M., Ichinose, H., & Togari, A. (2000). Changes in cytokines and neurotrophins in Parkinson's disease. *Advances in Research on Neurodegeneration* (pp. 277–290). *Journal of Neural Transmission. Supplementum*, (60), 277–290. http://doi.org/10.1007/978-3-7091-6301-6_19

Nagatsu, T., & Sawada, M. (2005). Inflammatory Process in Parkinsons Disease: Role for Cytokines. *Current Pharmaceutical Design*, *11*(8), 999–1016. http://doi.org/10.2174/1381612053381620

Nakagawa, Y., & Chiba, K. (2014). Role of microglial M1/M2 polarization in relapse and remission of psychiatric disorders and diseases. *Pharmaceuticals*. http://doi.org/10.3390/ph7121028

Nakamura, Y., Si, Q. S., & Kataoka, K. (1999). Lipopolysaccharide-induced microglial activation in culture: Temporal profiles of morphological change and release of cytokines and nitric oxide. *Neuroscience Research*, *35*(2), 95–100. http://doi.org/10.1016/S0168-0102(99)00071-1

Nakamura, K., Nemani, V. M., Azarbal, F., Skibinski, G., Levy, J. M., Egami, K., Edwards, R. H. (2011). Direct membrane association drives mitochondrial fission by the Parkinson disease-associated protein α-synuclein. *Journal of Biological Chemistry*, *286*(23), 20710–20726. http://doi.org/10.1074/jbc.M110.213538

Navarro, J. A., Ohmann, E., Sanchez, D., Botella, J. A., Liebisch, G., Moltó, M. D., Schneuwly, S. (2010). Altered lipid metabolism in a Drosophila model of Friedreich's ataxia. *Human Molecular Genetics*, *19*(14), 2828–2840. http://doi.org/10.1093/hmg/ddq183

Nemes, Z., Dietz, R., Lüth, J. B., Gomba, S., Hackenthal, E., & Gross, F. (1979). The pharmacological relevance of vital staining with neutral red. *Experientia*, *35*(11), 1475–1476. http://doi.org/10.1007/BF01962793

Nemeth, E., Valore, E. V., Territo, M., Schiller, G., Lichtenstein, A., & Ganz, T. (2003). Hepcidin, a putative mediator of anemia of inflammation, is a type II acute-phase protein. *Blood*, *101*(7), 2461–2463. http://doi.org/10.1182/blood-2002-10-3235

Nemeth, E., Rivera, S., Gabayan, V., Keller, C., Taudorf, S., Pedersen, B. K., & Ganz, T. (2004). IL-6 mediates hypoferremia of inflammation by inducing the synthesis of the iron regulatory hormone hepcidin. *Journal of Clinical Investigation*, *113*(9), 1271–1276. http://doi.org/10.1172/JCI200420945

Nemeth, E., Tuttle, M. S., Powelson, J., Vaughn, M. B., Donovan, A., & Ward, D. M. (2004). Hepcidin Regulates Cellular Iron Efflux by Binding to Ferroportin and Inducing Its

Internalization. *Science (New York, N.Y.)*, *306*(5704), 2090–2093. http://doi.org/10.1126/science.1104742

Neumann, J., Sauerzweig, S., Ronicke, R., Gunzer, F., Dinkel, K., Ullrich, O., Reymann, K. G. (2008). Microglia Cells Protect Neurons by Direct Engulfment of Invading Neutrophil Granulocytes: A New Mechanism of CNS Immune Privilege. *Journal of Neuroscience*, *28*(23), 5965–5975. http://doi.org/10.1523/JNEUROSCI.0060-08.2008

Nicklas, W. J., Youngster, S. K., Kindt, M. V., & Heikkila, R. E. (1987). IV. MPTP, MPP+ and mitochondrial function. *Life Sciences*, *40*(8), 721–729. http://doi.org/10.1016/0024-3205(87)90299-2

Nicolas, G., Chauvet, C., Viatte, L., Danan, J. L., Bigard, X., Devaux, I., Vaulont, S. (2002). The gene encoding the iron regulatory peptide hepcidin is regulated by anemia, hypoxia, and inflammation. *Journal of Clinical Investigation*, *110*(7), 1037–1044. http://doi.org/10.1172/JCI200215686

Nikolova, G. (2012). Oxidative Stress and Parkinson Disease. *Trakia Journal of Sciences*, *10*(1), 92–100. http://doi.org/10.3389/fnana.2015.00091

Nilsson, P. (2012). Neocuproine. *Encyclopedia of Reagents for Organic Synthesis*. Retrieved from http://onlinelibrary.wiley.com/doi/10.1002/047084289X.rn01440/full

Nimmerjahn, A., Kirchhoff, F., & Helmchen, F. (2005). Resting microglial cells are highly dynamic surveillants of brain parenchyma in vivo. *Neuroforum*, *11*(3), 95–96. http://doi.org/10.1126/science.1110647

Niranjan, R., Nath, C., & Shukla, R. (2012). Melatonin attenuated mediators of neuroinflammation and alpha-7 nicotinic acetylcholine receptor mRNA expression in lipopolysaccharide (LPS) stimulated rat astrocytoma cells, C6. *Free Radical Research*, *46*(9), 1167–1177. http://doi.org/10.3109/10715762.2012.697626

Niranjan, R. (2014). The Role of inflammatory and oxidative stress mechanisms in the pathogenesis of parkinson's disease: Focus on astrocytes. *Molecular Neurobiology*. http://doi.org/10.1007/s12035-013-8483-x

Noronha-Dutra, A. A., Epperlein, M. M., & Woolf, N. (1993). Reaction of nitric oxide with hydrogen peroxide to produce potentially cytotoxic singlet oxygen as a model for nitric oxide-mediated killing. *FEBS Letters*, *321*(1), 59–62. http://doi.org/10.1016/0014-5793(93)80621-Z

Noyce, A. J., Bestwick, J. P., Silveira-Moriyama, L., Hawkes, C. H., Giovannoni, G., Lees, A. J., & Schrag, A. (2012). Meta-analysis of early nonmotor features and risk factors for Parkinson disease. *Annals of Neurology*. http://doi.org/10.1002/ana.23687

Nulton-Persson, A. C., & Szweda, L. I. (2001). Modulation of Mitochondrial Function by Hydrogen Peroxide. *Journal of Biological Chemistry*, *276*(26), 23357–23361. http://doi.org/10.1074/jbc.M100320200

Nutt, J. G., Woodward, W. R., & Anderson, J. L. (1985). The effect of carbidopa on the pharmacokinetics of intravenously administered levodopa: The mechanism of action in the treatment of parkinsonism. *Annals of Neurology*, *18*(5), 537–543. http://doi.org/10.1002/ana.410180505

Nutt, J. G. (2008). Pharmacokinetics and pharmacodynamics of levodopa. *Movement Disorders*, *23*(SUPPL. 3). http://doi.org/10.1002/mds.22037

Nuytemans, K., Theuns, J., Cruts, M., & Van Broeckhoven, C. (2010). Genetic etiology of Parkinson disease associated with mutations in the SNCA, PARK2, PINK1, PARK7, and LRRK2 genes: A mutation update. *Human Mutation*. http://doi.org/10.1002/humu.21277

Oakley, A. E., Collingwood, J. F., Dobson, J., Love, G., Perrott, H. R., Edwardson, J. A., Morris, C. M. (2007). Individual dopaminergic neurons show raised iron levels in Parkinson disease. *Neurology*, *68*(21), 1820–1825. http://doi.org/10.1212/01.wnl.0000262033.01945.9a

Obeso, J., Olanow, C., & Rodriguez-Oroz, M. (2001). Deep-brain stimulation of the subthalamic nucleus or the pars interna of the globus pallidus in Parkinson's disease. *N Engl J Med*, *345*(13), 956–63. http://doi.org/10.1056/NEJMoa000827

Oestreicher, E., Sengstock, G. J., Riederer, P., Olanow, C. W., Dunn, A. J., & Arendash, G. W. (1994). Degeneration of nigrostriatal dopaminergic neurons increases iron within the substantia nigra: a histochemical and neurochemical study. *Brain Research*, 660(1), 8–18. http://doi.org/10.1016/0006-8993(94)90833-8

Oide, T., Yoshida, K., Kaneko, K., Ohta, M., & Arima, K. (2006). Iron overload and antioxidative role of perivascular astrocytes in aceruloplasminemia. *Neuropathology and Applied Neurobiology*, *32*(2), 170–176. http://doi.org/10.1111/j.1365-2990.2006.00710.x

Olanow, C. W., & Arendash, G. W. (1994). Metals and free radicals in neurodegeneration. *Curr Opin Neurol*, *7*(6), 548–558.

Oliviera, L., Bouton, C., & Drapier, J.-C. (1999). Thioredoxin Activation of Iron Regulatory Proteins: Redox Regulation of RNA Binding After Exposure to Nitric Oxide. *The Journal of Biological Chemistry,* 274(1), 516-521. http://www.jbc.org/content/274/1/516.full.pdf

Olivieri, S., Conti, a., Iannaccone, S., Cannistraci, C. V., Campanella, a., Barbariga, M., Alessio, M. (2011). Ceruloplasmin Oxidation, a Feature of Parkinson's Disease CSF, Inhibits Ferroxidase Activity and Promotes Cellular Iron Retention. *Journal of Neuroscience*, *31*(50), 18568–18577. http://doi.org/10.1523/JNEUROSCI.3768-11.2011

Olson, J. K., & Miller, S. D. (2004). Microglia initiate central nervous system innate and adaptive immune responses through multiple TLRs. *Journal of Immunology (Baltimore, MD: 1950)*, *173*(6), 3916–24. http://doi.org/10.4049/jimmunol.173.6.3916

Orihuela, R., McPherson, C. A., & Harry, G. J. (2016). Microglial M1/M2 polarization and metabolic states. *British Journal of Pharmacology*. http://doi.org/10.1111/bph.13139

Ouchi, Y., Yoshikawa, E., Sekine, Y., Futatsubashi, M., Kanno, T., Ogusu, T., & Torizuka, T. (2005). Microglial activation and dopamine terminal loss in early Parkinson's disease. *Annals of Neurology*, *57*(2), 168–175. http://doi.org/10.1002/ana.20338

Pacher, P., Beckman, J. S., & Liaudet, L. (2007). Nitric oxide and peroxynitrite in health and disease. *Physiological Reviews*, *87*(1), 315–424.

Pallis, C. (1971). Parkinsonism- Natural History and Clinical Features. *British Medical Journal*, *3*(5776), 683–686.

Palomo, G. M., Cerrato, T., Gargini, R., & Diaz-Nido, J. (2011). Silencing of frataxin gene expression triggers p53- dependent apoptosis in human neuron-like cells. *Human Molecular Genetics*, *20*(14), 2807–2822. http://doi.org/10.1093/hmg/ddr187

Pandey, A., Pain, J., Ghosh, A. K., Dancis, A., & Pain, D. (2015). Fe-S Cluster Biogenesis in Isolated Mammalian Mitochondria. *Journal of Biological Chemistry*, *290*(1), 640–657. http://doi.org/10.1074/jbc.M114.610402

Pantopoulos, K., Weiss, G., & Hentze, M. W. (1996). Nitric oxide and oxidative stress (H_2O_2) control mammalian iron metabolism by different pathways. *Molecular and Cellular Biology*, *16*(7), 3781–3788.

Pantopoulos, K., Mueller, S., Atzberger, A., Ansorge, W., Stremmel, W., & Hentze, M. W. (1997). Differences in the regulation of iron regulatory protein-1 (IRP-1) by extra- and intracellular oxidative stress. *Journal of Biological Chemistry*, *272*(15), 9802–9808. http://doi.org/10.1074/jbc.272.15.9802

Paolicelli, R. C., Bolasco, G., Pagani, F., Maggi, L., Scianni, M., Panzanelli, P., Gross, C. T. (2011). Synaptic pruning by microglia is necessary for normal brain development. *Science (New York, N.Y.)*, *333*(6048), 1456–8. http://doi.org/10.1126/science.1202529

Parkinson, J. (2002). An Essay on the Shaking Palsy. *Journal of Neuropsychiatry & Clinical Neuroscience*, *14*(2).

Patel, B. N., & David, S. (1997). A novel glycosylphosphatidylinositol-anchored form of ceruloplasmin is expressed by mammalian astrocytes. *Journal of Biological Chemistry*, *272*(32), 20185–20190. http://doi.org/10.1074/jbc.272.32.20185

Pechlaner, R., Kiechl, S., Mayr, M., Santer, P., Weger, S., Haschka, D., Weiss, G. (2016). Correlates of serum hepcidin levels and its association with cardiovascular disease in an elderly general population. *Clinical Chemistry and Laboratory Medicine*, *54*(1), 151–161. http://doi.org/10.1515/cclm-2015-0068

Pelizzoni, I., Zacchetti, D., Campanella, A., Grohovaz, F., & Codazzi, F. (2013). Iron uptake in quiescent and inflammation-activated astrocytes: A potentially neuroprotective control of iron burden. *Biochimica et Biophysica Acta - Molecular Basis of Disease*, *1832*(8), 1326–1333. http://doi.org/10.1016/j.bbadis.2013.04.007

Perry, T. L., Godin, D. V., & Hansen, S. (1982). Parkinson's disease: A disorder due to nigral glutathione deficiency? *Neuroscience Letters*, *33*(3), 305–310. http://doi.org/10.1016/0304-3940(82)90390-1

Peterson, P. K., & Toborek, M. (2014). *Neuroinflammation and neurodegeneration*. *Neuroinflammation and Neurodegeneration*. http://doi.org/10.1007/978-1-4939-1071-7

Petrat, F., Weisheit, D., Lensen, M., de Groot, H., Sustmann, R., & Rauen, U. (2002). Selective determination of mitochondrial chelatable iron in viable cells with a new fluorescent sensor. *The Biochemical Journal*, *362*(Pt 1), 137–147. http://doi.org/10.1042/0264-6021:3620137

Pietrangelo, A., Dierssen, U., Valli, L., Garuti, C., Rump, A., Corradini, E., Trautwein, C. (2007). STAT3 Is Required for IL-6-gp130-Dependent Activation of Hepcidin In Vivo. *Gastroenterology*, *132*(1), 294–300. http://doi.org/10.1053/j.gastro.2006.10.018

Piñero, D. J., Li, N. Q., Connor, J. R., & Beard, J. L. (2000). Variations in dietary iron alter brain iron metabolism in developing rats. *The Journal of Nutrition*, *130*(2), 254–63. Retrieved from http://www.ncbi.nlm.nih.gov/pubmed/10720179

Pinter, M. M., Pogarell, O., & Oertel, W. H. (1999). Efficacy, safety, and tolerance of the non-ergoline dopamine agonist pramipexole in the treatment of advanced Parkinson's disease: A double blind, placebo controlled, randomised, multicentre study. *Journal of Neurology, Neurosurgery & Psychiatry*, *66* (December 2005), 436–441.

Plassman, B. L., Havlik, R. J., Steffens, D. C., Helms, M. J., Newman, T. N., Drosdick, D., Breitner, J. C. S. (2000). Documented head injury in early adulthood and risk of Alzheimer's disease and other dementias. *Neurology*, *55*(8), 1158–1166. http://doi.org/10.1212/WNL.55.8.1158

Polazzi, E., Gianni, T., & Contestabile, A. (2001). Microglial cells protect cerebellar granule neurons from apoptosis: Evidence for reciprocal signaling. *GLIA*, *36*(3), 271–280. http://doi.org/10.1002/glia.1115

Ponka, P. (1999). Cellular iron metabolism. *Kidney International. Supplement*, *69*(S69), S2–S11. http://doi.org/10.1046/j.1523-1755.1999.055Suppl.69002.x

Porras, G., Li, Q., & Bezard, E. (2012). Modeling Parkinson's disease in primates: The MPTP model. *Cold Spring Harbor Perspectives in Medicine*, *2*(3). http://doi.org/10.1101/cshperspect.a009308

Possel, H., Noack, H., Putzke, J., Wolf, G., & Sies, H. (2000). Selective upregulation of inducible nitric oxide synthase (iNOS) by lipopolysaccharide (LPS) and cytokines in microglia: In vitro and in vivo studies. *GLIA*, *32*(1), 51–59. http://doi.org/10.1002/1098-1136(200010)32:1<51::AID-GLIA50>3.0.CO;2-4

Postuma, R. B., Berg, D., Stern, M., Poewe, W., Olanow, C. W., Oertel, W., Deuschl, G. (2015). MDS clinical diagnostic criteria for Parkinson's disease. *Movement Disorders*. http://doi.org/10.1002/mds.26424

Prasad, K. N., Carvalho, E., Kentroti, S., Edwards-Prasad, J., Freed, C., & Vernadakis, A. (1994). Establishment and characterization of immortalized clonal cell lines from fetal rat mesencephalic tissue. *In Vitro Cellular & Developmental Biology. Animal*, *30A*(9), 596–603. http://doi.org/10.1007/BF02631258

Pringsheim, T., Jette, N., Frolkis, A., & Steeves, T. D. L. (2014). The prevalence of Parkinson's disease: A systematic review and meta-analysis. *Movement Disorders*. http://doi.org/10.1002/mds.25945

Prus, E., & Fibach, E. (2007). Flow cytometry measurement of the labile iron pool in human hematopoietic cells. *Journal of the International Society for Advancement of Cytometry*, *73A*(1), 22–27.

Przedborski, S., Jackson-Lewis, V., Muthane, U., Jiang, H., Ferreira, M., Naini, A. B., & Fahn, S. (1993). Chronic levodopa administration alters cerebral mitochondrial respiratory chain activity. *Annals of Neurology*, *34*(5), 715–723. http://doi.org/10.1002/ana.410340515

Qian, Z. M., He, X., Liang, T., Wu, K. C., Yan, Y. C., Lu, L. N., Ke, Y. (2014). Lipopolysaccharides Upregulate Hepcidin in Neuron via Microglia and the IL-6/STAT3 Signaling Pathway. *Molecular Neurobiology*, *50*(3), 811–820. http://doi.org/10.1007/s12035-014-8671-3

Qin, L., Li, G., Qian, X., Liu, Y., Wu, X., Liu, B., Block, M. L. (2005). Interactive role of the toll-like receptor 4 and reactive oxygen species in LPS-induced microglia activation. *GLIA*, *52*(1), 78–84. http://doi.org/10.1002/glia.20225

Qin, L., Wu, X., Block, M. L., Liu, Y., Breese, G. R., Hong, J. S., Crews, F. T. (2007). Systemic LPS causes chronic neuroinflammation and progressive neurodegeneration. *GLIA*, *55*(5), 453–462. http://doi.org/10.1002/glia.20467

Quincozes-Santos, A., Bobermin, L. D., Kleinkauf-Rocha, J., Souza, D. O., Riesgo, R., Gonçalves, C. A., & Gottfried, C. (2009). Atypical neuroleptic risperidone modulates glial functions in C6 astroglial cells. *Progress in Neuro-Psychopharmacology and Biological Psychiatry*, *33*(1), 11–15. http://doi.org/10.1016/j.pnpbp.2008.08.023

Quintana, C., Bellefqih, S., Laval, J. Y., Guerquin-Kern, J. L., Wu, T. D., Avila, J., Patiño, C. (2006). Study of the localization of iron, ferritin, and hemosiderin in Alzheimer's disease hippocampus by analytical microscopy at the subcellular level. *Journal of Structural Biology*, *153*(1), 42–54. http://doi.org/10.1016/j.jsb.2005.11.001

Röhl, C., Armbrust, E., Kolbe, K., Lucius, R., Maser, E., Venz, S., & Gölden, M. (2008). Activated microglia modulate astroglial enzymes involved in oxidative and inflammatory stress and increase the resistance of astrocytes to oxidative stress in vitro. *GLIA*, *56*(10), 1114–1126. http://doi.org/10.1002/glia.20683

Raudino, F. (2012). The Parkinson disease before James Parkinson. *Neurological Sciences*, *33*(4), 945–948. http://doi.org/10.1007/s10072-011-0816-9

Reif, D. W. (1992). Ferritin as a source of iron for oxidative damage. *Free Radical Biology and Medicine*, *12*(5), 417–427. http://doi.org/10.1016/0891-5849(92)90091-T

Renault-Mihara, F., Okada, S., Shibata, S., Nakamura, M., Toyama, Y., & Okano, H. (2008). Spinal cord injury: emerging beneficial role of reactive astrocytes' migration. *The International Journal of Biochemistry & Cell Biology*, *40*(9), 1649–53. http://doi.org/10.1016/j.biocel.2008.03.009

Repetto, G., del Peso, A., & Zurita, J. L. (2008). Neutral red uptake assay for the estimation of cell viability/cytotoxicity. *Nature Protocols*, *3*(7), 1125–1131. http://doi.org/10.1038/nprot.2008.75

Revesz, T., McLaughlin, J. L., Rossor, M. N., & Lantos, P. L. (1997). Pathology of familial Alzheimer's disease with Lewy bodies. *Journal of Neural Transmission. Supplementum*, *51*, 121–35. Retrieved from http://www.ncbi.nlm.nih.gov/pubmed/9470133

Rhee, S. G., Kang, S. W., Chang, T. S., Jeong, W., & Kim, K. (2001). Peroxiredoxin, a novel family of peroxidases. In *IUBMB Life* (Vol. 52, pp. 35–41). http://doi.org/10.1080/15216540252774748

Rhee, S. G. (2006). H2O2, a necessary evil for cell signaling. *Science (New York, N.Y.)*, *312*(5782), 1882–1883. http://doi.org/10.1126/science.1130481

Rhodes, S. L., & Ritz, B. (2008). Genetics of iron regulation and the possible role of iron in Parkinson's disease. *Neurobiology of Disease*. http://doi.org/10.1016/j.nbd.2008.07.001

Riederer, P., & Youdim, M. B. H. (1986). Monoamine Oxidase Activity and Monoamine Metabolism in Brains of Parkinsonian Patients Treated with l-Deprenyl. *Journal of Neurochemistry*, *46*(5), 1359–1365. http://doi.org/10.1111/j.1471-4159.1986.tb01747.x

Riederer, P., Sofic, E., Rausch, W. -D, Schmidt, B., Reynolds, G. P., Jellinger, K., & Youdim, M. B. H. (1989). Transition Metals, Ferritin, Glutathione, and Ascorbic Acid in Parkinsonian Brains. *Journal of Neurochemistry*, *52*(2), 515–520. http://doi.org/10.1111/j.1471-4159.1989.tb09150.x

Riemer, J., Hoepken, H. H., Czerwinska, H., Robinson, S. R., & Dringen, R. (2004). Colorimetric ferrozine-based assay for the quantitation of iron in cultured cells. *Analytical Biochemistry*, *331*(2), 370–375. http://doi.org/10.1016/j.ab.2004.03.049

Righi, M., Mori, L., Libero, G. De, Sironi, M., Biondi, A., Mantovani, A., Ricciardi-Castagnoli, P. (1989). Monokine production by microglial cell clones. *European Journal of Immunology*, *19*(8), 1443–1448. http://doi.org/10.1002/eji.1830190815

Rival, T., Page, R. M., Chandraratna, D. S., Sendall, T. J., Ryder, E., Liu, B., Lomas, D. A. (2009). Fenton chemistry and oxidative stress mediate the toxicity of the beta-amyloid peptide in a Drosophila model of Alzheimer's disease. *European Journal of Neuroscience*, *29*(7), 1335–1347. http://doi.org/10.1111/j.1460-9568.2009.06701.x

Rodriguez-Pallares, J., Parga, J. A., Muñoz, A., Rey, P., Guerra, M. J., & Labandeira-Garcia, J. L. (2007). Mechanism of 6-hydroxydopamine neurotoxicity: The role of NADPH oxidase and microglial activation in 6-hydroxydopamine-induced degeneration of dopaminergic neurons. *Journal of Neurochemistry*, *103*(1), 145–156. http://doi.org/10.1111/j.1471-4159.2007.04699.x

Rohrdanz, E., Schmuck, G., Ohler, S., Tran-Thi, Q. H., & Kahl, R. (2001). Changes in antioxidant enzyme expression in response to hydrogen peroxide in rat astroglial cells. *Arch Toxicol*, *75*(3), 150–158.

Romero, L. I., Tatro, J. B., Field, J. A., & Reichlin, S. (1996). Roles of IL-1 and TNF-alpha in endotoxin-induced activation of nitric oxide synthase in cultured rat brain cells. *American Journal of Physiology*, *270*(2 Pt 2), R326–32.

Roncagliolo, M., Garrido, M., Walter, T., Peirano, P., & Lozoff, B. (1998). Evidence of altered central nervous system development in infants with iron deficiency anemia at 6 mo: Delayed maturation of auditory brainstem responses. *American Journal of Clinical Nutrition*, *68*(3), 683–690.

Rossi, E. (2005). Hepcidin--the iron regulatory hormone. *The Clinical Biochemist. Reviews: Australian Association of Clinical Biochemists*, *26*(3), 47–49.

Rouault, T. A. (2001). Iron on the brain. *Nature Genetics*, *28*(4), 299–300. http://doi.org/10.1038/91036

Rouault, T. A., & Cooperman, S. (2006). Brain Iron Metabolism. *Seminars in Pediatric Neurology*. http://doi.org/10.1016/j.spen.2006.08.002

Rouault, T. A. (2013). Iron metabolism in the CNS: implications for neurodegenerative diseases. *Nature Reviews Neuroscience*, *14*(8), 551–564. http://doi.org/10.1038/nrn3453

Sagara, J., Miura, K., & Bannai, S. (1993). Maintenance of Neuronal Glutathione by Glial Cells. *Journal of Neurochemistry*, *61*(5), 1672–1676. http://doi.org/10.1111/j.1471-4159.1993.tb09802.x

Saggu, H., Cooksey, J., Dexter, D., Wells, F. R., Lees, A., Jenner, P., & Marsden, C. D. (1989). A Selective Increase in Particulate Superoxide Dismutase Activity in Parkinsonian Substantia Nigra. *Journal of Neurochemistry*, *53*(3), 692–697. http://doi.org/10.1111/j.1471-4159.1989.tb11759.x

Salazar, J., Mena, N., Hunot, S., Prigent, A., Alvarez-Fischer, D., Arredondo, M., … Hirsch, E. C. (2008). Divalent metal transporter 1 (DMT1) contributes to neurodegeneration in animal models of Parkinson's disease. *Proceedings of the National Academy of Sciences of the United States of America*, *105*(47), 18578–18583.

Samokyszyn, V. M., Thomas, C. E., Reif, D. W., Saito, M., & Aust, S. D. (1988). Release of Iron from Ferritin and its Role in Oxygen Radical Toxicities. *Drug Metabolism Reviews*, *19*(3 & 4), 283–303.

Saura, J., Parés, M., Bové, J., Pezzi, S., Alberch, J., Marin, C., Martí, M. J. (2003). Intranigral infusion of interleukin-1beta activates astrocytes and protects from subsequent 6-hydroxydopamine neurotoxicity. *Journal of Neurochemistry*, *85*(3), 651–661. http://doi.org/1676

Sawada, M., Suzumura, A., & Marunouchi, T. (1992). TNF alpha induces IL-6 production by astrocytes but not by microglia. *Brain Research*, *583*(1–2), 296–299. http://doi.org/10.1016/S0006-8993(10)80037-X

Sawada, M., Imamura, K., & Nagatsu, T. (2006). Role of cytokines in inflammatory process in Parkinson's disease. *Journal of Neural Transmission. Supplementum*, (70), 373–81. Retrieved from http://www.ncbi.nlm.nih.gov/pubmed/17017556

Schäfer, K. H., Mestres, P., März, P., & Rose-John, S. (1999). The IL-6/sIL-6R fusion protein hyper-IL-6 promotes neurite outgrowth and neuron survival in cultured enteric neurons. *Journal of Interferon & Cytokine Research: The Official Journal of the International Society for Interferon and Cytokine Research*, *19*(5), 527–32. http://doi.org/10.1089/107999099313974

Schafer, D. P., Lehrman, E. K., & Stevens, B. (2013). The "quad-partite" synapse: Microglia-synapse interactions in the developing and mature CNS. *GLIA*, *61*(1), 24–36. http://doi.org/10.1002/glia.22389

Schapira, A. H., Cooper, J. M., Dexter, D., Clark, J. B., Jenner, P., & Marsden, C. D. (1990). Mitochondrial complex I deficiency in Parkinson's disease. *Journal of Neurochemistry*, *54*(3), 823–7. http://doi.org/10.1111/j.1471-4159.1990.tb02325.x

Schulz-Schaeffer, W. J. (2010). The synaptic pathology of α-synuclein aggregation in dementia with Lewy bodies, Parkinson's disease and Parkinson's disease dementia. *Acta Neuropathologica*. http://doi.org/10.1007/s00401-010-0711-0

Seidler, A., Hellenbrand, W., Robra, B. P., Vieregge, P., Nischan, P., Joerg, J., Schneider, E. (1996). Possible environmental, occupational, and other etiologic factors for Parkinson's disease: a case-control study in Germany. *Neurology*, *46*(5), 1275–1284. http://doi.org/10.1212/WNL.46.5.1275

Seiser, C., Teixeira, S., & Kühn, L. C. (1993). Interleukin-2-dependent transcriptional and post-transcriptional regulation of transferrin receptor mRNA. *The Journal of Biological Chemistry*, *268*(18), 13074–13080.

Shachar, D. Ben, Kahana, N., Kampel, V., Warshawsky, A., & Youdim, M. B. H. (2004). Neuroprotection by a novel brain permeable iron chelator, VK-28, against 6-hydroxydopamine lesion in rats. *Neuropharmacology*, *46*(2), 254–263. http://doi.org/10.1016/j.neuropharm.2003.09.005

Shankar, N., Tandon, O. P., Bandhu, R., Madan, N., & Gomber, S. (2000). Brainstem auditory evoked potential responses in iron-deficient anemic children. *Indian Journal of Physiology and Pharmacology*, *44*(3), 297–303.

Sherer, T. B., Betarbet, R., Stout, A. K., Lund, S., Baptista, M., Panov, A. V, Greenamyre, J. T. (2002). An In Vitro Model of Parkinson's Disease : Linking Mitochondrial Impairment to Altered α-Synuclein Metabolism and Oxidative Damage. *Science*, *22*(16), 7006–7015. http://doi.org/20026721

Sherer, T. B., Kim, J.-H., Betarbet, R., & Greenamyre, J. T. (2003). Subcutaneous Rotenone Exposure Causes Highly Selective Dopaminergic Degeneration and α-Synuclein Aggregation. *Experimental Neurology*, *179*(1), 9–16.

Shirwaikar, A., Rajendran, K., & Kumar, C. D. (2004). In vitro antioxidant studies of Annona squamosa Linn. Leaves. *Indian Journal of Experimental Biology*, *42*(8), 803–807.

Sian, J., Dexter, D. T., Lees, A. J., Daniel, S., Jenner, P., & Marsden, C. D. (1994). Glutathione-related enzymes in brain in Parkinson's disease. *Annals of Neurology*, *36*(3), 356–361. http://doi.org/10.1002/ana.410360306

Simard, M., & Nedergaard, M. (2004). The neurobiology of glia in the context of water and ion homeostasis. *Neuroscience*. http://doi.org/10.1016/j.neuroscience.2004.09.053

Simmons, M. L., & Murphy, S. (1993). Cytokines Regulate L-Arginine-Dependent Cyclic GMP Production in Rat Glial Cells. *European Journal of Neuroscience*, *5*(7), 825–831. http://doi.org/10.1111/j.1460-9568.1993.tb00934.x

Simovich, M. J., Conrad, M. E., Umbreit, J. N., Moore, E. G., Hainsworth, L. N., & Smith, H. K. (2002). Cellular location of proteins related to iron absorption and transport. *American Journal of Hematology*, *69*(3), 164–170. http://doi.org/10.1002/ajh.10052

Sinet, P. M., Heikkila, R. E., & Cohen, G. (1980). Hydrogen Peroxide Production by Rat Brain In Vivo. *Journal of Neurochemistry*, *34*(6), 1421–1428. http://doi.org/10.1111/j.1471-4159.1980.tb11222.x

Smirnov, I. M., Bailey, K., Flowers, C. H., Garrigues, N. W., & Wesselius, L. J. (1999). Effects of TNF-alpha and IL-1beta on iron metabolism by A549 cells and influence on cytotoxicity. *The American Journal of Physiology*, *277*(2 Pt 1), L257–L263. Retrieved from http://ajplung.physiology.org/content/277/2/L257

Smith, M. A., Harris, P. L., Sayre, L. M., & Perry, G. (1997). Iron accumulation in Alzheimer disease is a source of redox-generated free radicals. *Proceedings of the National Academy of Sciences of the United States of America*, *94*(18), 9866–8. http://doi.org/10.1073/pnas.94.18.9866

Smith, J. A., Das, A., Ray, S. K., & Banik, N. L. (2012). Role of pro-inflammatory cytokines released from microglia in neurodegenerative diseases. *Brain Research Bulletin*. http://doi.org/10.1016/j.brainresbull.2011.10.004

Snyder, B., Shell, B., Cunningham, J. T., & Cunningham, R. L. (2017). Chronic intermittent hypoxia induces oxidative stress and inflammation in brain regions associated with early-stage neurodegeneration. *Physiological Reports*, *5*(9), e13258. http://doi.org/10.14814/phy2.13258

Sofic, E., Riederer, P., Heinsen, H., Beckmann, H., Reynolds, G. P., Hebenstreit, G., & Youdim, M. B. H. (1988). Increased iron (III) and total iron content in post mortem substantia nigra of parkinsonian brain. *Journal of Neural Transmission*, *74*(3), 199–205. http://doi.org/10.1007/BF01244786

Sofic, E., Paulus, W., Jellinger, K., Riederer, P., & Youdim, M. B. H. (1991). Selective Increase of Iron in Substantia Nigra Zona Compacta of Parkinsonian Brains. *Journal of Neurochemistry*, *56*(3), 978–982. http://doi.org/10.1111/j.1471-4159.1991.tb02017.

Sofic, E., Lange, K. W., Jellinger, K., & Riederer, P. (1992). Reduced and oxidized glutathione in the substantia nigra of patients with Parkinson's disease. *Neuroscience Letters*, *142*(2), 128–130. http://doi.org/10.1016/0304-3940(92)90355-B

Soldin, O. P., Bierbower, L. H., Choi, J. J., Choi, J. J., Thompson-Hoffman, S., & Soldin, S. J. (2004). Serum iron, ferritin, transferrin, total iron binding capacity, hs-CRP, LDL cholesterol and magnesium in children; new reference intervals using the Dade Dimension Clinical Chemistry System. *Clinica Chimica Acta*, *342*(1–2), 211–217. http://doi.org/10.1016/j.cccn.2004.01.002

Spina, M. B., & Cohen, G. (1988). Exposure of striatal [corrected] synaptosomes to L-dopa increases levels of oxidized glutathione. *The Journal of Pharmacology and Experimental Therapeutics*, *247*(2), 502–7.

St-Pierre, J., Buckingham, J. A., Roebuck, S. J., & Brand, M. D. (2002). Topology of superoxide production from different sites in the mitochondrial electron transport chain. *Journal of Biological Chemistry*, *277*(47), 44784–44790.

Steinkellner, H., Scheiber-Mojdehkar, B., Goldenberg, H., & Sturm, B. (2010). A high throughput electrochemiluminescence assay for the quantification of frataxin protein levels. *Analytica Chimica Acta*, *659*(1–2), 129–132. http://doi.org/10.1016/j.aca.2009.11.036

Stemmler, T. L., Lesuisse, E., Pain, D., & Dancis, A. (2010). Frataxin and mitochondrial FeS cluster biogenesis. *Journal of Biological Chemistry*. http://doi.org/10.1074/jbc.R110.118679

Stephan, A. H., Barres, B. A., & Stevens, B. (2012). The Complement System: An Unexpected Role in Synaptic Pruning During Development and Disease. *Annual Review of Neuroscience*, *35*(1), 369–389. http://doi.org/10.1146/annurev-neuro-061010-113810

Streit, W. J., Semple-Rowland, S. L., Hurley, S. D., Miller, R. C., Popovich, P. G., & Stokes, B. T. (1998). Cytokine mRNA profiles in contused spinal cord and axotomized facial nucleus suggest a beneficial role for inflammation and gliosis. *Experimental Neurology*, *152*(1), 74–87. http://doi.org/10.1006/exnr.1998.6835

Streit, W. J., Hurley, S. D., McGraw, T. S., & Semple-Rowland, S. L. (2000). Comparative evaluation of cytokine profiles and reactive gliosis supports a critical role for interleukin-6 in neuron-glia signaling during regeneration. *Journal of Neuroscience Research*, *61*(1), 10–20.

Streit, W. J. (2002). Microglia as neuroprotective, immunocompetent cells of the CNS. *GLIA*. http://doi.org/10.1002/glia.10154

Streit, W. J., Sammons, N. W., Kuhns, A. J., & Sparks, D. L. (2004). Dystrophic Microglia in the Aging Human Brain. *GLIA*, *45*(2), 208–212. http://doi.org/10.1002/glia.10319

Suárez-Fernández, M. B., Soldado, A. B., Sanz-Medel, A., Vega, J. A., Novelli, A., & Fernández-Sánchez, M. T. (1999). Aluminum-induced degeneration of astrocytes occurs via apoptosis and results in neuronal death. *Brain Research*, *835*(2), 125–136. http://doi.org/10.1016/S0006-8993(99)01536-X

Sun, J., Zhang, X. J., Broderick, M., & Fein, H. (2003). Measurement of nitric oxide production in biological systems by using Griess Reaction assay. *Sensors*, *3*(8), 276–284.

Sun, C., Song, N., Xie, A., Xie, J., & Jiang, H. (2012). High hepcidin level accounts for the nigral iron accumulation in acute peripheral iron intoxication rats. *Toxicology Letters*, *212*(3), 276–281. http://doi.org/10.1016/j.toxlet.2012.05.022

Surmeier, D. J., Guzman, J. N., Sanchez-Padilla, J., & Schumacker, P. T. (2011). The role of calcium and mitochondrial oxidant stress in the loss of substantia nigra pars compacta dopaminergic neurons in Parkinson's disease. *Neuroscience*. http://doi.org/10.1016/j.neuroscience.2011.08.045

Tacchini, L., Bianchi, L., Bernelli-Zazzera, A., & Cairo, G. (1999). Transferrin receptor induction by hypoxia. HIF-1-mediated transcriptional activation and cell-specific post-transcriptional regulation. *Journal of Biological Chemistry*, *274*(34), 24142–24146. http://doi.org/10.1074/jbc.274.34.24142

Tacconi, M. T. (1998). Neuronal death: Is there a role for astrocytes? *Neurochemical Research*, *23*(5), 759–765. http://doi.org/10.1023/A:1022463527474

Tachiev, G., Roth, J., & Bowers, R. (2000). Kinetics of hydrogen peroxide decomposition with complexed and "free" iron catalysts. *International Journal of Chemical Kinetics*, *32*(1), 24–35.

Taetle, R., & Honeysett, J. M. (1987). Effects of monoclonal anti-transferrin receptor antibodies on in vitro growth of human solid tumor cells. *Cancer Research*, *47*(8), 2040–4. Retrieved from http://www.ncbi.nlm.nih.gov/pubmed/3828993

Tanaka, S., Ishii, A., Ohtaki, H., Shioda, S., Yoshida, T., & Numazawa, S. (2013). Activation of microglia induces symptoms of Parkinson's disease in wild-type, but not in IL-1 knockout mice. *Journal of Neuroinflammation*, *10*(1), 143. http://doi.org/10.1186/1742-2094-10-143

Tang, Y., & Le, W. (2016). Differential Roles of M1 and M2 Microglia in Neurodegenerative Diseases. *Molecular Neurobiology*. http://doi.org/10.1007/s12035-014-9070-5

Tatton, N. A., Maclean-Fraser, A., Tatton, W. G., Perl, D. P., & Olanow, C. W. (1998). A fluorescent double-labeling method to detect and confirm apoptotic nuclei in Parkinson's disease. *Annals of Neurology*, *44*(3 Suppl 1), S142-8. Retrieved from http://www.ncbi.nlm.nih.gov/pubmed/9749586

Teismann, P., & Schulz, J. B. (2004). Cellular pathology of Parkinson's disease: Astrocytes, microglia and inflammation. *Cell and Tissue Research*. http://doi.org/10.1007/s00441-004-0944-0

Tennant, G. B., & Greenman, D. a. (1969). Determination of iron in solutions containing iron complexes. *Journal of Clinical Pathology*, *22*(3), 301–3. Retrieved from http://www.pubmedcentral.nih.gov/articlerender.fcgi?artid=474064&tool=pmcentrez&rendertype=abstract

Testa, C. M., Sherer, T. B., & Greenamyre, J. T. (2005). Rotenone induces oxidative stress and dopaminergic neuron damage in organotypic substantia nigra cultures. *Molecular Brain Research*, *134*(1), 109–118. http://doi.org/10.1016/j.molbrainres.2004.11.007

Thacker, E. L., & Ascherio, A. (2008). Familial aggregation of Parkinson's disease: A meta-analysis. *Movement Disorders*, *23*(8), 1174–1183. http://doi.org/10.1002/mds.22067

Théry, C., Chamak, B., & Mallat, M. (1991). Cytotoxic Effect of Brain Macrophages on Developing. *The European Journal of Neuroscience*, *3*(11), 1155–1164. http://doi.org/ejn_03111155 [pii]

Thomas, C. E., Morehouse, L. A., & Aust, S. D. (1985). Ferritin and superoxide-dependent lipid peroxidation. *Journal of Biological Chemistry*, *260*(6), 3275–3280.

Tieu, K., Ischiropoulos, H., & Przedborski, S. (2003). Nitric oxide and reactive oxygen species in Parkinson's disease. *IUBMB Life*. http://doi.org/10.1080/1521654032000114320

Tomás-Camardiel, M., Rite, I., Herrera, A. J., De Pablos, R. M., Cano, J., Machado, A., & Venero, J. L. (2004). Minocycline reduces the lipopolysaccharide-induced inflammatory reaction, peroxynitrite-mediated nitration of proteins, disruption of the blood-brain barrier, and damage in the nigral dopaminergic system. *Neurobiology of Disease*, *16*(1), 190–201. http://doi.org/10.1016/j.nbd.2004.01.010

Torres-Platas, S. G., Comeau, S., Rachalski, A., Bo, G., Cruceanu, C., Turecki, G., … Mechawar, N. (2014). Morphometric characterization of microglial phenotypes in human cerebral cortex. *Journal of Neuroinflammation*, *11*(1), 12. http://doi.org/10.1186/1742-2094-11-12

Tórsdóttir, G., Kristinsson, J., Sveinbjornsdóttir, S., Snaedal, J., & Johannesson, T. (1999). Copper, Ceruloplasmin, Superoxide Dismutase and Iron Parameters in Parkinson's Disease. *Pl~armatology & Toxicology*, *85*, 239–243. http://doi.org/10.1111/j.1600-0773.1999.tb02015.x

Troy, C. M., Derossi, D., Prochiantz, A., Greene, L. A., & Shelanski, M. L. (1996). Downregulation of Cu/Zn superoxide dismutase leads to cell death via the nitric oxide-

peroxynitrite pathway. *The Journal of Neuroscience: The Official Journal of the Society for Neuroscience*, *16*(1), 253–61.

Turnbull, S., Tabner, B. J., El-Agnaf, O. M. A., Moore, S., Davies, Y., & Allsop, D. (2001). a-synuclein implicated in Parkinson's disease catalyses the formation of hydrogen peroxide in vitro. *Free Radical Biology and Medicine*, *30*(10), 1163–1170.

Twig, G., Jung, S.-K., Messerli, M. A., Smith, P. J. S., Shirihai, O. S. (2001). Real-Time Detection of Reactive Oxygen Intermediates from Single Microglial Cells. *The Biological Bulletin, 201*(2): 261-262.

Unterharnscheidt, F. (1995). A neurologist's reflections on boxing. *Revista de Neurologia, 23*(123): 1027-32.

Urrutia, P., Aguirre, P., Esparza, A., Tapia, V., Mena, N. P., Arredondo, M., … Núñez, M. T. (2013). Inflammation alters the expression of DMT1, FPN1 and hepcidin, and it causes iron accumulation in central nervous system cells. *Journal of Neurochemistry*, *126*(4), 541–549. http://doi.org/10.1111/jnc.12244

Uversky, V. N., Li, J., & Fink, A. L. (2001). Metal-triggered structural transformations, aggregation, and fibrillation of human alpha-synuclein. A possible molecular link between Parkinson's disease and heavy metal exposure. *Journal of Biological Chemistry*, *276*(47), 44284–44296. http://doi.org/10.1074/jbc.M105343200

Valko, M., Izakovic, M., Mazur, M., Rhodes, C. J., & Telser, J. (2004). Role of oxygen radicals in DNA damage and cancer incidence. *Molecular and Cellular Biochemistry*, *266*(1–2), 37–56. http://doi.org/10.1023/B:MCBI.0000049134.69131.89

Van, B., Gouel, F., Jonneaux, A., Timmerman, K., Gelé, P., Pétrault, M., Devedjian, J. C. (2016). Ferroptosis, a newly characterized form of cell death in Parkinson's disease that is regulated by PKC. *Neurobiology of Disease*, *94*, 169–178. http://doi.org/10.1016/j.nbd.2016.05.011

Van Den Eeden, S. K., Tanner, C. M., Bernstein, A. L., Fross, R. D., Leimpeter, A., Bloch, D. A., & Nelson, L. M. (2003). Incidence of Parkinson's Disease: Variation by Age, Gender, and Race/Ethnicity. *Am J Epidemiol American Journal of Epidemiology*, *157*(11), 1015–1022. http://doi.org/10.1093/aje/kwg068

Van Engeland, M., Nieland, L. J. W., Ramaekers, F. C. S., Schutte, B., & Reutelingsperger, C. P. M. (1998). Annexin V-affinity assay: A review on an apoptosis detection system based on phosphatidylserine exposure. *Cytometry*.

Venkateshappa, C., Harish, G., Mahadevan, A., Srinivas Bharath, M. M., & Shankar, S. K. (2012). Elevated oxidative stress and decreased antioxidant function in the human hippocampus and frontal cortex with increasing age: Implications for neurodegeneration in Alzheimer's disease. *Neurochemical Research*, *37*(8), 1601–1614. http://doi.org/10.1007/s11064-012-0755-8

Von Campenhausen, S., Bornschein, B., Wick, R., Bötzel, K., Sampaio, C., Poewe, W., … Dodel, R. (2005). Prevalence and incidence of Parkinson's disease in Europe. *European*

Neuropsychopharmacology, *15*(4), 473–490. http://doi.org/10.1016/j.euroneuro.2005.04.007

Wake, H., Moorhouse, A. J., Jinno, S., Kohsaka, S., & Nabekura, J. (2009). Resting Microglia Directly Monitor the Functional State of Synapses In Vivo and Determine the Fate of Ischemic Terminals. *Journal of Neuroscience*, *29*(13), 3974–3980. http://doi.org/10.1523/JNEUROSCI.4363-08.2009

Wake, H., & Fields, R. D. (2011). Physiological function of microglia. *Neuron Glia Biology*, *7*(1), 1–3. http://doi.org/10.1017/S1740925X12000166

Wang, X., You, G., Chen, H., & Cai, X. (2002). Clinical course and cause of death in elderly patients with idiopathic Parkinson's disease. *Chin Med J (Engl).*, *115*(9), 1409–11.

Wang, X., Garrick, M. D., Yang, F., Dailey, L. A., Piantadosi, C. A., & Ghio, A. J. (2005). TNF, IFN-gamma, and endotoxin increase expression of DMT1 in bronchial epithelial cells. *Am J Physiol Lung Cell Mol Physiol*, *289*(1), L24-33. http://doi.org/00428.2003 [pii]\r10.1152/ajplung.00428.2003

Wang, Q., Du, F., Qian, Z. M., Xiao, H. G., Zhu, L., Wing, H. Y., Ke, Y. (2008). Lipopolysaccharide induces a significant increase in expression of iron regulatory hormone hepcidin in the cortex and substantia nigra in rat brain. *Endocrinology*, *149*(8), 3920–3925. http://doi.org/10.1210/en.2007-1626

Wang, D., Wang, L. H., Zhao, Y., Lu, Y. P., & Zhu, L. (2010). Hypoxia regulates the ferrous iron uptake and reactive oxygen species level via divalent metal transporter 1 (DMT1) exon1B by hypoxia-inducible factor-1. *IUBMB Life*, *62*(8), 629–636. http://doi.org/10.1002/iub.363

Wang, J., Song, N., Jiang, H., Wang, J., & Xie, J. (2013). Pro-inflammatory cytokines modulate iron regulatory protein 1 expression and iron transportation through reactive oxygen/nitrogen species production in ventral mesencephalic neurons. *Biochimica et Biophysica Acta - Molecular Basis of Disease*, *1832*(5), 618–625.

Ward, D.M., & Kaplan, J. (2012). Ferroportin-mediated iron transport: expression and regulation. *Biochimica et Biophysica Acta- Molecular Cell Research*, *1823*(9): 1426-1433. https://www.sciencedirect.com/science/article/pii/S016748891200064X

Ward, R. J., Legssyer, R., Henry, C., & Crichton, R. R. (2000). Does the haemosiderin iron core determine its potential for chelation and the development of iron-induced tissue damage? *Journal of Inorganic Biochemistry*, *79*(1–4), 311–317. http://doi.org/10.1016/S0162-0134(99)00237-8

Ward, R. J., Crichton, R. R., & Dexter, D. T. (2013). *Mechanisms and Metal Involvement in Neurodegenerative Diseases*.

Ward, R. J., Zucca, F. A., Duyn, J. H., Crichton, R. R., & Zecca, L. (2014). The role of iron in brain ageing and neurodegenerative disorders. *The Lancet Neurology*. http://doi.org/10.1016/S1474-4422(14)70117-6

Weaver, F. M., Follett, K., Stern, M., Hur, K., Harris, C., Marks Jr., W. J., Huang, G. D. (2009). Bilateral deep brain stimulation vs best medical therapy for patients with advanced Parkinson disease: a randomized controlled trial. *Jama*, *301*(1), 63–73. http://doi.org/10.1001/jama.2008.929

Weinreb, O., Mandel, S., Youdim, M. B. H., & Amit, T. (2013). Targeting dysregulation of brain iron homeostasis in Parkinson's disease by iron chelators. *Free Radical Biology and Medicine*. http://doi.org/10.1016/j.freeradbiomed.2013.01.017

Weiss, G., Goossen, B., Doppler, W., Fuchs, D., Pantopoulos, K., Werner-Felmayer, G., … Hentze, M. W. (1993). Translational regulation via iron-responsive elements by the nitric oxide/NO-synthase pathway. *The EMBO Journal*, *12*(9), 3651–3657.

White, R. E., & Jakeman, L. B. (2008). Don't fence me in: harnessing the beneficial roles of astrocytes for spinal cord repair. *Restorative Neurology and Neuroscience*, *26*(2–3), 197–214. http://doi.org/10.1016/j.bbi.2008.05.010

Wills, J., Jones, J., Haggerty, T., Duka, V., Joyce, J. N., & Sidhu, A. (2010). Elevated tauopathy and alpha-synuclein pathology in postmortem Parkinson's disease brains with and without dementia. *Experimental Neurology*, *225*(1), 210–218.

Winterbourn, C. C. (1995). Toxicity of iron and hydrogen peroxide: The Fenton reaction. *Toxicology Letters*, *82–83*(C), 969–974. http://doi.org/10.1016/0378-4274(95)03532-X

Wright, G. J., Cherwinski, H., Foster-Cuevas, M., Brooke, G., Puklavec, M. J., Bigler, M., Barclay, a N. (2003). Characterization of the CD200 receptor family in mice and humans and their interactions with CD200. *Journal of Immunology (Baltimore, MD: 1950)*, *171*(6), 3034–3046. http://doi.org/10.4049/jimmunol.171.6.3034

Wrighting, D. M., & Andrews, N. C. (2006). Interleukin-6 induces hepcidin expression through STAT3. *Blood*, *108*(9), 3204–3209. http://doi.org/10.1182/blood-2006-06-027631

Wu, D.-C., Teismann, P., Tieu, K., Vila, M., Jackson-Lewis, V., Ischiropoulos, H., & Przedborski, S. (2003). NADPH oxidase mediates oxidative stress in the 1-methyl-4-phenyl-1,2,3,6-tetrahydropyridine model of Parkinson's disease. *Proceedings of the National Academy of Sciences of the United States of America*, *100*(10), 6145–50. http://doi.org/10.1073/pnas.0937239100

Wyss-Coray, T. (2006). Inflammation in Alzheimer disease: driving force, bystander or beneficial response? *Nature Medicine*, *12*(9), 1005–15. http://doi.org/10.1038/nm1484

Wyss-Coray, T., & Rogers, J. (2012). Inflammation in Alzheimer disease-A brief review of the basic science and clinical literature. *Cold Spring Harbor Perspectives in Medicine*, *2*(1). http://doi.org/10.1101/cshperspect.a006346

Xie, W., Li, X., Li, C., Zhu, W., Jankovic, J., & Le, W. (2010). Proteasome inhibition modeling nigral neuron degeneration in Parkinson's disease. *Journal of Neurochemistry*, *115*(1), 188–199. http://doi.org/10.1111/j.1471-4159.2010.06914.x

Xie, Y., Hou, W., Song, X., Yu, Y., Huang, J., Sun, X., Tang, D. (2016). Ferroptosis: process and function. *Cell Death and Differentiation*, *23*(3), 369–379. http://doi.org/10.1038/cdd.2015.158

Xu, J., & Ling, E. A. (1994). Upregulation and induction of surface antigens with special reference to MHC class II expression in microglia in postnatal rat brain following intravenous or intraperitoneal injections of lipopolysaccharide. *Journal of Anatomy*, (Pt 2), 285–96.

Xu, X., & Malave, A. (2000). P38 MAPK, but not p42/p44 MAPK mediated inducible nitric oxide synthase expression in C6 glioma cells. *Life Sciences*, *67*(26), 3221–3230. http://doi.org/10.1016/S0024-3205(00)00902-4

Xu, X., Pin, S., Gathinji, M., Fuchs, R., & Harris, Z. L. (2004). Aceruloplasminemia: An inherited neurodegenerative disease with impairment of iron homeostasis. *Annals of the New York Academy of Sciences*. http://doi.org/10.1196/annals.1306.024

Xu, X., Wang, Q., & Zhang, M. (2008). Age, gender, and hemispheric differences in iron deposition in the human brain: An in vivo MRI study. *NeuroImage*, *40*(1), 35–42. http://doi.org/10.1016/j.neuroimage.2007.11.017

Xu, Q., Kanthasamy, A. G., Jin, H., & Reddy, M. B. (2016). Hepcidin Plays a Key Role in 6-OHDA Induced Iron Overload and Apoptotic Cell Death in a Cell Culture Model of Parkinson's Disease. *Parkinson's Disease*, *2016*. http://doi.org/10.1155/2016/8684130

Yana, M. H., Wang, X., & Zhu, X. (2013). Mitochondrial defects and oxidative stress in Alzheimer disease and Parkinson disease. *Free Radical Biology and Medicine*. http://doi.org/10.1016/j.freeradbiomed.2012.11.014

Yang, W. S., & Stockwell, B. R. (2016). Ferroptosis: Death by Lipid Peroxidation. *Trends in Cell Biology*. http://doi.org/10.1016/j.tcb.2015.10.014

Yasuda, T., Niki, T., Ariga, H., & Iguchi-Ariga, S. M. M. (2017). Free radicals impair the anti-oxidative stress activity of DJ-1 through the formation of SDS-resistant dimer. *Free Radical Research*, *51*(4), 397–412. http://doi.org/10.1080/10715762.2017.1324201

Yokokura, M., Terada, T., Bunai, T., Nakaizumi, K., Takebayashi, K., Iwata, Y., Ouchi, Y. (2016). Depiction of microglial activation in aging and dementia: Positron emission tomography with [11C]DPA713 versus [11C](R)PK11195. *J Cereb Blood Flow Metab*. http://doi.org/10.1177/0271678x16646788

Yoshida, T., Tanaka, M., Sotomatsu, A., & Hirai, S. (1995). Activated microglia cause superoxide-mediated release of iron from ferritin. *Neuroscience Letters*, *190*(1), 21–24. http://doi.org/10.1016/0304-3940(95)11490-N

Yoshida, T., Tanaka, M., Sotomatsu, A., Hirai, S., & Okamoto, K. (1998). Activated microglia cause iron-dependent lipid peroxidation in the presence of ferritin. *Neuroreport*, *9*(9), 1929–1933. Retrieved from http://www.ncbi.nlm.nih.gov/pubmed/9674569

Youdim, M. B. H., Ben-Shachar, D., Yehuda, S., Levitsky, D. A., & Hill, J. M. (1989). Putative biological mechanisms of the effect of iron deficiency on brain biochemistry and behavior. *American Journal of Clinical Nutrition*, *50*(3 SUPPL.), 607–617.

Youdim, M. B. H., Ben-Shachar, D., & Riederer, P. (1989). Is Parkinson's disease a progressive siderosis of substantia nigra resulting in iron and melanin induced neurodegeneration? *Acta Neurologica Scandinavica*, *80*, 47–54. http://doi.org/10.1111/j.1600-0404.1989.tb01782.x

Youdim, M. B. H., Stephenson, G., & Shachar, D. Ben. (2004). Ironing iron out in Parkinson's disease and other neurodegenerative diseases with iron chelators: A lesson from 6-hydroxydopamine and iron chelators, desferal and VK-28. *Annals of the New York Academy of Sciences*, *1012*, 306–325. http://doi.org/10.1196/annals.1306.025

Young, S. P., Bomford, A., & Williams, R. (1984). The effect of the iron saturation of transferrin on its binding and uptake by rabbit reticulocytes. *Biochem J*, *219*(2), 505–510. http://doi.org/10.1042/bj2190505

Zecca, L., Pietra, R., Goj, C., Mecacci, C., Radice, D., & Sabbioni, E. (1994). Iron and Other Metals in Neuromelanin, Substantia Nigra, and Putamen of Human Brain. *Journal of Neurochemistry*, *62*(3), 1097–1101. http://doi.org/10.1046/j.1471-4159.1994.62031097.x

Zecca, L., Gallorini, M., Schünemann, V., Trautwein, A. X., Gerlach, M., Riederer, P., Tampellini, D. (2001). Iron, neuromelanin and ferritin content in the substantia nigra of normal subjects at different ages: Consequences for iron storage and neurodegenerative processes. *Journal of Neurochemistry*, *76*(6), 1766–1773. http://doi.org/10.1046/j.1471-4159.2001.00186.x

Zecca, L., Youdim, M. B. H., Riederer, P., Connor, J. R., & Crichton, R. R. (2004). Iron, brain ageing and neurodegenerative disorders. *Nature Reviews Neuroscience*, *5*(11), 863–873. http://doi.org/10.1038/nrn1537

Zhang, G., & Ghosh, S. (2001). Toll-like receptor-mediated NF-κB activation: A phylogenetically conserved paradigm in innate immunity. *Journal of Clinical Investigation*. http://doi.org/10.1172/JCI11837

Zhang, W., Wang, T., Qin, L., Gao, H.-M., Wilson, B., Ali, S. F., Liu, B. (2004). Neuroprotective effect of dextromethorphan in the MPTP Parkinson's disease model: role of NADPH oxidase. *FASEB Journal: Official Publication of the Federation of American Societies for Experimental Biology*, *18*, 589–91. http://doi.org/10.1096/fj.03-0983fje

Zhang, W. (2005). Aggregated α-synuclein activates microglia: a process leading to disease progression in Parkinson's disease. *The FASEB Journal*, *19*(6), 533–542. http://doi.org/10.1096/fj.04-2751com

Zhang, W., Wang, T., Pei, Z., Miller, D., Wu, X., Block, M., Zhang, J. (2005). Aggregated a-synuclein activates microglia: a process leading to disease progression in Parkinson's disease. *The FASEB Journal*, *19*(6), 533–542. http://doi.org/10.1096/fj.04-2751com

Zhang, X., Chen, Y., Wang, C., & Huang, L.-Y. M. (2007). Neuronal somatic ATP release triggers neuron-satellite glial cell communication in dorsal root ganglia. *Proceedings of the National Academy of Sciences of the United States of America*, *104*(23), 9864–9. http://doi.org/10.1073/pnas.0611048104

Zhang, S., Wang, J., Song, N., Xie, J., & Jiang, H. (2009). Up-regulation of divalent metal transporter 1 is involved in 1-methyl-4-phenylpyridinium (MPP+)-induced apoptosis in MES23.5 cells. *Neurobiology of Aging*, *30*(9), 1466–1476.

Zhang, Z., Hou, L., Song, J. L., Song, N., Sun, Y. J., Lin, X., Ge, Y. L. (2014). Pro-inflammatory cytokine-mediated ferroportin down-regulation contributes to the nigral iron accumulation in lipopolysaccharide-induced Parkinsonian models. *Neuroscience*, *257*, 20–30. http://doi.org/10.1016/j.neuroscience.2013.09.037

Zheng, H., Gal, S., Weiner, L. M., Bar-Am, O., Warshawsky, A., Fridkin, M., & Youdim, M. B. H. (2005). Novel multifunctional neuroprotective iron chelator-monoamine oxidase inhibitor drugs for neurodegenerative diseases: In vitro studies on antioxidant activity, prevention of lipid peroxide formation and monoamine oxidase inhibition. *Journal of Neurochemistry*, *95*(1), 68–78. http://doi.org/10.1111/j.1471-4159.2005.03340.x

Zheng, X., & Hunter, T. (2013). Parkin mitochondrial translocation is achieved through a novel catalytic activity coupled mechanism. *Cell Research*, *23*(7), 886–97.

Zhou, C., Huang, Y., & Przedborski, S. (2008). Oxidative stress in Parkinson's disease: A mechanism of pathogenic and therapeutic significance. In *Annals of the New York Academy of Sciences* (Vol. 1147, pp. 93–104). http://doi.org/10.1196/annals.1427.023

Zhou, Z. D., Lan, Y. H., Tan, E. K., & Lim, T. M. (2010). Iron species-mediated dopamine oxidation, proteasome inhibition, and dopaminergic cell demise: Implications for iron-related dopaminergic neuron degeneration. *Free Radical Biology and Medicine*, *49*(12), 1856–1871.

Zhu, W., Zheng, H., Shao, X., Wang, W., Yao, Q., & Li, Z. (2010). Excitotoxicity of TNF alpha derived from KA activated microglia on hippocampal neurons in vitro and in vivo. *Journal of Neurochemistry*, *114*(2), 386–396.

Zoratti, M., & Szabò, I. (1995). The mitochondrial permeability transition. *Biochimica et Biophysica Acta*, *1241*(2), 139–176.

Zucca, F. A., Segura-Aguilar, J., Ferrari, E., Muñoz, P., Paris, I., Sulzer, D., Zecca, L. (2017). Interactions of iron, dopamine and neuromelanin pathways in brain aging and Parkinson's disease. *Progress in Neurobiology*.